Dynamics of a translating cable subjected to unilateral constraints, friction and punctual loads

Charlélie Bertrand

NNT number : 2022LYSET009 Year 2022

THÈSE DE DOCTORAT DE L'UNIVERSITÉ DE LYON

opérée au sein de

l'École Nationale des travaux Publics de l'État

École Doctorale 162
Mécanique-Énergétique - Génie Civil - Acoustique
Spćialité de doctorat : Génie mécanique

Soutenue publiquement le 27/06/2022 par
Charlélie BERTRAND

Dynamics of a translating cable subjected to unilateral constraints, friction and punctual loads

Comportement dynamique d'un câble en translation soumis à des contraintes unilatérales, du frottement et à des efforts ponctuels

---

devant le jury composé de :

	Fabrice THOUVEREZ	Prof. EC Lyon, CNRS, LTDS
Rapporteurs :	Bruno COCHELIN	Prof. EC Marseille, CNRS, LMA
	Olivier BRULS	Prof. ordinaire Université de Liège, LSMM
Examinateurs :	Béatrice FAVERJON	MCF, INSA Lyon, LaMCoS
Co-Directeurs :	Claude-Henri LAMARQUE	Prof. ENTPE, CNRS, LTDS
	Vincent ACARY	DR2, CNRS, INRIALPES, Tripop

Acknowledgments

Heureux qui comme Ulysse, a fait un beau voyage - Ou comme celui-là qui conquit la Toison - Et puis s'en est retourné, plein d'usage et raison - Vivre entre ses parents le reste de son âge - Joachim Du Bellay.

This PhD have been filled with satisfaction and frustration but the journey was worth it. Longer the acknowledgments are, the less we remember the people without who this work would not have been possible.

I would like to thank from the bottom of the heart Pr. Claude-Henri Lamarque for his continuous support and supervision. His behavior and philosophy in both research and life have been a great inspiration to me.

I also thank Pr. Vincent Acary for his advised tips and for keeping me from being a cable goldfish. His culture and skills made this work a perpetual enrichment.

I thank, with all due gratitude, Pr. Alireza Ture Savadkoohi for his every day presence and his generosity. All along my years at ENTPE, he was a model of availability, curiosity and kindness.

I thank all the people in the shadow who are making research possible: research engineers, librarians, secretaries and students.

I personally thank my dear friend Loïc Bonnetain for his presence and relieving sense of humor during this past three years.

Eventually, I thank all my family for their moral support and the esteem they placed in me.

Abstract

In France, aerial ropeways are mostly present in mountain areas but their urban implantation is starting slowly by slowly. Although their static design seems well established, the understanding of the dynamical behavior remain a challenge.
This work aim at modeling and simulating the dynamical behavior of a translating cable subjected to unilateral constraint, friction and punctual loads. The interaction between the cable, the tower and the sheaves is modeled via frictional contact in order to satisfy a given line speed.
This work first focuses on the development of system equations according to Lagrangian mechanics. The latter is believed more applicable to any constitutive law and any constraints including obstacles.
Those same equations are used to derive a versatile cable element that can be used for any cable system. The treatment of contact and friction is realized thanks to the Siconos platform.
Ritz-Galerkin methods are often used in the literature to treat the nonlinear dynamics of cables. Here we proposed a general derivations of the latter which we compare to finite element methods.
Some applications focused on the dynamics of aerial ropeways are proposed to model the possible scenarios leading to global instabilities ate the scale of an installation.

Résumé long en français

En France, les installations de transport par câble sont majoritairement présentes en régions montagneuses mais leur implantation en zone urbaine se développe. Bien que leur dimensionnement statique semble maîtrisé, leur comportement dynamique n'est à ce jour pas totalement cerné.
Ce travail s'intéresse à la modélisation de la dynamique d'une installation de transport par câble. Plusieurs approches sont proposées avec pour objectif d'ouvrir des pistes sur la prise en compte des chargements ponctuels mais aussi de l'intéraction entre le câble, les appuis et les poulies de la ligne. Le contact entre le câble et ces éléments est supposé frottant dans le but de prendre en compte l'entraînement de câble à une certaine vitesse.
Mêlant à la fois développements analytiques et numériques, cette thèse a été co-encadrée par le LTDS à Lyon et l'INRIA à Grenoble. Le concours du STRMTG a rendu possible des échanges enrichissants et pratiques sur le contexte technique dans lequel s'inscrit cette thèse.
Ce travail a conduit aux publications suivantes :

- C. Bertrand, A. Ture Savadkoohi, and C.-H. Lamarque. Nonlinear oscillations of a pendulum cable with the effects of the friction and the radius of the support. Nonlinear Dynamics, 96:1303–1315, 2019 ;

- C. Bertrand, C. Plut, A. Ture Savadkoohi, and C.-H. Lamarque. On the modal response of mobile cables. Engineering Structures, 210, 2020 ;

- C. Bertrand, V. Acary, A. Ture Savadkoohi, and C.-H. Lamarque. A robust and efficient numerical finite element method for cables. International Journal for Numerical Method in Engineering, 121, 2020 ;

- C. Bertrand, A. Ture Savadkoohi, V. Acary, and C.-H. Lamarque. Reduced-order model for the non-linear dynamics of cables [accepted]. Journal of Engineering Mechanics, 2022.

ainsi qu'aux conférences internationales suivantes :

- **About the modal response of mobile cables**, Recent Advances in Nonlinear Mechanics (RANM), May 2019 Lodz, Poland

- **Equilibrium of a non-compressible cable subjected to unilateral constraints**, European Nonlinear Oscillation Conference (ENOC), 17-22 July 2022, Lyon, France

- **A robust numerical implementation of cable finite elements**, International Congress of Theoretical and Applied Mechanics (ICTAM), 23-28 August 2020+1, Milano, Italy

- **Numerical dynamics of a cable subjected to frictional impact**, Conference on the Numerical Solution of Differential and Differential-Algebraic Equations (NUMDIFF), 6-10 September 2021, Halle, Germany

Ce manuscrit comporte six chapitres rapportant les avancées scientifiques faites durant trois années de travail.

Le **chapitre 1** présente la littérature scientifique dans lequel s'inscrit les travaux. Deux principaux blocs existent séparemment : les méthodes analytiques et les méthodes numériques. Le manque de lien direct et de mélange entre les deux implique que les modèles disponibles sont soit trop simplistes pour le cas du téléphérique ou comportent trop de paramètres pour permettre des études paramériques à grande plus-value. Le positionnement de cette thèse est hybride dans la mesure où les deux approches peuvent se combiner pour étudier la réalité.

Le **chapitre 2** développe des principes lagrangiens pour la mécanique d'un câble. Cette approche permet d'inclure des conditions aux limites sophistiquées et des lois de comportements sophistiquées tout en permettant de généraliser les modèles existants dans la littérature. Les représentations classiques du câble parabolique et de la caténaire sont présentées dans ce chapitre tout en élargissant les perspectives de résultats analytiques au cas du contact persistant d'un câble inextensible sur un obstacle convexe.

Le **chapitre 3** traite des éléments finis appliqués au câble. Les difficultés numériques inhérentes à ce problème sont présentées objectivement et traitées en formulant un élément de câble n'admettant pas la compression. Ce même élément est utilisé pour intégrer une dynamique non-régulière avec impact et frottement. Ces développements permettent de simuler la dynamique de courroie, l'enroulement d'une amarre ou le rebond d'un câble sur un obstacle.

Le **chapitre 4** reprend le cas de la théorie des vibrations pour le câble pour les petites vibrations autour d'un équilibre. Ce cas est écrit dans la base locale -dite de Frenet- et utilisé pour formaliser l'écriture de modèles réduits numériques pour la réponse non-linéaire d'un câble bi-appuyé. Ces développements sont utilisés conjointement avec la continuation par longueur d'arc afin d'obtenir des tendances de réponses. D'autres méthodes sont aussi utilisées pour comparer cet outil : les éléments finis et la méthode des échelles multiples, permettant d'avoir des critères objectifs de validité et d'utilisation pratiques des approches proposées.

Les **chapitres 5 et 6** sont des applications spécifiques de la thèse au cas du télephérique. Des équations pour la dynamique d'une travée en translation sont proposées pour traiter le cas du "pompage". Il est montré que la vitesse seule ne peut expliquer une apparition soudaine d'une grosse amplitude. L'entrée d'une cabine dans une travée semble jouer un rôle prépondérant dans ce phénomène ce qui peut aussi être étudié par élément fini.

Contents

List of Figures

List of Tables

Introduction

Context

This thesis is financed by the French Ministry, namely 'Ministère de la Transition Écologique'. This opportunity granted me with three years of research about the modeling of cable dynamics with a particular focus on the dynamics of cable-car installations. In France, the 'lois Grenelle de l'Environnement' states that these transportation infrastructures may be an alternative to existing transportation solution [1]. Today, building such systems are at the heart of urban planning configurations which require more knowledge about their dynamic behavior [2].

Objectives

This work aims at developing a cable model which takes into account the correct geometry of the cable and the complex interactions between the cable and its supports. The model takes into account the point and distributed loads, the friction occurring between the cable and its supports and also the friction between the cable and the driving pulleys. The cable is in motion due to an imposed velocity at one of its boundaries. The thesis deals with the modeling of the described system associated with robust procedures for its numerical treatments. The reliability and applicability of each approaches will be discussed.

Results and Scientific Contributions

PhD Results

In this work several models and scenarios have been investigated to catch potential critical dynamic scenarios for ropeways. The main results are the following:

- Derive a robust basis for the cable model based upon the principle of variation and constrained optimization: Chapter 2;
- Develop a versatile cable element which can both ensure a non-compression condition for each cable segment and which can be used for nonsmooth analysis: Chapter 3;
- Propose a methodology to compute modes and reduced-order models to trace the essential features of the nonlinear dynamics of single-span cable (translating or not) 4: Chapter 4 and Chapter 5;
- Investigate a global methodology to model a whole ropeway. The latter considers the effect of friction, point loads, control velocity and the cable: Chapter 6.

All approaches have been considered to find clues about the proper way of simulating the dynamics of such cable systems. However, the developed tools are not strictly reserved for

ropeways and can be applied to other domain including cable networks, belt-sheave or off-shore cables.

Scientific Production

This work led to various type of scientific communication including:

- Publications dealing with:
  - The effects of friction on the amplitude of oscillations [3]
  - The modal response of translating cables [4]
  - The robustness of finite element methods for cable systems [5]
  - The generalization of reduced-order-model for cable nonlinear dynamics and its comparison with finite element method [6]
- Conferences:
  - **About the modal response of mobile cables**, Recent Advances in Nonlinear Mechanics (RANM), May 2019 Lodz, Poland
  - **Equilibrium of a non-compressible cable subjected to unilateral constraints**, European Nonlinear Oscillation Conference (ENOC), 17-22 July 2022, Lyon, France
  - **A robust numerical implementation of cable finite elements**, International Congress of Theoretical and Applied Mechanics (ICTAM), 23-28 August 2020+1, Milano, Italy
  - **Numerical dynamics of a cable subjected to frictional impact**, Conference on the Numerical Solution of Differential and Differential-Algebraic Equations (NUMDIFF), 6-10 September 2021, Halle, Germany
- Vulgarization events
  - **Rencontres Interdisciplinaires Doctorales de l'Architecture et de l'Aménagement durable** (RIDAAD), February 2019, Vaulx-en-Velin, France
  - **Café des Sciences**, October 2019, Vaulx-en-Velin, France

Organization of the manuscript

Outline

This PhD work is organized as follows:
The equations are developed from calculus of variation in Chapter 2. This chapter provides with the general cable equations that can be used for any situation. Some classical results are recalled in the framework proposed in this work. Chapter 3 presents a finite element method to tackle the computation of cable nonlinear dynamics while imposing a non-compression condition for each element. The latter is combined to nonsmooth dynamics in order to treat impact and friction numerically. Chapter 4 provides the equations for the dynamics of cables for single span problems. The modal analysis and the nonlinear dynamics are tackled via Ritz-Galerkin procedure. Those analyses are hybrid since they are mostly analytical but need a computer to evaluate the final results. Chapters 5 and 6 consist of applications of result of previous chapters to the case of ropeways. The single-span approach and the FEM approach are both discussed in the context of those infrastructures.

Suggestions for reading

Chapter 2 presents the essential equations of the cable mechanics. Chapter 3 and Chapter 4 can be read separately even though some comparisons are given in Chapter 4. They cannot be skipped at first reading. Chapters 5 and 6 consist on applications and extension of the results of Chapters 3-4 to the particular case of an aerial ropeway. Chapters 1, 5 and 6 can be skipped at first reading.

Introduction en Français

Contexte

Cette thèse est financée par le 'Ministère de la Transition Énergétique'. Cette opportunité m'a offert trois ans de recherche sur la dynamique des installations de téléphériques. En France, les lois 'Grenelle de l'Environnement' placent le téléphérique comme une alternative durable à d'autres moyens de transport en commun [1]. Il s'avère que ces installations sont au coeur de réflexions pour redéfinir les constructions des réseaux urbains mais que la simulation de leur comportement dynamique nécessite davantage de connaissances [2].

Objectifs

Ce travail a pour objectif de construire des modèles de câble qui prennent en compte la géométrie exacte ainsi que les interactions qui existent entre le câble et ses divers supports. Les modèles traiteront, dans la mesure du possible, des charges ponctuelles, des charges distribuées et du frottement entre le câble et ses roulements/poulies. Une vitesse est imposée au câble sous la forme d'une donnée de vitesse d'exploitation à la poulie motrice. Cette thèse traitera tout autant de la robustesse numérique que de la fiabilité des démarches proposées.

Résultats et Communication Scientifique

Résultats de la Thèse

Ce travail entend présenter plusieurs modélisations et scénarios pouvant aboutir à des scénarios critiques pour les installations de téléphériques. Les résultats principaux sont les suivants :

- Développements des équations fondamentales servant à la modélisation des câbles en partant des principes variationnels et de l'optimisation sous contraintes : Chapitre 2;
- Fabrication d'un élement fini de câble passe-partout assurant une condition de non-compression pour chaque élement du maillage et compatible avec des calculs non-lisses : Chapitre 3;
- Proposition d'une méthodologie de calcul des modes et des modèles réduits numériques pour capturer les comportements dynamiques non-linéaires d'un câble bi-appuyé, en translation ou non : Chapitres 4 et 5;
- Présentation d'un premier jet de modèle intégré d'une installation complète de téléphérique. Cette dernier comprend les effets du frottements sur pylônes et poulies, les charges ponctuelles, la vitesse d'entraînement et le câble : Chapitre 6.

Toutes les approches proposées permettent de choisir en âme et conscience la meilleure option de modélisation de la dynamique des systèmes à câbles. De plus, les outils présentés dans ce travail ne sont pas circonscrits aux seules installations à câbles mais reste assez générales pour s'appliquer aux courroies, aux câbles marins et aux réseaux de câbles.

Communication Scientifique

Ce travail a abouti à plusieurs publications dans des journaux à comité de lecture ayant pour sujet :

- L'effet du frottement sur une amplitude d'oscillation [3]
- Les modes de câble en translation [4]
- La robustesse des méthodes éléments finis appliquées aux systèmes à câbles [5]
- La généralisation des modèles réduits pour la dynamique nonlinéaire d'un câble et un comparatif de performance avec la méthode éléments finis [6]

Plusieurs conférences internationales ont permis de communiquer les résultats de thèse :

- **About the modal response of mobile cables**, Recent Advances in Nonlinear Mechanics (RANM), May 2019 Lodz, Poland
- **Equilibrium of a non-compressible cable subjected to unilateral constraints**, European Nonlinear Oscillation Conference (ENOC), 17-22 July 2022, Lyon, France
- **A robust numerical implementation of cable finite elements**, International Congress of Theoretical and Applied Mechanics (ICTAM), 23-28 August 2020+1, Milano, Italy
- **Numerical dynamics of a cable subjected to frictional impact**, Conference on the Numerical Solution of Differential and Differential-Algebraic Equations (NUMDIFF), 6-10 September 2021, Halle, Germany

Deux évènements de vulgarisation scientifique ont permis de communiquer les résultats à des publics larges :

- **Rencontres Interdisciplinaires Doctorales de l'Architecture et de l'Aménagement durable** (RIDAAD), February 2019, Vaulx-en-Velin, France
- **Café des Sciences**, October 2019, Vaulx-en-Velin, France

Organisation du document

Plan

La thèse est organisée comme suit :
Les équations du mouvements sont déduites de principes généraux de mécanique dans le Chapitre 2. Ce chapitre présente des équations générales pouvant être appliquées à de nombreuses situations. Le Chapitre 3 présente un élément fini de câble permettant de calculer la dynamique nonlinéaire d'un câble tout en assurant une condition de non-compression pour tous les éléments composant le maillage. Cet élément peut être utilisé dans le cas d'une dynamique à impact et pour le frottement. Le Chapitre 4 traite les équations de la dynamique d'un câble bi-appuyé. La théorie des vibrations linéaires est rappelée et un traitement de la

dynamique nonlinéaire par une méthode de Ritz-Galerkin est proposé. Ces méthodes sont dites analytico-numériques car elles reposent principalement sur des développements analytiques qui nécessitent une évaluation numérique à la toute fin des développements. Les Chapitres 5 et 6 sont des pplications des autres chapitres au cas des téléphériques. Les approches sur portée isolée et sur système complet sont toutes les deux présentées.

Suggestions de lecture

Le Chapitre 2 présente l'essentiel des équations utilisées dans tout le document. Les Chapitres 3 et 4 peuvent être lus séparémment et sont relativement indépendants. Ils ne peuvent pas être sautés en première lecture. Les Chapitres 5 et 6 sont des applications des autres chapitres donc doivent être lus en dernier. Les Chapitres 1, 5 et 6 peuvent être ignorés à la première lecture.

References

[1] Assemblée nationale de France et Sénat de France. Loi grenelle I de l'environnement, 2009-967, 2009.

[2] Y. Schneider and C. Clément-Werny. Transport par câble aérien en milieu urbain, June 2012.

[3] C. Bertrand, A. Ture Savadkoohi, and C.-H. Lamarque. Nonlinear oscillations of a pendulum cable with the effects of the friction and the radius of the support. *Nonlinear Dynamics*, 96:1303–1315, 2019.

[4] C. Bertrand, C. Plut, A. Ture Savadkoohi, and C.-H. Lamarque. On the modal response of mobile cables. *Engineering Structures*, 210, 2020.

[5] C. Bertrand, V. Acary, A. Ture Savadkoohi, and C.-H. Lamarque. A robust and efficient numerical finite element method for cables. *International Journal for Numerical Method in Engineering*, 121, 2020.

[6] C. Bertrand, A. Ture Savadkoohi, V. Acary, and C.-H. Lamarque. Reduced-order model for the non-linear dynamics of cables [accepted]. *Journal of Engineering Mechanics*, xxx, 2022.

Chapter 1

Literature review

This chapter starts with some few basic information about ropeways. Then some historical milestones in the cable mechanics are highlighted. Eventually, the positioning of this work is clarified and the global plan is provided.

1.1 Ropeways and French context

Ropeways refer to a circulating cable where cabins or chairs are carried from a bottom to a top station. This transportation devices were often dispatched in places with a limiting topography. Nowadays its usage is studied for urban optimization which is changing the context of the installation. This is the case in mountain areas but also when a river is crossing a city or when existing building are restraining the available space. The cable is constrained to move axially at a given velocity in the motor station which is often (not always) coinciding with the top station. The cable tension is ensured via hydraulic actuators (or counter-weight for some installations). A simplified illustration for such systems is provided in Figure 1.1. Cables are used to pull the cabins to the top or to bear the cabins. As suggested, several cables may be combined to fulfill the pulling or bearing tasks. Sometimes a single cable is used to do both tasks, i.e. carrying the cabins and pulling them to the top. The installations often cover large distances, then pylons are required to constrain the cable to a given path. The top of each pylon is composed of an assembly of rollers called a roller battery. A simplified drawing of the latter is provided in Figure 1.2. Those roller batteries constrain the cable in a unilateral way (Figures 1.3a and 1.3b) or in a bilateral way (Figure 1.3c). Sometimes cabins are equipped with a detachable grip to help people getting in/out easier. Comfort and safety reasons explain

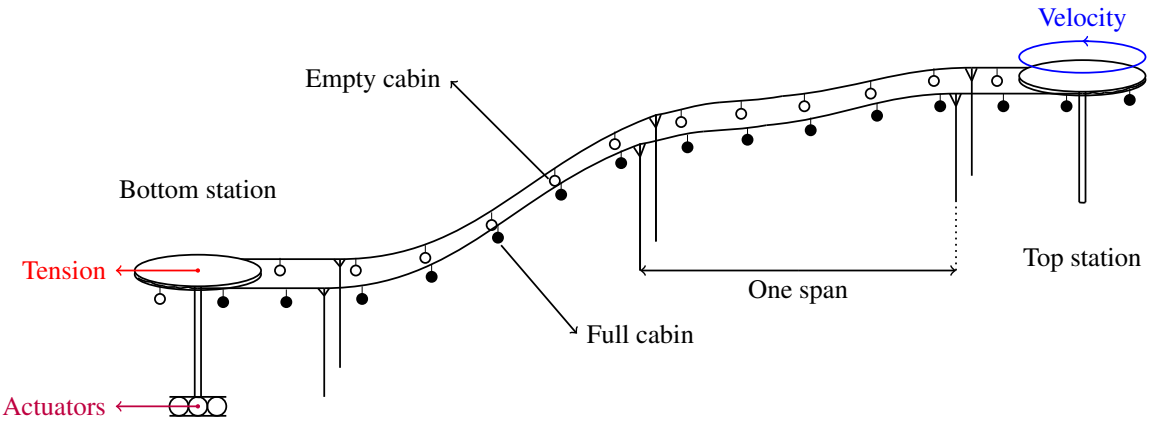

Figure 1.1: Simplified schematic of a ropeway

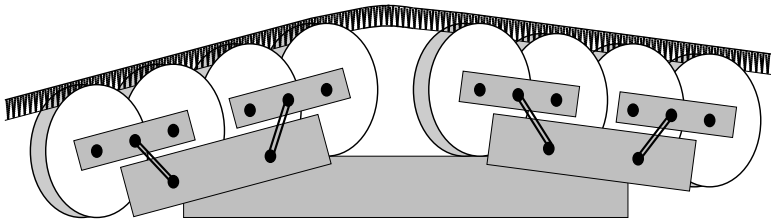

Figure 1.2: Drawing of a roller battery constraining a cable

(a) Compression roller battery - TSD4 Les pyramides / Les trois vallées

(b) Support roller battery - TSF4 Bisorne / Ax-les-Thermes

(c) Support/compression roller battery - TSD6 L'Oursière / Les sept Laux

Figure 1.3: Different kind of roller battery - Photo credit 'www.remontees-mecaniques.net'

most of improvements made on these devices. Among them is the axial speed is imposed to the cable which is provided by the French legislation depending on the type of installation as provided in Table 1.1. The ropeways are supposed to work with a constant axial velocity in the ordinary conditions. The velocity range is prescribed by law and tolerance levels can be found in [1]. Different braking situations exist. Most of the time, the cable revs up with a linear or parabolic profile. A lot of engineering data related to motor, brakes, actuators, cabins and way of operating these devices are available in [2].

1.2 Historical background of cable engineering related to ropeways

The cables in ropeways serve a precise function in a very particular context. Let us state a simple but very important fact: Their usage in this domain are far more different than in suspended bridges. Then, drawing parallel between these two disciplines must be done with special care. Indeed, cables in bridges are hopefully designed to stay in place and are not subjected to translating motion. For ropeways, cables are systematically in motion and their position is constantly varying. Moreover, a bridge cable is often designed to satisfy a given profile while a chair-lift cable is designed for a given tension [3]. In addition to that, environmental constraints

Table 1.1: In-line maximal velocities for ropeways [1]

Type of installation	Maximum authorized velocity	Maximum proposed velocity (construct
Reversible bicable aerial ropeway	12.5 m/s	12.5 m/s
Uni-directional bicable aerial ropeway	7.5-8 m/s	7 - 8 m/s
Double-monocable aerial ropeway	8 m/s	7 - 8 m/s
Monocable aerial ropeway	6 m/s	5 - 6 m/s

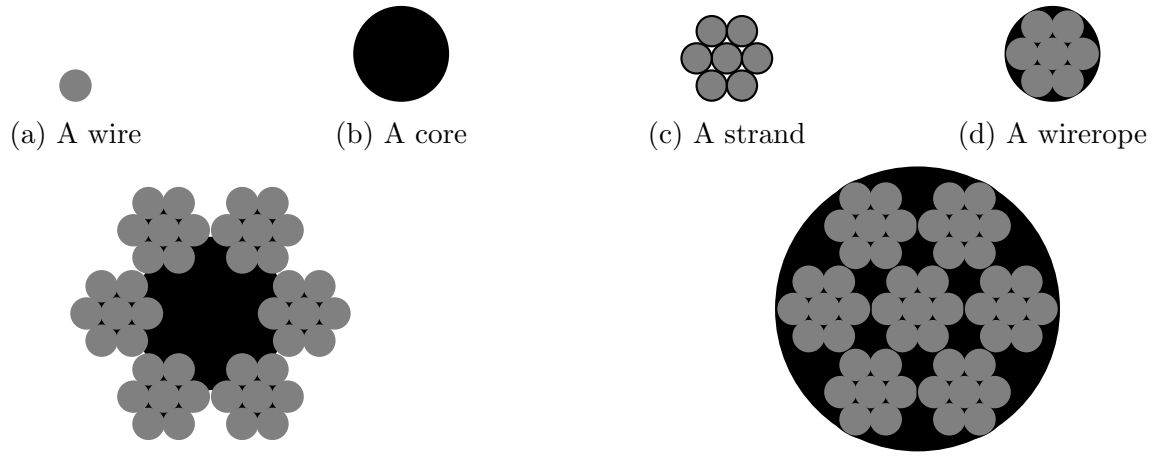

(a) A wire (b) A core (c) A strand (d) A wirerope

(e) A complex stranded rope (f) A complex stranded rope

Figure 1.4: Cable compositions and examples

are very different (wind, chemical reactions, temperature gradient) but most of them are out of the scope of this thesis.
A cable is an assembly of wires (Figure 1.4a) twisted into an helix which is called a strand (Figure 1.4c). A cable is often twisted into a circular shape. These wires are often coupled with an elastomere core (Figure 1.4b) and the process can be repeated: twisting wirerope (Figure 1.4d) into a stranded rope. Depending on the way the wires are twisted and on the core used there is a lot of possibilities for creating cables (Figures 1.4e and 1.4f).
Due to their slenderness, cables are often considered as a one-dimensional continuum. It is mostly considered that cables produce a force along their axial direction which is the only non trivial force that exists inside this continuum. This force is denoted as *tension*. Some approaches may take into account resisting moments or torques close to anchorage since they influence the local rotations. However, the simplest model for a cable is an assembly of infinitesimal segments which are freely rotating with each other. As cables are composed of elastomere and iron, the influence of temperature is often considered. Due to the combine effect of the elastomere core and the internal friction between elementary wires, the constitutive law of a cable remains a deep research subject. In this work, a linear elastic constitutive law is taken into account and the effects of temperature are discarded since our focus is drawn on the coupling between the geometrical nonlinearity and the contacting surfaces existing on rolls.
Nowadays, the design of ropeway relies on static analyses coupled to safety coefficients [3] and design guidelines[1]. When the cable is subjected to dynamic loads, quasi-static analysis is often performed in softwares [4] or simple models are considered to evaluate their maximum deflection. It has been more than eighty years that cable dynamics have a renewed interest but a lot of questions remain about the transient dynamics of complex cable structures. The latter is the most important factor for the safety and comfort of the ropeway. Moreover, those considerations will open the gate to a better understanding on the amplitude of vibrations during braking, acceleration or when cabins are crossing a roller battery.

1.3 Roadmap on cable modeling

In this section, a review about modeling the cable taking into account its correct geometry is proposed. The review is divided into the treatment of the dynamic analyses and then the

[1]Prescriptions de sécurité pour les installations à câbles destinées au transport de personnes - Calculs, NF EN 12930, Nov 2015, EU

numerical treatment of cable related problems. Until today, improvements, simplifications, clarifications, modifications and extensions never ceased.

Since the first observations about the equilibrium of a rope with non negligible self-weight dates from late XVII century with Galileo [5]. First theorems appeared in the work of Huygens who proved that the hanging rope profile was not a parabola [6]. Bernouilli and Leibniz [7, 8] characterize the profile of the catenary as we know it today via introducing logarithms operator to treat the equations of an inextensible cable. Those results were even taught in French applied mathematics classes [9] in the mid-eighteenth for the inextensible and elastic catenary. The static of cable has been very fast considered as well established including the use of approximation [10] depending on the type of situation:

- The cable exhibits large deflection (i.e. span depth ratio $> \frac{1}{8}$) or inclined supports $\rightarrow$ Catenary solution is used
- The cable exhibits small deflection (i.e. span depth ration $< \frac{1}{8}$) and aligned supports $\rightarrow$ Parabolic approximation is used

1.3.1 Cable dynamics

Linear free vibrations of cables

The first steps in the domain of the dynamics were made by Rohrs [11] who derived equations to approximate the frequencies of a inextensible cable which mass is uniformly distributed with a small sag to span length ratio. Routh [12] extended these equations later on for a heterogeneous mass distribution. However, this model was not asymptotically reproducing the results known for taut strings obtained by Kirchfoff [13]. The first engineering formulae appeared in the work of Pugsley [14] who derived approximation for the frequencies of a chain and compared them with experimental results. Mathematical solutions for the oscillation of a catenary were given for the first time by Saxon and Chan [15]. To the knowledge of the authors, the very first work which performed the asymptotic validity for the vibrating string case were the works of Soler [16] and Simpson [17] where the oscillations are investigated as a dynamic perturbation of a steady-state.
Various methods have been proposed for the evaluation of frequencies of the cable for the domain of bridges [18, 19, 20].
One of the most notable contributions is the one of Irvine and Caughey who unified all known developments and clarified the transition from the sagged elastic cable frequencies towards the vibrating string frequencies [10, 21] and validated experimentally their results. The work of Irvine [10] had so much impact that one the most remarkable parameter for the analysis of cable is now referred as Irvine's parameter and reads

$$\lambda_{\mathrm{Irv}} = \frac{\rho g d}{H}\sqrt{\frac{EA}{H\int_0^L \cos(\alpha(S))^3 \mathrm{d}S}} \tag{1.1}$$

where ρ is linear density of the cable, g is the gravity constant, d the horizontal span distance between two supports, H the horizontal constant component of the tension, EA is the cross-section rigidity of the cable, S the curvilinear abscissa and α the angle between the horizontal axis and the cable.
This parameter is often used in current literature as a fundamental cable parameter. It is often found in frequency plots in order to locate some zones where the cable modes exchange their nature. These zones have been called 'cross-overs' since the frequency curve for one mode gives the impression to cross another curve (see Figure 1.5). However their developments for

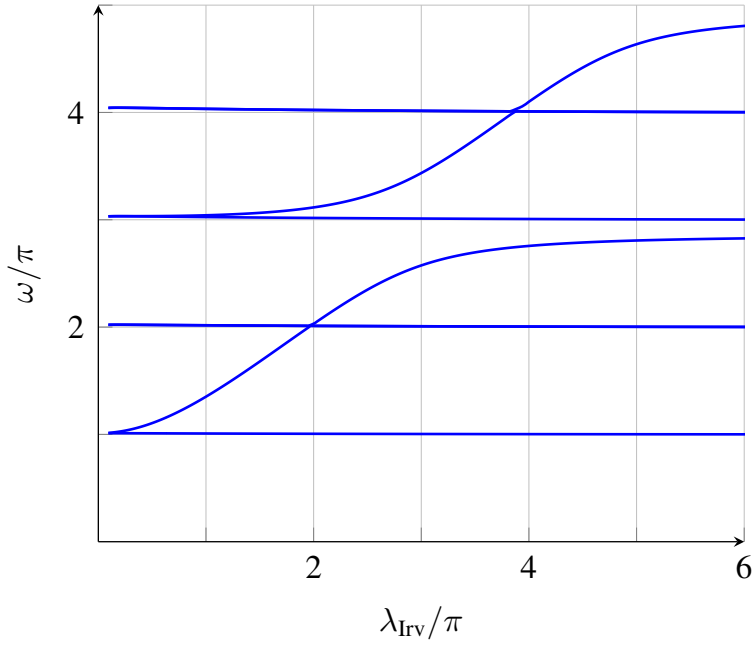

Figure 1.5: Illustration of the cross-over phenomenon

the inclined cable have been precised later on by Triantafyllou [22] who showed that taking into account the dynamic increment of the tension results into hybrid modes zones which is the biggest extension of the modal representation of cable modes. Before this, Routh [12] and Rannie and von Karman [18] respectively found that cable modes to be anti-symmetric or symmetric modes. From this point, cable modes are expected as being anti-symmetric or symmetric far from the bifurcating zones but close to bifurcation they are not symmetric and not anti-symmetric either (hybrid then). Wu *et al.* [23] proved that Irvine theory can be extended to account for those hybrid modes via considering a geometrical parameter:

$$\beta = \frac{\mu g \cos\theta \sqrt{d^2 + h^2}}{8H} \tag{1.2}$$

where h the vertical span distance between two supports and θ is the angle between the horizontal and the straight line joining the supports. All the parameters introduced in this section are presented on Figure 1.6. There are tremendous research works in this domain which we omit in this part of the review. More focus is given to newer subject as nonlinear dynamics.

Nonlinear vibrations of cables

Until the early 1980, only the linearized dynamics of cables were treated. Although the equations proposed by Irvine and Caughey [21] were nonlinear, the first work tracing a nonlinear response is from Hagedorn and Schäfer [24]. Their approach is the milestone of the nonlinear dynamics of cables as they introduced the combined use of Ritz-Galerkin and perturbation methods to treat the nonlinear terms in original system equations. This approach results in condensing the dynamics on some selected modes. Global methodology consists on using a Taylor truncated series of system variables and then decomposition of displacement along modes. The resulting equation (or its equivalent in higher dimension) has been studied for the last forty years

$$\ddot{q} + q + c_2 q^2 + c_3 q^3 = f(t) \tag{1.3}$$

A cluster of Italian researchers studied in detail the information contained in (1.3). The work of Luongo *et al.* [25] opened the discussion via a two degree of freedom model for an elastic

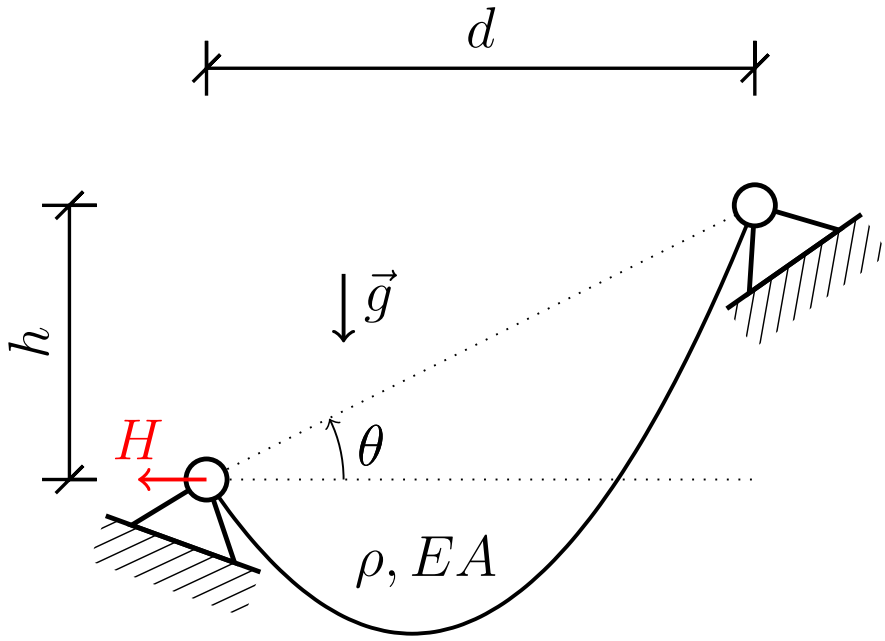

Figure 1.6: Illustration of an inclined cable with all parameters

cable with full geometrical nonlinearity. They showed how cubic and quadratic nonlinearities could alter the frequencies of the linear cable. The parameters which influence the nonlinear responses of the cable have been investigated by Rega *et al.* [26] and precised two years later by Luongo *et al.* [27]. Benedettini *et al.* [28] showed that the cable exhibits strong coupled oscillations and that the slacker the cable is, the more exchanges exists between the two first modes of the cable. The following year, Benedettini and Rega [29] highlighted a notable difference between the cable and the string: a cable exhibits softening-hardening behavior contrary to a string. Today this observation seems to find an explanation in the presence of both quadratic and cubic nonlinearities. The same duo found feature of subharmonic resonances in 1989 [30]. In 1991, Visweswara Rao and Iyengar [31] investigated the behavior of the cable when the two first modes are highly coupled to each other and they subjected the system to internal and external resonance. They arrived to the conclusion that chaotic behavior needs more investigations for the cable since Hopf bifurcation type was found. Meanwhile, the joined work of Lee and Perkins [32, 33] about the nonlinear oscillations of suspended cable near a 2:1 internal resonance was quite complete on the matter. Indeed, numerical simulations and experiments have been joined to investigate the stability of the cable system. Analytical and numerical studies were made with a two dof system composed of one symmetric mode and one out-of-plane mode. In 1995, two works have been published almost simultaneously from Benedettini *et al.* [34] who performed the bifurcation analysis of a four dof cable model (two symmetric in-plane modes and two out-of-plane modes) and of Lee and Perkins [35] for a three dof cable model where internal resonances have been deeply investigated. Lee and Perkins presented leads about the link between two modes resonance (resp. three modes resonance) and the quadratic (resp. cubic) nonlinearity.
In year 1996, Rega [36] investigated thoroughly the relevance of several cable models depending on the number and nature of dof retained in the computations. In-depth comparisons between those choices of models are given and are supplemented with experiments to testify for their possible applications. Moreover, Rega [36] gave a complete zoology of phenomenons hidden in the equations obtained from a condensed model such as chaos, periodic regime, subharmonic resonance or quasi-periodic response. Moreover, the contributions made two years later by Rega *et al.* [37, 38] showed complex internal resonance for a cable system and also some prac-

tical conditions to obtain those in experimental study.
In 2003, Srinil *et al.* [39, 40] proposed a numerical approach for the cable vibrations of arbitrary sagged inclined cable. Until this work, nonlinear vibrations were not considered for inclined arbitrarily sagged cable. However they depicted the traced phenomenons obtained on reduce order models. Later on, Rega [41] published the biggest cable oriented review with more than two hundreds references. Meanwhile, nonlinear dynamics of inclined cables continued to be investigated for example by Berlioz and Lamarque [42] who proposed a two dof model for an inclined cable and its treatment via the method of multiple scale to obtain the cable response in resonant regimes. They also exhibited examples of situation where cable systems are very sensitive to rounding errors making the experimental calibration particularly tedious. Rega *et al.* [43] also proposed a model for nonlinear vibrations of an inclined cable treated by finite differences and supplemented by experiments. Meanwhile, cable dynamics have been enriched with singularity as in the works of Sofi and Muscolino [44, 45] who proposed a model for an inclined cable carrying moving oscillators. They introduced modified series expansion to capture correctly the singularities due to point solicitations and improved it in their second work.
A lot of modeling aspects for cable have been collected, investigated and precised by Lacarbonara and Pacitti [46] who depicted a cable model with flexural stiffness and a visco-elastic constitutive law. It was also one of the very first work to emphasis on the non-compression condition inherent to cable equilibrium. Same modeling context was chosen by Arena et al [47] who studied the nonlinear vibrations of a cable derived from Cosserat theory with inclusion of the torsional stiffness. Other models have been proposed in the literature as for example the one of Pai and Nayfeh [48] where Poisson effects were considered.
Investigations about transient regimes of a cable carrying moving masses have been done by Wand and Rega [49] and they discussed about adaption of the condensed model for non-shallow cables. In 2016, Warminski *et al.* [50] revisited in details the four dof model of Benedettini [28] dating from 1995. They exhibits multiple resonances and primary resonance and improved the stability analysis done previously for this cable model.
Current considerations in nonlinear vibration of cables are for galloping phenomenon in shallow cables (e.g see the work of Ferretti [51]) or also complex structures where a cable is bonding two other structural elements for example the beam-cable-beam structure studied by Gatulli *et al.* [52].

Vibrations of translating continuum

A way of simplifying the ropeway at its simplest representation is to consider one span where there is an infinite flow of cable prescribed at a given tension and axial velocity. This scientific domain is what we could refer as *axially moving continuum*.
Its origin dates from 1897 with the early work of Skutch [53] who derived the frequencies of a string which is translating with a constant velocity between two eyelets. He was the first to investigate the response of a continuum media via the characteristics curves. Provided a suitable change of variable involving the velocity of translation, he proposed a method to derive analytical solutions. In 1954, Sack [54] proved that when a velocity of translation is considered, a change of phase in the vibration occurs then the nonlinear vibrations of a string cannot be represented with a sine function. His observations remain true for damped systems. Belt drives have been investigated via using the equations of axially moving beam between ideal supports solved via characteristics curves. Indeed Chubachi [55] also showed that the equations were relatively similar to the one of a continuous flow inside a pipe or solid-fluid interaction. In 1960, Miranker [56] developed equations from the principle of variations for a tape moving at arbitrary velocity between two ideal sheaves and investigated on the forced vibrations of a tape moving at constant velocity. In 1966, Mote [57, 58] studied the nonlinear oscillations of a string

and concluded that in presence of velocity of translation, the behavior of vibrating string cannot be interpolated to the one of the translating string. He even showed that the linear analysis is not relevant in the case of low tension combined to high velocities. Ames *et al.* [59, 60] studied the dynamics of a moving threadline in a three dimensional framework considered all string nonlinearities. They studied the response of the latter when subjected to boundary excitation and illustrated the notion of critical velocity with analytical developments validated by experimental results. Moreover, they re-developed governing equations to account for a general case. Shih [61] explored the elliptic ballooning for a three dimensional nonlinear string in 1971, which grossly means that the cable response to a planar boundary excitation is three-dimensional. He also investigated the existence of a steady-state regime for the nonlinear string subjected to axial velocity. One year later, Simpson [17] first studied the existence of modes for a translating elastic cable. He showed that for cables, the modal response consists on two waves traveling the cable upstream and downstream as Skutch [53] wrote for the linear string. His results were asymptotically valid for strings. Then Perkins and Mote [62] investigated on the vibrations of a three dimensional cable subjected to an axial velocity and extended their analysis to arbitrarily sagged cables. A lot of parallel between ropeways and belt drives can be drawn, thus the review of Abrate [63] about belts and drives gives insight about possible phenomenons in ropeway and also limit cases for the cable case. Recently, one can notice a renewed interest for derivations of system equations from general principles of continuum mechanics. It is the case with the works of O'Reilly and Varadi [64] who discussed the possible equilibria for a translating elastic cable and later with Luo and Mote [65] for an arbitrarily sagged cable. The incremental dynamics equations have been derived in three dimensions from continuum mechanics by Wang and Luo [66]. Several other domain exploit those situation where a system is translating between specific boundaries for example with lifts in the work of Gaiko and van Horssen [67].

1.3.2 Numerical methods for cable equilibrium

As it was explained, the research community of bridge cables deeply investigated on the analytical aspects of cable dynamics as they consider those approaches more relevant to extract key mechanisms and influences of parameters on the statics or dynamics. The statement of design suitability may be relevant for a bridge where vibrations around an equilibrium state are considered. However, some applications require to trace large displacements, slack cables, non-uniformity and combinations of various types of loading which general case is untraceable even in statics. Sub-marine cables, mooring lines or tethered satellites (for instance) cannot rely on incremental dynamics or intermediate configurations and require numerical approaches. The rise of Finite Element (FE) Methods (FEM) [68] in the mid-twentieth century also leads to advances in the domain of cables. Until now, researches never ceased to look for answers to overcome the geometrical nonlinearity of cable system as did Ernst [69] by introducing a correction to the Young modulus depending on the geometry. A lot of different cable elements have been developed aiming at the most versatility with Henghold and Russel [70] who proposed a FEM being able to catch cable modes already consistent with the results of Irvine [10] but are valid for arbitrary sag and any elastic deformation. Due to the cable slenderness, those models are often an assembly of segments which are able to trace finite motions for example in the work of Winget and Huston [71] for towed cables. These approaches allow to consider complex loading settings as the one of crane partially submerged and subjected to point loads. The latter have been extended also for pre-stressed cable nets in the work of Gambhir and de Batchelor [72] with applications to cable-roof structures and modal analyses. The nonlinear frequency is, according to their work, still to be investigated via FEM. The dynamics have also been studied via interpolating nodes and segments with different interpolation by Ozdemir [73].

The linearization of the stiffness matrix is used to build iterations and get the three-dimensional equilibrium configuration. Here, the statement of Irvine [10] is not confirmed in the review of Choo and Casarella [74]. Indeed FEM are considered as the best solutions in terms of versatility and in the framework of large displacement. However a kind of hybrid method appeared in 1979 with the work of Peyrot and Goulois [75] who first proposed a catenary based element which relies on the static equations of cable (elastic catenary equation). The main idea is to use the static solution of one cable to build a cable assembly. The following year, investigations on the energy functional linked to the formulation of two-nodes elements were made by Monforton and El-Hakim [76]. Cable truss elements were able to perform analysis for networks with a lot of joints and their low interpolation order allows to perfectly account for stress discontinuity. It is often pointed out that those approaches need a lot of elements to converge [77] but it is the case for any FE approach and for any system. Early approaches in dynamics of extensible cables suffered from this so-called limitation since computers capacities were not able to perform fast and heavy computations despite their applicability. See for example the work of Fried [78] who derived quadratic elements for the dynamics of cable. At that time, less than twenty elements were used which created fictitious compression out of Gauss points. However the physics of the problem were well reconstituted and experiments were there to supplement the numerical data. It appears that numerical approaches were intensively developed in the domain of mooring lines and as soon as the solicitation becomes sophisticated, for instance Tuah and Leonard [79] who subjected a cable to nonlinear load as drag, lift and inertial forces of the report about towed cable dynamics of Kamman and Nguyen [80].
Very few advances in FEM applied to cables were carried out by the beginning of current century. Investigation of absolute nodal coordinate formulation non-incremental procedures were carried out by Sugiyama *et al.* [81]. The latter allows to compute nonlinear FE analysis without using a local frame and comparisons with the results obtained by analytical tools are reproduced with FE without simplifying assumptions. Among other developments, catenary based approaches were still under investigation (e.g. [82]) until improvements able to trace responses to dynamics loading (e.g. earthquake) have been pursued by Thai and Kim in [83]. These approaches are very interesting to include cable as a super-element in a complex structure FE analysis. However, they rely on the analytic solution of the hanging catenary which is challenging for complex FE analysis when it comes to couple them to other kind of elements. Some interesting information lies on the work done by Tur et al [84]. Indeed cable networks FE analysis coupled to equality constraint seems to have a better convergence properties than complex assembly procedure. They were also able to connect cable elements to nonlinear bar elements which is quite encouraging for studying the cables systems via FE applied to cable. Moreover it appears that mixed formulation couple to a generalized α-method can definitely arrange numerical robustness of cable analysis as shown by Crussels-Girona et al [85]. Despite all these advances it appears that there is a lack of knowledge and practice on cable finite element applied to frictional cases even though theoretical results exists in the infinitesimal displacement domain [86].

References

[1] Y. Schneider and C. Clément-Werny. Transport par câble aérien en milieu urbain, June 2012.

[2] L. Berne. Les remontées mécaniques, 2003.

[3] S. Lehanneur. Conférence sur les téléphériques à voyageurs, 1962.

[4] J.P. Cassou. GHTyro 2.00 [software], 2008.

[5] Galileo. Discorsi e dimostrazioni matematiche intorno a due nuove scienze. *Edizione nazionale sotto gli auspicii di sua maesta il re d'Italia*, 7:186, 1638.

[6] C. Huygens. Correspondance no 21, letter to mersenne, proposition 8. *Dutch academy of sciences*, page 36, 1646.

[7] G.W. Leibniz. The string whose curve is described by bending under its own weight, and the remarkable resources that can be discovered from it by however many proportional means and logarithms. *Acta Eruditorum*, June 1691.

[8] G.W. Leibniz. Solutions to the problem of the catenary, or funicular curve, proposed by M. Jacques Bernoulli. *Acta Eruditorum*, September 1691.

[9] E. Bobillier and M. Finck. Questions résolues. *Annales de mathématiques pures et appliquées, Tome 17*, pages 59–68, 1826.

[10] H.M. Irvine. *Cable structures*. Dover, New York, 1981.

[11] J.H. Rohrs. On the oscillations o a suspension cable. *Transactions of the Cambridge Philosophical society*, 9:379–389, 1851.

[12] E.J. Routh. *Advanced Rigid Dynamics*. Mac Millan, New-York, 1868.

[13] *Vorlesungen über Mathematische Physik: Mechanik*. Druck une Verlag von B.G., Leipzig, 1876.

[14] A.G. Pugsley. On the natural frequencies of suspension chains. *The Quarterly Journal of Mechanics and Applied Mathematics*, 2:412–418, 1949.

[15] D.S. Saxon and A.S. Cahn. Modes of vibration of a suspended chain. *The Quarterly Journal of Mechanics and Applied Mathematics*, 6:273–285, 1953.

[16] J.F. Soler. Dynamic response of single cables with initial sag. *Journal of the Franklin Institute*, 290:377–387, 1970.

[17] A. Simpson. On the oscillatory motions of translating elestic cables. *20 of Sound and Vibration*, 290:177–189, 1972.

[18] W.D. Rannie and T. von Karman. The failure of the Tacoma narrows bridge. *Federal works agency applications*, VI, 1941.

[19] K. Kloppel and K.H. Lie. Die lotrechten Eingenschwingungen des Hangebrucken. *Bauingenieur*, 23:277, 1942.

[20] W.J. Goodey. On the natural modes and frequencies of a suspended chain. *Quarterly Journal of Mechanics and Applied Mathematics*, 14:118–127, 1961.

[21] H.M. Irvine and T.K. Caughey. The linear theory of free vibrations of a suspended cable. *Proceedings of the Royal Society*, 341:299–315, 1974.

[22] M.S. Triantafyllou. The dynamics of taut inclined cables. *The Quarterly Journal of Mechanics and Applied Mathematics*, 37(3):421–440, 1984.

[23] Q. Wu, K. Takahashi, and S. Nakamura. Formulae for frequencies and modes of in-plane vibrations of small-sag inclined cables. *Journal of Sound and Vibrations*, 279:1155–1169, 2005.

[24] P. Hagedorn and Schäfer. On non-linear free vibrations of an elastic cable. *International journal of non-linear mechanics*, 15:333–340, 1980.

[25] A. Luongo, G. Rega, and F. Vestroni. Monofrequent oscillations of a non-linear model of a suspended cable. *Journal of sound and vibrations*, 82:247–259, 1982.

[26] G. Rega, F. Vestroni, and F. Benedettini. Parametric analysis of large amplitude free vibrations of a sus pended cable. *International Journal of Solids and Structures*, 20:95–105, 1984.

[27] A. Luongo, G. Rega, and F. Vestroni. Planar non-linear free vibrations of an elastic cable. *International journal of non-linear mechanics*, 19:39–52, 1984.

[28] F. Benedettini, G. Rega, and F. Vestroni. Modal coupling in the free nonplanar finite motion of an elastic cable. *Meccanica*, 21:38–46, 1986.

[29] F. Benedettini and G Rega. Non-linear dynamics of an elastic cable under planar excitation. *International Journal of Non-linear Mechanics*, 22:497–509, 1987.

[30] G Rega and F. Benedettini. Planar non-linear oscillations of elastic cables under subharmonic resonance conditions. *Journal of Sound and Vibrations*, 132:367–381, 1989.

[31] G. Visweswara Rao and R.N. Iyengar. Internal resonance and non-linear response of a cable under periodic excitation. *Journal of Sound and Vibrations*, 149:25–41, 1991.

[32] C.L. Lee and N.C. Perkins. Nonlinear oscillations of suspended cables containing a two-to-one internal resonance. *Nonlinear dynamics*, 3:465–490, 1992.

[33] N.C. Perkins. Modal interactions in the non-linear response of elastic cables under parametric/external excitation. *International journal of Non-linear mechanics*, 27:233–250, 1992.

[34] F. Benedettini, G Rega, and R. Alaggio. Non-linear oscillations of a four-degree-of-freedom model of a suspended cable under multiple internal resonance conditions. *Journal of Sound and Vibrations*, 182:775–798, 1995.

[35] C.L. Lee and N.C. Perkins. Three-dimensional oscillations of suspended cables involving simultaneous internal resonance. *Nonlinear dynamics*, 8:45–63, 1995.

[36] G. Rega. Non-linearity, bifurcation and chaos in the finite dynamics of different cable models. *Chaos, Solitons and Fractals*, 7:1507–1536, 1996.

[37] G Rega, R. Alaggio, and F. Benedettini. Experimental investigation of the nonlinear response of a hanging cable. part I: Local analysis. *Nonlinear dynamics*, 14:89–117, 1997.

[38] F. Benedettini and G Rega. Experimental investigation of the nonlinear response of a hanging cable. part II: Global analysis. *Nonlinear dynamics*, 14:119–138, 1997.

[39] N. Srinil, G. Rega, and S. Chucheepsakul. Three-dimensional non-linear coupling and dynamic tension in the large-amplitude free vibrations of arbitrarily sagged cables. *Journal of Sound and Vibration*, 269:823–852, 2004.

[40] N. Srinil, G. Rega, and S. Chucheepsakul. Large amplitude three-dimensional free vibrations of inclined sagged elastic cables. *Nonlinear dynamics*, 33:129–154, 2003.

[41] G. Rega. Nonlinear vibrations of suspended cables—part I: Modeling and analysis. *Applied Mechanics Reviews*, 57:443–475, 2004.

[42] A. Berlioz and C.-H. Lamarque. A non-linear model for the dynamics of an inclined cable. *Journal of Sound and Vibration*, 279:619–639, 2005.

[43] G. Rega, N. Srinil, and R.. Alaggio. Experimental and numerical studies of inclined cables: free and parametrically-forced vibrations. *Journal of theoretical and applied mechanics*, 46:621–640, 2008.

[44] A. Sofi and G. Muscolino. Dynamic analysis of suspended cables carrying moving oscillators. *International Journal of Solids and Structues*, 44:6725–6743, 2007.

[45] A. Sofi. Nonlinear in-plane vibrations of inclined cables carrying moving oscillators. *Journal of Sound and Vibrations*, 332:1712–1724, 2013.

[46] W. Lacarbonara and A. Pacitti. Nonlinear modeling of cables with flexural stiffness. *Mathematical problem in Engineering*, 2008, 2008.

[47] A. Arena, A. Pacitti, and W. Lacarbonara. Nonlinear response of elastic cables with flexural-torsional stiffness. *International Journal of Solids and Structures*, 87:267–277, 2016.

[48] P.F. Pai and A.H. Nayfeh. Fully nonlinear model of cables. *AIAA Journal, Technical notes*, 30, 2012.

[49] Wang. L. and G. Rega. Modelling and transient planar dynamics of susênded cables with moving mass. *International Journal of Solids and Structures*, 47:2733–2744, 2010.

[50] J. Warminski, D. Zulli, G. Rega, and J. Latalski. Revisited modelling and multimodal nonlinear oscillations of a sagged cable under support motion. *Meccanica*, 51:2541–2575, 2016.

[51] M. Ferretti, D. Zulli, and A. Luongo. A continuum approach to the nonlinear in-plane galloping of shallow flexible cables. *Advances in Mathematical Physics*, 2019, 2019.

[52] V. Gatulli, M. Lepidi, F Potenza, and U. di Sabatino. Modal interactions in the nonlinear dynamics of a beam–cable–beam. *Nonlinear dynamics*, 96:2547–2566, 2019.

[53] R. Skutch. *Annalen der Physik und Chemie*, 61, 1897.

[54] R.A. Sack. Transverse oscillations in traveling strings. *British Journal of applied Physic*, 5, 1954.

[55] T. Chubachi. Lateral vibration of axially moving wire or belt form materials. *Bulletin of JSME*, 1, 1958.

[56] W.L. Miranker. The wave equation in a medium in motion. *IBM Journal*, 1960.

[57] C.D.Jr. Mote. On the nonlinear oscillation of an axially moving string. *Journal of Applied Mechanics*, 33:463–464, 1966.

[58] A.L. Thurman and C.D.Jr. Mote. Free, periodic, nonlinear oscillation of an axially moving strip. *Journal of Applied Mechanics*, 36:83–91, 1966.

[59] W.F. Ames, S.Y. Lee, and J.N. Zaiser. Non-linear vibration of a traveling threadline I. *International Journal of Non-linear Mechanics*, 3:449–469, 1968.

[60] W.F. Ames, S.Y. Lee, and A.A.Jr. Vicario. Non-linear vibration of a traveling threadline II. *International Journal of Non-linear Mechanics*, 5:413–426, 1970.

[61] L.Y. Shih. Three-dimensional non-linear vibration of a traveling string. *International Journal of Non-linear Mechanics*, 6:427–434, 1971.

[62] N.C. Perkins and C.D.Jr. Mote. Three-dimensional vibration of travelling elastic cables. *Journal of Sound and Vibrations*, 114, 1987.

[63] S. Abate. Vibrations of belts and belt drives. *Mechanics and Machine Theory*, 27:645–659, 1992.

[64] O.M. O'Reilly and P. Varadi. Elastic equilibria of translating cables. *Acta mechanica*, 108:189–206, 1995.

[65] A.C.J. Luo and C.D.Jr. Mote. Equilibrium solutions and existence for traveling, arbitrarily sagged elastic cables. *Transactions of the ASME*, 67:148–154, 2000.

[66] Y. Wang and A.C.J. Luo. Dynamics of traveling, inextensible cables. *COmmunications in Nonlinear Science and Numerical Simulation*, 9:531–542, 2004.

[67] N.V. Gaiko and W.T. van Horssen. On transversal oscillations of a vertically translating string with small time-harmonic length variations. *Journal of Sound and Vibrations*, 383:339–348, 2016.

[68] O. C. Zienkiewicz and R. L. Taylor. *The finite element method. Vol. 1: The basis*. Butterworth-Heinemann, Oxford, 5. ed., reprinted edition, 2002. OCLC: 249013082.

[69] H. J. Ernst. Der e-modul von seilen unter berücksichtigung des durchhanges. *Der Bauingenieur*, 40(2):52–55, 1965.

[70] W.M. Henghold and J.J. Russell. Equilibrium and natural frequencies of cable structures (a nonlinear finite element approach). *Computers & Structures*, 6:267–271, 1976.

[71] J.M. Winget and R.L. Huston. Cable dynamics - a finite segment approach. *Computers & Structures*, 6:475–480, 1976.

[72] M.L. Gambhir and Barrington de V. Batchelor. A finite element for 3d prestressed cablenets. *International journal for numerical methods in engineering*, 11:1699–1718, 1977.

[73] H. Ozdemir. A finite element approah for cable problems. *International journal os solids and structures*, 15:427–437, 1979.

[74] Y. Choo and M.J. Casarella. A survey of analytical methods fo dynamic simulation of cable-body systems. *Journal of Hydronautics*, 7:137–144, 1973.

[75] A.H. Peyrot and A.M. Goulois. Analysis of cable structures. *Computers & Structures*, 10:805–813, 1979.

[76] G.R. Monforton and N.M. El-Hakim. Analysis of truss-cable structures. *Computers & Structures*, 11:327–335, 1980.

[77] G. Tibert. Numerical analysis of cable roof structures [master thesis]. 1999.

[78] I. Fried. Large deformation static and dynamic finite element analysis of extensible cables. *Computers & Structures*, 15:315–319, 1982.

[79] H. tuah and J.W. Leonard. Strumming of nonlinear cable elements using modal superposition. *Engineering structures*, 14:282–290, 1989.

[80] J.W. Kamman and T.C. Nguyen. Modeling towed cable system dynamics. *Naval Coastal Systems Center*, 1990.

[81] H. Sugiyama, A.M. Mikkola, and A.A. Shabana. A non-incremental nonlinear finite element solution for cable problems. *American Society of Mechanical Engineering*, 125:746–756, 2003.

[82] Y.B. Yang and J.-Y. Tsay. Geometric nonlinear analysis of cable structures with a two-node cable element by generalized displacement control method. *International Journal of Structural Stability and Dynamics*, 7:571–588, 2007.

[83] H.-T. Thai and S.-E. Kim. Nonlinear static and dynamic analysis of cable structures. *Finite element in analysis and desig*, 57:237–246, 2011.

[84] M. Tur, E. Garcia, L. Baeza, and F.J. Fuenmayor. A 3d absolute nodal coordinate finite element model to compute the initial configuration of a railway catenary. *Engineering structures*, 71:234–243, 2014.

[85] M. Crussels-Girona, F.C. Filippou, and R.L. Taylor. A mixed formulation for nonlinear analysis of cable structures. *Computers & Structures*, 186:50–61, 2017.

[86] José Eduardo Souza de Cursi. Un problème issu de l'étude numérique d'un fil sans raideur soumis au frottement sec. *Annales de la Faculté des sciences de Toulouse : Mathématiques*, 5e série, 11(2):137–186, 1990.

Chapter 2

Cable mechanics

This chapter is presenting cable equations. A brief history of developments of such equations is provided. Although the subject is old, deep understanding of cable mechanics remains hard to grasp. Here we momentously step aside the ropeway applications to focus on a very specific structural element: the cable.
This chapter spans the following subjects:

- The cable statics main characteristics are highlighted from the 2D case for simplicity;
- Lagrangian mechanics are derived to introduce the 3D-dynamics of the cable;
- Analytical developments are performed for the case the statics and modal analysis of cables;

2.1 Description of a cable

A cable is a a very slender structure, meaning that it resembles a very long cylinder which cross-section dimensions are very small compare to its axial dimension. Our world is filled with those structural elements as suggested by Figure 2.1. In another words, cables can be assimilated to a curve. This simplification which shrinks spatial dependencies to a single spatial variable does not suffice to make everything clear and simple so that further vocabulary and geometrical description is needed.

2.1.1 Geometry of the cable

We consider the three-dimensionnal Cartesian space, $\mathbb{R}^3$, given by the Euclidean basis $(\mathcal{O}, \mathbf{x}, \mathbf{y}, \mathbf{z})$ where $\mathbf{x}$, $\mathbf{y}$ and $\mathbf{z}$ respectively stands for the horizontal, vertical and transversal unit vectors. The geometry of the cable is given by an application $S \longrightarrow \mathbf{q}(S)$ where $\mathbf{q} \in \mathbb{R}^3$ represents the cartesian coordinates of the position of the sections and S is an arc-length coordinate called the Lagrangian curvilinear abscissa of the cable. This coordinate should be understood as a

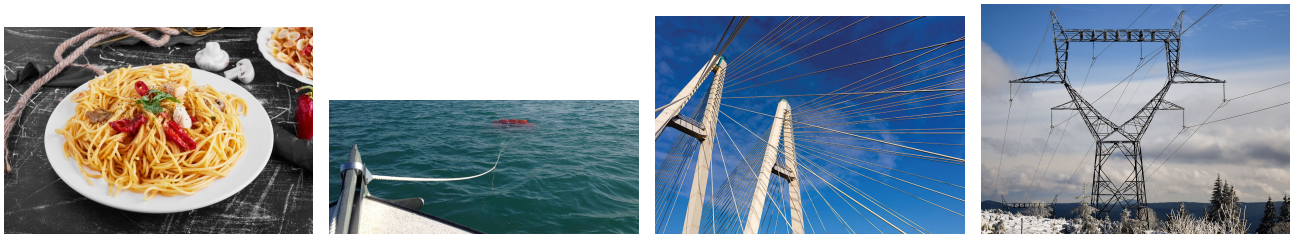

Figure 2.1: Various examples of cables (Engineering or not)

marker which skims from one tip of the cable the other. For practical and sensible reasons, this coordinate spans from 0 to L where L corresponds to the length of the cable when it is free of any action. This length is also referred as Lagrangian length, reference length, natural length or unstretched length.
The continuity condition of the system is assumed, i.e. we will assume that the cable is not broken neither splitted into pieces so that $\mathbf{q}$ is a continuous function of S, angular points may exists so that $\frac{\mathrm{d}\mathbf{q}}{\mathrm{d}S} = \mathbf{q}'$ admits a left and right limits for every S.

$$\mathbf{q} \in \mathcal{C}^1_{\text{pw}} = \left\{ \tilde{\mathbf{q}} \in (0, L) \longrightarrow \mathbb{R}^3, \text{ Piecewise differentiable } \right\} \tag{2.1}$$

From the last statements, it appears natural to describe the direction where the cable is pointing to. This direction is the main orientation of the cable and it is called the tangent vector. The latter is given by

$$\mathbf{e}(S) = \frac{\mathbf{q}'(S)}{\|\mathbf{q}'(S)\|} \ , \tag{2.2}$$

where $\|\cdot\|$ is the euclidean norm of $\mathbb{R}^3$. For an arbitrary vector $\mathbf{u}$ it reads

$$\|\mathbf{u}\| = \sqrt{\mathbf{u}_\mathbf{x}^2 + \mathbf{u}_\mathbf{y}^2 + \mathbf{u}_\mathbf{z}^2} \ . \tag{2.3}$$

It can be easily checked that $\mathbf{e}(S)$ has unit length but we also need to ensure that

$$\|\mathbf{q}'(S)\| \neq 0 \ . \tag{2.4}$$

The tangent vector is the first member of a local frame sometimes denoted as Frenet frame. Another vector providing a normal direction is necessary to obtain a complete local frame. A choice should be made at this stage, a right oriented local frame is obtained by considering $(\mathbf{e}(S), \mathbf{n}(S), \mathbf{z})$ where

$$\mathbf{n}(S) = \mathbf{z} \wedge \mathbf{e}(S) \ . \tag{2.5}$$

This choice keeps the local plane $(\mathbf{q}(S), \mathbf{e}(S), \mathbf{n}(S))$ contained into the Cartesian plane $(\mathcal{O}, \mathbf{x}, \mathbf{y})$ and will be justified later. The relationship between the local frame and the Eulerian frame is made by the tangent angle $\alpha(S)$ and the latter is connecting $(\mathbf{x}, \mathbf{y}, \mathbf{z})$ with $(\mathbf{e}, \mathbf{n}, \mathbf{z})$ as follows

$$\mathbf{e}(S) = \cos\left(\alpha(S)\right) \mathbf{x} + \sin\left(\alpha(S)\right) \mathbf{y} \ , \tag{2.6}$$
$$\mathbf{n}(S) = -\sin\left(\alpha(S)\right) \mathbf{x} + \cos\left(\alpha(S)\right) \mathbf{y} \ . \tag{2.7}$$

The spatial derivative of the angle α is called the curvature of the domain. The latter is difficult to interpret physically but it is the inverse of the best fitting circle to the domain at the abscissa S and also links the spatial derivative of $\mathbf{e}$ and $\mathbf{n}$ as follows:

$$\begin{cases} \mathbf{e}'(S) = \mathcal{K}(S)\mathbf{n}(S) \\ \mathbf{n}'(S) = -\mathcal{K}(S)\mathbf{e}(S) \end{cases} \quad \text{where} \quad \mathcal{K}(S) = \alpha'(S) \ . \tag{2.8}$$

2.1.2 Deformations of a cable

The cable is expected to move and to change of geometry when actions are applied. The description of its movements recquires to track the main characteristics of the motion. In another words, we need a proper way to measure its strain and displacements.
The idea of motion and deformations is associated to the transformation of the domain from a reference configuration to its current configuration. In this section, the quantities associated to the reference configuration will be subscripted with a 0 while the quantities associated to the

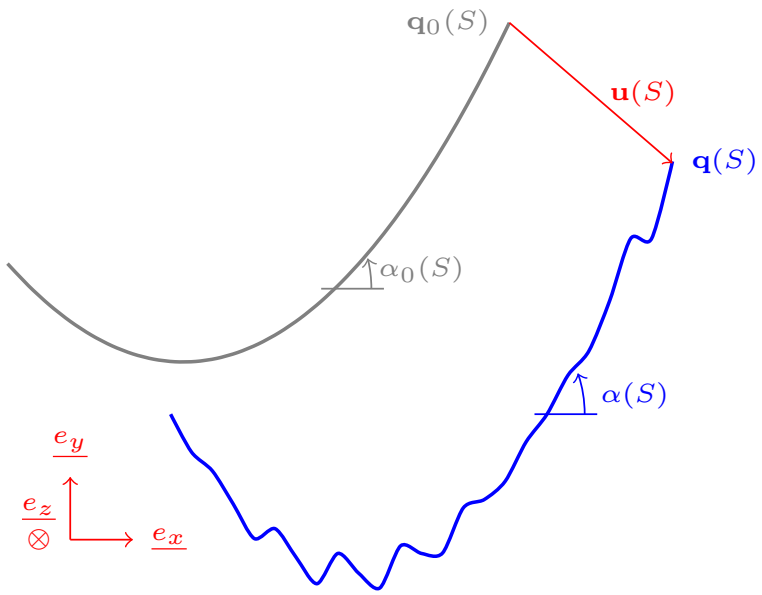

Figure 2.2: Reference and current configuration of a cable undergoing the displacement $\mathbf{u}$

current reference are kept unsubscripted.
Following the notations of Section 2.1.1, the reference configuration is fully given by:

$$\begin{cases} S \longrightarrow \mathbf{q}_0(S) \\ \mathbf{e}_0(S) = \dfrac{\mathbf{q}_0'(S)}{\|\mathbf{q}_0'(S)\|} = \cos\left(\alpha_0(S)\right)\mathbf{x} + \sin\left(\alpha_0(S)\right)\mathbf{y} \\ \mathbf{n}_0(S) = \mathbf{z} \wedge \mathbf{e}_0(S) = -\sin\left(\alpha_0(S)\right)\mathbf{x} + \cos\left(\alpha_0(S)\right)\mathbf{y} \\ \mathcal{K}_0(S) = \alpha_0'(S) \end{cases} . \tag{2.9}$$

One notable fact is that the current configuration is kept as a function of the Lagrangian curvilinear abscissa. One could have chosen the current curvilinear abscissa but the latter implies difficulties to impose boundary conditions or loads since it changes during the transformation. The current length is computed as

$$\int_0^L \|\mathbf{q}'(S)\| \, \mathrm{d}S \ . \tag{2.10}$$

Applying (2.10) to a segment of arbitrary length L^*, it appears that any segment could be shrunk to a point if the condition $\|\mathbf{q}'(S)\| > 0$ is not enforced. We will further assume that the cable is non-degenerate, i.e. $\mathbf{q}$ is such that $\|\mathbf{q}'(S)\| > 0$ for all S in $(0, L)$.
The transformation of the domain can be interpreted as the combination of a displacement $\mathbf{u}$ and a rotation ω, as depicted in Figure 2.2. The expressions of the displacement and the rotation are

$$\mathbf{u}(S) = \mathbf{q}(S) - \mathbf{q}_0(S) \ , \tag{2.11}$$
$$\omega(S) = \alpha(S) - \alpha_0(S) \ . \tag{2.12}$$

2.1.3 Rigid-body motion (strainless deformation)

A first type of transformation of notable interest are the congruent transformations of the cable. In another words, it is the case when the cable is only subjected to a rotation. Rotation are

operations that preserve the distance between two points. It is suitable, in physics at least, to restrain ourself to the rotations that also preserves the orientation of the curvilinear domain (i.e. we discard symmetries). We will denote the set of operator as **SO**. This a group called the special orthogonal group. To lighten notations, the operator of **SO** will be directly assimilated to their representation in matricial form (vectorial form or quaternion form).
Rigid body motions are obtained in the form of

$$\mathbf{q}(S) = \mathbf{d} + \mathbf{Q}\mathbf{q}_0(S) \tag{2.13}$$

where $\mathbf{d} \in \mathbb{R}^3$ is constant with S and $\mathbf{Q} \in \mathbf{SO}$ is uniform for the domain. This leads to

$$\mathbf{q}'(S) = \mathbf{Q}\mathbf{q}_0'(S) \ . \tag{2.14}$$

As $\mathbf{Q} \in \mathbf{SO}$, $\mathbf{q}'(S)$ is still a unit vector and the curvilinear abscissa is left unchanged in the motion. The tangent vector is obtained via a simple rotation of the reference tangent vector:

$$\mathbf{e}(S) = \mathbf{Q}\mathbf{e}_0(S) \tag{2.15}$$

In this case, the displacement field, $\mathbf{u}(S)$, and the rotation, $\omega(S)$, are both given by

$$\mathbf{u}(S) = \mathbf{d} + (\mathbf{Q} - \mathbf{I})\,\mathbf{q}_0(S) \ , \tag{2.16}$$
$$\omega(S) = \alpha(S) - \alpha_0(S) \ . \tag{2.17}$$

It follows that

$$\|\mathbf{q}'(S)\| = 1 \ , \tag{2.18}$$
$$\omega'(S) = 0 \ . \tag{2.19}$$

The extensional strain, ε, is therefore introduced via considering how far the slope's norm is from unity while and the flexural strain, ζ, is the derivative of the rotation. The latter reads

$$\varepsilon(S) = \|\mathbf{q}'(S)\| - 1 \ , \tag{2.20}$$
$$\zeta(S) = \omega'(S) \ . \tag{2.21}$$

However, the cable behavior is dominated by its axial forces and therefore no moment can be applied to it. It follows that it does not have any flexural stiffness and does not resist to torques. When it comes to beams, ζ has an important role to play and the three-dimensionnal (3D) representation of rotations is of major importance. This fact is highligthed by all the contributions in the domain of geometrically exact beams [6]. But for the cable, the 2D case directly extend to the 3D case since the balance of momentum induces that only the axial forces govern the equilibirum. In practice, the rotation is not regarded in cable mechanics since every mechanical information is contained in one position $\mathbf{q}(S = S_0)$ and the slope of the cable $\mathbf{q}'(S)$ including the angle of rotation.

2.1.4 Why axial forces govern the cable equilibrium ?

We will first build the equilibrium of the cable from a local point of view. Let us write the equilibrium of the segment (S_1, S_2) in terms of forces and moments. For the forces, we will assume that the cable produces a force denoted as $\mathbf{f}_i$ and that the cable is subjected to external forces density $\mathbf{f}_e$. It implies that the equilibrium of a segment with $S \in (S_1, S_2)$ is given by

$$\begin{cases} \mathbf{0} = -\mathbf{f}_i(S_1) + \displaystyle\int_{S_1}^{S_2} \mathbf{f}_e(S)\mathrm{d}S + \mathbf{f}_i(S_2) \\ \mathbf{0} = -\mathbf{q}(S_1) \wedge \mathbf{f}_i(S_1) + \displaystyle\int_{S_1}^{S_2} \mathbf{q}(S) \wedge \mathbf{f}_e(S)\mathrm{d}S + \mathbf{q}(S_2) \wedge \mathbf{f}_i(S_2) \end{cases} . \tag{2.22}$$

From (2.22) we can deduce that

$$\begin{cases} \mathbf{0} = \displaystyle\int_{S_1}^{S_2} \left(\frac{\mathrm{d}\mathbf{f}_i}{\mathrm{d}S}(S) + \mathbf{f}_e(S) \right) \mathrm{d}S \\ \mathbf{0} = \displaystyle\int_{S_1}^{S_2} \left(\frac{\mathrm{d}\left(\mathbf{q} \wedge \mathbf{f}_i\right)}{\mathrm{d}S}(S) + \mathbf{q}(S) \wedge \mathbf{f}_e(S) \right) \mathrm{d}S \end{cases} . \tag{2.23}$$

The local form of the equilibrium reads

$$\begin{cases} \mathbf{0} = \mathbf{f}_i'(S) + \mathbf{f}_e(S) \\ \mathbf{0} = \left(\mathbf{q} \wedge \mathbf{f}_i\right)'(S) + \mathbf{q}(S) \wedge \mathbf{f}_e(S) = \mathbf{q}'(S) \wedge \mathbf{f}_i(S) + \mathbf{q}(S) \wedge \left[\mathbf{f}_i'(S) + \mathbf{f}_e(S)\right] \end{cases} . \tag{2.24}$$

Injecting the first equation in the second leads to

$$\mathbf{q}'(S) \wedge \mathbf{f}_i(S) = \mathbf{0} \ , \tag{2.25}$$

which means that internal forces are necessarily directed along the axial direction. The internal forces are therefore named tension and assimilated to a scalar. In another words we have

$$\mathbf{f}_i(S) = \left(T\mathbf{e}\right)(S) \ . \tag{2.26}$$

2.2 Energy principles of a cable

Cable equations are often derived intuitively via a balance between internal forces and external forces. Newton's law of motions or the equilibrium of an infinitesimal segment are indeed enough to have every information about the cable equilibrium. However, the latter requires a constitutive law which is unnecessary for the case of cable.
This section demonstrates how Lagrangian mechanics and calculus of variations (see Appendix B) lead to the same equilibrium.
First, we are deriving general Lagrangian Mechanics based upon calculus of variations. The latter is developped in the particular case of curvilinear domains. Then applications to various cable related cases are proposed.

2.2.1 Calculus of variations for curvilinear domains

Unconstrained case

In this section, $\mathbf{q} \in \mathbb{R}^3$ is a function of S and t. Its derivatives with regards to S and t are denoted as $\mathbf{q}'$ and $\dot{\mathbf{q}}$ respectively. We consider the following functional

$$\mathcal{S}(f) = \int_{t=t_0}^{t=t_1} \int_{S=0}^{S=L} \mathcal{L}(\mathbf{q}, \mathbf{q}', \dot{\mathbf{q}}, S, t) \ \mathrm{d}S\mathrm{d}t \ . \tag{2.27}$$

We are concerned with finding extremal values of $\mathcal{S}$ for the set of functions that are satisfying the following boundary conditions

$$\mathbf{q}(S = 0, t) = \mathbf{q}(0, t) \ , \ \mathbf{q}(S = L, t) = \mathbf{q}(L, t) \ , \tag{2.28}$$

$$\mathbf{q}(S, t = t_0) = \mathbf{q}(S, t_0) \ , \ \mathbf{q}(S, t = t_1) = \mathbf{q}(0, t_1) \ , \tag{2.29}$$

The idea is to apply $\mathcal{S}$ to a function $\mathbf{q} + \epsilon\mathbf{g}$ such that

$$\mathbf{g}(S = 0, t) = \mathbf{0} \ , \ \mathbf{g}(S = L, t) = \mathbf{0} \ \ \mathbf{g}(S, t = t_0) = \mathbf{0} \ , \ \mathbf{g}(S, t = t_1) = \mathbf{0} \tag{2.30}$$

The first order variation of $\mathcal{S}$ reads

$$\mathrm{d}\mathcal{S} = \mathcal{S}(\mathbf{q} + \epsilon\mathbf{g}) - \mathcal{S}(\mathbf{q}) \ . \tag{2.31}$$

At first order in ϵ the latter expands as follows

$$\mathrm{d}\mathcal{S} = \epsilon \int_{t=t_0}^{t=t_1} \int_{S=0}^{S=L} \frac{\partial \mathcal{L}}{\partial \mathbf{q}} \cdot \mathbf{g} + \frac{\partial \mathcal{L}}{\partial \mathbf{q}'} \cdot \mathbf{g}' + \frac{\partial \mathcal{L}}{\partial \dot{\mathbf{q}}} \cdot \dot{\mathbf{g}} \ \mathrm{d}S\mathrm{d}t + \mathcal{O}(\epsilon^2) \ . \tag{2.32}$$

Using integral by part with the second and third integral term yields

$$\int_{S=0}^{S=L} \frac{\partial \mathcal{L}}{\partial \mathbf{q}'} \cdot \mathbf{g}' \mathrm{d}S = \left[\frac{\partial \mathcal{L}}{\partial \mathbf{q}'} \cdot \mathbf{g}\right]_{S=0}^{S=L} - \int_{S=0}^{S=L} \frac{\mathrm{d}}{\mathrm{d}S}\left(\frac{\partial \mathcal{L}}{\partial \mathbf{q}'}\right) \cdot \mathbf{g} \mathrm{d}S \ , \tag{2.33}$$

$$\int_{t=t_0}^{t=t_1} \frac{\partial \mathcal{L}}{\partial \dot{\mathbf{q}}} \cdot \dot{\mathbf{g}} \mathrm{d}t = \left[\frac{\partial \mathcal{L}}{\partial \dot{\mathbf{q}}} \cdot \mathbf{g}\right]_{t=t_0}^{t=t_1} - \int_{t=t_0}^{t=t_1} \frac{\mathrm{d}}{\mathrm{d}t}\left(\frac{\partial \mathcal{L}}{\partial \dot{\mathbf{q}}}\right) \cdot \mathbf{g} \mathrm{d}t \ . \tag{2.34}$$

Using the conditions on $\mathbf{g}$ and factorizing by g inside the integral yields

$$\mathrm{d}\mathcal{S} = \epsilon \int_{t=t_0}^{t=t_1} \int_{S=0}^{S=L} \left[\frac{\partial \mathcal{L}}{\partial \mathbf{q}} - \frac{\mathrm{d}}{\mathrm{d}S}\left(\frac{\partial \mathcal{L}}{\partial \mathbf{q}'}\right) - \frac{\mathrm{d}}{\mathrm{d}t}\left(\frac{\partial \mathcal{L}}{\partial \dot{\mathbf{q}}}\right)\right] \cdot \mathbf{g} \ \mathrm{d}S\mathrm{d}t + \mathcal{O}(\epsilon^2) \ . \tag{2.35}$$

If f is an extreme point of $\mathcal{S}$, then $\mathrm{d}\mathcal{S}$ should vanish at first order for all $\mathbf{g}$. As a consequence, $\mathbf{q}$ should satisfy the following differential equation

$$\frac{\partial \mathcal{L}}{\partial \mathbf{q}} - \frac{\mathrm{d}}{\mathrm{d}S}\left(\frac{\partial \mathcal{L}}{\partial \mathbf{q}'}\right) - \frac{\mathrm{d}}{\mathrm{d}t}\left(\frac{\partial \mathcal{L}}{\partial \dot{\mathbf{q}}}\right) = \mathbf{0} \ . \tag{2.36}$$

The latter is a vector equation and it can be enriched with constraints which is th etopic of next section.

Constrained case

We want to extend the last result to the case where the domain is subjected to a constraint of the form

$$\mathbf{a}(\mathbf{q}, \mathbf{q}', \dot{\mathbf{q}}) = \mathbf{0} \ . \tag{2.37}$$

We consider a modified Lagrangian given by

$$\mathcal{L}^*\left(\mathbf{q}, \lambda, \mathbf{q}', \dot{\mathbf{q}}, S, t\right) = \mathcal{L}\left(\mathbf{q}, \mathbf{q}', \dot{\mathbf{q}}, S, t\right) - \mathbf{a}(\mathbf{q}, \mathbf{q}', \dot{\mathbf{q}}) \cdot \lambda(S, t) \ , \tag{2.38}$$

and we define

$$\mathcal{S}^*(f) = \int_{t=t_0}^{t=t_1} \int_{S=0}^{S=L} \mathcal{L}^*\left(\mathbf{q}, \lambda, \mathbf{q}', \dot{\mathbf{q}}, S, t\right) \ \mathrm{d}S\mathrm{d}t \ . \tag{2.39}$$

We are concerned with finding extremal values of $\mathcal{S}^*$ for the set of functions that are satisfying the following boundary conditions

$$\mathbf{q}(S = 0, t) = \mathbf{q}(0, t) \ , \ \mathbf{q}(S = L, t) = \mathbf{q}(L, t) \ , \tag{2.40}$$

$$\mathbf{q}(S, t = t_0) = \mathbf{q}(S, t_0) \ , \ \mathbf{q}(S, t = t_1) = \mathbf{q}(0, t_1) \ . \tag{2.41}$$

We derive the first order linearization of $\mathcal{S}^*$. This time, we use a 2-uplet $(\mathbf{g}, \mathbf{g}_\lambda)$ such that both satisfy homogeneous boundary conditions. The variation of $\mathcal{S}^*$ is given by

$$\mathrm{d}\mathcal{S}^* = \mathrm{d}\mathcal{S} - \mathrm{d}\left(\int_{t=t_0}^{t=t_1} \int_{S=0}^{S=L} \mathbf{a}(\mathbf{q}, \mathbf{q}', \dot{\mathbf{q}}) \cdot \lambda(S, t) \ \mathrm{d}S\mathrm{d}t\right) \ , \tag{2.42}$$

and reads at first-order in ϵ

$$\begin{aligned}\mathrm{d}\mathcal{S}^* =&\epsilon \int_{t=t_0}^{t=t_1}\int_{S=0}^{S=L} \frac{\partial \mathcal{L}}{\partial \mathbf{q}}\cdot\mathbf{g}+\frac{\partial \mathcal{L}}{\partial \mathbf{q}'}\cdot\mathbf{g}'+\frac{\partial \mathcal{L}}{\partial \dot{\mathbf{q}}}\cdot\dot{\mathbf{g}}\ \mathrm{d}S\mathrm{d}t\\ &-\epsilon \int_{t=t_0}^{t=t_1}\int_{S=0}^{S=L} \frac{\partial \mathbf{a}}{\partial \mathbf{q}}\cdot\mathbf{g}+\frac{\partial \mathbf{a}}{\partial \mathbf{q}'}\cdot\mathbf{g}'+\frac{\partial \mathbf{a}}{\partial \dot{\mathbf{q}}}\cdot\dot{\mathbf{g}}+\mathbf{a}(\mathbf{q},\mathbf{q}',\dot{\mathbf{q}})\cdot\mathbf{g}_\lambda\ \mathrm{d}S\mathrm{d}t+\mathcal{O}(\epsilon^2)\ .\end{aligned} \tag{2.43}$$

Using the integral by part as in previous subsection, we have that

$$\begin{aligned}\mathrm{d}\mathcal{S}^* =&\epsilon \int_{t=t_0}^{t=t_1}\int_{S=0}^{S=L} \left[\frac{\partial \mathcal{L}}{\partial \mathbf{q}}-\frac{\mathrm{d}}{\mathrm{d}S}\left(\frac{\partial \mathcal{L}}{\partial \mathbf{q}'}\right)-\frac{\mathrm{d}}{\mathrm{d}t}\left(\frac{\partial \mathcal{L}}{\partial \dot{\mathbf{q}}}\right)\right]\cdot\mathbf{g}\ \mathrm{d}S\mathrm{d}t\\ &-\epsilon \int_{t=t_0}^{t=t_1}\int_{S=0}^{S=L} \left[\frac{\partial \mathbf{a}}{\partial \mathbf{q}}^\top\lambda-\ \frac{\mathrm{d}}{\mathrm{d}S}\left[\frac{\partial \mathbf{a}}{\partial \mathbf{q}'}^\top\lambda\right]-\frac{\mathrm{d}}{\mathrm{d}t}\left[\frac{\partial \mathbf{a}}{\partial \dot{\mathbf{q}}}^\top\lambda\right]\right]\cdot\mathbf{g}\ \mathrm{d}S\mathrm{d}t\\ &-\epsilon \int_{t=t_0}^{t=t_1}\int_{S=0}^{S=L} \mathbf{a}(\mathbf{q},\mathbf{q}',\dot{\mathbf{q}})\cdot\mathbf{g}_\lambda\ \mathrm{d}S\mathrm{d}t+\mathcal{O}(\epsilon^2)\end{aligned} \tag{2.44}$$

The function $\mathbf{g}$ and $\mathbf{g}_\lambda$ being arbitrary, we have the following coupled differential equations satisfied by $\mathbf{q}$ and λ

$$\begin{cases}\mathbf{0}=\dfrac{\partial \mathcal{L}}{\partial \mathbf{q}}-\dfrac{\mathrm{d}}{\mathrm{d}S}\left(\dfrac{\partial \mathcal{L}}{\partial \mathbf{q}'}\right)-\dfrac{\mathrm{d}}{\mathrm{d}t}\left(\dfrac{\partial \mathcal{L}}{\partial \dot{\mathbf{q}}}\right)-\dfrac{\partial \mathbf{a}}{\partial \mathbf{q}}^\top\lambda+\ \dfrac{\mathrm{d}}{\mathrm{d}S}\left[\dfrac{\partial \mathbf{a}}{\partial \mathbf{q}'}^\top\lambda\right]+\dfrac{\mathrm{d}}{\mathrm{d}t}\left[\dfrac{\partial \mathbf{a}}{\partial \dot{\mathbf{q}}}^\top\lambda\right]\\ \mathbf{0}=\mathbf{a}(\mathbf{q},\mathbf{q}',\dot{\mathbf{q}})\end{cases} \tag{2.45}$$

2.2.2 Inextensible cable

We are modeling a cable which linear density at rest is ρ. The reference length of the cable is denoted as L and the cable is assumed perfectly flexible (no resistance to moment and torques). The particle positions are represented via $\mathbf{q}$ and the velocity of the cable is denoted by $\dot{\mathbf{q}}$. The global energy of the cable is given by the sum of its kinetic energy and its potential energy:

$$\mathcal{S}(\mathbf{q})=\int_{t_0}^{t_1}\int_0^L\left(\frac{\rho}{2}\dot{\mathbf{q}}\cdot\dot{\mathbf{q}}+\mathbf{f}_e\cdot\mathbf{q}\right)\mathrm{d}S\mathrm{d}t \tag{2.46}$$

We further assume that the cable is subjected to an inextensibility constraint:

$$\mathbf{a}(\mathbf{q}')=\|\mathbf{q}'\|-1=0 \tag{2.47}$$

We can build an augmented functional as follows:

$$\mathcal{S}^*(\mathbf{q},\lambda)=\int_{t_0}^{t_1}\int_0^L\left(\frac{\rho}{2}\dot{\mathbf{q}}\cdot\dot{\mathbf{q}}+\mathbf{f}_e\cdot\mathbf{q}\right)\mathrm{d}S\mathrm{d}t-\int_{t_0}^{t_1}\int_0^L\mathbf{a}(\mathbf{q}')\lambda\mathrm{d}S\mathrm{d}t \tag{2.48}$$

Equation (2.48) is similar to the case provided in Appendix B. As a consequence, the equations of motions reads:

$$\begin{cases}\dfrac{\mathrm{d}}{\mathrm{d}t}\left(\rho\dot{\mathbf{q}}\right)=\ \dfrac{\mathrm{d}}{\mathrm{d}S}\left(\lambda\dfrac{\mathbf{q}'}{\|\mathbf{q}'\|}\right)+\mathbf{f}_e\\ 0=\ \|\mathbf{q}'\|-1\end{cases} \tag{2.49}$$

We clearly see that the tension is in fact the Lagrange multiplier associated to the inextensibility constraint. In another words, the constraint enforcement induces a reaction force directed along the tangent vector. The latter can be illustrated clearly with (2.24) where internal forces are explicitly written as

$$\mathbf{f}_i(S)=T\mathbf{e}=T\frac{\mathbf{q}'}{\|\mathbf{q}'\|}, \tag{2.50}$$

leading to

$$\begin{cases} \dfrac{\mathrm{d}}{\mathrm{d}t}\left(\rho\dot{\mathbf{q}}\right) = \dfrac{\mathrm{d}}{\mathrm{d}S}\left(T\dfrac{\mathbf{q}'}{\|\mathbf{q}'\|}\right) + \mathbf{f}_e \\ 0 = \|\mathbf{q}'\| - 1 \end{cases} . \tag{2.51}$$

Often, the constraint $\|\mathbf{q}'\| = 1$ is directly used to arrange system equations leading to the equation known as the 'catenary' equation.

2.2.3 Non-compressible cable

It is often stated that a cable cannot be compressed. It is interesting to see the implication of this assumption on the structure of the dynamical problem. The inextensibility constraint can be modified by a non-compression condition which reads

$$\mathbf{g}(\mathbf{q}') = \|\mathbf{q}'\| - 1 \geqslant 0 . \tag{2.52}$$

The same methodology can by applied to this constraint. In this case, the Signorini law [17] appears naturally, as explained in Appendix B.

$$\begin{cases} \dfrac{\mathrm{d}}{\mathrm{d}t}\left(\rho\dot{\mathbf{q}}\right) = \dfrac{\mathrm{d}}{\mathrm{d}S}\left(\lambda\dfrac{\mathbf{q}'}{\|\mathbf{q}'\|}\right) + \mathbf{f}_e \\ 0 \leqslant \|\mathbf{q}'\| - 1 \perp \lambda \geqslant 0 \end{cases} . \tag{2.53}$$

In this case it is clear that elongation is permitted whereas compression is forbidden. However the choice of rigidity is not possible and we see that the satisfaction of the Signorini law implies that tension and elongation cannot happen simultaneously. If the cable is elongated then λ vanishes and if the cable does not elongate then there is an axial force. In the case where elasticity is significant, the introduction of an elastic potential is required, however the equilibrium is reduced to the classical inextensible case with one more information: λ, the tension, is positive.

2.2.4 The elastic cable

If now the cable is assumed elastic and to obey the Hooke's law, its global energy of the cable is given by the sum of its kinetic energy and its potential energy

$$\mathcal{S}(\mathbf{q}) = \int_{t_0}^{t_1}\int_0^L \frac{\rho}{2}\dot{\mathbf{q}}\cdot\dot{\mathbf{q}} + \frac{EA}{2}\left(\|\mathbf{q}'\| - 1\right)^2 + \mathbf{f}_e\cdot\mathbf{q}\mathrm{d}S\mathrm{d}t . \tag{2.54}$$

Equation (2.54) is similar to the case provided in Appendix B. As a consequence, the equations of motions reads

$$\frac{\mathrm{d}}{\mathrm{d}t}\left(\rho\dot{\mathbf{q}}\right) = \frac{\mathrm{d}}{\mathrm{d}S}\left(EA\left(\|\mathbf{q}'\| - 1\right)\frac{\mathbf{q}'}{\|\mathbf{q}'\|}\right) + \mathbf{f}_e . \tag{2.55}$$

This derivation highlights the fact the governing equations of the elastic and the inextensible cable are way different. Even though the elastic case is stated to be asymptotically valid for the inextensible one, both systems derive from different functional. Particular attention must be paid to the elastic cable case since the latter admits intrinsically several solutions (see 2.2.5) while the inextensible cable only admits one.
We recall that in this case we have

$$T(S) = EA\varepsilon(S) = EA\left(\|\mathbf{q}'\| - 1\right) . \tag{2.56}$$

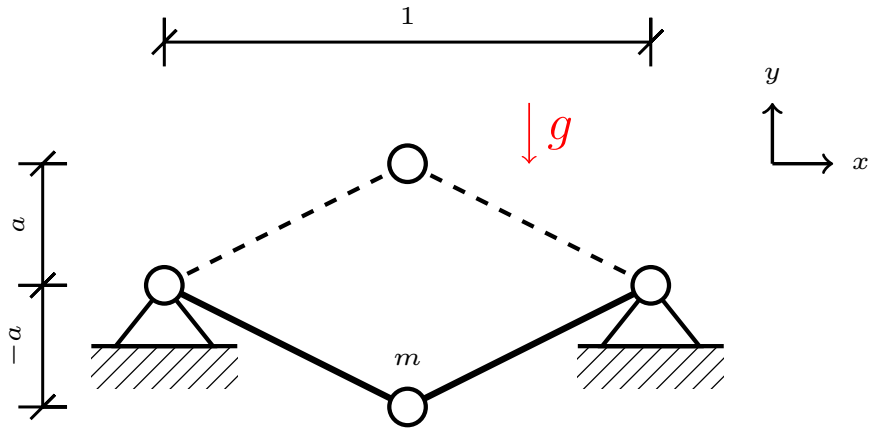

Figure 2.3: A cable at rest holding a mass

2.2.5 An example of multiple solutions for the elastic case

Considering the static case, i.e. $\dot{\mathbf{q}} = \mathbf{0}$, solving (2.55) consists of the following minimization problem:

$$\min_{\mathbf{q}\in\mathcal{C}_a} \left(\frac{1}{2}\int_0^L EA\left(\|\mathbf{q}'\|-1\right)^2 \, \mathrm{d}S + \int_0^L \mathbf{q}\cdot\mathbf{f}_e \, \mathrm{d}S \right) , \tag{2.57}$$

where $\mathcal{C}_a$ refers to the set of admissible solutions. The latter will be precised just below. Indeed, for a cable, the existence of compressive internal actions is not admitted. The latter means that the condition $\varepsilon > 0$ should be enforced in the research of an equilibrium. Therefore, the admissible solutions set is given as:

$$\mathcal{C}_a = \left\{ \mathbf{q} \in \mathcal{C}^1_{\mathrm{pw}}, \ \|\mathbf{q}'\| - 1 \geqslant 0 \right\} . \tag{2.58}$$

The latter set can be understood as the set of tension-only cable. In preparation of a FE code for cable, the conditions described in (2.58) should be included and supervised carefully. As an example, let us consider the following cable composed of two equal length linear elements. A concentrated mass has been considered at the connection points of the two segments. This case is illustrated in Figure 2.3. This example is not just a simple counter-example, it is what can actually happen in typical finite element simulations. Let x and y denote for the horizontal and vertical position of cable particles. Due to the symmetry of the presented case, we consider the following parametrization

$$x(S) = \frac{S}{L} \tag{2.59}$$

$$y(S) = \begin{cases} \dfrac{2a}{L}S & , \quad 0 \leqslant S \leqslant L/2 \\ \dfrac{2a(L-S)}{L} & , \quad L/2 \leqslant S \leqslant L \end{cases} . \tag{2.60}$$

It follows that:

$$\varepsilon = \sqrt{x'(S)^2 + y'(S)^2} - 1 = \frac{\sqrt{1+4a^2}}{L} - 1 . \tag{2.61}$$

For a given length L, one should find a that solves (2.57), i.e.

$$\min_a \left(\frac{L}{2} EA \left(\frac{\sqrt{1+4a^2}}{L} - 1 \right)^2 - mga \right) . \tag{2.62}$$

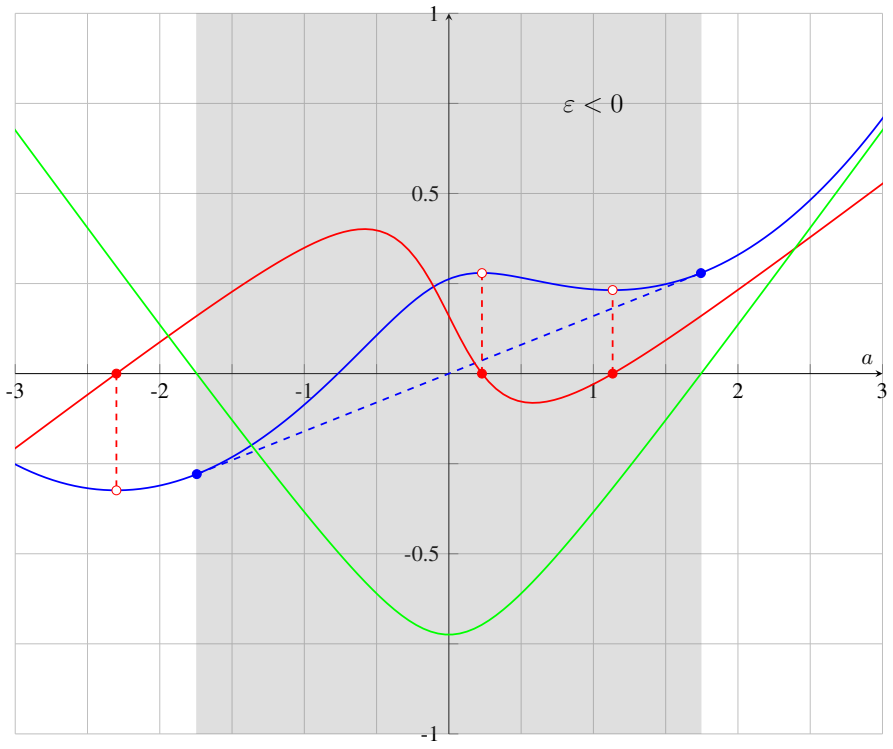

Figure 2.4: (solid line ——) $\mathcal{E}(a)$ without $\varepsilon > 0$ condition; (dashed line - - -) $\mathcal{E}(a)$ with $\varepsilon > 0$ condition; (solid line ——) $\mathcal{E}'(a)$; (solid line ——) ε

An equivalent minimization can be written as

$$\min_a \left(\frac{1}{2} \left(\frac{\sqrt{1+4a^2}}{L} - 1 \right)^2 - Ga \right) = \min_a \mathcal{E}(a) \quad , \quad G = \frac{mg}{EAL} \, . \tag{2.63}$$

The first order Karush-Kuhn-Tucker (KKT) optimality conditions [8] reads

$$0 = \frac{4a}{L^2\sqrt{1+4a^2}} \left(\sqrt{1+4a^2} - L \right) - G \, . \tag{2.64}$$

Without imposing the given non-compressibility conditions in (2.58), this equation admits one, two or three zeros. Additional features is needed to ensure the uniqueness of the solution. One way to do it is to enforce the tension state, i.e. $\varepsilon \geqslant 0$. To illustrate this claim, the plot of (2.63), its gradient and the associated strain are depicted in Figure 2.4. One can see, that two local minima exist and both are locally stable. However, only one corresponds to the global minimum. When the condition $\varepsilon > 0$ is enforced, it destroys the local stability of the non-global equilibrium. This example will be remembered as the reason why the no-compression condition should be enforced in numerical investigations. We see in the case presented here that we manage to create a convex potential which is more likely to converge toward the downward state ($a < 0$) whatever the initial condition is. Let us formalize the problem in terms of constrained optimization. The method of Lagrangian multipliers is used here via defining the following functional

$$L(a, \lambda) = \frac{1}{2} \left(\frac{\sqrt{1+4a^2}}{L} - 1 \right)^2 - Ga - \lambda \left(\frac{\sqrt{1+4a^2}}{L} - 1 \right) \, . \tag{2.65}$$

In this case Karush-Kuhn-Tucker conditions read:

$$\begin{cases} 0 = \dfrac{4a}{L^2\sqrt{1+4a^2}}\left(\sqrt{1+4a^2}-L\right) - G - \lambda\dfrac{4a}{L\sqrt{1+4a^2}} \\ 0 \leqslant \lambda \perp \left(\dfrac{\sqrt{1+4a^2}}{L} - 1\right) \geqslant 0 \end{cases} . \tag{2.66}$$

When the constraint is active, meaning that $\lambda \geqslant 0$, the functional reduces to a linear function as shown in the dashed part of the plot (Figure 2.4). When the constraint is not active, meaning that $\lambda = 0$, the elastic part of the potential is activated. In this case, the feasible directions are given by the ones pointing outward the gray zone.
An equivalent analysis can be performed via considering the following functional

$$L^*(a) = \frac{1}{2}\left[\max\left(0, \frac{\sqrt{1+4a^2}}{L} - 1\right)\right]^2 - Ga \ , \tag{2.67}$$

which directly provides with the convex envelope of the functional (2.63). The latter has been widely discussed and experimented by Souza de Cursi in [18] where the lack of numerical convergence drew the author to investigate the existence and uniqueness of the solution for cable problems.

2.2.6 The unilateral cable

As a concluding remark, we introduce a unilateral formulation of the cable. The latter requires to introduce one elastic potential plus a non-compressible constraint. It can be seen as the Lagrangian mechanics associated to the elastic cable with an inequality constraint. In other words, we consider the following Lagrangian

$$\mathcal{L}^* = \frac{\rho}{2}\dot{\mathbf{q}}\cdot\dot{\mathbf{q}} + \frac{EA}{2}\left(\|\mathbf{q}'\| - 1\right)^2 + \mathbf{f}_e\cdot\mathbf{q} - \lambda\left(\|\mathbf{q}'\| - 1\right) \ . \tag{2.68}$$

Applying the Calculus of Variations on the latter provides with

$$\begin{cases} \dfrac{\mathrm{d}}{\mathrm{d}t}\left(\rho\dot{\mathbf{q}}\right) = \dfrac{\mathrm{d}}{\mathrm{d}S}\left(\left[EA\left(\|\mathbf{q}'\| - 1\right) + \lambda\right]\dfrac{\mathbf{q}'}{\|\mathbf{q}'\|}\right) + \mathbf{f}_e \\ 0 \leqslant \|\mathbf{q}'\| - 1 \perp \lambda \geqslant 0 \end{cases} , \tag{2.69}$$

or, written in terms of strain, as

$$\begin{cases} \dfrac{\mathrm{d}}{\mathrm{d}t}\left(\rho\dot{\mathbf{q}}\right) = \dfrac{\mathrm{d}}{\mathrm{d}S}\left(\left[EA\varepsilon + \lambda\right]\dfrac{\mathbf{q}'}{\|\mathbf{q}'\|}\right) + \mathbf{f}_e \\ 0 \leqslant \varepsilon \perp \lambda \geqslant 0 \\ \varepsilon = \|\mathbf{q}'\| - 1 \end{cases} \tag{2.70}$$

The formulation given by (2.69) is similar to the no-tension formulation used in brick assemblies [1, 15] of similar to the no-compression formulation used in truss network available in [11].
As a conclusion, particular attention must be paid to the physical and mathematical modeling of cables. Without this particular care, numerical applications can lead to spurious solutions as shown in several works for cable structures [14, 19]. The numerical problems inherent to cable systems encouraged a lot of approximate analytical developments which are more suitable to enforce tension state and then derived various analysis as static analysis, modal analysis, linear stability or nonlinear dynamics.

2.3 The elastic catenary and the parabolic cable

This section briefly presents the derivations of the catenary and the parabola which have been used a lot for the design of cables. The catenary choice will be assessed via a comparison with the parabola. Using the elastic catenary rather than the inextensible one does not add any more difficulty and accounts for more generic cases.
For cable car application, the elasticity consideration is required as soon as the span gets long and that tensions are expected to vary a lot span-wise.

2.3.1 Equations for the fixed-fixed cable and its non-dimensional form

The name elastic catenary refers to the position taken by an elastic cable acting under its self-weight only and which ends are imposed. Usually, a nonlinear problem is to be solved to obtain this configuration since the tension or the length is unknown.
From last section, it has been shown that the dynamics of a cable reads:

$$\frac{\mathrm{d}}{\mathrm{d}t}\left(\rho\dot{\mathbf{q}}\right) = \frac{\mathrm{d}}{\mathrm{d}S}\left(\left[EA\left(\|\mathbf{q}'\|-1\right)\right]\frac{\mathbf{q}'}{\|\mathbf{q}'\|}\right)+\mathbf{f}_e \ . \tag{2.71}$$

For the case of interest, we further assume that the cable has a homogeneous linear density ρ and a homogeneous rigidity EA. The cable is pinned in $S=0$ and $S=L$ such that:

$$\mathbf{q}(0)=\begin{bmatrix}0\\0\end{bmatrix} \quad , \quad \mathbf{q}(L)=\begin{bmatrix}d\\h\end{bmatrix} \ . \tag{2.72}$$

The external forces read

$$\mathbf{f}_e=\begin{bmatrix}0\\-\rho g\end{bmatrix}+\mathbf{f}(t)=-\rho g\mathbf{y}++\mathbf{f}(t) \ , \tag{2.73}$$

where $\mathbf{y}$ is the unit vector in the vertical direction.
Moreover, some structural damping is added, resulting in

$$\rho\ddot{\mathbf{q}}+\alpha\dot{\mathbf{q}}=EA\left[\left(\|\mathbf{q}'\|-1\right)\mathbf{e}\right]'+\mathbf{f}_e \ . \tag{2.74}$$

The latter is made non-dimensional via the following mappings

$$\tilde{\mathbf{q}}\rightsquigarrow\frac{\mathbf{q}}{d} \quad , \quad \tilde{S}\rightsquigarrow\frac{S}{d} \quad , \quad \tilde{t}\rightsquigarrow\frac{t}{d\sqrt{\frac{\rho}{H}}} \ , \tag{2.75}$$

providing with the following dynamical equilibrium ,

$$\ddot{\tilde{\mathbf{q}}}+\tilde{\alpha}\dot{\tilde{\mathbf{q}}}=\frac{1}{\epsilon}\left[\left(\|\tilde{\mathbf{q}}'\|-1\right)\tilde{\mathbf{e}}\right]'-\delta\mathbf{y}+\tilde{f} \tag{2.76}$$

where we have set

$$\tilde{\alpha}=\frac{d}{\sqrt{\rho H}}\alpha \quad , \quad \epsilon=\frac{H}{EA} \quad , \quad \delta=\frac{\rho g d}{H} \quad , \quad \tilde{f}=\frac{d}{H}f \quad , \quad l=\frac{L}{d} \ . \tag{2.77}$$

In the sequel, the $\tilde{\cdot}$ are removed but we are working with the non-dimensional system of equations.

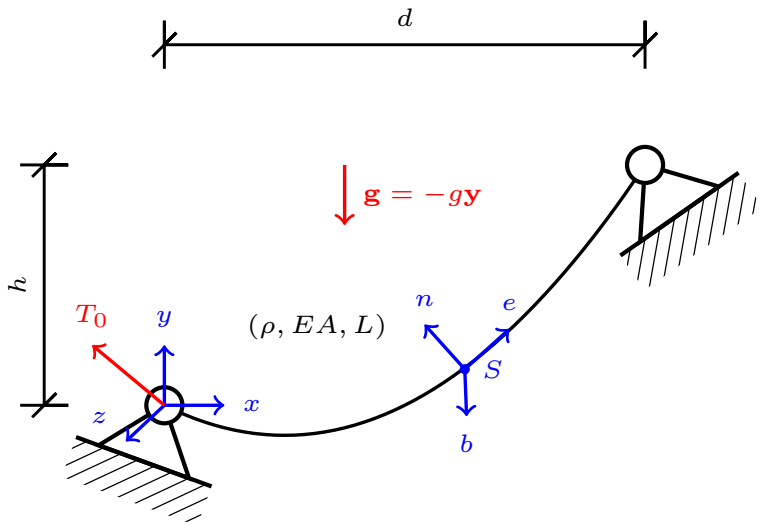

Figure 2.5: Elastic catenary position

2.3.2 The elastic catenary

Here is provided a detailed derivation of the elastic catenary equation. This can be obtained when no inertial effects are considered and when the cable is subjected to its self-weight only. In the literature and also in this work, we will coin this situation as the static situation and we denote by $\mathbf{x}$ the profile taken by the cable in this case. Equation (2.76) simplifies as

$$\mathbf{0} = \frac{1}{\epsilon}\left[\left(\|\mathbf{x}'(S)\| - 1\right)\mathbf{e}(S)\right]' - \delta\mathbf{y} \ , \tag{2.78}$$

where we have set

$$\mathbf{e}(S) = \frac{\mathbf{x}'(S)}{\|\mathbf{x}'(S)\|} \ . \tag{2.79}$$

The initial slope is given as

$$\mathbf{e}(0) = \frac{1}{\sqrt{1+\eta^2}}\begin{bmatrix}1\\ \eta\end{bmatrix} \ , \tag{2.80}$$

that corresponds to the case of an imposed tension which reads

$$T(0)\mathbf{e}(0) = T_0\mathbf{e}(0) = \begin{bmatrix}H\\ V\end{bmatrix} \tag{2.81}$$

in the physical domain.
No transverse load is applied so the equilibrium is planar. Due to the non-dimensional form of equations, the first extremity of the cable is pinned in $(0,0)$ and the second extremity in $(1, h^* = \frac{h}{d})$. This physical situation is depicted in Figure 2.5. Equation (2.78) implies that the horizontal component of the internal forces is constant. The strain field and tangent vector are obtained via integrating (2.78) between 0 and $0 \leqslant S \leqslant l$

$$\|\mathbf{x}'(S)\| - 1 = \epsilon\sqrt{1 + (\eta + \delta S)^2} \tag{2.82}$$

$$\mathbf{e}(S) = \frac{1}{\sqrt{1 + (\eta + \delta S)^2}}\begin{bmatrix}1\\ \eta + \delta S\end{bmatrix} \ , \tag{2.83}$$

where η is the ratio of the vertical component of the internal forces by its horizontal counterpart. The latter is also linked to the sine of (2.6) at $S = 0$ and l is the non-dimensional length of the

cable.
To obtain the profile of the cable, we use the following relation which can be derived by combination of (2.82) with (2.79)

$$\mathbf{x}'(S) = \|\mathbf{x}'(S)\|\,\mathbf{e}(S)\ . \tag{2.84}$$

Using (2.82)-(2.83) while integrating $\mathbf{x}'$ between $0 \leqslant S \leqslant l$ and l yields the following:

$$1 - x(S) = \epsilon\,(l - S) + \frac{\sinh^{-1}(\eta + \delta l) - \sinh^{-1}(\eta + \delta S)}{\delta}\ , \tag{2.85}$$

$$h^* - y(S) = \epsilon\eta\,(l - S) + \frac{\delta\epsilon}{2}\left(l^2 - S^2\right) + \frac{\sqrt{1 + (\eta + \delta l)^2} - \sqrt{1 + (\eta + \delta S)^2}}{\delta}\ . \tag{2.86}$$

Equations (2.85)-(2.86) provide with the non-dimensional profile of the cable. Admissibility conditions are obtained via solving the nonlinear system obtained via setting $S = 0$. The latter produces the elastic catenary equation which reads

$$\begin{bmatrix}0\\0\end{bmatrix} = \begin{bmatrix}x(0)\\y(0)\end{bmatrix} = \begin{bmatrix} 1 - \epsilon l - \dfrac{\sinh^{-1}(\eta + \delta l) - \sinh^{-1}(\eta)}{\delta} \\ h^* - \epsilon\eta l - \dfrac{\delta\epsilon}{2}l^2 - \dfrac{\sqrt{1 + (\eta + \delta l)^2} - \sqrt{1 + \eta^2}}{\delta} \end{bmatrix}\ . \tag{2.87}$$

Depending on the domain of application, variables can change. Indeed for a ropeway the couple (l, η) is unknown while for a bridge cable (δ, η) or (ϵ, η) is unknown.
The normal vector $\mathbf{n}$ and the curvature $\mathcal{K}$, are obtained via expressions given in (2.5) and (2.8), we have:

$$\mathbf{n}(S) = -\frac{1}{\sqrt{1 + (\eta + \delta S)^2}}\begin{bmatrix}\eta + \delta S\\ -1\end{bmatrix}\ , \tag{2.88}$$

$$\mathcal{K}(S) = \frac{\delta}{1 + (\eta + \delta S)^2}\ . \tag{2.89}$$

The following procedure accounts for the inextensible cable via setting $EA \to +\infty$ or $\varepsilon = 0$ which yields

$$\begin{bmatrix}0\\0\end{bmatrix} = \begin{bmatrix}x(0)\\y(0)\end{bmatrix} = \begin{bmatrix} 1 - \dfrac{\sinh^{-1}(\eta + \delta l) - \sinh^{-1}(\eta)}{\delta} \\ h^* - \dfrac{\sqrt{1 + (\eta + \delta l)^2} - \sqrt{1 + \eta^2}}{\delta} \end{bmatrix}\ . \tag{2.90}$$

A remark on numerical treatments of the elastic catenary equation

This problem can meet some numerical difficulties but for carefully chosen starting points, Newton-Raphson procedure succeeds to solve it. Problem (2.87) can also be formulated using log function instead of $\sinh^{-1}$ but this has to be considered carefully to avoid numerical errors in the process.
The problem can also be formulated via using T_0 instead of H, however the latter is trickier to tackle numerically especially with sagged cable. Alternative formulations and Jacobians used in Newton-Raphson methods are given in Appendix A.

2.3.3 The parabolic cable

A handy approximation is often made for cables which is called the parabolic cable. The latter consists on assuming that the vertical position of the cable is a parabolic function of its horizontal position. Moreover, this configuration is often accompanied with an inextensibility condition (i.e. $EA = +\infty$). Writing system equations (2.78) for an inextensible cable, following system is obtained

$$\begin{cases} \dfrac{\mathrm{d}}{\mathrm{d}S}\left[T(S)\dfrac{\mathrm{d}x}{\mathrm{d}S}\right] = 0 \\ \dfrac{\mathrm{d}}{\mathrm{d}S}\left[T(S)\dfrac{\mathrm{d}y}{\mathrm{d}S}\right] = \delta \end{cases} , \tag{2.91}$$

where the inextensibility condition directly have been substituted into equations.
The horizontal component of tension is constant according to the first equation of (2.91) and unit due to the non-dimensional form of the system equation. The second equation is therefore manipulated as follows

$$\frac{\mathrm{d}}{\mathrm{d}S}\left[T(S)\frac{\mathrm{d}y}{\mathrm{d}S}\right] = \frac{\mathrm{d}}{\mathrm{d}S}\left[\frac{\mathrm{d}S}{\mathrm{d}x}\frac{\mathrm{d}y}{\mathrm{d}S}\right] \approx \frac{\mathrm{d}^2 y}{\mathrm{d}x^2} , \tag{2.92}$$

where $\mathrm{d}S$ is assimilated with $\mathrm{d}x$.
No numerical solvers is required to access this static solution. This approximation provides the exact solution when the vertical load is proportional to $\cos\alpha$ [9]. The parabolic profile and tension are therefore obtained as

$$\begin{aligned} y(x) &= \left(h^* - \frac{\delta}{2}\right)x + \frac{\delta}{2}x^2 , \\ T(x) &= \sqrt{1 + \left(\left(h^* - \frac{\delta}{2}\right) + \delta x\right)^2} . \end{aligned} \tag{2.93}$$

The maximum deflection of the cable is therefore obtained by setting

$$x_{\min} = \frac{1}{2} - \frac{h^*}{\delta} \implies y_{\min} = -\frac{\delta}{2}\left(\frac{h^*}{\delta} - \frac{1}{2}\right)^2 , \tag{2.94}$$

while for the inextensible catenary, we have the following expression

$$y_{\min} = h^* - \frac{\sqrt{1 + (\eta + \delta l)^2} - 1}{\delta} . \tag{2.95}$$

Comparisons with the catenary can be endowed from the latter. It is interesting to account for the differences between both solutions. The main one is the sag difference which becomes significant. Several references state the limit sag-to-span ratio to be 1/8. The latter is shown on Figure 2.6. We recall that δ stands for the ratio of the self-weight of the cable by the horizontal component of internal forces. The depart from the parabolic approximation from the exact value of it obtained via catenary becomes bigger when the load increases which is critical for the case of ropeways subjected to double their self-weight when cabins or chairs are fully loaded and dispatched along the span. In this work, the catenary is used rather than the parabola. Moreover, the further need of precision for long span installations where the elasticity plays a significant role in the sag justifies this strategy.

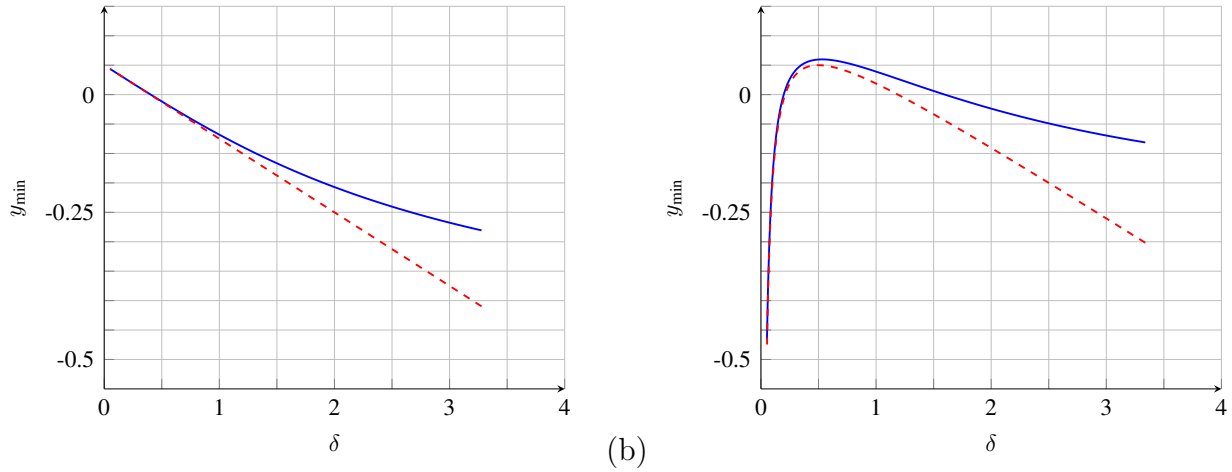

Figure 2.6: Maximum non-dimensional deflection for the inextensible catenary (solid line —) and the parabola (dashed line - - -) as a function of δ
(a) Aligned cable ; (b) Inclined cable with $h^* = 1/4$

2.4 Cables in the presence of obstacles

In the following sections space and time variables are removed for the sake of conciseness.
This section is dealing with simple properties that can be derived from the cable equations (inextensible case - (2.49)) when the domain is subjected to the presence of obstacles. The latter is embedded into an inequality constraint

$$\mathbf{g}(\mathbf{q}) \geqslant 0 \ . \tag{2.96}$$

When $\mathbf{g} = 0$ the gap is closed meaning that a reaction force is applied to the domain to ensure non-penetration.
The proposed results are given in the framework of the inextensible cable of constant linear density, i.e. for the following governing equations:

$$\begin{cases} \rho \dfrac{\mathrm{d}}{\mathrm{d}t}(\dot{\mathbf{q}}) = \dfrac{\mathrm{d}}{\mathrm{d}S}(T\mathbf{q}') + \mathbf{f}_e - \bar{\boldsymbol{\lambda}} \dfrac{\partial \mathbf{g}}{\partial \mathbf{q}} \\ 0 = \|\mathbf{q}'\| - 1 \\ 0 \leqslant \mathbf{g}(\mathbf{q}) \perp \bar{\boldsymbol{\lambda}} \geqslant 0 \end{cases} , \tag{2.97}$$

where T denotes the tension of the cable, that plays the role of the multiplier associated to the constraint $\|\mathbf{q}'\| = 1$.

2.4.1 Persistent contact

Let us assume that a segment of the domain, $S \in [S_0, S_1]$, remains in contact of the obstacle, $\mathbf{g}(\mathbf{q}) = 0, \forall S \in [S_0, S_1]$, for a time interval $[t_c, t_c^*]$ where $t_c < t_c^*$. Let us decompose the velocity $\dot{\mathbf{q}}$ as a normal and tangent velocity as follows

$$\dot{\mathbf{q}} = \mathbf{u_e}\mathbf{e} + \mathbf{u_n}\mathbf{n} \ , \tag{2.98}$$

where $\mathbf{e}$ and $\mathbf{n}$ are the directors defined in (2.2) and (2.5). Then the derivative of the velocity reads

$$\frac{\mathrm{d}\dot{\mathbf{q}}}{\mathrm{d}t} = (\dot{\mathbf{u}}_\mathbf{e} - \dot{\alpha}\mathbf{u_n})\,\mathbf{e} + (\dot{\mathbf{u}}_\mathbf{n} + \dot{\alpha}\mathbf{u_e})\,\mathbf{n} \tag{2.99}$$

As the contact is persistent, we have that

$$\forall t \in [t_c, t_c^*],\ \forall S \in [S_0, S_1], \frac{\mathrm{d}}{\mathrm{d}t}\mathbf{g}(\mathbf{q}) = \frac{\partial \mathbf{g}}{\partial \mathbf{q}}\dot{\mathbf{q}} = 0\ , \tag{2.100}$$

which means that from the cable perspective we have

$$\forall t \in [t_c, t_c^*],\ \forall S \in [S_0, S_1], \dot{\mathbf{q}} \cdot \mathbf{n} = \mathbf{u_n} = 0\ , \tag{2.101}$$

and that $\mathbf{n}$ and $\frac{\partial \mathbf{g}}{\partial \mathbf{q}}$ are aligned but not necessarily sharing the same sign.
This implies from (2.8) and (2.97) that

$$\forall t \in [t_c, t_c^*],\ \forall S \in [S_0, S_1], \begin{cases} \rho\ \dot{\mathbf{u}}_\mathbf{e} = & T' + \mathbf{f}_e \cdot \mathbf{e} \\ \rho\ \dot{\alpha}\mathbf{u}_\mathbf{e} = & \mathcal{K}T + \mathbf{f}_e \cdot \mathbf{n} - \bar{\boldsymbol{\lambda}}\dfrac{\partial \mathbf{g}}{\partial \mathbf{q}} \cdot \mathbf{n} \end{cases}\ . \tag{2.102}$$

As a preliminary result, we obtain the fact that the reaction is contained in the plane given by the directors of the cable. The latter results gives an interesting conclusion for the case of a string of negligible weight, i.e. $T' = 0$ and $\mathbf{f}_e = \mathbf{0}$, since it results into the following condition for the persistent contact

$$\forall t \in [t_c, t_c^*],\ \forall S \in [S_0, S_1], \bar{\boldsymbol{\lambda}}\frac{\partial \mathbf{g}}{\partial \mathbf{q}} \cdot \mathbf{n} = \mathcal{K}T\ , \tag{2.103}$$

which can be interpreted as the fact that the obstacle and the string should share the same convexity for the contact to persist. This result have been first shown in a weightless case to prove that contact cannot persists when the obstacle has the opposite convexity of the cable [5]. Indeed, as $\bar{\boldsymbol{\lambda}} \geqslant 0$ and $\mathcal{K}T \geqslant 0$, if $\frac{\partial \mathbf{g}}{\partial \mathbf{q}} \cdot \mathbf{n} < 0$ the equation is trivially violated making impossible for a vibrating string to remain in contact of a concave obstacle.

2.4.2 Inextensible cable contacting a sheave

The equilibrium of a cable contacting a sheave has been quite investigated in the past years. The static equilibrium of a cable contacting a sheave has been well studied [4, 7, 12, 13, 16] for applications in transportation and in electric lines. The key idea is to consider the cable-sheave assembly as a super-element connected to two other cables.
In this section, the general equations are derived and the Capstan Law is endowed to accommodate for the tension loss in the contacting zone. Several cases are considered depending on the sheave orientation. Then, the 3D equations for connecting a cable-sheave element to another cable systems are given. Every derivations are done with the inextensibility assumption. Indeed, elasticity requires additional assumptions about the contact between the cable and the sheave that are not in the scope of analytical derivations.

Equations for the cable-sheave contact with Capstan law

The sheave is viewed as a cylindrical obstacle of radius R around which the cable is wrapped. The contacting part of the cable is subjected to a left force T_1 and a right force T_2. Those tension are assumed known here but are unknown in general application. Even though the description of this equilibrium when the cable is partially in contact, we will assume that all the cable is in contact all along the cylinder frontier given by the contacting angle $\theta_1 + \theta_2$. We further assume that the cable is in a persistent contact case. The situation is depicted on Figure 2.7. Equation (2.97) can be applied to this case and after projection on the local basis

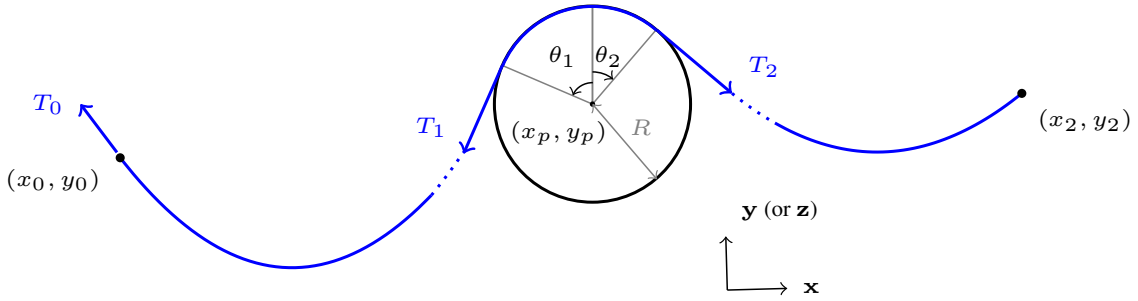

Figure 2.7: Cable segment with end forces in contact with a cylinder

we have

$$\begin{cases} \widehat{r}_T - \sin(\alpha)\rho g = T' \\ \widehat{r}_N + \cos(\alpha)\rho g = \mathcal{K}T \end{cases} \rightsquigarrow \begin{cases} r_T = T' \\ r_N = \mathcal{K}T \end{cases} , \tag{2.104}$$

where $\mathbf{r}_T$ and $\mathbf{r}_N$ respectively stand for the equivalent tangent and normal reaction applied to the cable by the cylinder. Assuming a Coulomb friction law [3] for the cable-sheave interface, we have

$$|\mathbf{r}_T| \leqslant \mu \mathbf{r}_N \tag{2.105}$$

where μ is the Coulomb coefficient.
We can obtain the following differential inequality satisfied by the tension

$$-\mu\mathcal{K}T \leqslant T' \leqslant \mu\mathcal{K}T \ . \tag{2.106}$$

As the cable is inextensible, the integration can be performed via using the change of variable $S = \frac{\theta}{\mathcal{K}}$ where $\frac{1}{\mathcal{K}} = R$ since the section of the cylinder is a circle. This yields

$$T_1 e^{-\mu(\theta_2 - \theta_1)} \leqslant T_2 \leqslant T_1 e^{+\mu(\theta_2 - \theta_1)} \ . \tag{2.107}$$

The equilibrium is achieved for T_2 satisfying (2.107), if not the cable is slipping on the sheave.

The cable-sheave super-element

With in mind the objective of building an assembly of cables and sheaves, we need to describe the sheave-cable element which is joining two cables derived via the inextensible catenary equations. The assembly is illustrated by Figure 2.7. The sheave is located in $\mathbf{q}_p$ and has radius R. The relative position of the whole cable should be inferred to avoid spurious or multiple solutions. We assume that we are in a critical equilibrium configuration given by the equality case of (2.107). Both cable segments should satisfy the catenary equations and should satisfy the joint condition

$$T_2 = T_1 e^{\mu(\theta_2 - \theta_1)} \ , \tag{2.108}$$

where μ is the coulomb friction of the sheave.
Two possible configurations are of notable interest:

- The cable is above the sheave (Support configuration)
- The cable is below the sheave (Compression configuration)

The detailed derivations are given for the support configuration. Other derivations are direct fall-out of the derived case. All configurations are given in Appendix C including 3D-equations without proof. These derivations are equivalent to the work done in previous research [2, 4, 13] with a small 3D-extension to the frictional case done in [10]. The equations consists in an

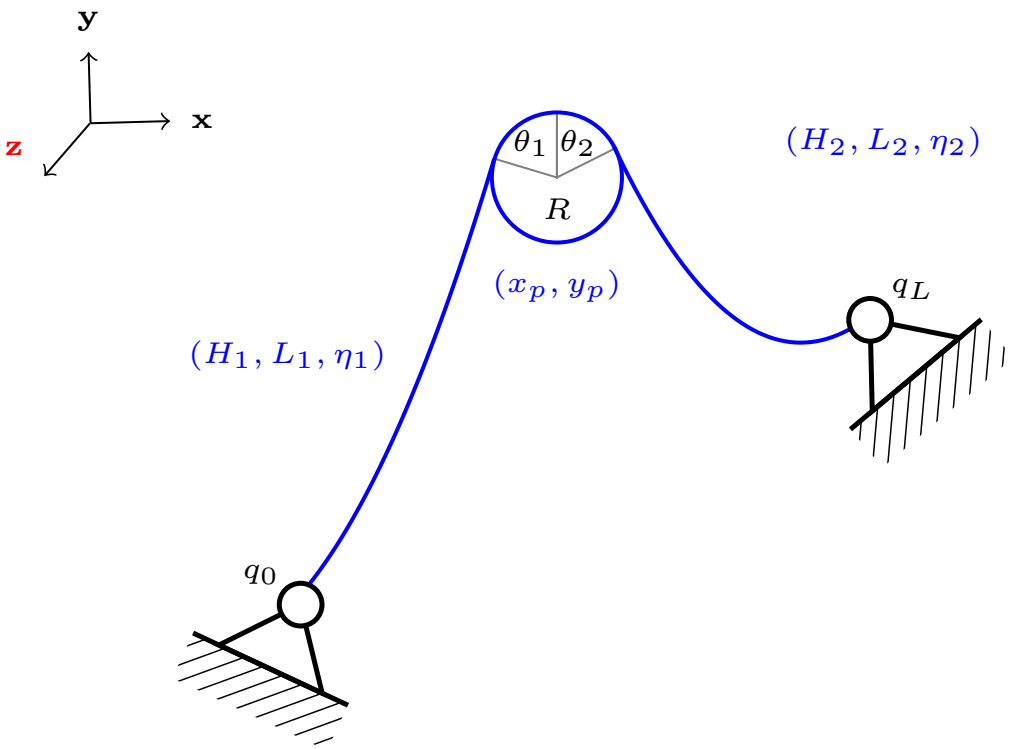

Figure 2.8: Two cables connected via a sheave

inextensible catenary for the left and right part. The sheave satisfies the profile continuity and the Capstan law for the tension. The latter reads:

$$\text{(C1):} \begin{cases} 0 = d_1 - \dfrac{H_1}{\rho g}\left(\sinh^{-1}(\eta_1 + \dfrac{\rho g}{H_1}L_1) - \sinh^{-1}(\eta_1)\right) \\ 0 = h_1 - \dfrac{H_1}{\rho g}\left(\sqrt{1+\left(\eta_1 + \dfrac{\rho g}{H_1}L_1\right)^2} - \sqrt{1+\eta_1^2}\right) \end{cases}$$

$$\text{(P):} \begin{cases} d_1 = (x_p - R\sin(\theta_1)) - x_0 \\ h_1 = (y_p + R\cos(\theta_1)) - y_0 \\ d_2 = x_2 - (x_p + R\sin(\theta_2)) \\ h_2 = y_2 - (y_p + R\cos(\theta_2)) \\ T_2 = T_1 e^{\mu(\theta_2 - \theta_1)} \end{cases} \tag{2.109}$$

$$\text{(C2):} \begin{cases} 0 = d_2 - \dfrac{H_2}{\rho g}\left(\sinh^{-1}(\eta_2 + \dfrac{\rho g}{H_2}L_2) - \sinh^{-1}(\eta_2)\right) \\ 0 = h_2 - \dfrac{H_2}{\rho g}\left(\sqrt{1+\left(\eta_2 + \dfrac{\rho g}{H_2}L_2\right)^2} - \sqrt{1+\eta_2^2}\right) \end{cases}$$

The geometric compatibility between θ_1 and η_1 and also between θ_2 and η_2 reads

$$\cos(\theta_1) = \frac{1}{\sqrt{1+\left(\eta_1 + \frac{\rho g}{H_1}L_1\right)^2}} \quad , \quad \sin(\theta_1) = \frac{\eta_1 + \frac{\rho g}{H_1}L_1}{\sqrt{1+\left(\eta_1 + \frac{\rho g}{H_1}L_1\right)^2}} \tag{2.110}$$

$$\cos(\theta_2) = \frac{1}{\sqrt{1+\eta_2^2}} \quad , \quad \sin(\theta_2) = -\frac{\eta_2}{\sqrt{1+\eta_2^2}} \tag{2.111}$$

Table 2.1: Parameters used for the comparison of the cable sheave and the catenary

ρ (kg/m)	L (m)	Ends(m)	sheave Radius (m)	sheave position
5.56	50.5	$(0,0,0)$; $(50,0,0)$	3	$(25,-3,0)$
5.56	50.5	$(0,0,0)$; $(50,0,0)$	3	$(37.5,-4,0)$
5.56	51	$(0,0,0)$; $(50,8,0)$	3	$(25,-1,0)$

Combining and reducing (2.109-2.111), provides with the following set of nonlinear equations:

$$
\begin{aligned}
&\text{(C1):} \begin{cases} 0 = x_p - \dfrac{R\left(\eta_1 + \frac{\rho g}{H_1} L_1\right)}{\sqrt{1 + \left(\eta_1 + \frac{\rho g}{H_1} L_1\right)^2}} - x_0 - \dfrac{H_1}{\rho g}\left(\sinh^{-1}(\eta_1 + \dfrac{\rho g}{H_1} L_1) - \sinh^{-1}(\eta_1)\right) \\ 0 = y_p + \dfrac{R}{\sqrt{1 + \left(\eta_1 + \frac{\rho g}{H_1} L_1\right)^2}} - y_0 - \dfrac{H_1}{\rho g}\left(\sqrt{1 + \left(\eta_1 + \dfrac{\rho g}{H_1} L_1\right)^2} - \sqrt{1+\eta_1^2}\right) \end{cases} \\
&\text{(P):} \quad \left\{ H_2\sqrt{1+\eta_2^2} = H_1\sqrt{1 + \left(\eta_1 + \frac{\rho g}{H_1} L_1\right)^2}\, e^{\mu(\tan^{-1}(-\eta_2) - \tan^{-1}(\eta_1))} \right. \\
&\text{(C2):} \begin{cases} 0 = x_2 - x_p + \dfrac{R\eta_2}{\sqrt{1+\eta_2^2}} - \dfrac{H_2}{\rho g}\left(\sinh^{-1}(\eta_2 + \dfrac{\rho g}{H_2} L_2) - \sinh^{-1}(\eta_2)\right) \\ 0 = y_2 - y_p - \dfrac{R}{\sqrt{1+\eta_2^2}} - \dfrac{H_2}{\rho g}\left(\sqrt{1 + \left(\eta_2 + \dfrac{\rho g}{H_2} L_2\right)^2} - \sqrt{1+\eta_2^2}\right) \end{cases}
\end{aligned}
\tag{2.112}
$$

The small angles assumptions is not done here which explains the presence of radicals in (2.112). Those equations constitute the simplest way of implementing the cable-sheave super-element in any code. Although we may simplify (2.112), it makes implementation more tedious. The latter considerably change the behavior of the numerical algorithms. Both tension or length can be used as an unknown for this problem. However, using the tension as an unknown seems more unstable since multiple solutions exist for this problem [7]. Some example are given on Figure 2.9 via using (2.112) with parameters in Table 2.1.

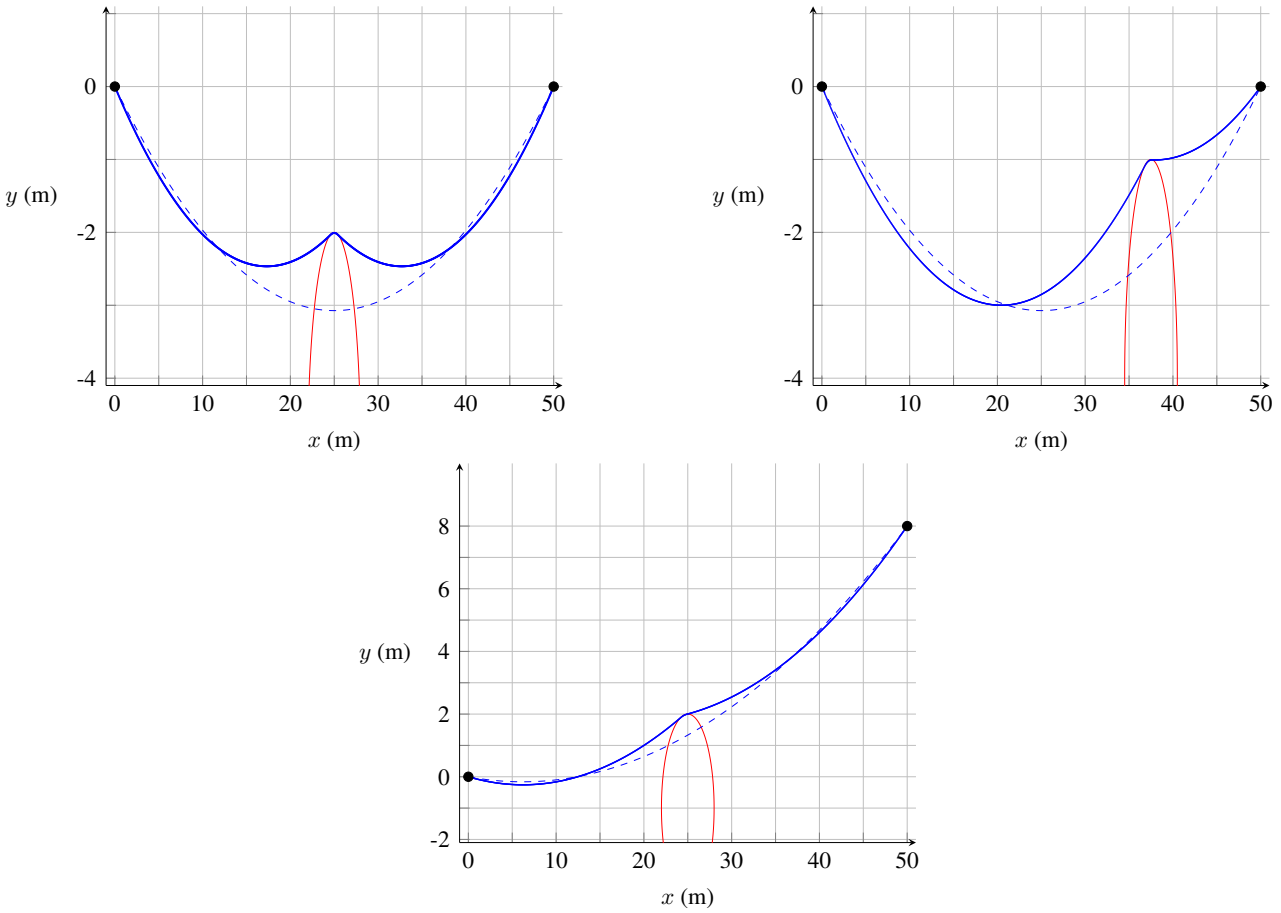

Figure 2.9: Profile obtained via using the cable-sheave solution (solid line —) versus the same cable not subjected to the obstacle (dashed line - - -)

Conclusion of the chapter

This chapter provides with the essential tools and models that can be endowed to derive the cable equations and to prepare both analytical and numerical application. Main contributions and results are

- The different model derivation via Lagrangian mechanics including unilateral models;
- A first illustration about possible multiple solutions;
- The illustration of the precision superiority of the elastic catenary compared to the parabolic cable;
- Preliminary results about the cables subjected to the presence of obstacles.

Some perspectives can already be pointed out such as:

- Develop more sophisticated models which embed visco-elastic behavior and torsion (mainly for fatigue analysis) or thermo-mechanical coupling;
- Proving mathematically the existence and the non-uniqueness of the solutions of the different cable model provided in the chapter;
- Investigate more sophisticated geometries for the obstacle;
- Develop a geometrically exact beams model suitable for comparisons with the presented models and the presence of obstacles.

References

[1] Angelillo, M. (1994). A finite element approach to the study of no-tension structures. *Finite Elements in Analysis and Design*, 17(1):57–73.

[2] Aufaurre, M. (1991). A finite elemen of cable passing through a pulley. *Computers and Structures*, 46:807–812.

[3] Bastien, J., Bernardin, F., and Lamarque, C.-H. (2003). *Non-Smooth Deterministic or Stochastic Discrete Dynamical Systems: Applications to models with Friction or Impacts.* Wiley.

[4] Bruno, D. and Leonardi, A. (1999). Nonlinear structural models in cableway transport systems. *Simulation Practice and Theory*, 7(3):207–218.

[5] Cabannes, H. (1984). Cordes vibrantes avec obstacles. *Acta Acustica united with Acustica*, pages 14–20.

[6] Cardona, A. and Geradin, M. (1988). A beam finite element non-linear theory with finite rotations. *International Journal for Numerical Methods in Engineering*, 26(11):2403–2438.

[7] Crusells-Girona, M., Filippou, F. C., and Taylor, R. L. (2017). A mixed formulation for nonlinear analysis of cable structures. *Computers & Structures*, 186:50–61.

[8] Fletcher, R. (1993). *Practical Methods of Optimization.*

[9] Fuss, N. (1796). Chapter x: On strings of a treatyise on analytical statics by Routh. *University press.*

[10] Ju, F. and Choo, Y. (2005). Super element approach to cable passing through multiple pulleys.

[11] Kanno, Y. and Ohsaki, M. (2003). Minimum principle of complementary energy of cable networks by using second-order cone programming. *International Journal of Solids and Structures*, 40(17):4437–4460.

[12] Marigo, J. J. (2014). *Mécanique des Milieux Continus I.* Paris, École polytechnique. Lecture notes, HAL-ID: *cel-01023392.*

[13] McDonald, B. and Peyrot, A. (1988). Analysis of cables suspended in sheaves. *Journal of the Structural Engineering*, 114:693–706.

[14] Monforton, G. and El-Hakim, N. (1980). Analysis of truss-cable structures. *Computers & Structures*, 11:327–335.

[15] Panagiotopoulos, P. D. (1975). Stress-unilateral analysis of discretized cable and membrane structure in the presence of large displacements. *Ingenieur-Archiv*, 44(5):291–300.

[16] Pérès, J. (1953). *Mécanique générale.* Masson & Cie.

[17] Signorini, S. (1933). Sopra akune questioni di elastostatica. *Atti della Sicieta Italiana per il Progresso delle Scienze.*

[18] Souza de Cursi, J. E. (1990). Un problème issu de l'étude numérique d'un fil sans raideur soumis au frottement sec. *Annales de la Faculté des sciences de Toulouse : Mathématiques*, 5e série, 11(2):137–186.

[19] Tibert, G. (1999). Numerical analysis of cable roof structures [master thesis].

Chapter 3

Finite element method for cable systems

Equilibria and dynamics of cable systems continue to be studied until now as it is reported in the detailed review of Rega [32] with a focus on the modal analyses and the dynamics of cable systems. However, those studies often rely on reduced-order models which are neither applicable to generic situations nor to non-smooth phenomenons. This chapter deals with the FEM applied to cable structures.

A truss formulation [14] has been proposed in the early stage of FE investigations about cables. The latter is considering an apparent rigidity for a truss element in order to take into account geometrical nonlinearities. The possibility of doing modal analysis (e.g.[19]) and studying the dynamics (e.g. [18]) is an ongoing investigation in the domain of cable structures. In most cases, cable problems are ill-conditioned, badly scaled and the convergence results of the FE are compromised [43]. Numerical damping, load control step and a smart initial guess [15] or also constrained optimization [25] can be combined to increase the robustness of those methods. However, spurious solutions continue to be observed [15, 41] or the criteria on the positive internal actions (i.e. tension) are not satisfied out of Gauss integration points [18].

More sophisticated cable systems and cable dynamics are often studied for nets and mooring lines. Indeed, the complex shape taken by the system in its current state requires a minimum number of assumption and to consider all the effects of the geometrical nonlinearity.

Geometrically nonlinear aspects of the problem have been tackled using the nodal coordinate formulations [39] or also using co-rotational formulation [16] rather than displacement-based computations. This method is endowed since the small displacement assumption produces wrong tension estimates and potential instabilities [42]. In a recent work [10], a proper mixed FE formulation is proposed for a neo-Hookean cable material with the possibility of having a discontinuous axial force. Further discussion about the robustness of finite element procedure for cable systems composed of a large number of nodes is still needed. Our purpose is to expose the numerical problems that can be encountered with such systems and to propose bypasses for the occurrence of compressive solutions during the calculations.

The main assumption for cables is that they cannot bear compression stresses. In other words, the strains and stresses should remain positive. Proof of existence of mentionned conditions has been given via a complementary energy principles in the work of Kanno [22]. Moreover dual formulation also provides with the possibility of imposing tension only as presented in the work of Santos and Almeida [36]. The statics of cables or cable networks is then well established however there is a lack of formalism for the dynamics even if this problem is addressed in [38] where the dynamic increment is modified to ensure a positive strain.

A proper formalism can be endowed to impose a given sign to stresses [3, 31], coined as no-tension materials with application for masonry structures. For nonlinear cable structures,

there is the lack of a problem formulation with a no-compression formulation, although a formalism exists for bar/truss elements [22], no work currently treats this aspect combined to other constraints, geometrical non linearity and dynamics.

A lot of work have been carried out by the community of computer graphics. It often involves various implementations of geometrically exact beams combined with a rotation parametrization via quaternions, parallel transport, rotation vector or Euler angles. It is often stated that those methods are very satisfying for materials subjected to small stresses and not so stiff. Those models already have some industrial implementation (IPS cable for instance) allowing interactivity which requires real-time integration of the dynamics. This can be performed at the cost of having critical or almost critical modal damping combined to a behavior which is dominated by flexural stiffness which is unfortunately not acceptable to describe dynamics of a slender structure which behavior is dominated by its axial forces with extra light damping.

In this chapter, we will present a FE formulation of the cable which is able to trace the statics and the dynamics of cable systems. Focus will be drawn to the viable strategies to overcome the no-compression condition.
A self-standing presentation is available in [6]. Here the focus is drawn to pedagogy and details that made the approach efficient.

3.1 Formulation of a Cable Finite Element

Let us consider the equilibrium of an elastic cable of rigidity EA and of length L. The cable is located via the positions of its particles $\mathbf{q}$ and the velocity of its particles $\mathbf{v}$. The linear density of the cable, ρ, is assumed constant along the curvilinear abscissa S. Its local undamped dynamics are given by

$$\rho \frac{\mathrm{d}\mathbf{v}}{\mathrm{d}t} = [T\mathbf{e}]' + \mathbf{b} \ . \tag{3.1}$$

We also need to emphasize on the fact that cables are materials which can resist only to tensile forces. Indeed, the cable in its simplest representation can be tensed or slack. As a consequence, the internal forces produced by a cable can only be positive and oriented along the axial direction, $\mathbf{e}$, of one cable segment leading to the following formulation of cable tension

$$T = \begin{cases} EA\left(\|\mathbf{q}'\| - 1\right) & \text{if} \quad \|\mathbf{q}'\| - 1 \geqslant 0 \\ 0 & \text{if} \quad \|\mathbf{q}'\| - 1 < 0 \end{cases} \ . \tag{3.2}$$

A particular attention is given to (3.2) since unexpected numerical behavior can happen due to this mechanical inconsistency. The position of cable sections are kept as unknown rather than displacements. This strategy allows to keep the current orientation and length of each cable segment arbitrary.
Choosing nodal positions instead of displacements in the case of cable is of major relevance. Indeed, the motion of a cable often exhibits large displacements combined to small strain. As a consequence, the full geometrical non linearity must be kept in developments to avoid spurious estimations of the strain. An interesting illustration is provided by Zhu [42], injecting the strain-displacement relationship into a quadratic strain approximation yields

$$\widetilde{\varepsilon} = \cos(\omega) - 1 + \frac{1}{2}\sin^2(\omega) \ , \tag{3.3}$$

which is non-zero in the case of pure rigid body motion. For this reason, approximations of the strain and rotations cannot be used in the sequel. The latter is true for other order of expansion used.
Unknown functions $\mathbf{q}$ and $\mathbf{v}$ are assumed to belong to the following Sobolev space

$$\mathbf{v} \ , \ \mathbf{q} \ \in \mathcal{H}^1 = \left\{ \mathbf{u} \in \mathbb{R}^3 \text{ s.t. } \mathbf{u} \in \mathcal{L}^2\left([0,L]\right), \mathbf{u}' \in \mathcal{L}^2\left([0,L]\right) \right\} \ , \tag{3.4}$$

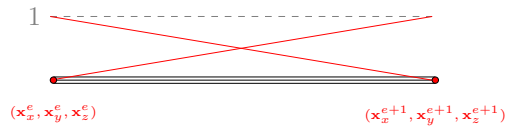

Figure 3.1: Linear interpolation of a cable e^{th} element

accompanied with its norm

$$\|\mathbf{u}\|_1 = \left[\int_0^L \mathbf{u}\cdot\mathbf{u} + \mathbf{u}'\cdot\mathbf{u}' \mathrm{d}S\right]^{\frac{1}{2}} . \tag{3.5}$$

Equation (3.1) is multiplied by an arbitrary function $\varphi \in \mathcal{H}^1$ and integrated by parts over the spatial domain

$$\int_0^L \rho\frac{\mathrm{d}\mathbf{v}}{\mathrm{d}t}\cdot\varphi \mathrm{d}S + \int_0^L T\mathbf{e}\cdot\varphi' \mathrm{d}S = [T\mathbf{e}\cdot\varphi]_0^L + \int_0^L \mathbf{b}\cdot\varphi \mathrm{d}S . \tag{3.6}$$

This manipulation highlights the fact the the boundary condition in force should be given in this case. However the latter is an unknown of this problem in general. Thus, the global equilibrium reads

$$\int_0^L \rho\frac{\mathrm{d}\mathbf{v}}{\mathrm{d}t}\cdot\varphi \mathrm{d}S + \int_0^L T\mathbf{e}\cdot\varphi' \mathrm{d}S = T(L)\mathbf{e}(L)\cdot\varphi(L) - T(0)\mathbf{e}(0)\cdot\varphi(0) + \int_0^L \mathbf{b}\cdot\varphi \mathrm{d}S , \tag{3.7}$$

where $T(L)\mathbf{e}(L)$ and $T(0)\mathbf{e}(0)$ are given or a consequence of boundary conditions. The most compliant and versatile approach is to include those boundary condition as a reaction to a constraint in the form of

$$\mathbf{a}(\mathbf{q}) = 0 \quad , \quad \nabla_{\mathbf{q}}\mathbf{a} = \mathbf{A} , \tag{3.8}$$

which implies that a reaction force is directed along the direction given by $\nabla_{\mathbf{q}}\mathbf{a} = \mathbf{A}$.
The Sobolev space is approximated via linear polynomials p^1 [43]. Then, the cable is described as an assembly of N cable segments. In another words, the interval $[0, L]$ is parted into sub-intervals $[S^e, S^e + L^e]$ such that $\sum_e L^e = L$. Positions and velocities are approximated as follows

$$\mathbf{q}(S) \approx \sum_{e=1}^{N} \mathbf{N}(S)\mathbf{q}^e , \tag{3.9}$$

$$\mathbf{v}(S) \approx \sum_{e=1}^{N} \mathbf{N}(S)\mathbf{v}^e , \tag{3.10}$$

where $\mathbf{N}$ is a linear interpolation matrix

$$\mathbf{N}(S) = \begin{bmatrix} 1-\xi^e & 0 & 0 & \xi^e & 0 & 0 \\ 0 & 1-\xi^e & 0 & 0 & \xi^e & 0 \\ 0 & 0 & 1-\xi^e & 0 & 0 & \xi^e \end{bmatrix} \quad , \quad \xi^e = \frac{S - S^e}{L_e} . \tag{3.11}$$

Vectors $\mathbf{q}^e$ and $\mathbf{v}^e$ are respectively the nodal positions and the nodal velocities associated to the e^{th} cable segment. The element considered is depicted in Figure 3.1. This choice implies that the tension and the orientation are constant element-wise.
Let us consider an arbitrary weight function φ approximated the same way over one cable segment, meaning

$$\varphi(S) \approx \sum_{e=1}^{N} \mathbf{N}(S)\varphi^e . \tag{3.12}$$

The global equilibrium given by (3.7) can be reformulated into the following equation in the approximate $\mathcal{H}_1^1$-space as

$$\sum_{e=1}^{N} {\varphi^e}^\top \left[\mathbf{M}^e \frac{\mathrm{d}\mathbf{v}^e}{\mathrm{d}t} + \mathbf{K}^e(\mathbf{q}^e)\mathbf{q}^e - \mathbf{f}^e \right] = \varphi^\top \left[\mathbf{A}^\top \boldsymbol{\lambda} \right] \ , \tag{3.13}$$

where

$$\mathbf{M}^e = \rho \int_0^{L^e} \mathbf{N}(S)^\top \mathbf{N}(S) \mathrm{d}S \ , \tag{3.14}$$

$$\mathbf{K}^e(\mathbf{q}^e) = EA \int_0^{L^e} \left(\|\mathbf{N}'(S)\mathbf{q}^e\| - 1 \right) \frac{\mathbf{N}'(S)^\top \mathbf{N}'(\xi)}{\|\mathbf{N}'(S)\mathbf{q}^e\|} \mathrm{d}S \ , \tag{3.15}$$

$$\mathbf{f}^e = \int_0^{L^e} \mathbf{N}(S)^\top \mathbf{b} \ \mathrm{d}S \ , \tag{3.16}$$

which read in matrix forms

$$\begin{cases} \mathbf{M}^e = \dfrac{\rho L^e}{6} \begin{bmatrix} 2 & 0 & 0 & 1 & 0 & 0 \\ 0 & 2 & 0 & 0 & 1 & 0 \\ 0 & 0 & 2 & 0 & 0 & 1 \\ 1 & 0 & 0 & 2 & 0 & 0 \\ 0 & 1 & 0 & 0 & 2 & 0 \\ 0 & 0 & 1 & 0 & 0 & 2 \end{bmatrix} \quad , \quad \mathbf{f}^e = \dfrac{L^e}{2} \begin{bmatrix} \mathbf{b_x} \\ \mathbf{b_y} \\ \mathbf{b_z} \\ \mathbf{b_x} \\ \mathbf{b_y} \\ \mathbf{b_z} \end{bmatrix}^\top \\ \mathbf{K}^e(\mathbf{q}^e) = \dfrac{EA}{L} \dfrac{\|\mathbf{N}'(\xi)\mathbf{q}^e\| - 1}{\|\mathbf{N}'(\xi)\mathbf{q}^e\|} \begin{bmatrix} 1 & 0 & 0 & -1 & 0 & 0 \\ 0 & 1 & 0 & 0 & -1 & 0 \\ 0 & 0 & 1 & 0 & 0 & -1 \\ -1 & 0 & 0 & 1 & 0 & 0 \\ 0 & -1 & 0 & 0 & 1 & 0 \\ 0 & 0 & -1 & 0 & 0 & 1 \end{bmatrix} \end{cases} . \tag{3.17}$$

Once assembled into a global problem the latter yields the dynamics of a cable. Structural damping may be considered for practical reasons which is added to the global problem as follows

$$\begin{cases} \mathbf{0} = \mathbf{M}\dfrac{\mathrm{d}\mathbf{v}}{\mathrm{d}t} + \mathbf{C}(\mathbf{q}, \mathbf{v})\mathbf{v} + \mathbf{K}(\mathbf{q})\mathbf{q} - \mathbf{f} - \mathbf{A}^\top \boldsymbol{\lambda} \\ \mathbf{0} = \mathbf{a}(\mathbf{q}) \end{cases} . \tag{3.18}$$

The expression of $\mathbf{a}$ should be supplied in accordance with the system physics.
The form of the matrix $\mathbf{C}(\mathbf{q}, \mathbf{v})$ is left general since the latter depends on the domain considered.
The equilibrium given by (3.18) is nonlinear and non regular if we consider that the cable can only support tensile forces.
Eventually the assembly process, the boundary conditions and the numerical methods should be adapted for the study at stake. Among the possibilities is

- A linear assembly with fixed end nodes (Bridge cables, cable vibrations)
- A linear assembly with one fixed endpoint (Elastic n-pendulums, mooring lines)
- A closed-loop composed of n-segment (Belt-sheaves)
- An arbitrary assembly of segments whose ends are connected to another segment or anchored-fixed (Cable nets)

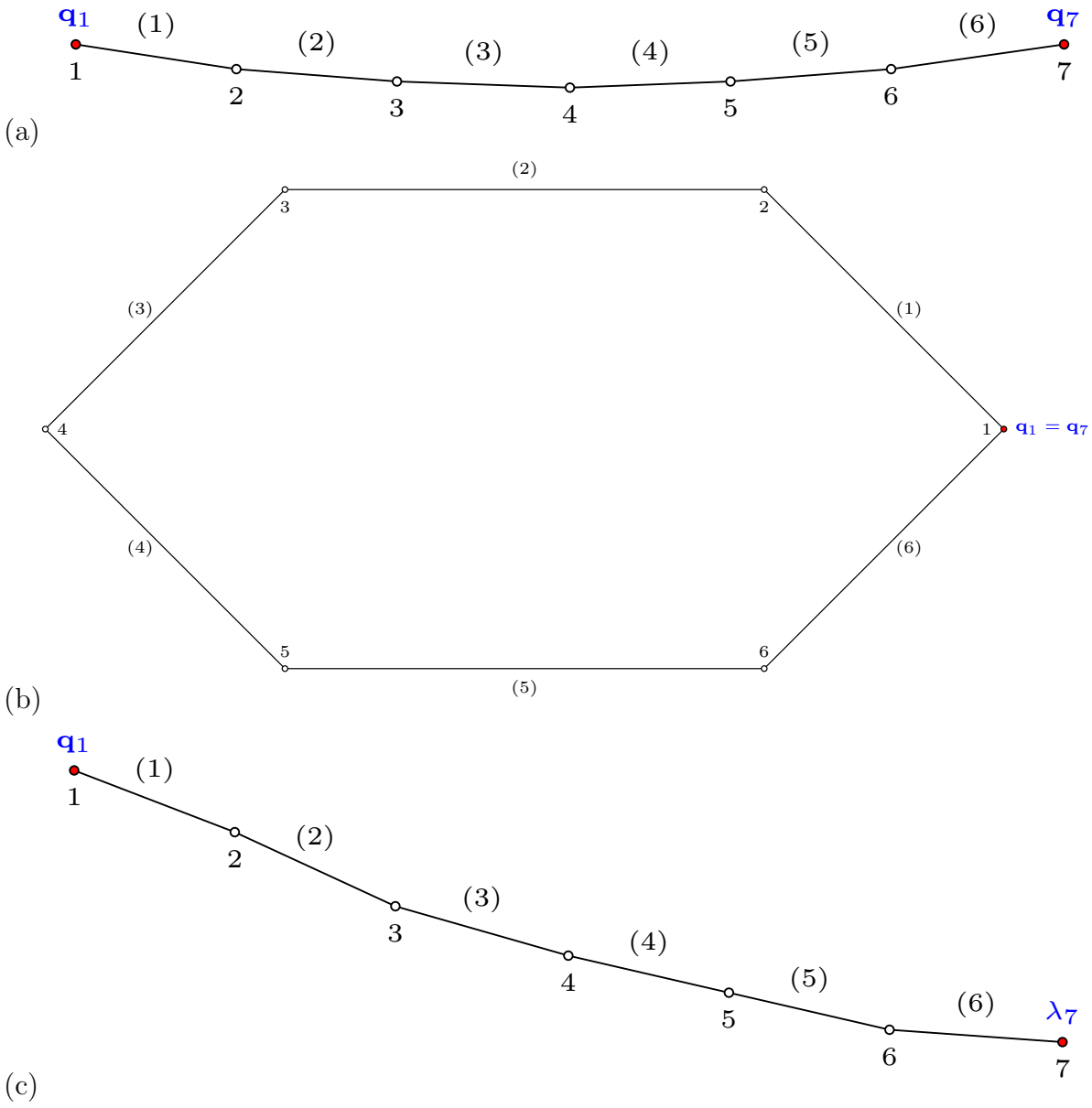

Figure 3.2: (a) Fixed cable configuration, (b) closed-loop configuration and (c) mooring Line (or n-pendulum) configuration with their given boundary condition in blue

A quick insight of various possibilities are illustrated in Figure 3.2. Some investigations about the consequence of the mesh on the integrability of such system have already been done by Kozlov in [26]. Statics and dynamics of a general cable system are two different challenges. Indeed, the static problem is to find the shape of the system at rest and to estimate its tension while the dynamics aims to predict the accurate system response when subjected to a dynamic load.

3.2 Statics of cables

The statics of cable systems are given by the following general equation

$$\mathbf{K}(\mathbf{q})\mathbf{q} - \mathbf{f} = \mathbf{0} \ , \tag{3.19}$$

coupled to some boundary conditions or more generally

$$\begin{cases} \mathbf{K}(\mathbf{q})\mathbf{q} - \mathbf{f} = \mathbf{A}^\top \boldsymbol{\lambda} \\ \mathbf{0} = \mathbf{a}(\mathbf{q}) \end{cases} . \tag{3.20}$$

Performing the static analysis of cable structures has at least three following interests

- Finding the shape of a given system
- Tension estimation of cables
- Provide suitable initial conditions for dynamics analyses

Following difficulties may be encountered during numerical treatment of cables

- Ill-conditioning of the residual equation
- Inaccurate topology of the cable (knots, folds or arches)
- Singularity of the stiffness matrix (due to the possible slackness of cable segments)

First, this section highlights the weaknesses of the direct solving of the residual equation obtained by FEM. Then, various numerical strategies to compute the equilibrium of tensed cables are presented. Eventually, a summary about Dynamic Relaxation Method (DRM) is given since it had a significant impact on the community of cable network and cable-roof structures.

3.2.1 Direct solving via FEM

Let us give the expressions for the stiffness and tangent stiffness matrices

$$\begin{cases} \mathbf{K}^e = EA \displaystyle\int_0^{L^e} \left(\|\mathbf{N}'(S)\mathbf{q}^e\| - 1\right) \frac{\mathbf{N}'(S)^\top \mathbf{N}'(\xi)}{\|\mathbf{N}'(S)\mathbf{q}^e\|} \mathrm{d}S \\ \Delta\mathbf{K}^e = \mathbf{K}^e + EA \displaystyle\int_0^{L^e} \frac{\mathbf{N}'(S)^\top \mathbf{N}'(S)\mathbf{q}^e \mathbf{q}^{e\top} \mathbf{N}'(S)^\top \mathbf{N}'(S)}{\|\mathbf{N}'(S)\mathbf{q}^e\|^3} \mathrm{d}S \end{cases} . \tag{3.21}$$

Without precautions, it allows for compression since a compressed segment still produce forces. This can lead to the situation explained in Section 2.2.5. When it comes to study the rest position of a hanging cable, non acceptable shapes can be obtained such as knots, arches or folds. A plot of a "wrong" solution obtained by solving (3.19) using a direct Newton-Raphson algorithm is provided in Figure 3.3. Facing this example, two solutions may be thought of

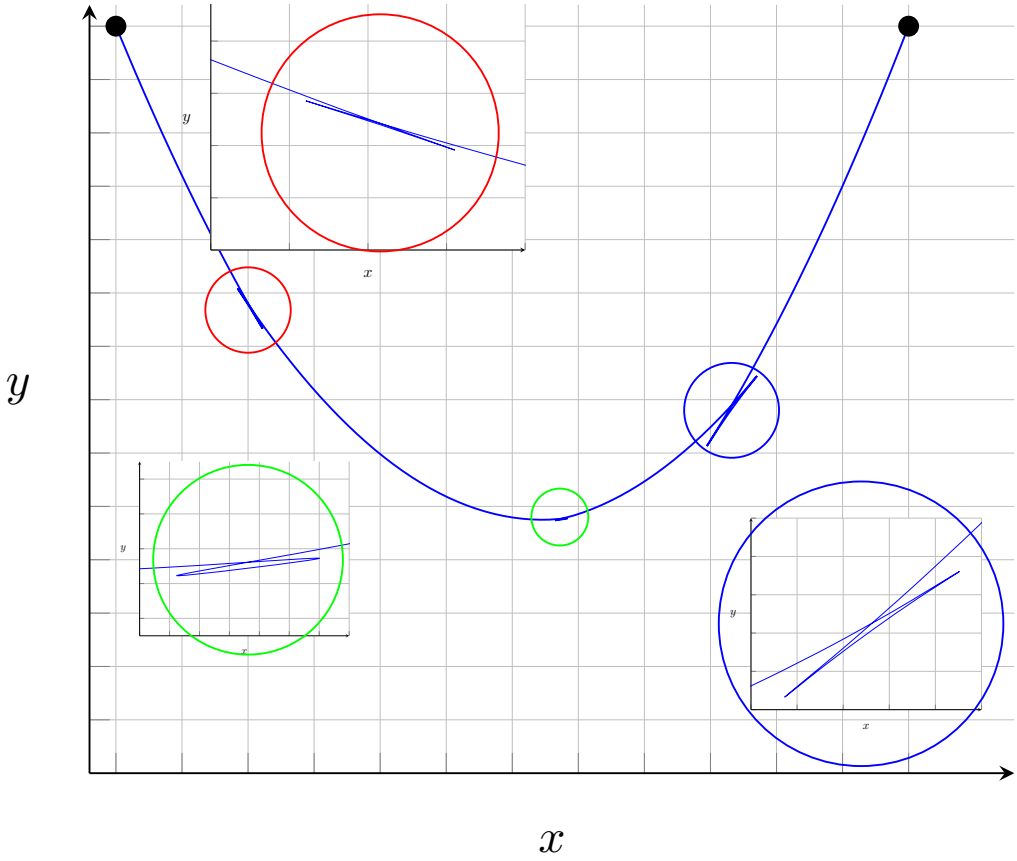

Figure 3.3: A numerical equilibrium obtained by naive implementation of FEM relying on (3.21) instead of its modified version. The compressed parts are zoomed in.

- Change the initial guess
- Change the nature of the internal forces so that compression is forbidden

The first choice relies mostly on experience and the physical sense of the user. As an example, initial guesses relatively close to the final equilibrium are also subjected to those phenomenon (for instance the parabolic profile). Moreover, the rest shape of complex structures cannot be so easily inferred. The second choice could be applied for a wider variety of problems. Some pioneering work for a truss assembly already has viable implementation and proof of convergence [21].
The system needs a bypass in order to have a physically acceptable solution which is the topic of next section.

3.2.2 Numerical strategies to avoid compressed segments

The key explanation for the situation depicted in Figure 3.3 relies on Figure 2.4. It has been shown in Section 2.2.5 that the elastic problem has several solutions when both traction and compression are allowed. The idea is to introduce a bias in the numerical computations that bents the simulation towards the tensed cable configuration.
One simple way to favor tensed configurations is to have a modified constitutive law which decrease the internal compressive forces. Several approaches may be endowed but the theoretically perfect one is the unilateral law which case has already been discussed in (2.68). The perfect unilateral law can be approximated by a piecewise linear law with a very small slope for negative strain as depicted in Figure 3.4. The ideal physical choice is of course the unilateral law since it simply discards locally the internal forces when it corresponds to a compressed

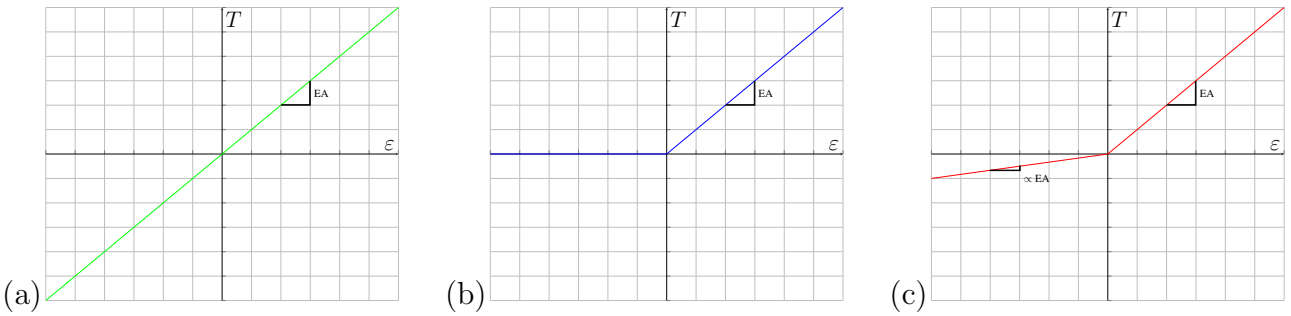

Figure 3.4: (a) Classic Hooke's law (solid line —) , (b) Unilateral Hooke's law (solid line —) and (c) linear-by-part Hooke's law (solid line —)

cable segment. However, the tangent stiffness matrix is no longer invertible due to a multi-diagonal slot of zeros. This encourages to investigate further the piecewise linear case. The latter leads to the matrice given in (3.17) where a small stiffness is considered when a segment is compressed. Even though this approach slightly increases the success rate of the numerical procedures it still has the drawback of presenting compressed equilibrium or convergence issues. A interesting way of searching equilibrium is to discard elastic forces corresponding to compression. The stiffness matrix, $\mathbf{K}$, and the tangent stiffness matrix, $\Delta\mathbf{K}$, must be adapted in order to choose a descent direction which is consistent with the physics expected of a cable and also to provide with an invertible problem. Moreover, as we investigate tensed configuration the latter should hold

$$\varepsilon(S) = |\varepsilon(S)| \iff \|\mathbf{N}'(S)\mathbf{q}^e\| - 1 = |\|\mathbf{N}'(S)\mathbf{q}^e\| - 1| \ , \tag{3.22}$$

Then we should have

$$\frac{\varepsilon(S)}{\varepsilon(S)+1} = \frac{|\varepsilon(S)|}{|\varepsilon(S)|+1} \ . \tag{3.23}$$

We therefore use the latter to enforce a tensed equilibrium. In this case, a vanishing residual equation implies that $\varepsilon \geqslant 0$. For one cable segment the latter reads

$$\varepsilon^e(S) = \|\mathbf{N}'(S)\mathbf{q}^e\| - 1 \ , \tag{3.24}$$

$$\mathbf{K}^e = \begin{cases} EA \displaystyle\int_0^{L^e} \frac{\mathbf{N}'(S)^\top \mathbf{N}'(S)}{1+|\varepsilon^e(S)|^{-1}} \mathrm{d}S & ; \quad \varepsilon^e(S) \geqslant 0 \\ \mathbf{0} & ; \quad \varepsilon^e(S) < 0 \end{cases} , \tag{3.25}$$

$$\Delta\mathbf{K}^e = \begin{cases} \mathbf{K}^e + EA \displaystyle\int_0^{L^e} \frac{\mathbf{N}'(S)^\top \mathbf{N}'(S)\mathbf{q}^e\mathbf{q}^{e\top}\mathbf{N}'(S)^\top \mathbf{N}'(S)}{(|\varepsilon^e(S)|+1)^3} \mathrm{d}S & ; \quad \varepsilon^e(S) \geqslant 0 \\ EA \displaystyle\int_0^{L^e} \frac{\mathbf{N}'(S)^\top \mathbf{N}'(S)}{1+|\varepsilon^e(S)|^{-1}} \mathrm{d}S & ; \quad \varepsilon^e(S) < 0 \end{cases} . \tag{3.26}$$

The parallel between this formulation and the particular case given in Section 2.2.5 is clear. The contribution of compressive forces is discarded so that only tensile forces will be considered in the equilibrium.
Some researchers developed several approaches among which penalty methods formulation, pendulums assembly [35] or constrained optimization [21] in order to fully account for the non-compressibility of cable systems.

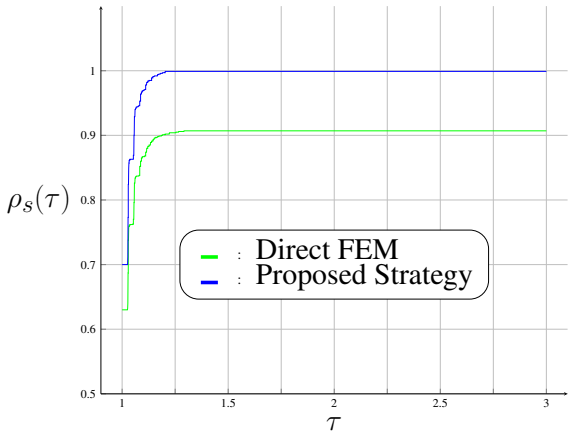

Figure 3.5: Performance profiles for naive approach (3.17) and the proposed approach (3.26)

3.2.3 Comparisons between the direct FEM and the proposed approach

The direct FEM given by (3.21) is not of practical interest for the computation of cable equilibrium compared to an approach based on the matrices given in (3.26). In order to assess for the following statement, an efficiency test has been ran for our approach [13]. According to p random problems, we can define an objective indicator of efficiency for each method possible denoted by subscript s which is the number of iterations (or CPU-time) needed to reach a numerical equilibrium penalized with the number of compressed segments in the domain

$$\text{crit}_{p,s} = n_{\text{it}} + n_{\varepsilon<0} \times \mathbf{max}_{\text{it}} \quad \text{or} \quad \text{crit}^*_{p,s} = \text{CPU-time} + n_{\varepsilon<0} \times t^* \ , \tag{3.27}$$

where n_{it} and $n_{\varepsilon<0}$ respectively stand for the number of iterations and the number of compressed segments in the domain. A performance ratio is defined as follows

$$r_{p,s} = \frac{\text{crit}_{p,s}}{\min\limits_{s} \left(\text{crit}_{p,s}\right)} \ . \tag{3.28}$$

We can build the probability that a performance ratio for a given method s is within a factor τ of the best possible method, which reads

$$\rho_s(\tau) = \frac{1}{p}\text{card}\left(\{\tilde{p} \ , \ r_{\tilde{p},s} \leqslant \tau\}\right) \ . \tag{3.29}$$

We used this methodology to compare objectively the robustness of our approach. We randomly selected $p = 1600$ static configurations problems over the set of parameters (ρ, L, EA, q_0, q_L) and ran the direct FEM (3.17) and the proposed strategy (3.26) on all problems. More details and strategies are available in our published work [6]. The main result is that a nonlinear approach based on formulation given by (3.26) instead of (3.21) is a better choice in the sense that it statistically improves the numerical success as illustrated by Figure 3.5. For large τ we see that all problem are solved since $\rho_s(\tau) \to 0$. Furthermore, the proposed approach is more computationally efficient.

3.2.4 Dynamic relaxation method

The Dynamic Relaxation Method (DRM) is a method endowed to compute static or quasi-static solutions for structures where large displacements are expected. Its name is due to the fact that the actual rest position of one system is obtained as the fixed point of a fictitious temporal

evolution. A lot of work have been done in order to optimize the choice for the fictitious time parameters: the mass matrix, the damping matrix and the time-step. The main advantages are the better conditioning of the time-evolution problem, the equilibrium obtained is an actual fixed-point of the dynamics and it can be applied to complex structures. Moreover the fictitious matrices are often diagonal and the evaluations of the fictitious dynamics are explicit which makes memory requirement smaller than actual nonlinear dynamics.
Its first developments [11, 23, 30, 40] have considerably improved until today [4, 33] to cite a few. This method is very suitable for systems subject to large motions and large deformations. Although this method has been used a lot and has been proven reliable, it does not explain the observed numerical instability. A very practical summary and review is accessible in this research note [34].
As stated just above, the idea is to compute a fictitious transient for the cable system over $\bigcup_{k=0}^{n}(t_k, t_{k+1}]$ where the mass matrix and the damping matrix are chosen to accelerate the convergence towards the rest position. The time-step h is also to be chosen to fasten the computation.
Applying the Wilson θ-Method to (3.18) with the particular choice $\theta = 1/2$ we have the following

$$\begin{cases} \left[\mathbf{M}_k + \frac{h}{2}\mathbf{C}_k\right]\mathbf{v}_{k+1} + \frac{h}{2}\mathbf{K}_{k+1}\mathbf{q}_{k+1} = \mathbf{M}_k\mathbf{v}_k - \frac{h}{2}\mathbf{C}_k\mathbf{v}_k - \frac{h}{2}\mathbf{K}_k\mathbf{q}_k + \frac{h}{2}\mathbf{f}_{k+1} + \frac{h}{2}\mathbf{f}_k \\ \mathbf{q}_{k+1} = \mathbf{q}_k + \frac{h}{2}\mathbf{v}_{k+1} + \frac{h}{2}\mathbf{v}_k \end{cases}, \tag{3.30}$$

which can also be written as

$$\begin{bmatrix} \mathbf{M}_k + \frac{h}{2}\mathbf{C}_k & \frac{h}{2}\mathbf{K}_{k+1} \\ -\frac{h}{2}\mathbf{M}_k & \mathbf{M}_k \end{bmatrix} \begin{pmatrix} \mathbf{v}_{k+1} \\ \mathbf{q}_{k+1} \end{pmatrix} = \begin{bmatrix} \mathbf{M}_k - \frac{h}{2}\mathbf{C}_k & \frac{h}{2}\mathbf{K}_k \\ \frac{h}{2}\mathbf{M}_k & \mathbf{M}_k \end{bmatrix} \begin{pmatrix} \mathbf{v}_k \\ \mathbf{q}_k \end{pmatrix} + \frac{h}{2} \begin{pmatrix} \mathbf{f}_{k+1} + \mathbf{f}_k \\ \mathbf{0} \end{pmatrix} . \tag{3.31}$$

The subscripts $\bullet_{k+1}$ and $\bullet_k$ respectively refer to a quantity evaluated in $t = t_{k+1}$ and $t = t_k$. The detailed derivations of the θ-method is given in Section 3.3.1.
The fictitious mass and damping matrices are taken diagonal most of the time. Popular choices are often the following

- Mass matrix:
  - $\mathbf{M}_k = \alpha\mathbf{I}$ where α is an arbitrary constant
  - $\mathbf{M}_k = \beta\mathbf{K}_k$ where β is an arbitrary constant
  - $(\mathbf{M}_k)_{ii} = \sum_j |\,(\mathbf{K}_k)_{ij}\,|$
  - $(\mathbf{M}_k)_{ii} \geqslant \frac{h^2}{4}\sum_j |\,(\mathbf{K}_k)_{ij}\,|$ (Gerschgorin's theorem)
- Damping matrix is always supposed to be diagonal with form $c_k\mathbf{I}$:
  - Proportional to the lowest frequency $c_k = 2\omega_0$
  - $c_k = 2\left[\frac{\omega_k}{1+\omega_k}\right]^{1/2}$ where $\omega_k = \frac{\mathbf{q}_k{}^\top \Delta\mathbf{K}_k\mathbf{q}_k}{\mathbf{q}_k{}^\top\mathbf{M}_k\mathbf{q}_k}$ [37]
  - $c_k = 2\left[\frac{\mathbf{q}_k{}^\top\mathbf{K}_k\mathbf{q}_k}{\mathbf{q}_k{}^\top\mathbf{M}_k\mathbf{q}_k}\right]^{1/2}$
  - Adaptative damping [40] obtained from Rayleigh theory $c_k = 2\left[\frac{\mathbf{q}_k{}^\top\widehat{\mathbf{K}}_{k+1}\mathbf{q}_k}{\mathbf{q}_k{}^\top\mathbf{M}\mathbf{q}_k}\right]^{1/2}$ where $\mathbf{M}$ is taken as the Gerschgorin's theorem and $\widehat{\mathbf{K}}_{k+1} = \frac{2}{h}\mathbf{diag}\left(\frac{[\mathbf{K}_{k+1}\mathbf{q}_{k+1}]_i - [\mathbf{K}_k\mathbf{q}_k]_i}{[\mathbf{v}_{k+1}-\mathbf{v}_k]_i}\right)$

- Time-step h:
  - A constant time-step is often used when the frequency content is known $h \leqslant \frac{2}{\omega_{\max}}$ or even 1 to avoid the computation of the system's eigenvalues
  - When the mass and damping matrices are taken via Gerschgorin's theorem and Rayleigh's theorem, we set $h_k = \frac{2}{\sqrt{1+\omega_k}}$ where $\omega_k = \frac{\mathbf{q}_k{}^\top \Delta\mathbf{K}_k \mathbf{q}_k}{\mathbf{q}_k{}^\top \mathbf{M}_k \mathbf{q}_k}$ [37]

This calculation tool is used in this work to obtain initial condition for the dynamics of complex systems especially the ones subjected to unilateral constraints, see (2.97).

3.2.5 Tension estimation of cable networks

This section entails the application of our proposed methodology for the computation of some various cable structures. The developed tools is applicable to any structure composed totally or partially of cables. The assembly process can be very tedious. As an example, we formed a spider web made of 26 segments. Each segment has a density of at least four nodes per meter. The parameters for the spider web are given in Table 3.1. The unknowns in this case are 9126 dof, 21 Lagrange multipliers for the clamped boundary conditions and 375 Lagrange multipliers for the connections between the different cables. For the starting configuration, each sub-cable was given a random straight configuration inside of the final center of the net. The presented example remains academic but suffices to illustrate the case of slack assembly. Any further application could be enhanced with a better interface to facilitate the assembly and the matrices building.
We see that the proposed FEM is able to trace the catenary shape and to build tension estimations for the cable net. The robustness of the gradient direction proposed in (3.26) is assessed by this difficult numerical example. We insist on the fact that the DRM was not used for the presented examples, proving that the approach suffices to compute complex cable equilibriums. Moreover we see that the method is able to trace combined slack and taut cables in a complex assembly. Some perspectives to improve DRM associated to nets form-finding problems are open by the usage of the proposed approach. The final obtained equilibrium are depicted in Figure 3.6. The tension equilibrium is visible on each views, even though some cable are way slacker than other we are still able to catch this equilibrium and to evaluate the tension in each cable segment.

3.3 Dynamic analyses

The time-evolution of a cable is of utmost interest to predict the responses to dynamic loads and the stability of a given equilibrium. As we are mainly interested into the response of a constrained cable, the numerical scheme has to be adapted. Its derivation and use will be presented in the next section.

The nonlinear dynamics of cable systems are a major issue and challenging task. Contrary to analytical methods that trace a small displacement around and equilibrium, FEM is more adapted to compute the full dynamics of cable systems [35, 42]. In this section, we describe the detailed treatment of the non-smooth time evolution via the suitable θ-method. Then a qualitative validation of the performed integration is proposed. Eventually, a time-stepping scheme for cables subjected to frictional impact is derived.

Table 3.1: Parameters used for the spider web examples

Cable index	EA (MN)	ρ (kg/m)	L(m)	N	Clamped to ...	Connected to cables ...
0	1.5	0.8	4.1	60	$(0, 0, 0)$	$7, 13, 14$
1	1.5	0.8	2.336	30	$(5, 0, 7)$	$7, 8, 15$
2	1.5	0.8	2.336	30	$(13, 0, 7)$	$8, 9, 16$
3	1.5	0.8	3.262	45	$(18, 0, 1)$	$9, 10, 17$
4	1.5	0.8	2.549	30	$(16, 0, -8)$	$10, 11, 18$
5	1.5	0.8	4.1	60	$(8, 0, 12)$	$11, 12, 19$
6	1.5	0.8	3.706	45	$(2, 0, -8)$	$12, 13, 20$
7	1.5	0.8	6.503	90	None	$0, 1, 13, 14, 15$
8	1.5	0.8	6.1	90	None	$1, 2, 7, 9, 15, 16$
9	1.5	0.8	5.931	75	None	$2, 3, 8, 10, 16, 17$
10	1.5	0.8	6.183	90	None	$3, 4, 9, 11, 17, 18$
11	1.5	0.8	6.425	90	None	$4, 5, 10, 12, 18, 19$
12	1.5	0.8	5.485	75	None	$5, 6, 11, 13, 19, 20$
13	1.5	0.8	6.183	90	None	$0, 6, 7, 12, 14, 20$
14	1.5	0.8	4.223	60	None	$0, 7, 13, 15, 21, 22$
15	1.5	0.8	4.1	60	None	$1, 7, 8, 14, 21, 22$
16	1.5	0.8	5.1	75	None	$2, 8, 9, 22, 23$
17	1.5	0.8	4.572	60	None	$3, 9, 10, 18, 23, 24$
18	1.5	0.8	5.1	75	None	$4, 10, 11, 17, 23, 24$
19	1.5	0.8	4.223	60	None	$5, 11, 12, 24, 25$
20	1.5	0.8	4.343	60	None	$6, 12, 13, 21, 25$
21	1.5	0.8	4.1	60	None	$14, 15, 20, 22, 25$
22	1.5	0.8	3.1	45	None	$14, 15, 16, 21, 23$
23	1.5	0.8	3.706	45	None	$16, 17, 18, 22, 24$
24	1.5	0.8	2.928	30	None	$17, 18, 19, 23, 25$
25	1.5	0.8	3.262	45	None	$19, 20, 21, 24$

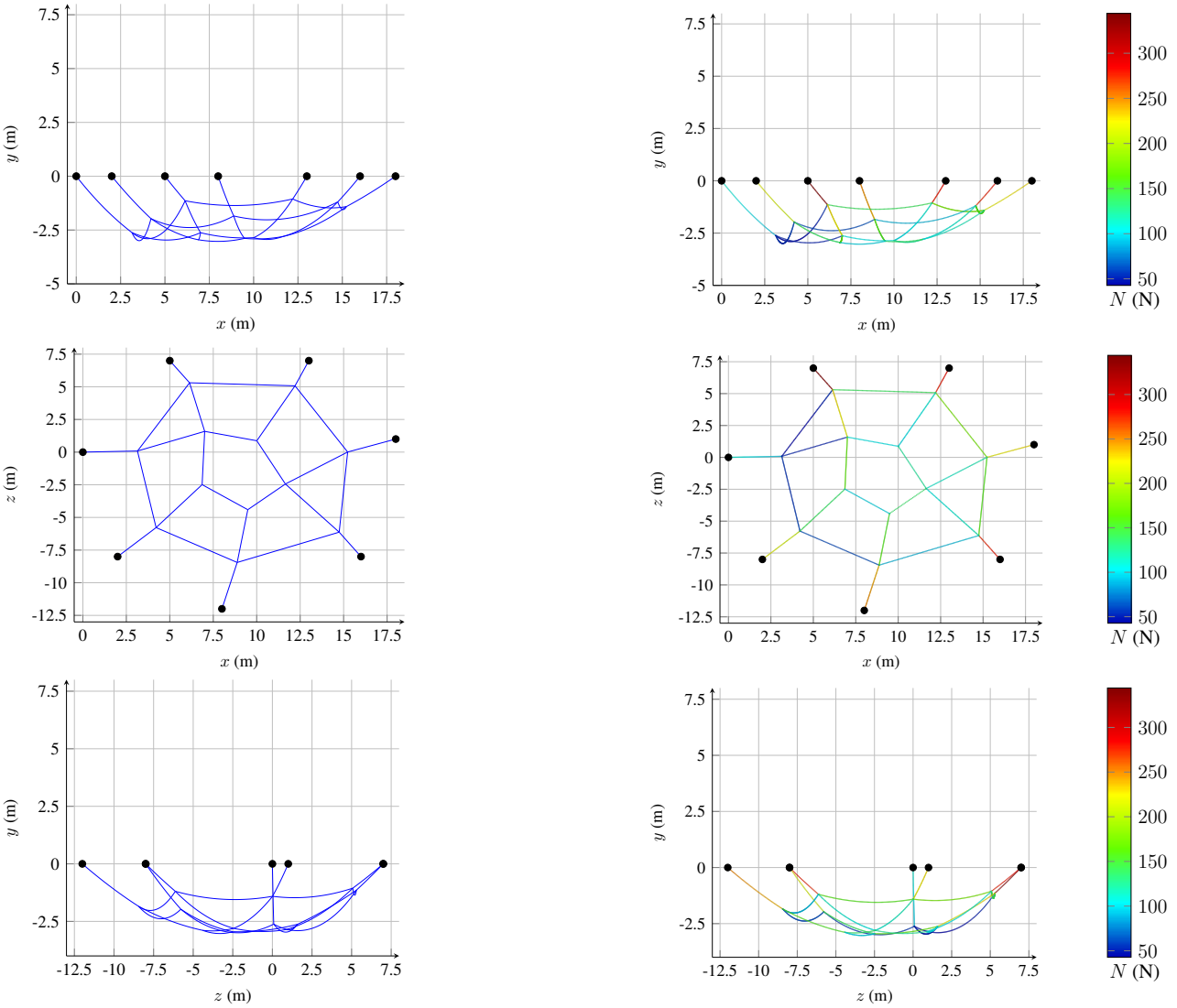

Figure 3.6: Static equilibrium of a cable net and its tension estimates computed via FEM under different views - Parameters in Table 3.1

3.3.1 θ-Method applied to cable dynamics

We suppose that the velocity $\mathbf{v}$ is a function of local bounded variation. In another words, the discontinuity occurrences of $\mathbf{v}$ are finite and countable. Some jumps can occur at some time t_i such that the left and right limit of the velocity are always defined. We take the following notations to refer to the right and left limits respectively

$$\mathbf{v}^+ = \mathbf{v}(t_i^+) = \lim_{\epsilon \to 0} \mathbf{v}(t_i + \epsilon) \quad , \quad \mathbf{v}^- = \mathbf{v}(t_i^-) = \lim_{\epsilon \to 0} \mathbf{v}(t_i - \epsilon) \ . \tag{3.32}$$

Besides, the positions are assumed to be absolutely continuous and are obtained via considering the Lebesgue integral of the velocity

$$\mathbf{q} = \mathbf{q}(t=0) + \int_0^t \mathbf{v} \ \mathrm{d}t \ . \tag{3.33}$$

The dynamics are recast into the following differential measure equality

$$\begin{cases} \mathbf{M}\mathrm{d}\mathbf{v} + \left[\mathbf{C}(\mathbf{q})\mathbf{v}^+ + \mathbf{K}(\mathbf{q})\mathbf{q}\right] \mathrm{d}t = \mathbf{f}\mathrm{d}t \\ \dfrac{\mathrm{d}\mathbf{q}}{\mathrm{d}t} = \mathbf{v}^+ \\ (\text{I.C.}) : \mathbf{q}(0) = \mathbf{q}_0 \quad , \quad \mathbf{v}^-(0) = \mathbf{v}_0 \end{cases} , \tag{3.34}$$

where we have that

$$\mathrm{d}\mathbf{v} = \boldsymbol{\gamma}\mathrm{d}t + \sum_i \left[\mathbf{v}^+ - \mathbf{v}^-\right] \delta_{t_i} + \mathrm{d}\mathbf{v}_s \ , \tag{3.35}$$

where $\boldsymbol{\gamma}$ is the acceleration in the classical sense and

- $\mathrm{d}t$ is the Lebesgue measure
- δ_{t_i} is the Dirac measure at discontinuity times t_i
- $\mathrm{d}\mathbf{v}_s$ is a singular measure with respect to $\mathrm{d}t + \sum_i \delta_{t_i}$ that will be neglected in the sequel

The differential measure equality is integrated over a time segment $(t_k, t_{k+1}]$ which yields

$$\begin{cases} \mathbf{M}\left(\mathbf{v}(t_{k+1}) - \mathbf{v}(t_k)\right) + \displaystyle\int_{t_k}^{t_{k+1}} \left[\mathbf{C}(\mathbf{q})\mathbf{v}^+ + \mathbf{K}(\mathbf{q})\mathbf{q}\right] \mathrm{d}t = \int_{t_k}^{t_{k+1}} \mathbf{f}\mathrm{d}t \\ \mathbf{q}(t_{k+1}) = \mathbf{q}(t_k) + \displaystyle\int_{t_k}^{t_{k+1}} \mathbf{v}^+ \mathrm{d}t \end{cases} . \tag{3.36}$$

The Wilson θ-Method is used to approximated integral quantities as follows

$$\int_{t_k}^{t_{k+1}} f(t)\mathrm{d}t \approx \theta h f(t_{k+1}) + (1-\theta) h f(t_k) \ . \tag{3.37}$$

As a consequence we have that

$$\int_{t_k}^{t_{k+1}} \left[\mathbf{C}(\mathbf{q})\mathbf{v}^+\right] \mathrm{d}t \approx \theta h \mathbf{C}(\mathbf{q}(t_{k+1}))\mathbf{v}(t_{k+1}) + (1-\theta) h \mathbf{C}(\mathbf{q}(t_k))\mathbf{v}(t_k) \ , \tag{3.38}$$

$$\int_{t_k}^{t_{k+1}} \left[\mathbf{K}(\mathbf{q})\mathbf{q}\right] \mathrm{d}t \approx \theta h \mathbf{K}(\mathbf{q}(t_{k+1}))\mathbf{q}(t_{k+1}) + (1-\theta) h \mathbf{K}(\mathbf{q}(t_k))\mathbf{q}(t_k) \ , \tag{3.39}$$

$$\int_{t_k}^{t_{k+1}} \mathbf{f}\mathrm{d}t \approx \theta h \mathbf{f}(t_{k+1}) + (1-\theta) h \mathbf{f}(t_k) \ . \tag{3.40}$$

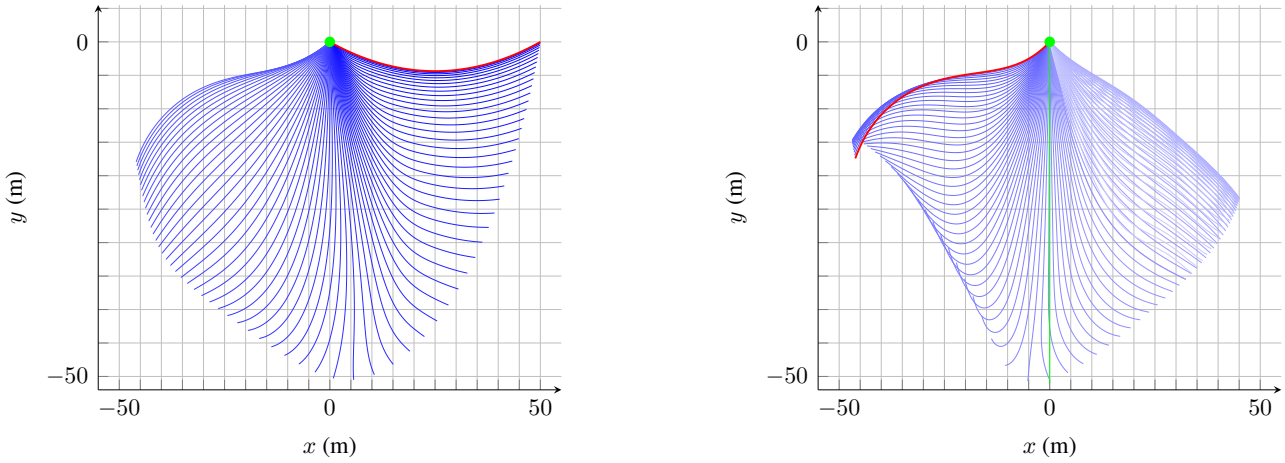

Figure 3.7: Stations of a falling cable (solid line —) starting without velocity from rest position (solid line —) and final equilibrium (solid line —)

This provides with the following problem

$$\begin{aligned}&[\mathbf{M}+h\theta\mathbf{C}(t_{k+1})]\,\mathbf{v}(t_{k+1})+h\theta\mathbf{K}(\mathbf{q}(t_{k+1}))\mathbf{q}(t_{k+1})=\mathbf{M}\mathbf{v}(t_k)\\&\quad-(1-\theta)h\mathbf{C}(\mathbf{q}(t_k))\mathbf{v}(t_k)-(1-\theta)h\mathbf{K}(\mathbf{q}(t_k))\mathbf{q}(t_k)+\theta h\mathbf{f}(t_{k+1})+(1-\theta)h\mathbf{f}(t_k)\end{aligned}\ , \tag{3.41}$$

$$\mathbf{q}(t_{k+1})=\mathbf{q}(t_k)+\theta h\mathbf{v}(t_{k+1})+(1-\theta)h\mathbf{v}(t_k)\ , \tag{3.42}$$

which is an implicit method in $(\mathbf{v}(t_{k+1}),\mathbf{q}(t_{k+1}))$. The latter can be used to trace the dynamics of cable systems or also to derive the statics via Dynamic Relaxation Methods as explained in Section 3.2.4. Several classical cases can be obtained as it follows

Method	Explicit Euler	Crank-Nicholson Finite Difference Method	Implicit Euler
θ	0	1/2	1

3.3.2 Application to the cable pendulum and qualitative validation

A benchmark example, is the falling cable pendulum. A fixed-free cable is released at time $t=0$ without initial velocity. The latter is oscillating in a pendulum-like motion until it converges to the vertical position.
The discrete equations of motion given in (3.18) are injected with the approximations of time derivatives given in Section 3.3.1. Some simplifications in the case $\theta=1/2$ are made to obtain the following nonlinear problem in $\mathbf{q}^{n+1}$

$$\left[\mathbf{M}+\frac{h}{2}\mathbf{C}+h^2\mathbf{K}\left(\mathbf{q}^{n+1}\right)\right]\mathbf{q}^{n+1}-h^2\mathbf{f}^{n+1}-\mathbf{M}\left(2\mathbf{q}^n-\mathbf{q}^{n-1}\right)-\frac{h}{2}\mathbf{C}\mathbf{q}^{n-1}=\mathbf{0}\ , \tag{3.43}$$

This test is typical of a situation with large displacements with small strains. The whipping effect of the cable tip is a good indicator of the nonlinear response of the system. The latter is easily comparable with a light experimental set-up [18]. Our own simulation reproduced correctly this phenomenon (see Figure 3.7) but a qualitative comparison with reality is therefore more interesting. An elastic cable of linear density $\rho=3.324\times10^{-2}$ kg.m^{-1} and rigidity $EA=750.77N$ has been considered. The rigidity of the cable has been estimated via a simple traction test. A picture of the considered cable in a tensed state is given in Figure 3.8 and the strain has been measured compared with an initial pre-stressed cable to ensure the uniform tension distribution in the domain. 30 measure points have been taken with different load paths

Figure 3.8: Extension of a linear elastic cable-type material

to check the linear elasticity assumption. The least-square method [7] has been endowed to estimate the cable rigidity as implied by Figure 3.9. We obtained the following results

$$\Delta T = 750.77 \Delta\varepsilon \quad ; \quad R^2 = 0.9692 \ . \tag{3.44}$$

The experiment consists on a 1.8 m cable hanged between two hinges which is released without initial velocity. We set up some targets that can be followed by a rapid/speed camera and the planar motion of the cable have been tested and ensured via using a suitable hinge which can be seen on Figure 3.10. The trajectory of the cable has been built according to video-correlation technique [24]. The software Kilonewton has been used to build back the 2D motion of the system. Some frames of the cable fall are depicted for illustration purpose only in Figure 3.11. The presence of the targets has been modeled with additional punctual masses dispatched along the reference curvilinear abscissa. Using a logarithmic decrement technique (details in Appendix D), we could estimate an acceptable value for the damping. Then prediction given by FEM can be compared with an actual trajectory which is given in Figure 3.12.
We can see the qualitative agreement between the motion of the targets and the motion computed via FEM. This simple test allows to validate the ability of the model to trace large displacements with small strain.
Current limitations of the protocol are listed below:

- The planar motion have been imposed roughly. Even though the motion remained planar, it has induced high dissipation in the hinged end of the cable
- The effect of initial curvature (torsional and flexural) of the material were neglected
- Even though every measure have been taken in the same room, no temperature test has been done to ensure the material was evolving in the same environment

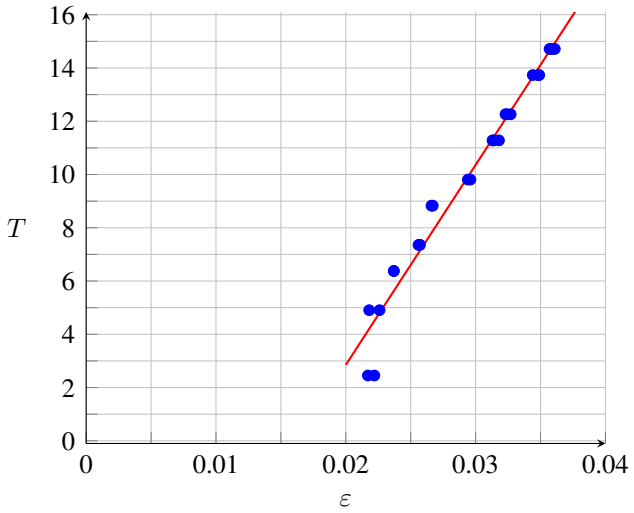

Figure 3.9: Measure points (•) and linear regression (solid line —) obtained from the traction test - $R^2 = 0.9692$

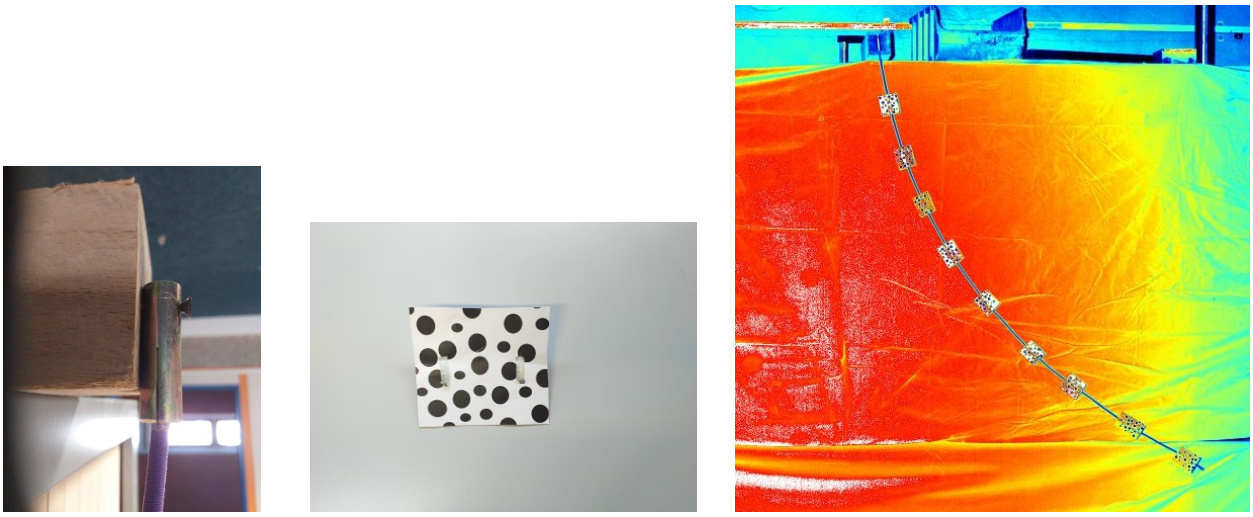

Figure 3.10: Hinge and target used for the experiment - Cable with targets mounted on

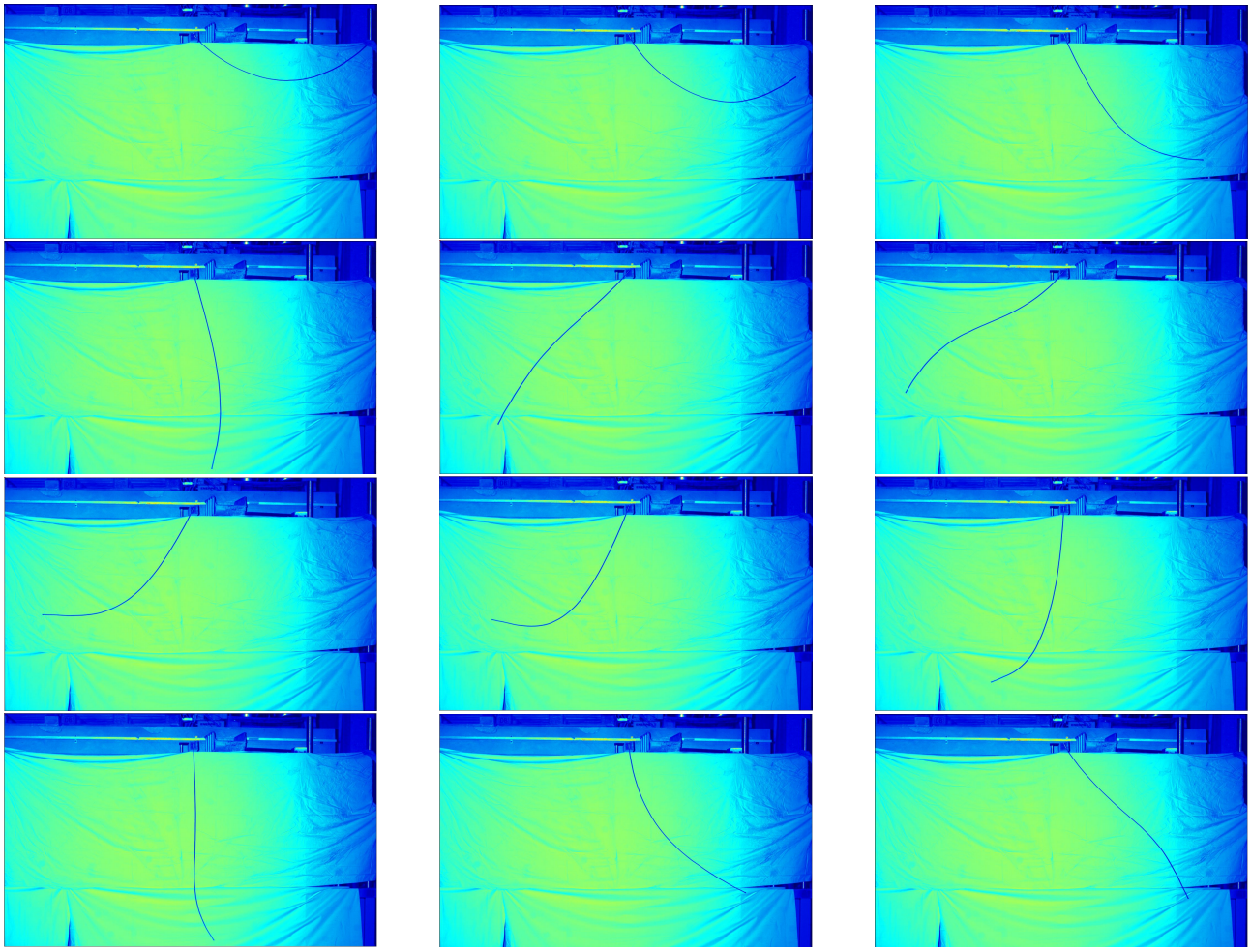

Figure 3.11: Snapshots of the falling cable obtained with a high speed camera (Illustration purpose only)

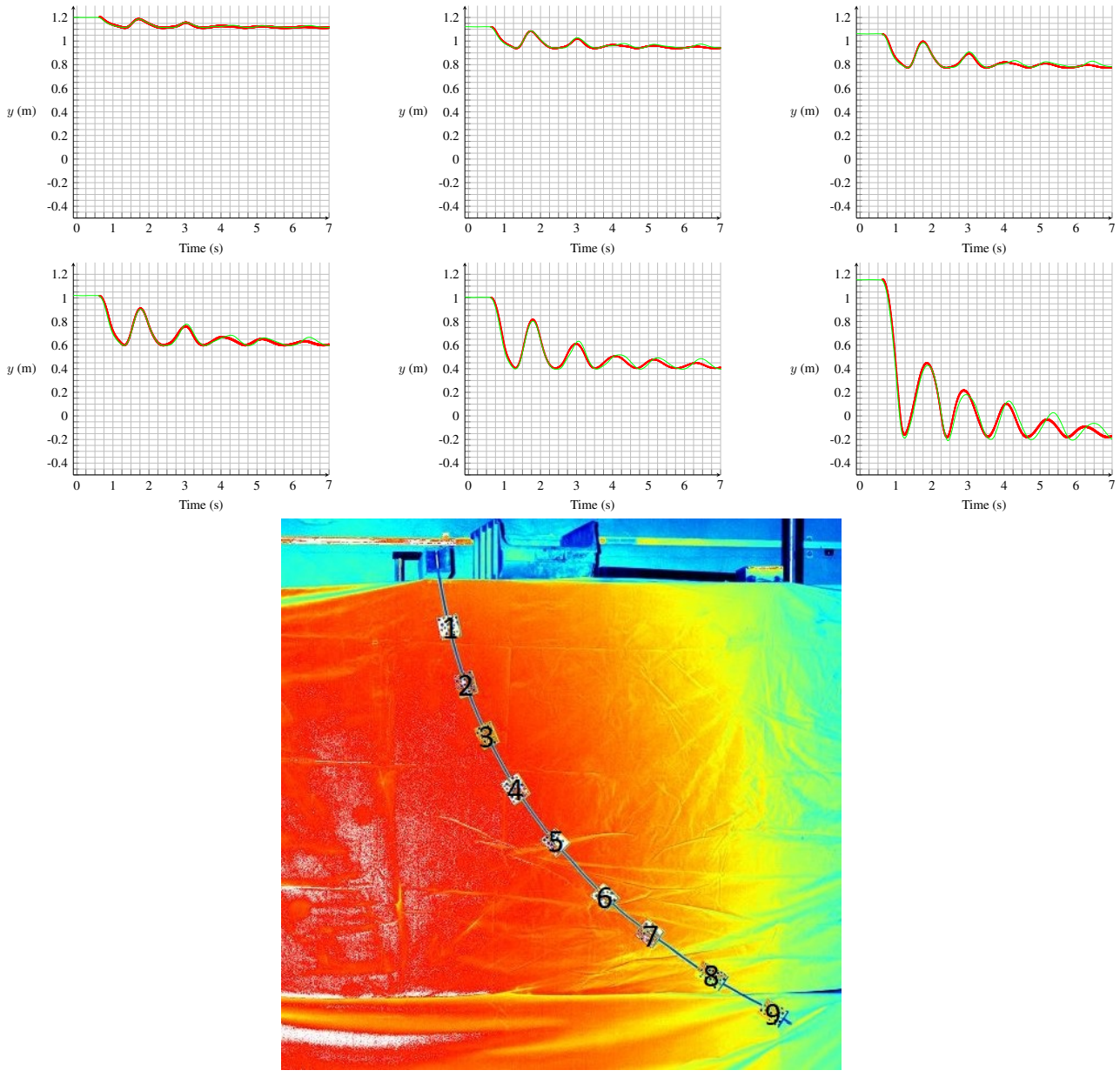

Figure 3.12: Trajectories of targets 1,2,3,4,5 and 8 obtained with a high speed camera (solid line —) and with FEM (solid line —)

3.4 Dynamics of a constrained cable

3.4.1 Discrete dynamics formulated as an inclusion

We assume that the cable is now subjected to inequality constraints which are given by

$$\mathbf{g}^{(j)}(\mathbf{q},t) \geqslant 0 \quad ; \quad j = 1, ..., m_i \ . \tag{3.45}$$

For instance, $\mathbf{g}$ can model the presence of an obstacle or friction.
The goal of the present approach is to take those constraints into account in the numerical process. The latter are considered at nodes of the system. Provided the finite element discretization, we can consider the vector of inequality constraints

$$\mathbf{g}(\mathbf{q},t) \geqslant 0 \ , \tag{3.46}$$

Each component of this vector is denoted as $\mathbf{g}^{(j)}$ and corresponds to the j^{th} constraint applied to the system. Let us introduce the following subset

$$\mathcal{C}(t) = \{\mathbf{q}, \quad \mathbf{g}(\mathbf{q},t) \geqslant 0\} \ , \tag{3.47}$$

where the dynamics are constrained to evolve in.
The smooth dynamics of the constrained cable is given as

$$\begin{cases} \mathbf{M}\dfrac{\mathrm{d}\mathbf{v}}{\mathrm{d}t} + \mathbf{C}\mathbf{v} + \mathbf{K}(\mathbf{q})\mathbf{q} = \mathbf{f} \\ \dfrac{\mathrm{d}\mathbf{q}}{\mathrm{d}t} = \mathbf{v} \\ \mathbf{q} \in \mathcal{C}(t) \end{cases} . \tag{3.48}$$

For perfect unilateral constraints, the reaction force is directed along the normal vector and when $\mathbf{g}^{(j)} > 0$ the reaction force is zero. This consideration leads to the Signorini formalism

$$\mathbf{g}^{(j)}(\mathbf{q},t) \geqslant 0, \quad \bar{\boldsymbol{\lambda}}^{(j)} \geqslant 0, \quad \bar{\boldsymbol{\lambda}}^{(j)}\mathbf{g}^{(j)}(\mathbf{q},t) = 0, \quad j = 1, ..., m_i \ , \tag{3.49}$$

which is denoted concisely as

$$\mathbf{0} \leqslant \mathbf{g}(\mathbf{q},t) \perp \bar{\boldsymbol{\lambda}} \geqslant \mathbf{0} \ . \tag{3.50}$$

As the system is subjected to unilateral conditions, the evolution of the general velocity is no longer smooth. Instead, we use the right limit of $\mathbf{v}$ denoted as $\mathbf{v}^+$ and the evolution problem is recast into the Karush-Kuhn-Tucker formalism as follows

$$\begin{cases} \mathbf{M}\dfrac{\mathrm{d}\mathbf{v}}{\mathrm{d}t} + \mathbf{C}\mathbf{v}^+ + \mathbf{K}(\mathbf{q})\mathbf{q} = \mathbf{f} + (\nabla_{\mathbf{q}}\mathbf{a})^\top\boldsymbol{\lambda} + (\nabla_{\mathbf{q}}\mathbf{g})^\top\bar{\boldsymbol{\lambda}} \\ \dfrac{\mathrm{d}\mathbf{q}}{\mathrm{d}t} = \mathbf{v}^+ \\ \mathbf{a}(\mathbf{q},t) = \mathbf{0} \\ \mathbf{0} \leqslant \mathbf{g}(\mathbf{q},t) \perp \bar{\boldsymbol{\lambda}} \geqslant \mathbf{0} \end{cases} , \tag{3.51}$$

where the vectors $\boldsymbol{\lambda}$ and $\bar{\boldsymbol{\lambda}}$ collects components $\boldsymbol{\lambda}^{(j)}$ and $\bar{\boldsymbol{\lambda}}^{(j)}$.
The vector given by $\nabla_{\mathbf{q}}\mathbf{g}^{(j)}$ is a normal vector to the frontier of $\mathcal{C}(t)$ and it is directed toward the admissible region $\mathcal{C}(t)$. In another words, the gradient of the constraints describes the outward normal cone to $\mathcal{C}(t)$ as

$$\mathcal{N}_{\mathcal{C}(t)}(\mathbf{q}) = \left\{ \begin{array}{r} \mathbf{s} \in \mathbb{R}^n \text{ such that } \mathbf{s} = -\displaystyle\sum_j^{m_i} \bar{\boldsymbol{\lambda}}^{(j)} \nabla_{\mathbf{q}}\mathbf{g}^{(j)} \\ \bar{\boldsymbol{\lambda}}^{(j)} \geqslant 0 \text{ for every } j \text{ s.t. } \mathbf{g}^{(j)} = 0 \end{array} \right\} . \tag{3.52}$$

The smooth dynamics can be written as an inclusion into $\mathcal{N}_{\mathcal{C}(t)}(\mathbf{q})$

$$\mathbf{M}\frac{\mathrm{d}\mathbf{v}}{\mathrm{d}t} + \mathbf{C}\mathbf{v}^+ + \mathbf{K}(\mathbf{q})\mathbf{q} - \mathbf{f} \in \mathcal{N}_{\mathcal{C}(t)}(\mathbf{q}) \ , \tag{3.53}$$

and the global discrete problem can be recast into a measure differential equation

$$\begin{cases} \mathbf{M}\mathrm{d}\mathbf{v} + \left[\mathbf{C}\mathbf{v}^+ + \mathbf{K}(\mathbf{q})\mathbf{q} - \mathbf{f}\right]\mathrm{d}t = \mathrm{d}\mathbf{s} \\ \mathrm{d}\mathbf{q} = \mathbf{v}^+\mathrm{d}t \\ \mathrm{d}\mathbf{s} \in -\mathcal{N}_{\mathcal{C}(t)}(\mathbf{q}) \end{cases} . \tag{3.54}$$

It is difficult in practice to satisfy the latter. This is the reason why we also define the tangent cone to the set $\mathcal{C}(t)$ as

$$\mathcal{T}_{\mathcal{C}(t)}(\mathbf{q}) = \left\{\mathbf{s} \in \mathbb{R}^n \ , \mathbf{s}^\top \nabla_{\mathbf{q}} \mathbf{g}^\alpha(\mathbf{q}, t) \geqslant 0 \ , \forall \alpha \in \mathcal{A}\right\} \ , \tag{3.55}$$

where we set

$$\mathcal{A} = \{\alpha \in [1, ..., n], \mathbf{g}^\alpha(\mathbf{q}, t) \leqslant 0\} \ . \tag{3.56}$$

According to Moreau Viability Lemma[29], the inclusion into $\mathcal{N}_{\mathcal{C}(t)}$ can be replaced by the inclusion into $\mathcal{N}_{\mathcal{T}_{\mathcal{C}(t)}(\mathbf{q})}(\mathbf{v}^+)$ if the time evolution starts with an admissible intial condition since in this case

$$\mathcal{N}_{\mathcal{T}_{\mathcal{C}(t)}(\mathbf{q})}(\mathbf{v}^+) \subset \mathcal{T}_{\mathcal{C}(t)}(\mathbf{q}) \ , \tag{3.57}$$

$$\begin{cases} \mathbf{M}\mathrm{d}\mathbf{v} + \left[\mathbf{C}\mathbf{v}^+ + \mathbf{K}(\mathbf{q})\mathbf{q} - \mathbf{f}\right]\mathrm{d}t = \mathrm{d}\mathbf{s} \\ \mathrm{d}\mathbf{q} = \mathbf{v}^+\mathrm{d}t \\ \mathrm{d}\mathbf{s} \in -\mathcal{N}_{\mathcal{T}_{\mathcal{C}(t)}(\mathbf{q})}(\mathbf{v}^+)(\mathbf{q}) \end{cases} . \tag{3.58}$$

In this section, we only considered unilateral condition since the difficulty is mainly due to treatment of the latter.
Injecting the measures expressions into (3.58) and splitting the dynamics with regards to measures yields

$$\begin{cases} \mathbf{M}\left[\mathbf{v}^+ - \mathbf{v}^-\right] = \mathbf{p} \\ \mathbf{M}\boldsymbol{\gamma}^+ + \left[\mathbf{C}\mathbf{v}^+ + \mathbf{K}(\mathbf{q})\mathbf{q} - \mathbf{f}\right] = \mathbf{0} \end{cases} . \tag{3.59}$$

3.4.2 Deriving a time-stepping scheme for the evolution problem

This section presents a time-integration scheme for the non-smooth time evolution problem given in (3.58). It can be seen at a particular update of a right-hand side via a One Step Non-Smooth Problem (OSNSP). The latter is obtained via discretizing the Moreau's Sweeping Process [29, Moreau] and computing the discrete evolution of the system between the step k and $k+1$.
A θ-method is endowed to approximate integrals with regards to Lebesgue measure over $[t_k, t_{k+1}]$ i.e.

$$\int_{t_k}^{t_{k+1}} \zeta(t)\mathrm{d}t \approx (t_{k+1} - t_k)\left[\theta\zeta(t_k) + (1-\theta)\zeta(t_{k+1})\right] \ . \tag{3.60}$$

We will refer to quantities evaluated in t_k (resp. t_{k+1}) as $\bullet_k$ (resp. $\bullet_{k+1}$) and the time step $(t_{k+1} - t_k)$ will be denoted h. The left hand side of (3.58) is obtained as

$$\begin{aligned} \int_{t_k}^{t_{k+1}} \mathbf{M}\mathrm{d}\mathbf{v} + \int_{t_k}^{t_{k+1}} \left[\mathbf{C}\mathbf{v}^+ + \mathbf{K}(\mathbf{q})\mathbf{q} - \mathbf{f}\right]\mathrm{d}t = \\ \mathbf{M}\left(\mathbf{v}_{k+1} - \mathbf{v}_k\right) + h\theta\left[\mathbf{C}\mathbf{v}^+ + \mathbf{K}(\mathbf{q})\mathbf{q} - \mathbf{f}\right]_k + h(1-\theta)\left[\mathbf{C}\mathbf{v}^+ + \mathbf{K}(\mathbf{q})\mathbf{q} - \mathbf{f}\right]_{k+1} \end{aligned} . \tag{3.61}$$

The integral of the impulse is given by

$$\int_{t_k}^{t_{k+1}} \mathrm{d}\mathbf{s} = \mathbf{p}_{k+1} \ . \tag{3.62}$$

The compatibility condition for position and velocity yields

$$\mathbf{q}_{k+1} = \mathbf{q}_k + h\theta\mathbf{v}_k + h(1-\theta)\mathbf{v}_{k+1} \ . \tag{3.63}$$

The overall dynamics in the global coordinate system reads

$$\begin{cases} \widehat{\mathbf{M}}_k \left(\mathbf{v}_{k+1} - \mathbf{v}_k\right) - \widehat{\mathbf{f}}_k = \mathbf{p}_{k+1} \\ \mathbf{q}_{k+1} = \mathbf{q}_k + h\theta\mathbf{v}_k + h(1-\theta)\mathbf{v}_{k+1} \end{cases} , \tag{3.64}$$

where we have set

$$\widehat{\mathbf{M}}_k = \mathbf{M} + h\theta\mathbf{C} + h^2\theta^2\Delta\mathbf{K}_k \ , \tag{3.65}$$

$$\widehat{\mathbf{f}}_k = h\theta\mathbf{f}_{k+1} + h(1-\theta)\mathbf{f}_k - h\mathbf{C}\mathbf{v}_k - h\mathbf{K}_k\mathbf{q}_k - h^2\theta\Delta\mathbf{K}_k\mathbf{v}_k \ , \tag{3.66}$$

$$\mathbf{p}_{k+1} = \int_{t_k}^{t_{k+1}} \mathrm{d}\mathbf{s} \ . \tag{3.67}$$

The velocity at the end of the time step is taken as

$$\mathbf{v}_{k+1} = \mathbf{v}_f + \Delta\mathbf{v}_{k+1} \ , \tag{3.68}$$

where $\mathbf{v}_f$ denotes the free velocity, i.e. the velocity of the system when the impact are null. The correction term $\Delta\mathbf{v}_{k+1}$ is computed via $\mathbf{p}_{k+1}$ which corresponds to unilateral constraints enforcement. Everything is gathered just below

$$\begin{cases} \mathbf{v}_{k+1} = \mathbf{v}_f + \widehat{\mathbf{M}}_k^{-1}\mathbf{p} \\ \mathbf{v}_f = \mathbf{v}_k + \widehat{\mathbf{M}}_k^{-1}\widehat{\mathbf{f}}_k \\ \mathbf{q}_{k+1} = \mathbf{q}_k + h\theta\mathbf{v}_k + h(1-\theta)\mathbf{v}_{k+1} \\ \mathbf{p} \approx \displaystyle\int_{t_k}^{t_{k+1}} \mathrm{d}\mathbf{s} \end{cases} . \tag{3.69}$$

We clearly see that the velocity computed as the end of the time step is a correction of the free-velocity, $\mathbf{v}_f$, due to the impact occurring at $t \in (t_k, t_{k+1}]$. If no impact occurs, i.e. $\mathbf{p} = \mathbf{0}$, then $\mathbf{v}_1 = \mathbf{v}_f$. Moreover, this scheme benefits of the unconditional stability of the θ-method for $0.5 < \theta \leqslant 1$.
Depending of the nature of the measure $\mathrm{d}\mathbf{s}$, several physical situations are described. Two cases are presented in the following sections: the impact dynamics (with Newton's law) and the frictional impact (with Newton's law and Coulomb friction) cases. Indeed, the value of $\mathbf{p}_{k+1}$ is the only value that has been left ambiguous in the above derivations but the latter need adequate developments.

3.4.3 Local kinematics and Delassus operator

This section is mainly designed to introduce some vocabulary and operators that will be of notable use in the sequel.
We are going to described the kinematics locally for a contacting point, i.e. a particle of the domain that is likely to close the distance between the studied system and an exterior geometry.

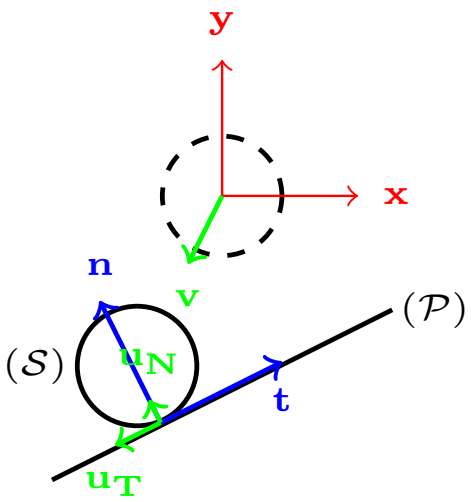

Figure 3.13: Cartesian and local frame of a ball, $(\mathcal{S})$, impacting an inclined plane, $(\mathcal{P})$

We are assuming that the distance between the studied domain $(\mathcal{S})$ and exterior geometries $(\mathcal{P})$ is given by a function $\mathbf{g}(\cdot)$. The function g is assumed to provide directly with the distance between $(\mathcal{S})$ and $(\mathcal{P})$, i.e. the minimum distance existing between $(\mathcal{S})$ particles and $(\mathcal{P})$ particles. Denoting by M and M' the points at concern, the relative velocity of $(\mathcal{S})$ with respect to $(\mathcal{P})$ reads

$$\mathbf{u} = \mathbf{v}(M) - \mathbf{v}(M') \ . \tag{3.70}$$

Those points are sometimes denoted as proximal points. A local frame is defined via the distance function $\mathbf{g}$. Indeed, as the latter is a signed distance between $(\mathcal{S})$ and $(\mathcal{P})$, a unit normal vector, $\mathbf{n}$ is given as the unit vector oriented in the direction $M'M$. Then, one or two tangential vectors are used to trace tangential components of the relative velocity.
The relative velocity is parted along its normal and tangential components and the subscript N and T will refer to normal and tangential components respectively. A 2D-representation of the local frame of a ball impact an inclined plane is visible in Figure 3.13.
Situations where a collection of contacting points are at stake will be accompanied with a superscript α which assesses for the 'active' contact between $(\mathcal{S})$ and $(\mathcal{P})$ at the considered time t. Transpose linear mapping which links the velocity in the reference frame and in the local frame are denoted as

$$\mathbf{u}_N = \mathbf{H}_N(\mathbf{q})\mathbf{v} \quad , \quad \text{Normal velocity at t} \ , \tag{3.71}$$
$$\mathbf{u}_T = \mathbf{H}_T(\mathbf{q})\mathbf{v} \quad , \quad \text{Tangential velocity at t} \ . \tag{3.72}$$

The local reaction forces $(\mathbf{r}_N, \mathbf{r}_T)$ can be projected back to the reference frame by using the transpose of $\mathbf{H}_N$ and $\mathbf{H}_T$ so that the forces created during contact are projected in the correct basis as

$$\mathbf{p} = {\mathbf{H}_N}^\top \mathbf{r}_N + {\mathbf{H}_T}^\top \mathbf{r}_T \ . \tag{3.73}$$

When we go back to dynamics, equations of the form

$$\mathbf{M}\frac{\mathrm{d}}{\mathrm{d}t}\mathbf{v} = \mathbf{f} + \mathbf{p} \ , \tag{3.74}$$

can be expressed with local variables by pre-multiplying by $\mathbf{H}_N\mathbf{M}^{-1}$ or $\mathbf{H}_T\mathbf{M}^{-1}$. This passage from reference to local frame is done via the Delassus operator which is defined as

$$\mathbf{W} = \begin{bmatrix} \mathbf{W}_{NN} & \mathbf{W}_{NT} \\ \mathbf{W}_{TN} & \mathbf{W}_{TT} \end{bmatrix} = \begin{bmatrix} \mathbf{H}_N\mathbf{M}^{-1}{\mathbf{H}_N}^\top & \mathbf{H}_N\mathbf{M}^{-1}{\mathbf{H}_T}^\top \\ \mathbf{H}_T\mathbf{M}^{-1}{\mathbf{H}_N}^\top & \mathbf{H}_T\mathbf{M}^{-1}{\mathbf{H}_T}^\top \end{bmatrix} \ . \tag{3.75}$$

Using the Delassus operator, the Cartesian dynamics can be projected into local dynamics as follows

$$\mathbf{M}\frac{\mathrm{d}}{\mathrm{d}t}\mathbf{v} = \mathbf{f} + \mathbf{p} \iff \frac{\mathrm{d}}{\mathrm{d}t}\mathbf{u} = \tilde{\mathbf{f}} + \mathbf{W}\mathbf{r} \ . \tag{3.76}$$

3.4.4 Dynamics with frictionless contact

The impact term is obtained via considering the following inclusion

$$\begin{cases} \mathbf{p} \in -\mathcal{N}_{\mathcal{T}_{\mathcal{C}(t)}(\widehat{\mathbf{q}})}\left(\dfrac{\mathbf{v}_{k+1} + e\mathbf{v}_k}{1+e}\right) \\ \widehat{\mathbf{q}} = \mathbf{q}_k + \gamma h \mathbf{v}_f \quad , \quad 0 \leqslant \gamma \leqslant 1 \end{cases} , \tag{3.77}$$

where e is a restitution coefficient describing an elastic impact law. The velocity of the particle subjected to the contact is restored with amplitude $e\mathbf{v}_0$ in the normal direction of the contacting surface.
The need for a restitution coefficient remains unclear for the case of continuum mechanics. However, finite element model are intrinsically discrete so that the usage of e is required. Moreover, the case of a finitely represented admissible domain can be written as a complementarity problem which is tractable numerically [1].
The kinematics at contacting points are described with local coordinates, namely tangent and normal velocities respectively associated to tangent and normal reactions. The latter will be denoted as follows

$$\mathbf{u}_{N,k+1} = \mathbf{H}_N(\mathbf{q}_{k+1})\mathbf{v}_{k+1} \quad , \quad \text{Normal velocity at t=}t_{k+1} \ , \tag{3.78}$$
$$\mathbf{u}_{Nk} = \mathbf{H}_N(\mathbf{q}_k)\mathbf{v}_k \quad , \quad \text{Normal velocity at t=}t_k \ , \tag{3.79}$$
$$\mathbf{u}_{T,k+1} = \mathbf{H}_T(\mathbf{q}_{k+1})\mathbf{v}_{k+1} \quad , \quad \text{Tangential velocity at t=}t_{k+1} \ , \tag{3.80}$$
$$\mathbf{u}_{Tk} = \mathbf{H}_T(\mathbf{q}_k)\mathbf{v}_k \quad , \quad \text{Tangential velocity at t=}t_k \ , \tag{3.81}$$

where the operators $\mathbf{H}_N$ and $\mathbf{H}_T$ are transpose linear mappings which project a vector along the corresponding component of the local basis centered at the contacting point (see Section 3.4.3 for details).
The use of the local kinematics is essential for all $\alpha \in \mathcal{A}$, the outward normal to the surface is given by the gradient of the unilateral constraints $\mathbf{H}_N^\alpha(\mathbf{q}) = \nabla_{\mathbf{q}}\mathbf{g}^\alpha(\mathbf{q})$. The velocity along this normal direction can be approximated as follows

$$\mathbf{u}_{Nk}^\alpha = \nabla_{\mathbf{q}}\mathbf{g}^\alpha(\mathbf{q}_k)^\top \mathbf{v}_k \ , \tag{3.82}$$
$$\mathbf{u}_{N,k+1}^\alpha = \nabla_{\mathbf{q}}\mathbf{g}^\alpha(\mathbf{q}_k)^\top \mathbf{v}_{k+1} \ , \tag{3.83}$$

where the active set is predicted according to $\mathbf{g}(\widehat{\mathbf{q}}) = \mathbf{g}\left(\mathbf{q}_0 + \gamma h \mathbf{v}_f\right)$, the latter corresponds to a discretized description of the tangent cone at $\mathbf{q}_0 + \gamma h \mathbf{v}_f$

$$\mathcal{A} = \{\alpha, \quad \mathbf{g}^\alpha(\widehat{\mathbf{q}}) \leqslant 0\} \ . \tag{3.84}$$

All α are collected and we can build a Linear Complemantarity Problem (LCP)

$$0 \leqslant \mathbf{r}_{N,k+1}^\alpha \perp \mathbf{u}_{N0}^\alpha + e\mathbf{u}_{N1}^\alpha \geqslant 0 \quad , \quad \forall \alpha \in \mathcal{A} \ . \tag{3.85}$$

The reaction forces vector is built and the velocity at t_{k+1} is recovered as

$$\begin{cases} \mathbf{v}_f = \widehat{\mathbf{M}}_k^{-1}\mathbf{f}_k \\ \mathbf{r}_{N,k+1} = \begin{cases} 0 \ , \ \alpha \notin \mathcal{A} \\ \mathbf{r}_{N,k+1}^\alpha \ , \ \alpha \in \mathcal{A} \end{cases} \\ \mathbf{p} = \nabla_{\mathbf{q}}\mathbf{g}(\mathbf{q}_k)\mathbf{r}_{N,k+1} \\ \mathbf{v}_{k+1} = \mathbf{v}_f + \widehat{\mathbf{M}}_k^{-1}\mathbf{p}_{k+1} \end{cases} . \tag{3.86}$$

The methodology described in the previously is coined as a OSNSP [1] and can be written in the form of a Linear Complementarity Problem (LCP). In the case of pure impact, reactions are purely normal. The key idea is to manipulate the equation so that the Delassus Operator appears in equation. Indeed, we have that

$$\begin{aligned}
&(\mathbf{v}_{k+1} - \mathbf{v}_f) = \widehat{\mathbf{M}}_k^{-1}\mathbf{p}_{k+1} \\
\Longrightarrow \quad &\mathbf{H}_N\mathbf{v}_{k+1} = \mathbf{H}_N\mathbf{v}_f + \mathbf{H}_N\widehat{\mathbf{M}}_k^{-1}\mathbf{p}_{k+1} \\
\Longrightarrow \quad &\mathbf{H}_N\mathbf{v}_{k+1} = \mathbf{H}_N\mathbf{v}_f + \mathbf{H}_N\widehat{\mathbf{M}}_k^{-1}\mathbf{H}_N{}^\top\mathbf{r}_{N,k+1} \\
\Longrightarrow \quad &\mathbf{u}_{Nk+1} = \mathbf{u}_{Nf} + \widehat{\mathbf{W}}_{NN}\mathbf{r}_{N,k+1}
\end{aligned}$$

The latter can be directly injected into the impact law so that

$$\begin{aligned}
&\mathbf{0} \leqslant \mathbf{r}^\alpha_{N,k+1} \perp \mathbf{u}^\alpha_{N,k+1} + e\mathbf{u}^\alpha_{Nk} \geqslant \mathbf{0} \\
\Longrightarrow \quad &\mathbf{0} \leqslant \mathbf{r}^\alpha_{N,k+1} \perp \widehat{\mathbf{W}}_{NN}\mathbf{r}^\alpha_{N,k+1} + \mathbf{u}^\alpha_{Nf} + e\mathbf{u}^\alpha_{Nk} \geqslant \mathbf{0} \\
\Longrightarrow \quad &\mathbf{0} \leqslant \mathbf{M}_{\text{lcp}}\mathbf{z}_{\text{lcp}} + \mathbf{q}_{\text{lcp}} \perp \mathbf{z}_{\text{lcp}} \geqslant \mathbf{0}
\end{aligned}$$

where

$$\mathbf{M}_{\text{lcp}} = \widehat{\mathbf{W}}_{NN} \quad , \quad \mathbf{q}_{\text{lcp}} = \mathbf{u}^\alpha_{Nf} + e\mathbf{u}^\alpha_{Nk} \quad , \quad \mathbf{z}_{\text{lcp}} = \mathbf{r}^\alpha_{N,k+1} \ .$$

A summary of the OSNSP, given in the process of computation reads

$$\begin{cases}
\mathbf{v}_f = \mathbf{v}_k + \widehat{\mathbf{M}}_k^{-1}\widehat{\mathbf{f}}_k \\
\mathbf{u}^\alpha_{Nf} = \mathbf{H}_N(t_k)^\alpha\mathbf{v}_f \\
\mathbf{u}^\alpha_{Nk} = \mathbf{H}_N(t_k)^\alpha\mathbf{v}_k \\
\forall \alpha \in \mathcal{A} \quad , \quad \text{Solve LCP:} \\
\left\{\mathbf{0} \leqslant \mathbf{r}^\alpha_{N,k+1} \perp \widehat{\mathbf{W}}_{NN}\mathbf{r}^\alpha_{N,k+1} + \mathbf{u}^\alpha_{Nf} + e\mathbf{u}^\alpha_{Nk} \geqslant \mathbf{0}\right. \ . \\
\mathbf{p}_{k+1} = \begin{cases} \mathbf{r}^\alpha_{N,k+1}\mathbf{H}_N{}^\top \forall \alpha \in \mathcal{A} \\ \mathbf{0} \quad , \quad \forall \alpha \notin \mathcal{A} \end{cases} \\
\widehat{\mathbf{M}}_k\left(\mathbf{v}_{k+1} - \mathbf{v}_f\right) = \mathbf{p}_{k+1}
\end{cases} \tag{3.87}$$

3.4.5 Dynamics with frictional contact

This section gives insights about the treatment of the frictional impact. Even though applications of this PhD work are directed toward cables, the formulation presented here stays applicable for any discrete mechanical system. First, generalities about Coulomb friction is recalled. Then the simplified case of the two-dimensional friction problem is presented. Eventually, a formulation for treating the general frictional contact is provided.
Numerical treatments are done with the Siconos[1] software developed by the INRIA-Tripop [2, Iniria-tripop]. Although various implementations of friction exist, the focus is drawn to a velocity-level formulation without any guidance imposed to the algorithm. Indeed, several works investigated the applications of this formulation and assessed for its robustness and versatility.

[1]Siconos is an open-source scientific software primarily targeted at modeling and simulating nonsmooth dynamical systems in C++ and in Python.

General aspects about the friction

The Coulomb friction model [5] has been written down as a series of observations to an experimental setup. It has been highlighted that when an object contacting a surface starts sliding along the surface, the tangential force applied on the object is proportional to the weight of the object and opposed to the object motion. The proportionality coefficient has been named later the Coulomb friction coefficient and the latter is only dependent on the kind of material considered.
The state of the art formulation is done via considering the following second-order cone

$$\mathbf{K} = \left\{ \mathbf{r} \in \mathbb{R}^3 \quad , \quad \|\mathbf{r}_T\| \leqslant \mu \mathbf{r}_N \right\} \ , \tag{3.88}$$

where $\mathbf{u}$ is the relative velocity at a contacting point. The tangential component of $\mathbf{u}$, denoted by $\mathbf{u}_T$, belongs to the plane which is orthogonal to the out-pointing normal vector to the contacting surface.
If a contact is active between $(\mathcal{S})$ and $(\mathcal{P})$, then $(\mathcal{P})$ exerts a reaction force on $(\mathcal{S})$ given by $\mathbf{r}$ and $(\mathcal{S})$ moves with relative velocity $\mathbf{u}$ with respect to $(\mathcal{P})$. The Coulomb law states that at least one the following statements is correct

- $(\mathcal{S})$ leaves the contact then $\mathbf{r} = \mathbf{0}$ and $\mathbf{u}_N \geqslant 0$;
- $(\mathcal{S})$ sticks to $(\mathcal{P})$ then $\mathbf{r} \in \mathbf{K}$ and $\mathbf{u} = \mathbf{0}$;
- $(\mathcal{S})$ slides along $(\mathcal{P})$ then $\mathbf{r} \in \partial\mathbf{K} - \{\mathbf{0}\}$, $\mathbf{u}_T = 0$ and $\exists \alpha > 0,\ \mathbf{r}_T = -\alpha \mathbf{u}_T$.

If a couple $(\mathbf{u}, \mathbf{r})$ satisfies the Coulomb law, we will write $(\mathbf{u}, \mathbf{r}) \in \mathcal{C}$. This formulation contains every possible scenario. In this work, we will rather keep the sophisticated structure of this problem without regularization and without rough simplifications.
Two approaches are used in the numerical process, therefore a quick oversight is proposed. First, the two dimensional case and its resolution via a LCP are detailed. Then, the general formulation of the frictional contact problem via a cone complementarity problem is given. The key references about its numerical treatment are provided.

Frictional contact formulated as a LCP (2D case)

The friction is added into consideration via considering a Coulomb friction law. The latter states that the tangential reaction is contained into a circle whose radius is proportional to the normal reaction. When the equality case is reached, i.e. the tangential reaction is on the circle, the relative velocity is non-zero. The latter can be written as follows for the time step $t = t_{k+1}$. The superscript $\cdot^{\alpha}$ are dropped for conciseness

$$\begin{cases} |\mathbf{r}_{T,k+1}| \leqslant \mu \mathbf{r}_{N,k+1} & \text{then} \quad \mathbf{u}_{T,k+1} = \mathbf{0} \\ |\mathbf{r}_{T,k+1}| = \mu \mathbf{r}_{N,k+1} & \text{then} \quad \mathbf{u}_{T,k+1} \propto -\mathbf{r}_{T,k+1} \end{cases} . \tag{3.89}$$

Here we present a derivation that enriches (3.87) with the friction law. The inequality (3.89) can be reformulated into the following

$$|\mathbf{r}_{T,k+1}| \leqslant \mu \mathbf{r}_{N,k+1} \begin{cases} \mathbf{0} \leqslant \mu \mathbf{r}_{N,k+1} - \mathbf{r}_{T,k+1} \perp \mathbf{u}^-_{T,k+1} \geqslant \mathbf{0} \\ \mathbf{0} \leqslant \mu \mathbf{r}_{N,k+1} + \mathbf{r}_{T,k+1} \perp \mathbf{u}^+_{T,k+1} \geqslant \mathbf{0} \end{cases} , \tag{3.90}$$

where the superscripts $\cdot^+$ and $\cdot^-$ refer to the positive part and negative part respectively.
The following change of variable is used

$$\begin{cases} \bar{\boldsymbol{\lambda}}_1 = \mu \mathbf{r}_{N,k+1} - \mathbf{r}_{T,k+1} \\ \bar{\boldsymbol{\lambda}}_2 = \mu \mathbf{r}_{N,k+1} + \mathbf{r}_{T,k+1} \end{cases} \quad \text{so that we have} \quad \begin{cases} \mathbf{r}_{T,k+1} = \mu \mathbf{r}_{N,k+1} - \bar{\boldsymbol{\lambda}}_1 \\ \bar{\boldsymbol{\lambda}}_2 = 2\mu \mathbf{r}_{N,k+1} - \bar{\boldsymbol{\lambda}}_1 \end{cases} . \tag{3.91}$$

A similar manipulation on the tangential relative velocity is performed as

$$\mathbf{u}_{T,k+1} = \mathbf{u}^{+}_{T,k+1} - \mathbf{u}^{-}_{T,k+1} \quad \Longleftrightarrow \quad \mathbf{u}^{-}_{T,k+1} = \mathbf{u}^{+}_{T,k+1} - \mathbf{u}_{T,k+1} \ . \tag{3.92}$$

The LCP given in (3.90) can be reformulated as

$$\begin{cases} \mathbf{0} \leqslant \mathbf{u}^{+}_{T,k+1} - \mathbf{u}_{T,k+1} \perp \bar{\boldsymbol{\lambda}}_1 \geqslant \mathbf{0} \\ \mathbf{0} \leqslant 2\mu\mathbf{r}_{N,k+1} - \bar{\boldsymbol{\lambda}}_1 \perp \mathbf{u}^{+}_{T,k+1} \geqslant \mathbf{0} \end{cases} . \tag{3.93}$$

A fully detailed derivation of the LCP with frictional impact is given for the reader understanding. The developments done in Section 3.4.4 are done again in the presence of friction. In this case, the tangential forces are non-zero so that

$$\begin{aligned} & (\mathbf{v}_{k+1} - \mathbf{v}_f) = \widehat{\mathbf{M}}_k^{-1}\mathbf{p}_{k+1} \\ \Longrightarrow \quad & \mathbf{H}_N\mathbf{v}_{k+1} = \mathbf{H}_N\mathbf{v}_f + \mathbf{H}_N\widehat{\mathbf{M}}_k^{-1}\mathbf{p}_{k+1} \\ \Longrightarrow \quad & \mathbf{H}_N\mathbf{v}_{k+1} = \mathbf{H}_N\mathbf{v}_f + \mathbf{H}_N\widehat{\mathbf{M}}_k^{-1}\left(\mathbf{H}_N{}^{\top}\mathbf{r}_{N,k+1} + \mathbf{H}_T{}^{\top}\mathbf{r}_{T,k+1}\right) \\ & \Longrightarrow \quad \begin{cases} \mathbf{u}_{Nk+1} = \mathbf{u}_{Nf} + \widehat{\mathbf{W}}_{NN}\mathbf{r}_{N,k+1} + \widehat{\mathbf{W}}_{NT}\mathbf{r}_{T,k+1} \\ \mathbf{u}_{Tk+1} = \mathbf{u}_{Tf} + \widehat{\mathbf{W}}_{TN}\mathbf{r}_{N,k+1} + \widehat{\mathbf{W}}_{TT}\mathbf{r}_{T,k+1} \end{cases} \end{aligned}$$

Lagrange multipliers associated to the tangential reaction are substituted to the other variables presented into (3.91). So that we have

$$\begin{cases} \mathbf{u}_{Nk+1} = \mathbf{u}_{Nf} + \widehat{\mathbf{W}}_{NN}\mathbf{r}_{N,k+1} + \widehat{\mathbf{W}}_{NT}\left(\mu\mathbf{r}_{N,k+1} - \bar{\boldsymbol{\lambda}}_1\right) \\ \mathbf{u}_{Tk+1} = \mathbf{u}_{Tf} + \widehat{\mathbf{W}}_{TN}\mathbf{r}_{N,k+1} + \widehat{\mathbf{W}}_{TT}\left(\mu\mathbf{r}_{N,k+1} - \bar{\boldsymbol{\lambda}}_1\right) \end{cases} . \tag{3.94}$$

The latter can be substituted jointly into the impact law and the friction law, then (3.94) is substituted so that

$$\begin{aligned} & \begin{cases} \mathbf{0} \leqslant \mathbf{u}_{N,k+1} + e\mathbf{u}_{Nk} \perp \mathbf{r}_{N,k+1} \geqslant \mathbf{0} \\ \mathbf{0} \leqslant \mathbf{u}^{+}_{T,k+1} - \mathbf{u}_{T,k+1} \perp \bar{\boldsymbol{\lambda}}_1 \geqslant \mathbf{0} \\ \mathbf{0} \leqslant 2\mu\mathbf{r}_{N,k+1} - \bar{\boldsymbol{\lambda}}_1 \perp \mathbf{u}^{+}_{T,k+1} \end{cases} \\ \Longrightarrow \quad & \begin{cases} \mathbf{0} \leqslant \widehat{\mathbf{W}}_{NN}\mathbf{r}_{N,k+1} + \widehat{\mathbf{W}}_{NT}\left(\mu\mathbf{r}_{N,k+1} - \bar{\boldsymbol{\lambda}}_1\right) + \mathbf{u}_{Nf} + e\mathbf{u}_{Nk} \perp \mathbf{r}_{N,k+1} \geqslant \mathbf{0} \\ \mathbf{0} \leqslant -\widehat{\mathbf{W}}_{TN}\mathbf{r}_{N,k+1} - \widehat{\mathbf{W}}_{TT}\left(\mu\mathbf{r}_{N,k+1} - \bar{\boldsymbol{\lambda}}_1\right) + \mathbf{u}^{+}_{T,k+1} - \mathbf{u}_{Tf} \perp \bar{\boldsymbol{\lambda}}_1 \geqslant \mathbf{0} \\ \mathbf{0} \leqslant 2\mu\mathbf{r}_{N,k+1} - \bar{\boldsymbol{\lambda}}_1 \perp \mathbf{u}^{+}_{T,k+1} \end{cases} \\ \Longrightarrow \quad & \mathbf{0} \leqslant \mathbf{M}_{\text{lcp}}\mathbf{z}_{\text{lcp}} + \mathbf{q}_{\text{lcp}} \perp \mathbf{z}_{\text{lcp}} \geqslant \mathbf{0} \end{aligned}$$

where

$$\mathbf{M}_{\text{lcp}} = \begin{bmatrix} \widehat{\mathbf{W}}_{NN} + \mu\widehat{\mathbf{W}}_{NT} & -\widehat{\mathbf{W}}_{NT} & \mathbf{0} \\ -\widehat{\mathbf{W}}_{TN} - \mu\widehat{\mathbf{W}}_{TT} & \widehat{\mathbf{W}}_{TT} & \mathbf{I} \\ 2\mu\mathbf{I} & -\mathbf{I} & \mathbf{0} \end{bmatrix} \quad , \quad \mathbf{q}_{\text{lcp}} = \begin{bmatrix} \mathbf{u}_{Nf} + e\mathbf{u}_{Nk} \\ -\mathbf{u}_{Tf} \\ \mathbf{0} \end{bmatrix} \quad , \quad \mathbf{z}_{\text{lcp}} = \begin{bmatrix} \mathbf{r}_{N,k+1} \\ \bar{\boldsymbol{\lambda}}_1 \\ \mathbf{u}^{+}_{T,k+1} \end{bmatrix} .$$

The OSNSP problem for frictional impact reads

$$\begin{cases} \mathbf{v}_f = \mathbf{v}_k + \widehat{\mathbf{M}}_k^{-1}\widehat{\mathbf{f}}_k \\ \mathbf{u}_{Nf}^\alpha = \mathbf{H}_N(t_k)^\alpha \mathbf{v}_f \\ \mathbf{u}_{Nk}^\alpha = \mathbf{H}_N(t_k)^\alpha \mathbf{v}_k \\ \mathbf{u}_{Tf}^\alpha = \mathbf{H}_T(t_k)^\alpha \mathbf{v}_f \\ \\ \forall \alpha \in \mathcal{A} \quad , \quad \text{Solve LCP:} \\ \begin{cases} \mathbf{0} \leqslant \widehat{\mathbf{W}}_{NN}\bar{\boldsymbol{\lambda}}_{N,k+1}^\alpha + \widehat{\mathbf{W}}_{NT}\left(\mu\bar{\boldsymbol{\lambda}}_{N,k+1}^\alpha - \bar{\boldsymbol{\lambda}}_1^\alpha\right) + \mathbf{u}_{Nf}^\alpha + e\mathbf{u}_{Nk}^\alpha \perp \mathbf{r}_{N,k+1}^\alpha \geqslant \mathbf{0} \\ \mathbf{0} \leqslant -\widehat{\mathbf{W}}_{TN}\mathbf{r}_{N,k+1}^\alpha - \widehat{\mathbf{W}}_{TT}\left(\mu\mathbf{r}_{N,k+1}^\alpha - \bar{\boldsymbol{\lambda}}_1^\alpha\right) + \mathbf{u}_{T,k+1}^{+,\alpha} - \mathbf{u}_{Tf}^\alpha \perp \bar{\boldsymbol{\lambda}}_1^\alpha \geqslant \mathbf{0} \\ \mathbf{0} \leqslant 2\mu\mathbf{r}_{N,k+1}^\alpha - \bar{\boldsymbol{\lambda}}_1^\alpha \perp \mathbf{u}_{T,k+1}^{+,\alpha} \geqslant \mathbf{0} \end{cases} \\ \\ \mathbf{p}_{k+1} = \begin{cases} \mathbf{r}_{N,k+1}^\alpha {\mathbf{H}_N}^\top + \left(\mu\mathbf{r}_{N,k+1}^\alpha - \bar{\boldsymbol{\lambda}}_1^\alpha\right){\mathbf{H}_T}^\top & , \quad \forall \alpha \in \mathcal{A} \\ \mathbf{0} & , \quad \forall \alpha \notin \mathcal{A} \end{cases} \\ \widehat{\mathbf{M}}_k\left(\mathbf{v}_{k+1} - \mathbf{v}_f\right) = \mathbf{p}_{k+1} \end{cases} \tag{3.95}$$

If the geometry is simple enough, this 2D friction case can be used to simulate the friction occurring at the interface between the cable and its surroundings.

Another choice of variables

We derive $\mathbf{M}_{\text{lcp}}$ as a consequence of the choice of $\mathbf{z}_{\text{lcp}}$. Another choice possible is

$$\mathbf{M}_{\text{lcp}} = \begin{bmatrix} \widehat{\mathbf{W}}_{NN} - \mu\widehat{\mathbf{W}}_{NT} & \widehat{\mathbf{W}}_{NT} & \mathbf{0} \\ \widehat{\mathbf{W}}_{TN} - \mu\widehat{\mathbf{W}}_{TT} & \widehat{\mathbf{W}}_{TT} & \mathbf{I} \\ 2\mu\mathbf{I} & -\mathbf{I} & \mathbf{0} \end{bmatrix} \quad , \quad \mathbf{q}_{\text{lcp}} = \begin{bmatrix} \mathbf{u}_{Nf} + e\mathbf{u}_{Nk} \\ \mathbf{u}_{Tf} \\ \mathbf{0} \end{bmatrix} \quad , \quad \mathbf{z}_{\text{lcp}} = \begin{bmatrix} \mathbf{r}_{N,k+1} \\ \bar{\boldsymbol{\lambda}}_2 \\ \mathbf{u}_{T,k+1}^- \end{bmatrix} .$$

By this choice, one should also compute the impact as follows

$$\mathbf{p}_{k+1} = \begin{cases} \mathbf{r}_{N,k+1}^\alpha {\mathbf{H}_N}^\top + \left(\bar{\boldsymbol{\lambda}}_2^\alpha - \mu\mathbf{r}_{N,k+1}^\alpha\right){\mathbf{H}_T}^\top & , \quad \forall \alpha \in \mathcal{A} \\ \mathbf{0} & , \quad \forall \alpha \notin \mathcal{A} \end{cases} .$$

Solving the LCPs corresponding to the OSNSP

In order to solve the LCP, we used the library provided in the Siconos platform developed at the INRIA [2].
The preferred numerical alternative is the Lemke pivot [27] since it solves exactly the LCP provided that a solution exists.

Frictional impact formulated as a cone complementarity problem (3D Case)

Let us introduce the dual cone to $\mathbf{K}$ given by

$$\mathbf{K}^* = \left\{\mathbf{u} \in \mathbb{R}^3 \quad , \quad \forall \mathbf{r} \in \mathbf{K} \quad , \quad \mathbf{u}\cdot\mathbf{r} \geqslant 0\right\} . \tag{3.96}$$

In their paper, De Saxcé and Feng [12] proved the following theorem

$$(\mathbf{u}, \mathbf{r}) \in \mathcal{C} \iff \mathbf{K}^* \ni \tilde{\mathbf{u}} \perp \mathbf{r} \in \mathbf{K} , \tag{3.97}$$

where the following change of variable is performed

$$\tilde{\mathbf{u}} = \mathbf{u} + \mu \left\|\mathbf{u}_T\right\| \mathbf{n} . \tag{3.98}$$

The proof of (3.97) is done via the bipotential for the contact law. This theorem opens with the possibility of computing fast and accurate solution for time-evolution problem with frictional impact for instance in [1, 8].
Numerical solutions to this formulation are sought in the following form

$$\begin{cases} \mathbf{u}_{k+1} = \widehat{\mathbf{W}}\mathbf{r}_{k+1} + \tilde{\mathbf{u}}_f \\ \tilde{\mathbf{u}}_{k+1} = \mathbf{u}_{k+1} + \begin{bmatrix} \mu \left\| \mathbf{u}_{T,k+1} \right\| \\ 0 \\ 0 \end{bmatrix} \\ \mathbf{K}^* \ni \tilde{\mathbf{u}}_{k+1} \perp \mathbf{r}_{k+1} \in \mathbf{K} \end{cases} . \tag{3.99}$$

Although some practical implementations still rely on unproved algorithms, this formulation appears far more robust than other approaches and a lot of solvers use this formulation. Later on the manuscript, frictional contact will be solved with the solver fc2d (or fc3d) available in the Siconos software[2].

3.4.6 Equality constraints embedding

The cable can also be subjected to equality constraints. But it is computationally heavy to trace all Lagrange multipliers and constraints satisfaction. It is more interesting to project the generalized positions and velocities into the kernel of the gradient of the equality constraints. Indeed, if we consider the equality constraints given by $\mathbf{a}$ in vector form, we have

$$\mathbf{0} = \mathbf{a}(\mathbf{q}_{k+1}) = \mathbf{a}(\mathbf{q}_k + (\mathbf{q}_{k+1} - \mathbf{q}_k)) \approx \mathbf{a}(\mathbf{q}_k) + \nabla_{\mathbf{q}}\mathbf{a}(\mathbf{q}_k)\left(\mathbf{q}_{k+1} - \mathbf{q}_k\right) , \tag{3.100}$$

$$\mathbf{0} = \frac{\mathrm{d}}{\mathrm{d}t}\left(\mathbf{a}(\mathbf{q}_{k+1})\right) = \nabla_{\mathbf{q}}\mathbf{a}(\mathbf{q}_k)\frac{\mathrm{d}}{\mathrm{d}t}\mathbf{q}_{k+1} \approx \nabla_{\mathbf{q}}\mathbf{a}(\mathbf{q}_k)\mathbf{v}_{k+1} . \tag{3.101}$$

The latter provides with 2 inclusions that can be used to project the dynamics suitably

$$\left[\mathbf{q}_{k+1} - \mathbf{q}_k + \nabla_{\mathbf{q}}\mathbf{a}(\mathbf{q}_k)^{-1}\mathbf{a}(\mathbf{q}_k)\right] \in \mathbf{ker}\left(\nabla_{\mathbf{q}}\mathbf{a}(\mathbf{q}_k)\right) , \tag{3.102}$$

$$\mathbf{v}_{k+1} \in \mathbf{ker}\left(\nabla_{\mathbf{q}}\mathbf{a}(\mathbf{q}_k)\right) . \tag{3.103}$$

3.4.7 Possible applications

The possibility offered by unilateral constraints including frictions are numerous. Among research examples one could cite the cable-pendulum falling against a wall, the bouncing of a cable against a circular obstacle, the shape-finding of a fish-net, the rockfall problem, the bouncing-ball paradigm, the mooring line knots, the sliding of a cable against a sheave. The scope of this work is way beyond the case of cable-cars. Every single system in this list is an ode to complexity and sophisticated dynamics. For each possible situation where impact and friction are considered, there is a wide variety of behavior and phenomenon. Although every single system are interesting, we present here different examples which illustrate key aspects of the dynamics that should be rendered in our future developments in the cable-car domain.

3.5 Applications to various systems with frictional contact

This section is dedicated to the application of the described numerical procedures in several cases. Those cases are mostly academic examples to illustrate the method and the interaction between the cable FE and the non-smooth dynamics.

[2]Documentations and basic formulations can be found online here `https://nonsmooth.gricad-pages.univ-grenoble-alpes.fr/siconos/users_guide/problems_and_solvers/friction_contact.html`

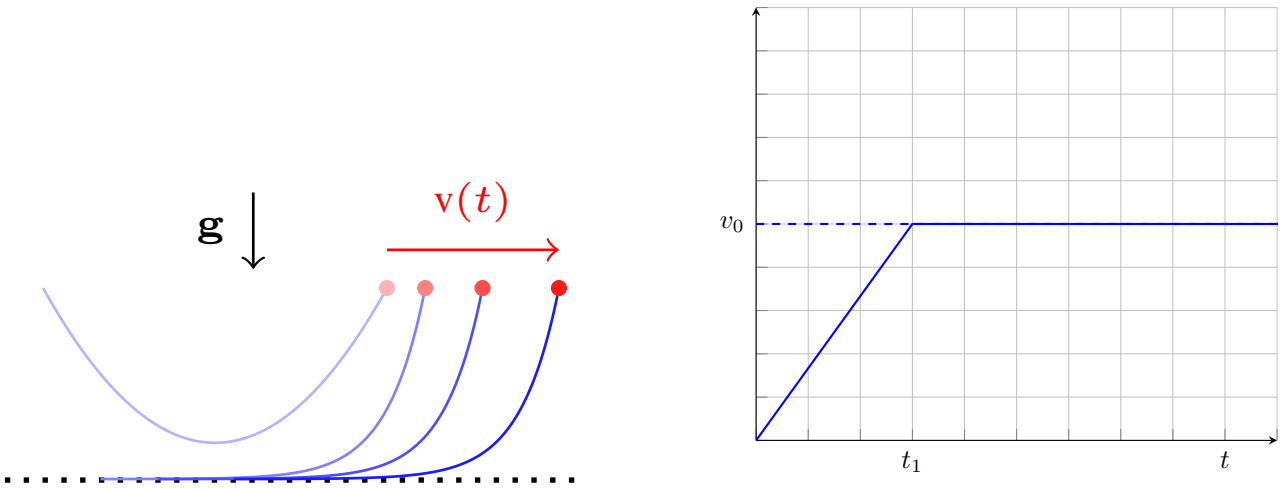

Figure 3.14: (Left) Dragged cable contacting the floor - (Right) Driving velocity

3.5.1 Cable dragged against the floor

This simulation consists on three phases. Starting from an initial position where the cable takes a catenary shape, then the left tip is released and falls in a pendulum-like motion. When the cable is set on the floor, the right tip of the cable is pulled with a controlled velocity. All along the motion, the contact mechanics may be activated and friction is considered.
The situation is simple and allows us to see how the friction and the cable finite element interact. The effect of meshing and time-steps can be investigated on this simple model before moving to more sophisticated situations and geometries.
The simulation is performed in a two-dimensional framework and the floor is modeled via a linear function $\mathbf{g}(\mathbf{q}) = \mathbf{G}\mathbf{q}$ which selects the vertical dofs of the cable. The piecewise definition of the driving velocity is

$$v(t) = \begin{cases} v_0 \dfrac{t}{t_1} & , \quad 0 \leqslant t \leqslant t_1 \\ v_0 & , \quad t_1 < t \leqslant t_2 \end{cases} . \tag{3.104}$$

The situation is illustrated in Figure 3.14. The main goal of this simple test is to assess the ability of the FE to trace a large displacement motion with a global translation motion. We want to check if the FEM is valid to trace both the global translation and the small vibration around it in particular. This first example highlights the idea that two displacement mechanisms are at stake and that the scaling between both does not affect the FEM precision. Here the parameters used for this example are given in Table 3.2. We see in Figure 3.15 that the ratio $\frac{\mathbf{r}_T}{\mathbf{r}_N}$ is varying a lot during the transient dynamics. The latter is erratic which displays the interest of including the friction as a nonsmooth problem. Those complex behaviors could explain some tension fluctuation at contact for the cable that cannot be explained by the freefall and the vibration alone. The evolution of the ratio may be smooth or non-smooth (jumps) however there is a common trend to converge toward a purely resisting friction. This goes in favor of assuming the friction equality case for established regime.

3.5.2 The conveyor-belt system

The conveyor-belt system is the perfect example of a system with an imposed velocity with friction along the pulling zone. Indeed, the sheaves are known to exhibit at least one slipping-contact zone and one stick-contact zone [9].

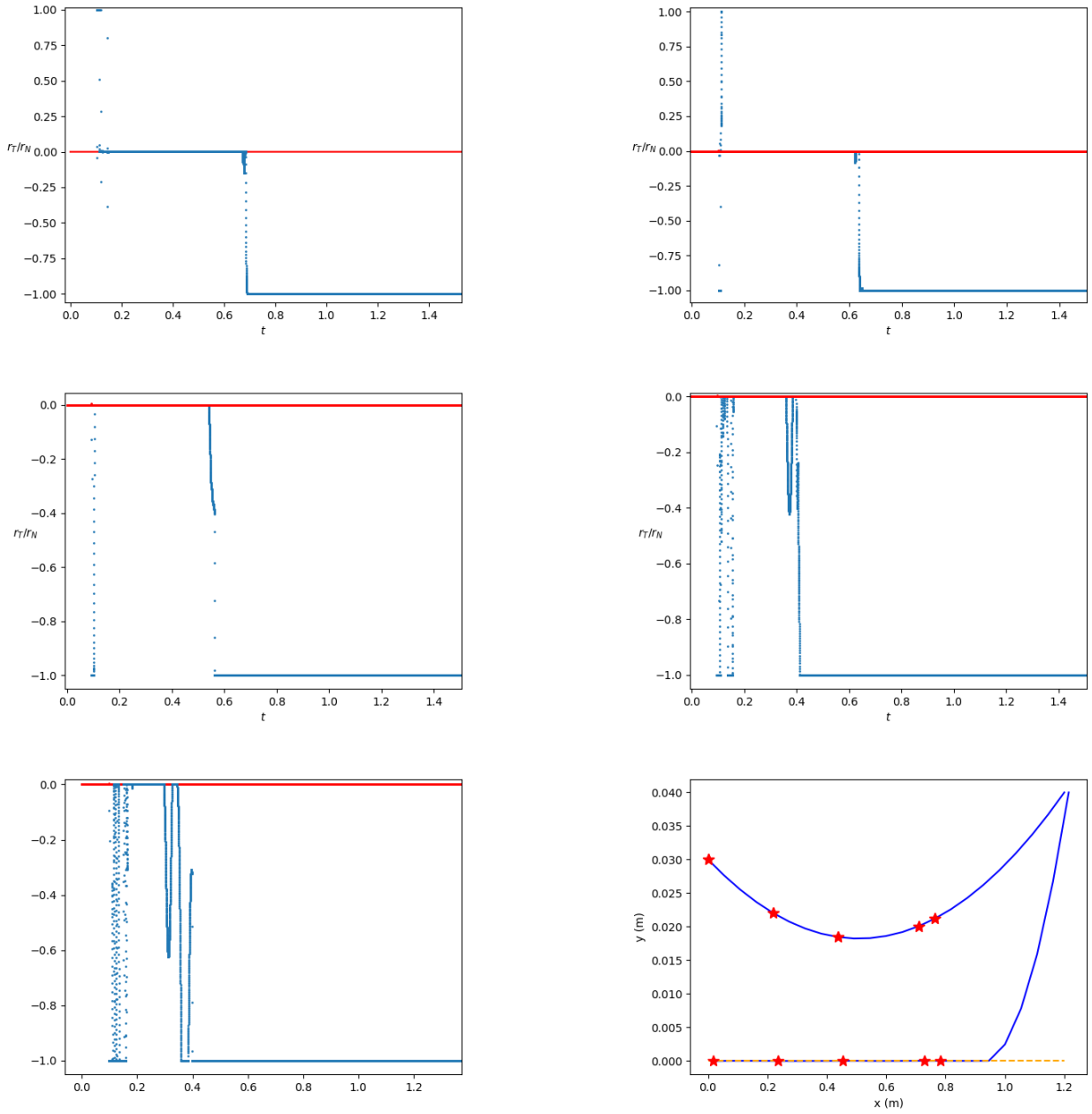

Figure 3.15: Ratio of the tangential by the normal component of the ground reaction for the 1st, 5th, 9th, 14th and 15th node of the cable versus time in seconds - Nodes are represented on the cable by a $\star$

Table 3.2: Parameters used for the simulation of a dragged cable with a contacting floor

Attributes	Values	Attributes	Values
EA (N)	30400	h (s)	6.67×10^{-5}
ρ (kg.m^{-1})	0.15	μ	1
α (kg.m^{-1}.s^{-1})	0.011	θ	1
L (m)	1.2	γ	0
x_0 (m)	$[0, 0.03]^\top$	e	0
x_L (m)	$[1.2, 0.04]^\top$		

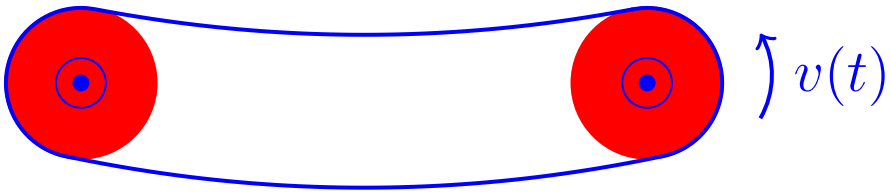

Figure 3.16: A cable pulled by a driving sheave at velocity $v(t)$

Table 3.3: Parameters used for the simulation of a conveyor belt

Attributes	Values	Attributes	Values
EA (N)	30400	h (s)	3.33×10^{-4}
ρ (kg.m^{-1})	0.096	μ	1
α (kg.m^{-1}.s^{-1})	0.011	θ	1
L (m)	1.2	γ	0
x_{P_1} (m)	$[0, 0]^\top$	R_1 (m)	0.05
x_{P_2} (m)	$[0.45, 0]^\top$	R_2 (m)	0.05
e	0		

However, the modeling of the latter remains an open question of computing. The majority of the approaches tends to ignore the direct modeling of the sheaves and rather focus on the influence of the driven and driving velocities on the vibration of the belt. It leads to interpret the dynamics as a perturbation of a rigid-body motion directly imposed by the sheave. FEM allow to embody the sheaves, the velocities of every sheave and the interaction between the belt and each interface (friction).
Here we modeled the sheaves as perfect circles of given radius and the belt is composed of cable elements. Parameters are given in Table 3.3. The system is closed in the sense that the first and last nodes are the same. The velocity of the sheaves are inputs and the combined effect of tension, friction and the velocity should suffice to create a flow of cable as illustrated in Figure 3.16. This modeling choice avoids the dilemma of imposing a status to each nodes (contacting, slipping, sticking or free of the contact) and allows to trace sophisticated mechanisms on the sheave interface.
Several observations can be made on that system:

- Once the stationary regime is reached, the global energy of the system remains the same. However the kinetic energy of one given node follows a cycle of progressive energy de-load until entering the driving sheave again;
- Along the sheave interface, a very stiff stick-slip phenomenon seems to appear which creates some oscillations and may cause numerical errors if not treated with a very refined time step size;
- The overall motion looks like a vibration around a mean position of the belt which goes in favor of some simplification of the dynamics in analytical or pseudo-analytical treatments of the PDEs. The vibration seems directly related to the driving velocity. Indeed, each moment where a cable segment leaves the contact creates a periodic excitation due to the tension variation rate at the sheave exit;
- The increase (or decrease) of the tension due to the resistant effect of the friction can be traced. Moreover the tension of the belt does not vary significantly around the static equilibrium which is visible in Figure 3.17.

The simple model shows effectively the bias in the choice of representation of the system. Indeed, one can choose to represent the motion in a local or global way. If we look at the trajectory of one given node, the motion looks strongly modulated and erratic whereas if we look at the global trajectory, i.e. screenshots of the whole belt at given moment, the motion seems more fluid and to follow an overall path. This is exactly the difference between the Lagrangian and Eulerian viewpoint which is illustrated in Figure 3.18. This highlights the pros and the cons of each representation:

- The Lagrangian viewpoint access to the particular dynamics with accuracy and permits to trace friction forces. The latter is not adapted to have an idea about the overall system since it only accounts for the motion of a node;
- The Eulerian viewpoint access the global dynamics of the system and the envelope of the motion. This representation seems adapted to the visualization of the global system trend which carries an information about the design of a physical system.

Depending on the application both formulations remain of interest. The Eulerian viewpoint seems more transportable to analytical developments in the means of reduced-order-model. The different possible representation choices should be adapted to the situation although the Eulerian viewpoint seems more likely to be used for design purpose and engineering. The Lagrangian viewpoint is more adapted for local information which can be of interest if a particular point of a system is at stake. Focus can be drawn to a specific node or cable segment which is essential if we want to follow the grip of a cabin for example.

3.6 Modes of constrained cables

A wide-range of mechanical applications relies on the concept of modes. Even though the constrained dynamics can be computed, an overall understanding of the system physics and its basic responses remains a strong tool for design. In order to simplify the analysis and to reduce the number of dofs, a basis suitable for projecting the dynamics is needed. This is why deriving modes is at stake in dynamics. The closer the mode is to the physics, the more accurate the prediction is.
We can take advantage of the constrained formalism to build an associated linear system. Indeed, let us consider that $\mathbf{q}$ corresponds to an equilibrium of (3.51) i.e.

$$\begin{cases} \mathbf{0} = \mathbf{M}\dfrac{\mathrm{d}\mathbf{v}}{\mathrm{d}t} + \mathbf{C}\mathbf{v} + \mathbf{K}(\mathbf{q})\mathbf{q} - \mathbf{f} - (\nabla_{\mathbf{q}}\mathbf{a})^{\top}\boldsymbol{\lambda} - (\nabla_{\mathbf{q}}\mathbf{g})^{\top}\bar{\boldsymbol{\lambda}} \\ \mathbf{0} = \dfrac{\mathrm{d}\mathbf{q}}{\mathrm{d}t} - \mathbf{v} \\ \mathbf{0} = \mathbf{a}(\mathbf{q}) \\ \mathbf{0} \leqslant \mathbf{g}(\mathbf{q}) \perp \bar{\boldsymbol{\lambda}} \geqslant \mathbf{0} \end{cases} . \tag{3.105}$$

We use here a subscript $\mathcal{A}$ to refer to active constraints. If $\mathbf{q}$ corresponds to an equilibrium, we can simplify the latter as

$$\begin{cases} \mathbf{0} = \mathbf{K}(\mathbf{q})\mathbf{q} - \mathbf{f} - (\nabla_{\mathbf{q}}\mathbf{a})^{\top}\boldsymbol{\lambda} - (\nabla_{\mathbf{q}}\mathbf{g})^{\top}\bar{\boldsymbol{\lambda}} \\ \mathbf{0} = \mathbf{a}(\mathbf{q}) \\ \mathbf{0} = \mathbf{g}_{\mathcal{A}}(\mathbf{q}) \quad \text{and} \quad \mathbf{0} = \bar{\boldsymbol{\lambda}}_{\bar{\mathcal{A}}} \end{cases} , \tag{3.106}$$

where we can assume

$$\mathbf{g}(\mathbf{q}) = \begin{bmatrix} \mathbf{g}_{\mathcal{A}}(\mathbf{q}) \\ \mathbf{g}_{\bar{\mathcal{A}}}(\mathbf{q}) \end{bmatrix} \quad ; \quad \bar{\boldsymbol{\lambda}} = \begin{bmatrix} \bar{\boldsymbol{\lambda}}_{\mathcal{A}} \\ \bar{\boldsymbol{\lambda}}_{\bar{\mathcal{A}}} \end{bmatrix} \tag{3.107}$$

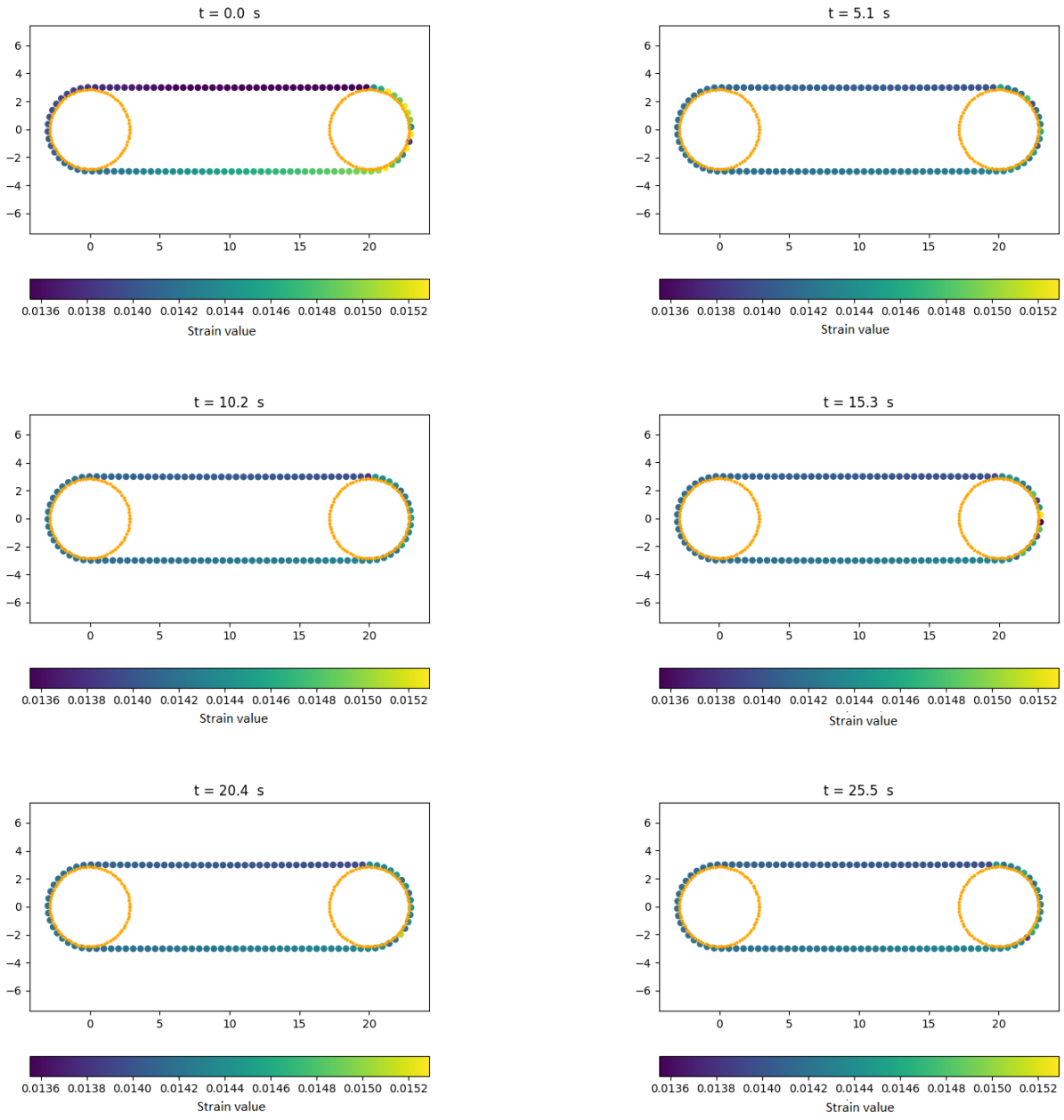

Figure 3.17: Strain along the belt; Axis in meters; A snapshot every five seconds

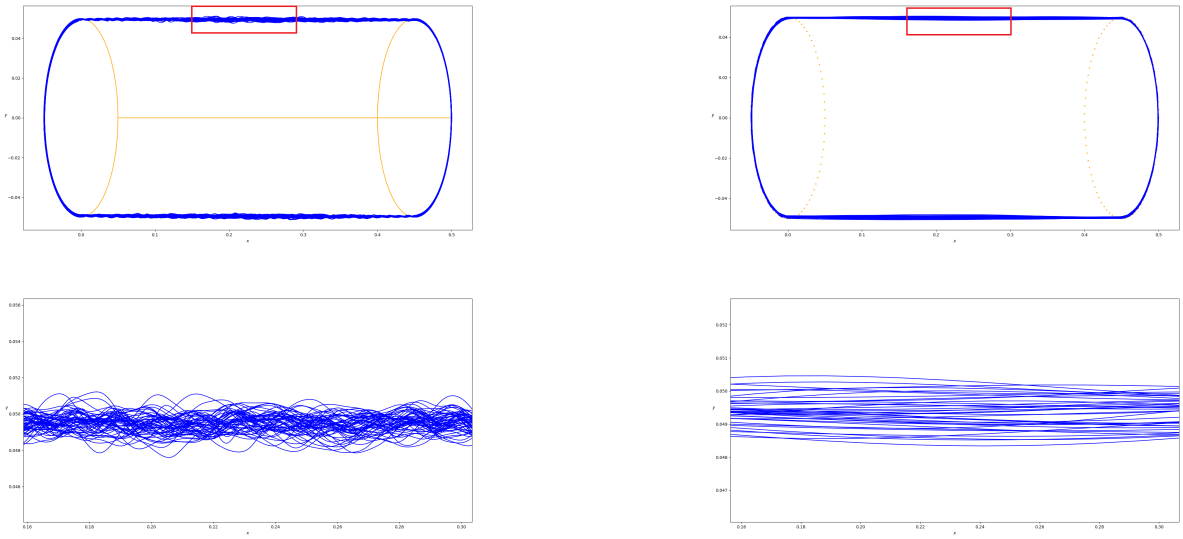

Figure 3.18: Differences between the Lagrangian (one node followed for the whole simulation - left) and Eulerian viewpoint (a belt snapshot every second - right) for a belt-sheave; Axis in meters; The zoomed area correspond to the red rectangle

We are now interested into a small undamped vibration around this equilibrium. The latter reads

$$\begin{cases} \mathbf{0} = \mathbf{M}\ddot{\mathbf{u}} + \mathbf{K}(\mathbf{q}+\mathbf{u})(\mathbf{q}+\mathbf{u}) - \mathbf{f} - (\nabla_{\mathbf{q}}\mathbf{a})^{\top}(\boldsymbol{\lambda}_{\mathbf{q}} + \boldsymbol{\lambda}_{\mathbf{u}}) - (\nabla_{\mathbf{q}}\mathbf{g})^{\top}(\bar{\boldsymbol{\lambda}}_{\mathbf{q}} + \bar{\boldsymbol{\lambda}}_{\mathbf{u}}) \\ \mathbf{0} = \mathbf{a}(\mathbf{q}+\mathbf{u}) \\ \mathbf{0} = \mathbf{g}_{\mathcal{A}}(\mathbf{q}+\mathbf{u}) \quad \text{and} \quad \mathbf{0} = \bar{\boldsymbol{\lambda}}_{\bar{\mathcal{A}}} \end{cases} . \tag{3.108}$$

Linearizing around $\mathbf{q}$ and injecting (3.106) gives

$$\begin{cases} \mathbf{0} = \mathbf{M}\ddot{\mathbf{u}} + \Delta\mathbf{K}(\mathbf{q})\mathbf{u} - (\nabla_{\mathbf{q}}\mathbf{a})^{\top}\boldsymbol{\lambda}_{\mathbf{u}} - (\nabla_{\mathbf{q}}\mathbf{g})^{\top}\bar{\boldsymbol{\lambda}}_{\mathbf{u}} \\ \mathbf{0} = \nabla_{\mathbf{q}}\mathbf{a}\ \mathbf{u} \\ \mathbf{0} = \nabla_{\mathbf{q}}\mathbf{g}_{\mathcal{A}}\ \mathbf{u} \end{cases} . \tag{3.109}$$

In order to correctly embed the constraints into modes, we should suitably project the first equation on the kernels of $\nabla_{\mathbf{q}}\mathbf{a}$ and $\nabla_{\mathbf{q}}\mathbf{g}_{\mathcal{A}}$. Then, we will search for $\mathbf{u}$ in the following form

$$\mathbf{u} = \mathbf{Q}\mathbf{P}\tilde{\mathbf{u}} \ , \tag{3.110}$$

where $\mathbf{P}$ is an orthogonal basis of $\nabla_{\mathbf{q}}\mathbf{a}$ and $\mathbf{Q}$ is an orthogonal basis of $(\nabla_{\mathbf{q}}\mathbf{g}_{\mathcal{A}}\mathbf{P})$. Therefore, if the first equation is premultiplied by $\mathbf{P}^{\top}\mathbf{Q}^{\top}$, the following equation is obtained

$$\mathbf{0} = \ \mathbf{P}^{\top}\mathbf{Q}^{\top}\mathbf{M}\mathbf{Q}\mathbf{P}\ddot{\tilde{\mathbf{u}}} + \mathbf{P}^{\top}\mathbf{Q}^{\top}\Delta\mathbf{K}(\mathbf{q})\mathbf{Q}\mathbf{P}\tilde{\mathbf{u}} - \mathbf{P}^{\top}\mathbf{Q}^{\top}(\nabla_{\mathbf{q}}\mathbf{a})^{\top}\boldsymbol{\lambda}_{\mathbf{u}} - \mathbf{P}^{\top}\mathbf{Q}^{\top}(\nabla_{\mathbf{q}}\mathbf{g})^{\top}\bar{\boldsymbol{\lambda}}_{\mathbf{u}} \ . \tag{3.111}$$

Due to the properties of $\mathbf{Q}$ and $\mathbf{P}$, it simplifies to

$$\mathbf{0} = \ \widetilde{\mathbf{M}}\ddot{\tilde{\mathbf{u}}} + \widetilde{\Delta\mathbf{K}}(\mathbf{q})\tilde{\mathbf{u}} \ , \tag{3.112}$$

where

$$\begin{cases} \widetilde{\mathbf{M}} = (\mathbf{Q}\mathbf{P})^{\top}\mathbf{M}\,(\mathbf{Q}\mathbf{P}) \\ \widetilde{\Delta\mathbf{K}}(\mathbf{q}) = (\mathbf{Q}\mathbf{P})^{\top}\Delta\mathbf{K}(\mathbf{q})\,(\mathbf{Q}\mathbf{P}) \end{cases} , \tag{3.113}$$

which corresponds to a classical eigenvalue problem

$$\left(\widetilde{\mathbf{M}}^{-1}\widetilde{\Delta\mathbf{K}}(\mathbf{q}) - \omega^2\mathbf{I}\right)\tilde{\mathbf{u}} = \mathbf{0} \ . \tag{3.114}$$

Table 3.4: Parameters used for the arc-length continuation example (Physical value of a ropeway span)

Attributes	Values
EA (N)	1×10^8
ρ (kg.m^{-1})	5.56
d (m)	300
h (m)	10
H (N)	26141 - 1750775

This methodology remains true and applicable for very simple cases since it consists of an extension of the theory of linear vibrations to a system subjected to both unilateral and bilateral constraints [17].

3.6.1 Modes and frequencies of the fixed-fixed cable

The modes of the fixed-fixed cable are usually derived as three families of solutions: the out-of-plane modes, the symmetric modes and the anti-symmetric modes. Here we proposed to show that the FE reproduces these analytical results accurately. A standard representation is to plot the frequencies versus the 'Irvine' parameter given by

$$\lambda_{\text{Irv}} = \frac{\rho g d}{H}\sqrt{\frac{EA}{H\int_0^L \cos(\alpha(S))^3 \mathrm{d}S}} \ . \tag{3.115}$$

Here we use the horizontal component of cable tension as the parameter and the frequencies are collected along the way. The frequency plot is known to exhibit crossover between the different continuums. At those intersections, modes exchange their symmetry so that the modal content is considerably altered. Moreover, the configurations leading to those cross-overs lead to severe resonance issues since three modes share approximately the same frequency. The latter might be interesting to study from a theoretical point of view although this case should be avoided if possible in engineering applications. To account for the FEA ability to reproduce the modal content of the cable, we challenged it with the solutions obtained via the finite differences and via the analytical approximation of frequencies.
The cable considered is given in Table 3.4. The comparison between FEM versus analytical approximation and also FEM versus FDM is illustrated in Figure 3.19. The FEA is shown able to reproduce the cross-over phenomenon and to predict accurately the frequencies in low-tension zones. Moreover the FEM can trace easier the frequencies than the FDM which often requires manual manipulation in low tension zone to sort complex frequencies (even though there is no damping or centrifugal forces in the case considered here) arising from the numerical process.
It is worth noting that for relatively high-tension, which is often the case for fixed-fixed cable in engineering application, the three approaches are accurate and provide with very similar results.

3.6.2 Modes of a cable net

Here is provided an example of applying (3.114) to the cable net given in Table 3.1. This case corresponds to a linearly constrained system so that we have

$$\mathbf{a}(\mathbf{q}) = \mathbf{0} \iff \mathbf{A}\mathbf{q} = \mathbf{0} \ . \tag{3.116}$$

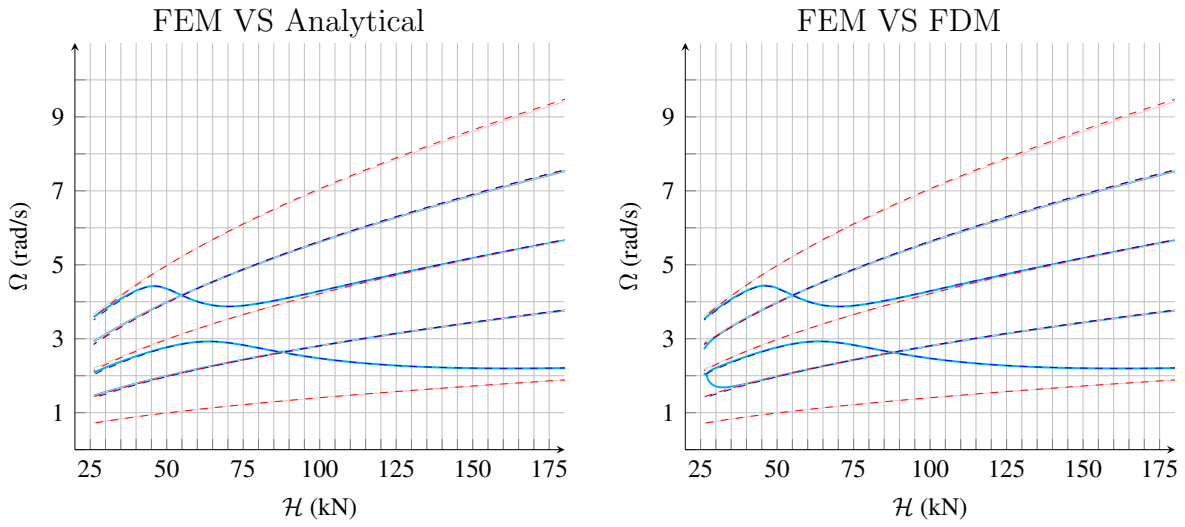

Figure 3.19: Frequencies versus horizontal component of tension. The FEM solution is classified along in-plane frequencies (dashed line - - -) and out-of-plane frequencies (dashed line - - -)
The analytical and the FDM solution are parted along in-plane frequencies (solid line —) and out-of-plane frequencies (solid line —)

Figure 3.20 illustrates the motion by superimposing the position of highest displacement to the rest position. The three different views of the system are provided to highlight the three-dimensional aspect of the vibration mode. This approach allows to trace which part of a cable structure is the more subjected to large motions. Here it seems that the slacker subpart of the net are more inclined to exhibit large displacement. Even though there is no decoupling between directions (as it is for the hanged cable), the modes are a good tool to simulated the dynamics quicker and accurately. Indeed, building reduced order model is an efficient way to decrease significantly the number of dofs. In the case of a this spider web, the total mesh is composed of 9126 dofs while a ROM version of it could be composed of less dofs considering the modes that are prone to reply to the solicitation. This direction has to be investigated further when it comes to complex cable structures and even more when the constraints applied to the system require high CPU-time.

3.6.3 Cable contacting a sheave

We already presented some analytical developments for an inextensible cable contacting a cylinder in Section 2.4.2. However those developments are true when it comes to an inextensible cable. The developed methodology gives the opportunity of investigating the case of an elastic cable contacting a cylinder. The flexibility of our approach is that FEM does not require to choose a law to wrap the cable around the sheave.

Obtaining the static profile of a cable contacting a sheave

The example developed here is a cable pinned at both ends. The parameters given in Table 3.6 are used. This system is subjected to the presence of a cylinder obstacle located at $(x_p, y_p, 0)$ given by the following constraint

$$\mathbf{g}_i(\mathbf{q}) = \sqrt{\left(\mathbf{q}^{(3i)} - x_p\right)^2 + \left(\mathbf{q}^{(3i+1)} - y_p\right)^2} \quad , \quad i \in \text{nodes} \; . \tag{3.117}$$

This constraint is applied to every node of the cable. The static configuration is obtained via combined usage of DRM (3.2.4) and the Cone Complementarity Problem (3.99). The

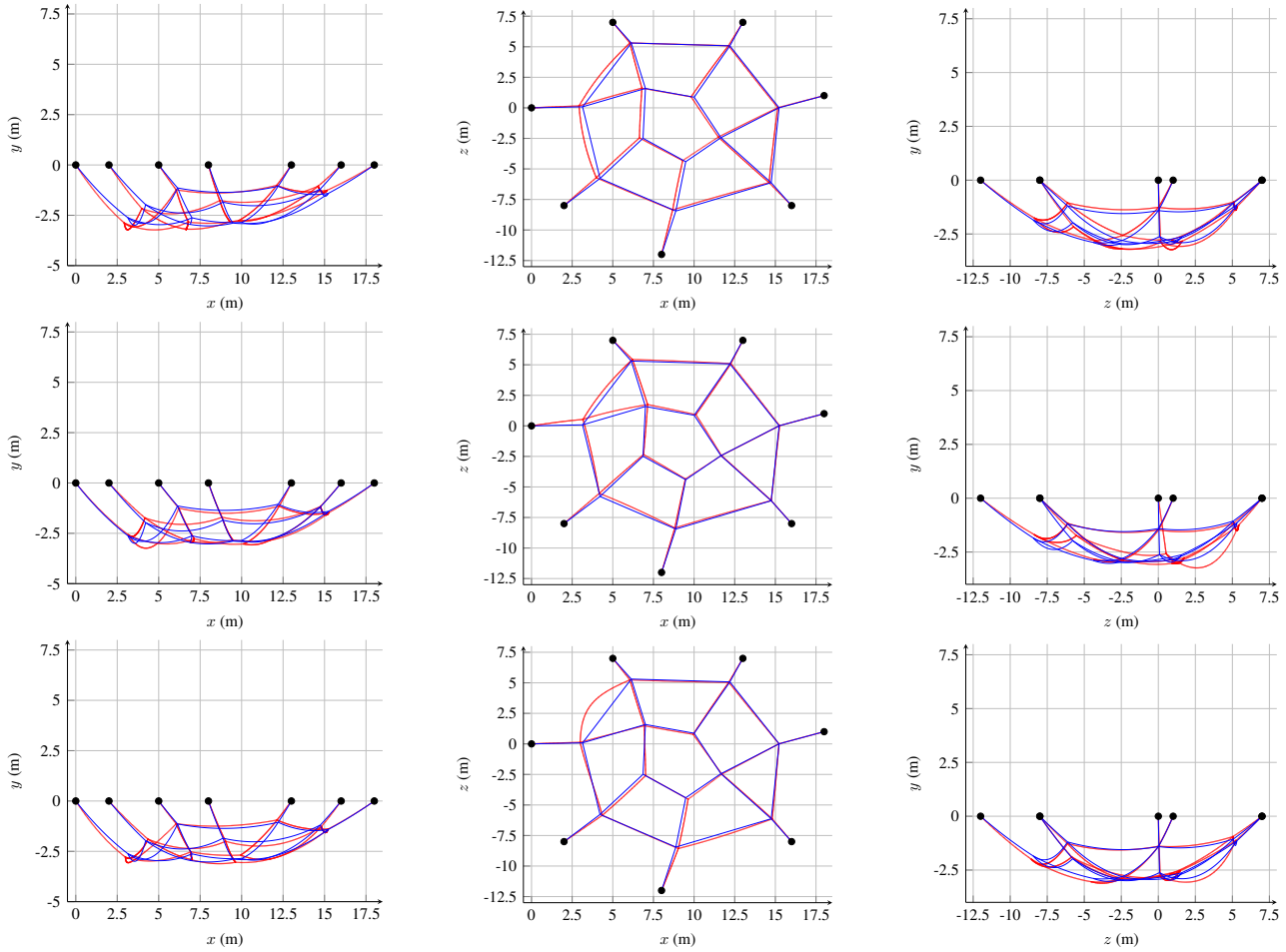

Figure 3.20: First three modes of a spider web computed via (3.114) - Parameters in Table 3.1

Table 3.5: Parameters used for the cable contacting a sheave - Static analysis

Method	EA (GN)	H (kN)	ρ (kg/m)	L (m)	N	Ends(m)	Radius (m)	sheave
FEM	1.5	N.A.	5.56	301	1500	$(0,0,0)$; $(300,0,0)$	10	$(150,-8,0)$
FEM	1.5	N.A.	5.56	301	1500	$(0,0,0)$; $(300,0,0)$	10	$(50,-5,0)$
Analytic	1.5	28.937	5.56	N.A.	1500	$(0,0,0)$; $(300,0,0)$	10	$(150,-8,0)$
Analytic	1.5	52.294	5.56	N.A.	1500	$(0,0,0)$; $(300,0,0)$	10	$(50,-5,0)$

Table 3.6: Parameters used for the cable contacting a sheave - Modal analysis

EA (MN)	ρ (kg/m)	L (m)	N	Clamped to ...	Radius (m)
1.5	5.56	300.6	1500	$(0,0,0)$ and $(300,0,0)$	10

internal forces obtained by such computations are consistent with the analytical prediction. The parameters used in the statics applications are gathered in Table 3.5. In order to compare fairly both approach, we consider a case of near inextensibility (high EA and relatively 'low' tension). We are looking to the static profile of an aligned cable which is likely to be supported by the sheave along the span. Two configurations are presented: one symmetrical with a centered sheave and one asymmetrical where the sheave is located arbitrarily on one end. The interest in using the DRM is that we obtain a dynamical equilibrium that is also a static equilibrium. We cannot be sure that this equilibrium is unique [10] however we are relatively close to the analytical solution. Indeed, the profiles obtained by both methods are pretty similar. The difference lies in the tension field: the analytical solution relies on the principle that tension is perfectly balanced ($\mu = 0$ here) whereas no assumption is made for FEM. This is the reason why we can see a difference only along the sheave. The FEM allows to catch tension variations along contacting zones which is more accurate and closer to the physics. This is shown in Figure 3.21 where static quantities obtained from analytical solutions and FEM are superimposed. We even see that limiting cases for the analytical solution are smoothed by the numerical approach. The global trend of having the same tension in and out is still obtained by our numerical tool and the almost linear variation of the vertical forces are well caught which is satisfying and encouraging to explore more sophisticated geometries instead of a cylinder.

Modes of a cable contacting a sheave

Then the frequencies and modes are computed via (3.114). We investigate the changes on the first frequencies of this particular cable when the obstacle translates along the horizontal axis. The situation is depicted in Figure 3.22. The horizontal span is meshed from 15m to 285m with a step size of 0.5m. The coupling between direction appears for every position of the obstacle and the planar modes always come by pairs. Two different natures of modes are found, some involve only one span and others involve the two parts of the span as shown in Figures 3.23-3.24. The latter case is interesting to explain instabilities that could be initiated from another span in complex cable structures. Indeed, the dynamics are explained by both single-span and double-span modes. Moreover, the sensitivity of the modes and frequency is shown by the abrupt changes in mode natures and frequencies. We see here that the design of this type of structures should be endowed very cautiously to avoid resonant scenarios.
The plotted examples considered a configuration where the normal displacement is blocked but the tangential displacement is still allowed. The analysis is linear in the sense that we used the methodology described in (3.114) with a configuration requiring prior nonsmooth computations.

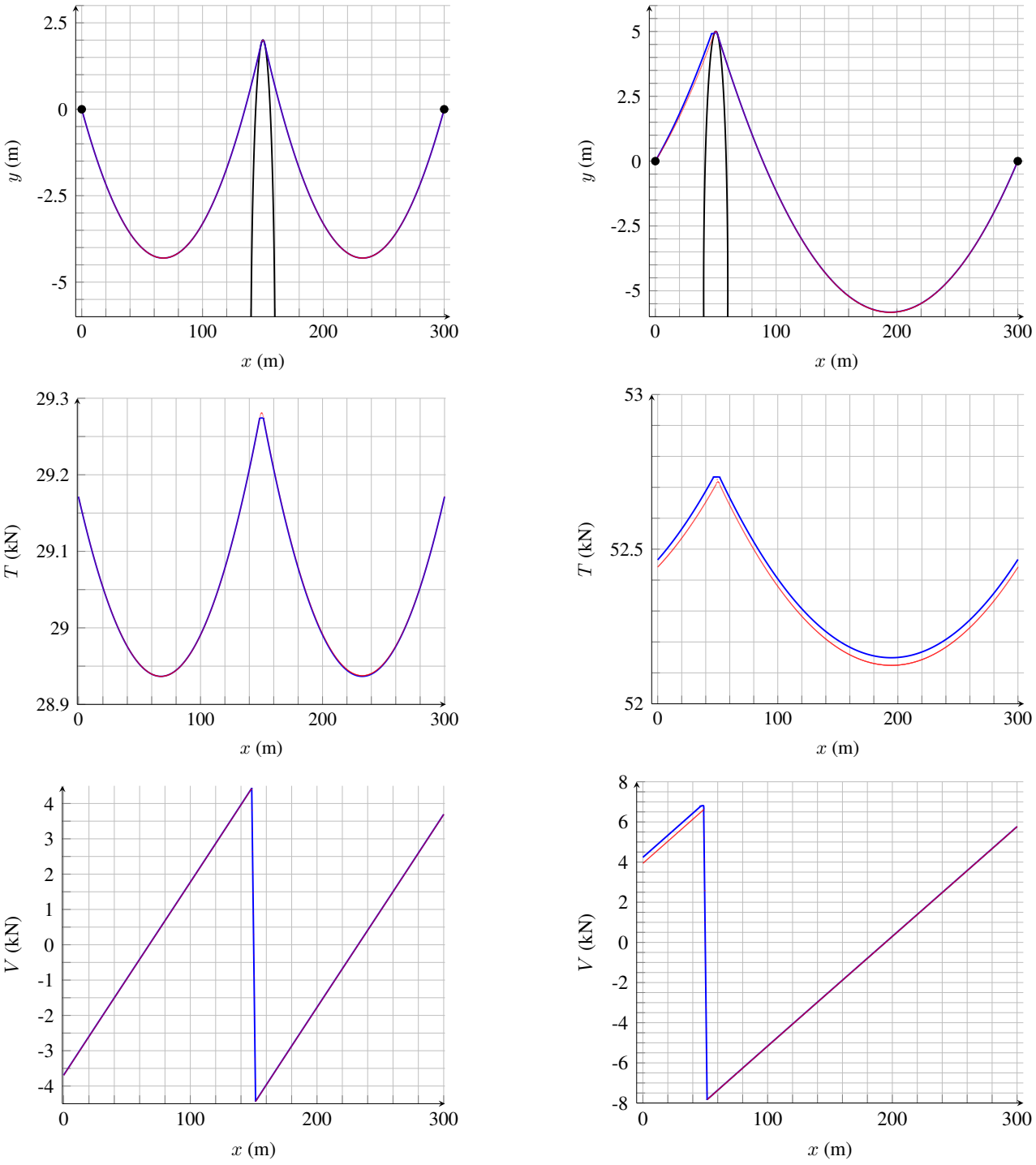

Figure 3.21: Profile and internal forces (T is the tension and V is the vertical component of the internal forces) of a cable contacting a sheave computed via an analytical solution (solid line ——) and via FEM (dotted line ·····)

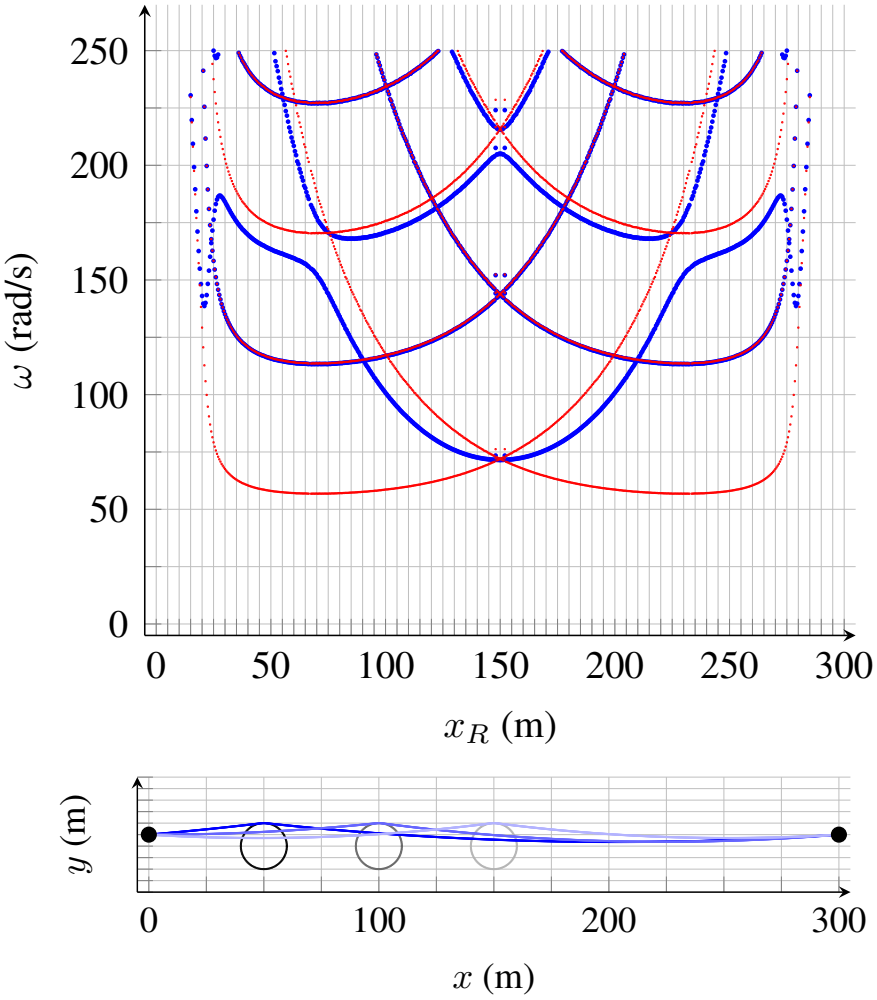

Figure 3.22: Change of the cable frequencies and variation of its profile with the translation of the obstacle

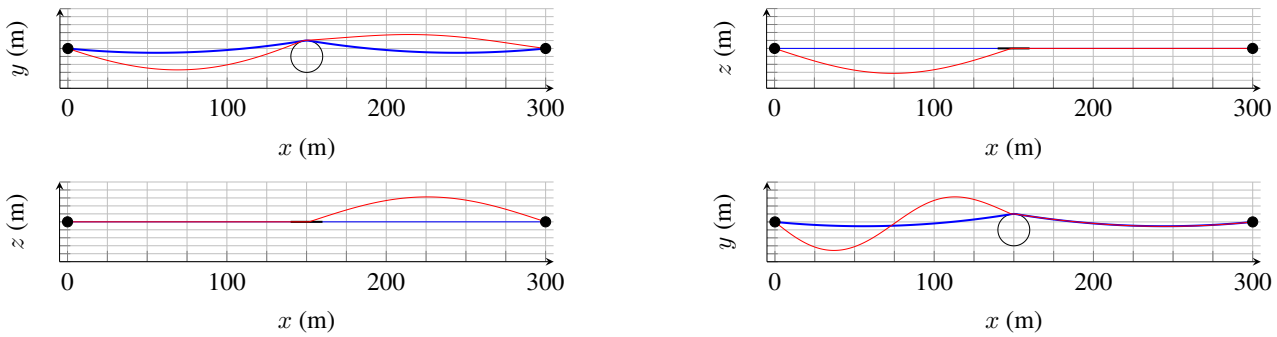

Figure 3.23: First four modes of the cable when the cylinder is at midspan ($x = 150$)m - Planar modes (solid line —) and transversal modes (solid line —)

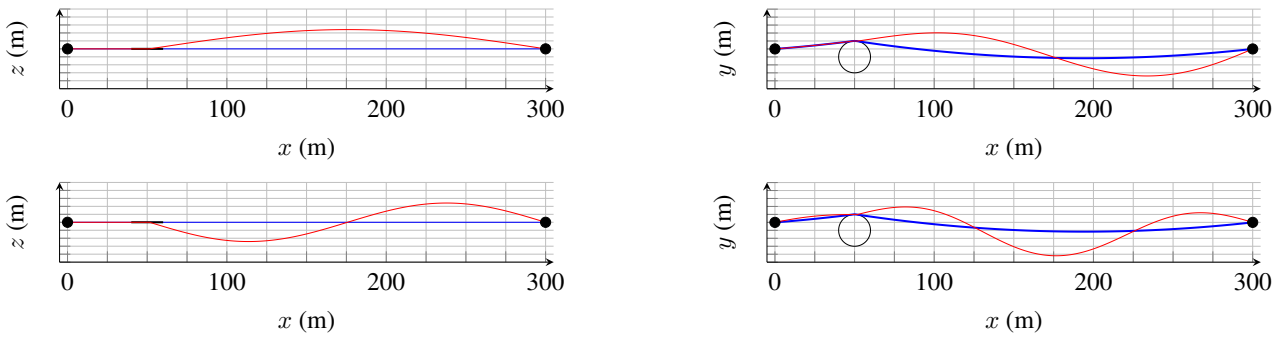

Figure 3.24: First four modes of the cable when the cylinder is not centered ($x = 50$m) - Planar modes (solid line —) and transversal modes (solid line —)

Conclusion of the chapter

This chapter highlights the key point to the finite element method applied to cable systems. Every part of this chapter can be applied to a large panel of system which is a powerful tool for research. Main contributions are:

- A general finite element framework applicable to any cable systems;
- A strategy to overcome compression in any cable segment;
- The dynamics are treated in a very general way with application to impact and friction;
- A methodology to compute the statics and the modes of any cable systems.

The limitations are the following:

- The numerical procedure relies on low-order schemes and therefore requires high CPU-time;
- The ill-conditioning and stiff nature of the ODE built according to our approach considerably affect the numerical accuracy;
- The methodology and tools developed in this section is rather difficult for practical engineers and its applications are not direct. The output data need more post-processing and analyses which requires more investigations. Indeed the methodology should be detailed and challenged with experiments which has not been done in this work.

Following improvements could be done:

- Investigate the possibility of faster numerical results via generalization of a α- generalized time integration scheme specific for cable subjected to unilateral constraint;
- Improve the accuracy via developing a suitable (and probably cunning) conditioning tool adapted to those problems;
- Confront the obtained results with robust and reliable experiment to validate or invalidate the proposed methods;
- Open the computations to more sophisticated constitutive law and mechanisms. A particular focus could be given to the extension of this work to visco-elastic behaviors, thermo-mechanical coupling and to geometrically-exact beams in order to trace torsion variations;

- Self-contact are ignored in this work, the latter may be included for the sake of generality and a wider range of application.

References

[1] Acary, V. and Brogliato, B. (2008). *Numerical methods for nonsmooth dynamical systems. Applications in mechanics and electronics.* Lecture Notes in Applied and Computational Mechanics 35. Berlin: Springer. xxi, 525 p. .

[2] Acary, V. and Pérignon, F. (2007). An introduction to siconos (technical report).

[3] Angelillo, M. (1994). A finite element approach to the study of no-tension structures. *Finite Elements in Analysis and Design*, 17(1):57–73.

[4] Barnes, M. (1977). Form finding and analysis of tension space structures by dynamic relaxation. *PhD Dissertation.*

[5] Bastien, J., Bernardin, F., and Lamarque, C.-H. (2003). *Non-Smooth Deterministic or Stochastic Discrete Dynamical Systems: Applications to models with Friction or Impacts.* Wiley.

[6] Bertrand, C., Acary, V., Lamarque, C.-H., and Ture Savadkoohi, A. (2020). A robust and efficient numerical finite element method for cables. *International Journal for Numerical Methods in Engineering*, 121(18):4157–4186.

[7] Bjorck, A. (1996). *Numerical Methods for Least Squares Problems.* SIAM.

[8] Cadoux, F. (2008). An optimization-based algorithm for coulomb's frictional contact. *Congrés National d'Analyse Numérique*, pages 54–69.

[9] Cepon, G. and Boltezar, M. (2009). Dynamics of a belt-drive system using a linear complementarity problem for the belt–pulley contact description. *Journal of Sound and Vibration*, 319:pp 1019–1035.

[10] Crusells-Girona, M., Filippou, F. C., and Taylor, R. L. (2017). A mixed formulation for nonlinear analysis of cable structures. *Computers & Structures*, 186:50–61.

[11] Day, A. (1965). An introduction to dynamic relaxation. *The Engineer*, 219:218 –221.

[12] De Saxcé, G. and Feng, Z. (1998). The bipotential method: A constructive aooriach to design the complete contact law with friction and improved numerical algorithms. *Mathematical and COmputer Modelling*, pages 225–245.

[13] Dolan, E.-D. and Moré, J.-J. (2002). Benchmarking optimization software with performance profiles. *Mathematical Programming*, 91:201–213.

[14] Ernst, H. J. (1965). Der e-modul von seilen unter berücksichtigung des durchhanges. *Der Bauingenieur*, 40(2):52–55.

[15] Felippa, C. A. (1974). Finite element analysis of three-dimensional cable structures. *Proc. 1st Int. Conf. Computational Methods in Nonlinear Mechanics; Austin TX*, pages 311–324.

[16] Felippa, C. A. and Haugen, B. (2005). A unified formulation of small-strain corotational finite elements: I. Theory. *Computer Methods in Applied Mechanics and Engineering*, 194(21-24):2285–2335.

[17] Fraejis de Veubeke, B., Gérardin, M., and Huck, A. (1974). *Structural dynamics*. LTAS, Liège.

[18] Fried, I. (1982). Large deformation static and dynamic finite element analysis of extensible cables. *Computers & Structures*, 15(3):315–319.

[19] Henghold, W. M. and Russell, J. J. (1976). Equilibrium and natural frequencies of cable structures (a nonlinear finite element approach). *Computers & Structures*, 6(4-5):267–271.

[Iniria-tripop] Iniria-tripop. Tripop: Modeling, simulation and control of nonsmooth dynamical systems.

[21] Kanno, Y. (2011). *Nonsmooth Mechanics and Convex Optimization, Chapter 4: Principles of Potential Energy for Cable Networks*. CRC Press, Taylor and Francis Group.

[22] Kanno, Y. and Ohsaki, M. (2003). Minimum principle of complementary energy of cable networks by using second-order cone programming. *International Journal of Solids and Structures*, 40(17):4437–4460.

[23] Key, S., Stone, C., and Krieg, R. (1981). *Dynamic Relaxation Applied to the Quasi-Static, Large Deformation, Inelastic Response of Axisymmetric Solid*. Springer Berlin Heidelberg.

[24] KiloNewton (2008). Kilonewton: Vibrations and optical measurements.

[25] Kim, B., Sung, H., Hong, S., and Jung, H. (2010). Finite Element Nonlinear Analysis for Catenary Structure Considering Elastic Deformation. *Computer Modeling in Engineering & Sciences*, 63(1):29–46.

[26] Kozlov, V. and Polekhin, I. (2020). On the non-integrability and dynamics of discrete models of threads. *arXiv : Chaotic Dynamics*.

[27] Lemke, C. (1967). *On Complementary Pivot Theory*. Dantzig, G.B. and Veinott, A.F.

[Moreau] Moreau, J.-J. *On Unilateral Constraints, Friction and Plasticity*. Springer.

[29] Moreau, J.-J. (1999). Numerical aspects of the sweeping process. *Computer Methods in Applied Mechanics and Engineering*, pages 329–349.

[30] Otter, J. (1966). Dynamic relaxation. *Proceedings of the Institution of Civil Engineers*, 35:633–656.

[31] Panagiotopoulos, P. D. (1975). Stress-unilateral analysis of discretized cable and membrane structure in the presence of large displacements. *Ingenieur-Archiv*, 44(5):291–300.

[32] Rega, G. (2004). Nonlinear vibrations of suspended cables - Part I: Modeling and analysis. *Applied Mechanics Reviews*, 57(6):443.

[33] Rezaiee-Pajand, M. and Mohammadi-Khatami, M. (2019). A fast and accurate dynamic relaxation scheme. *Frontiers of Structural and Civil Engineering*, 13:176–189.

[34] Rezaiee-Pajand, M. and Taghavian Hakkak, M. (2006). Research note : Nonlinear analysis of truss structures using dynamic relaxation. *IJE Transactions B*, 19:11–22.

[35] Rupe, R. and Thresher, R. (1975). The anchor-last deployment problem for inextensibe mooring lines. *ASME, J. Eng. Ind.*, 97:1046–1052.

[36] Santos, H. and Almeida Paulo, C. (2011). 0n a pure complementary energy principle and a force-based finite element formulation for non-linear elastic cables. *International Journal of Non-Linear Mechanics*, 46(2):395–406.

[37] Shizhong, Q. (1988). An adaptative dynamic relaxation method for non-linear problem. *Comput. Struc.*, 30:855–859.

[38] Srinil, N., Rega, G., and Chucheepsakul, S. (2004). Three-dimensional non-linear coupling and dynamic tension in the large-amplitude free vibrations of arbitrarily sagged cables. *Journal of Sound and Vibration*, 269(3-5):823–852.

[39] Tur, M., Garcia, E., Baeza, L., and Fuenmayor, F. (2014). A 3d absolute nodal coordinate finite element model to compute the initial configuration of a railway catenary. *Engineering Structures*, 71:234–243.

[40] Underwood, P. (1983). Dynamic relaxation. In Belytschko, T. and Hughes, T., editors, *Computational Method for Transient Analysis*, pages 245–265.

[41] Wang, C. and Watson, L. (1982). The elastic catenary. *International Journal of Mechanical Science*, 24:349–357.

[42] Zhu, Z. (2008). Nodal position finite element method and its application to dynamics of cable systems. *ASME, Int. Mech. Eng. Congress and Exposition*, 11:167–173.

[43] Zienkiewicz, O. C. and Taylor, R. L. (2002). *The finite element method. Vol. 1: The basis.* Butterworth-Heinemann, Oxford, 5. ed., reprinted edition. OCLC: 249013082.

Chapter 4

Cable vibrations

In this chapter the equations for the dynamics of a pinned-end cable are presented. It is often assumed that the main dynamics of a cable is dominated by the first modes. For this reason, we recall the derivations of cable modes in the particular framework of curvilinear mechanics and in the Frenet basis. Then, the nonlinear equations are developed and treated via Ritz-Galerkin procedure. Several applications of the obtained equations are proposed.

4.1 Free vibrations of the elastic catenary

In this section we are looking to the free vibrations problem of a cable. A lot of investigations have been already carried out in the literature, as detailed in Chapter 1. Here we present the equations for the free vibrations and the modes are obtained in the local basis. Often modes are obtained as vibrations around a parabolic cable position which means that the displacement is computed along the Cartesian frame.
We seek for the cable vibration around the current catenary equilibrium in the local basis. First, the incremental dynamics will be derived, then an analytical approximate treatment will be proposed and validation will be performed numerically.

4.1.1 Rescaling of the system

The dynamics of the cable in a undamped case and without any additional forces are given in a non-dimensional form by

$$\ddot{\mathbf{q}} = \frac{1}{\epsilon}\left[\left(\|\mathbf{q}'\| - 1\right)\mathbf{e}\right]' - \delta\mathbf{y} \ , \tag{4.1}$$

$$\epsilon = \frac{H}{EA} \quad , \quad \delta = \frac{\rho g d}{H} \ . \tag{4.2}$$

Nota: Be careful, $\epsilon \neq \varepsilon$ in this work.
With this particular form, the domain spans for $0 \leqslant S \leqslant l = \frac{L}{d}$ and the boundary conditions in $S = l$ now reads $x(l) = 1$ and $y(l) = h^* = \frac{h}{d}$. The physical representation of the situation is given in Figure 2.5. Let us recall the cable static profile given by $\mathbf{x} = [x, y]^\top$ (see Section 2.3.2) and notations just below

$$x = 1 - \epsilon\left(l - S\right) - \frac{\sinh^{-1}\left(\eta + \delta l\right) - \sinh^{-1}\left(\eta + \delta S\right)}{\delta} \ , \tag{4.3}$$

$$y = h^* - \epsilon\eta\left(l - S\right) - \frac{\delta\epsilon}{2}\left(l^2 - S^2\right) - \frac{\sqrt{1 + \left(\eta + \delta l\right)^2} - \sqrt{1 + \left(\eta + \delta S\right)^2}}{\delta} \ , \tag{4.4}$$

$$\|\mathbf{x}'\| = 1 + \epsilon\sqrt{1 + (\eta + \delta S)^2} \ . \tag{4.5}$$

Table 4.1: Parameters value for the example cases used throughout this chapter

Name	Type	EA (MN)	ρ (kg/m)	d (m)	h (m)
Case 1	Track rope	235	12.94	100	0 - 33
Case 2	Carrying hauling rope	40	6	100	0 - 33
Case 3	Fictitious cable	1	3	100	0 - 33

The local frame is given by

$$\mathbf{e} = \frac{1}{\sqrt{1+(\eta+\delta S)^2}}\begin{bmatrix}1\\ \eta+\delta S\end{bmatrix} \quad , \quad \mathbf{n} = -\frac{1}{\sqrt{1+(\eta+\delta S)^2}}\begin{bmatrix}\eta+\delta S\\ -1\end{bmatrix} . \tag{4.6}$$

The latter also obeys the following rule

$$\mathbf{e}' = \mathcal{K}\mathbf{n} \quad , \quad \mathbf{n}' = -\mathcal{K}\mathbf{e} \quad , \quad \mathcal{K} = \frac{\delta}{1+(\eta+\delta S)^2} \quad , \quad \varepsilon = \epsilon\sqrt{1+(\eta+\delta S)^2} . \tag{4.7}$$

Compatibility curves can be plotted for any given cable described by the uplet $(EA, \rho, \frac{h}{d})$, some examples are given in Figure 4.1. These examples will be continuously used in the manuscript since they are drawing differences between archetypal cable structures, see Table 4.1. The two first lines correspond to typical values of a cable-car installation and a hauling-rope respectively whereas the last line is a fictitious cable which exaggerates sag in low tension zones and where longitudinal waves can propagate easily.

4.1.2 Incremental Dynamics

In this section, we are interested in the linearized dynamics of the cable given by the rescaled equation (4.1). We consider a small displacement $\mathbf{u}$ around the static position given by $\mathbf{x}$, i.e. $\mathbf{q} = \mathbf{x} + \mathbf{u}$. As $\mathbf{x}$ is a position defined from the statics, we have that

$$\ddot{\mathbf{q}} = \ddot{\mathbf{x}} + \ddot{\mathbf{u}} = \ddot{\mathbf{u}} . \tag{4.8}$$

The geometrical nonlinearity is linearized up to first order $\mathcal{O}(\|\mathbf{u}\|)$ which reads

$$\frac{\mathbf{q}'}{\|\mathbf{q}'\|} = \frac{\mathbf{x}'+\mathbf{u}'}{\|\mathbf{x}'+\mathbf{u}'\|} \approx \frac{\mathbf{x}'}{\|\mathbf{x}'\|} + \frac{\mathbf{u}'}{\|\mathbf{x}'\|} - \frac{(\mathbf{x}'\cdot\mathbf{u}')}{\|\mathbf{x}'\|^3}\mathbf{x}' \tag{4.9}$$

$$= \mathbf{e} + \frac{1}{\|\mathbf{x}'\|}\left(\mathbf{u}' - (\mathbf{e}\cdot\mathbf{u}')\mathbf{e}\right) . \tag{4.10}$$

It is therefore more tractable to decompose the displacement $\mathbf{u}$ along the local basis as follows

$$\mathbf{u} = u\ \mathbf{e} + v\ \mathbf{n} + w\ \mathbf{z} , \tag{4.11}$$

where $(\mathbf{e}, \mathbf{n}, \mathbf{z})$ corresponds to the local basis in the configuration associated to $\mathbf{x}$. Using (2.8), we can obtain the following relations

$$\mathbf{u}' = (u' - \mathcal{K}v)\ \mathbf{e} + (v' + \mathcal{K}u)\ \mathbf{n} + w'\ \mathbf{z} , \tag{4.12}$$

$$\mathbf{u}'' = \left[(u' - \mathcal{K}v)' - \mathcal{K}(v' + \mathcal{K}u)\right]\ \mathbf{e} + \left[(v' + \mathcal{K}u)' + \mathcal{K}(u' - \mathcal{K}v)\right]\ \mathbf{n} + w''\ \mathbf{z} . \tag{4.13}$$

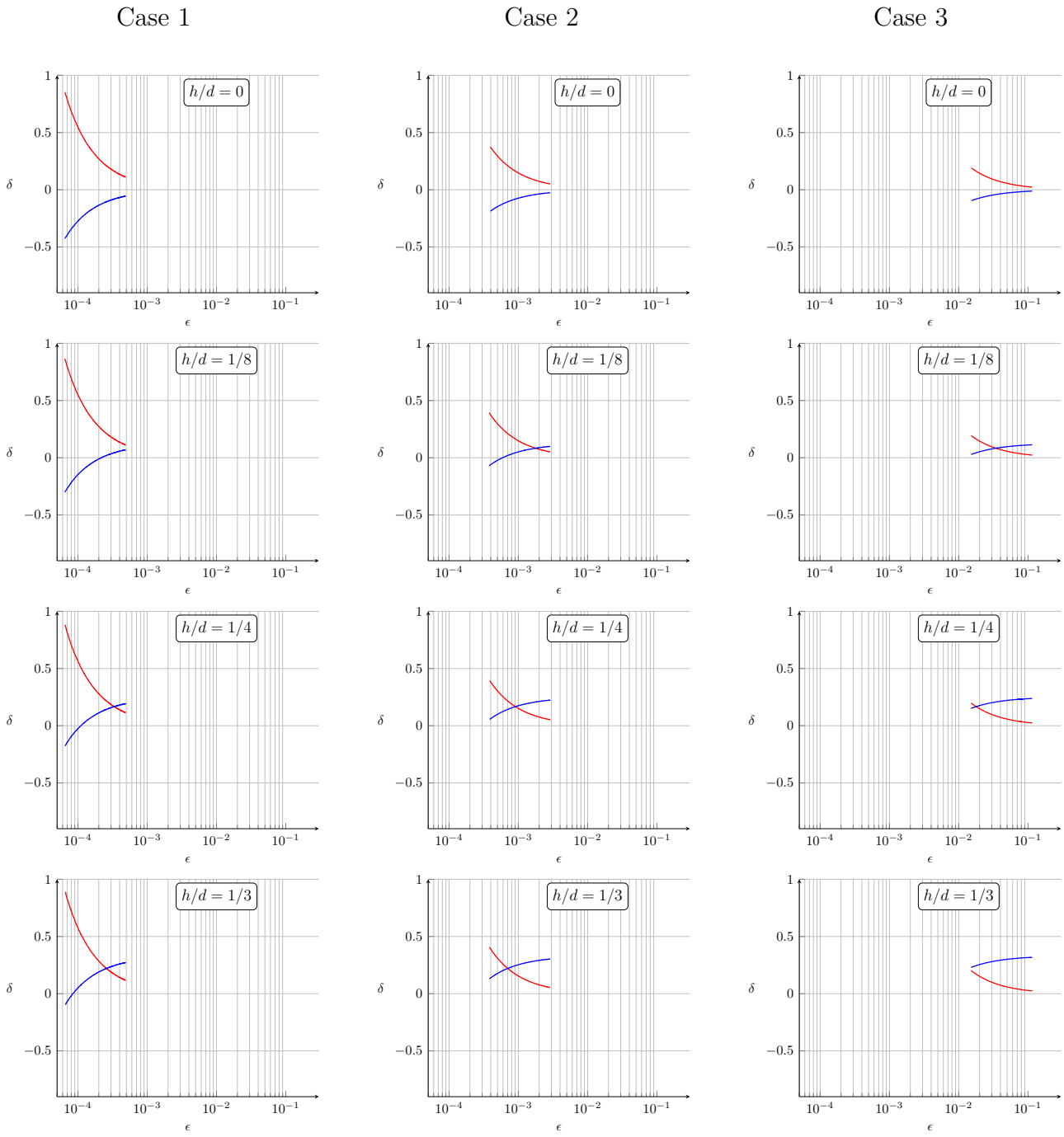

Figure 4.1: Relationship between ϵ and δ (solid line —) and relationship between ϵ and η (solid line —) with an increasing slope h/d and various cable type

Injecting the relations (4.10-4.13) into (4.1) yields in compact manner

$$\ddot{u} = \frac{1}{\epsilon}\left[(u' - \mathcal{K}v)' - \frac{\varepsilon}{1+\varepsilon}\mathcal{K}\left(v' + \mathcal{K}u\right)\right] , \tag{4.14}$$

$$\ddot{v} = \frac{1}{\epsilon}\left[\left(\frac{\varepsilon}{1+\varepsilon}\left(v' + \mathcal{K}u\right)\right)' + \mathcal{K}\left(u' - \mathcal{K}v\right)\right] , \tag{4.15}$$

$$\ddot{w} = \frac{1}{\epsilon}\left[\frac{\varepsilon}{1+\varepsilon}w'\right]' , \tag{4.16}$$

where we recall that $\varepsilon = \|\mathbf{x}'\| - 1$.
Equations (4.14 - 4.16) is a set of linear equations with continuous coefficients. Even though these equations are linear in u, v and w, the non-constant nature of the coefficients makes it difficult to solve exactly. However, we see that in the linear regime, 3D dynamics of the cable are the superposition of a planar vibration (4.14 -4.15) and a transverse vibration (4.16) which corresponds to the linear vibrations of a string with varying tension. The theory of linear free vibrations of cable is quite extensive and treated a lot in the literature. For simplicity, we give the extensive set of assumptions that leads to find approximate frequencies and mode-shapes for the hanging cable.

4.1.3 Out-of-plane vibrations

We first focus on (4.16). This kind of motion is a modified pendulum motion. The reader may imagine the bouncing of a hammock suspended between two trees as an illustration for these motions. Let us assume that the transverse displacement is given by

$$w(S,t) = W(S)e^{i\omega t} \quad ; \quad i^2 = -1 , \tag{4.17}$$

which can be inserted into (4.16) and yields

$$\omega^2 W + \frac{1}{\epsilon}\left[\frac{\varepsilon}{1+\varepsilon}W'\right]' = 0 . \tag{4.18}$$

Numerical studies have shown that $\dfrac{\varepsilon}{1+\varepsilon}$ is almost a constant function of S for high values of EA (which is often true in reality) then its derivative is neglected. This claim is supported by Figure 4.2. It results into the following differential equation

$$\omega^2 W + k^2 W'' = 0 , \tag{4.19}$$

where we have set the following

$$k^2 = \frac{1}{\epsilon}\,\frac{\varepsilon}{1+\varepsilon} . \tag{4.20}$$

If we take into account the positiveness of physical parameters, it leads to the following solution

$$W = b_1 \cos\left(\frac{\omega}{k}S\right) + b_2 \sin\left(\frac{\omega}{k}S\right) \quad ; \quad (b_1, b_2) \in \mathbb{R}^2 . \tag{4.21}$$

Once the boundary conditions are injected, constants b_1 and b_2 are found and the frequencies are obtained as

$$\sin\left(\frac{\omega}{k}l\right) = 0 \iff \omega = n\frac{k\pi}{l} , \tag{4.22}$$

and the normalized solutions ($\mathcal{L}^2$-norm) are given by

$$W_n = \sqrt{2}\sin\left(\frac{n\pi}{l}S\right) \; ; n \in \mathbb{N}^* . \tag{4.23}$$

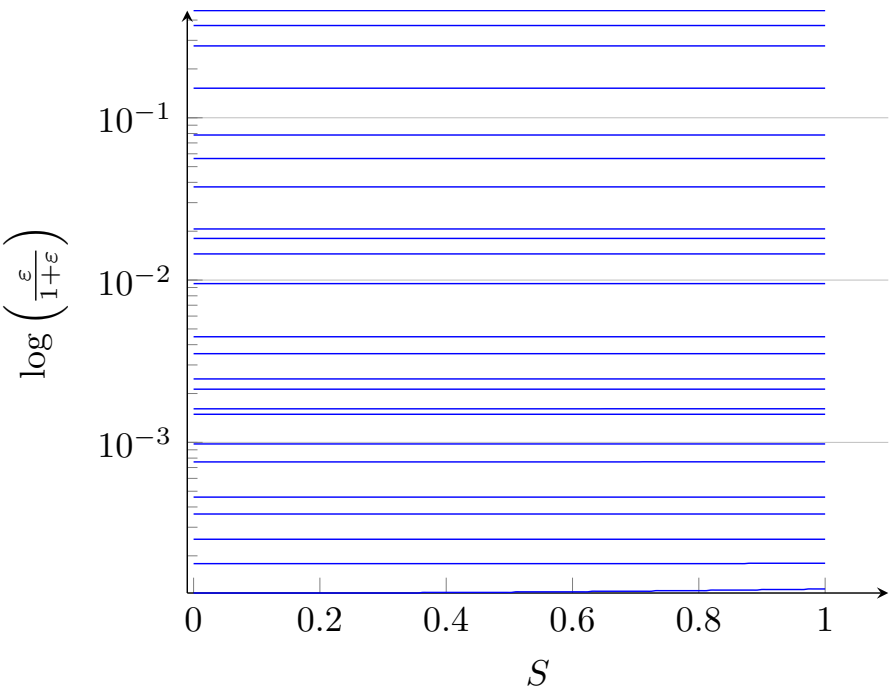

Figure 4.2: Highlights of the fact that $\frac{\varepsilon}{1+\varepsilon}$ is almost constant with S for $\epsilon \in [10^{-4}, 1]$ and $h^* = 1/8$

The validity of the current development should be checked carefully, indeed we must have the following condition

$$\left(\frac{\varepsilon}{1+\varepsilon}\right)' \approx 0 \ , \tag{4.24}$$

which is often true in practice as shown in Figure 4.2. Further developments provide with a set of orthogonal modes i.e.

$$\begin{cases} \left(\int_0^l W_n^2 \mathrm{d}S\right)^{\frac{1}{2}} = 1 \\ \int_0^l W_{n_1} W_{n_2} \mathrm{d}S = 0 \quad , \quad n_2 > n_1 \end{cases} . \tag{4.25}$$

4.1.4 In-plane normal vibrations

Let us focus on (4.14) and (4.15). This set of equations is a coupled set of linear equations with continuous coefficients. We assume that the planar displacement is given by

$$u = U(S)e^{i\omega t} \ , \tag{4.26}$$
$$v = V(S)e^{i\omega t} \ , \tag{4.27}$$

which can be inserted into (4.14) and (4.15) and yields:

$$\begin{cases} 0 = \omega^2 U + \frac{1}{\epsilon}\left[(U' - \mathcal{K}V)' - \mathcal{K}\frac{\varepsilon}{1+\varepsilon}(V' + \mathcal{K}U)\right] \\ 0 = \omega^2 V + \frac{1}{\epsilon}\left[\mathcal{K}\left(U' - \mathcal{K}V\right) + \left(\frac{\varepsilon}{1+\varepsilon}(V' + \mathcal{K}U)\right)'\right] \end{cases} . \tag{4.28}$$

In earlier developments for an aligned cable, in-plane modes were sorted by symmetry with regard to the half-span. Two types of vibrations are named in the literature:

- 'Anti-symmetric' ones that result in no increment of tension τ along the cable span at first order in $\|\mathbf{u}'\|$ and create a node at $S = \frac{l}{2}$;
- 'Symmetric' by opposition to the 'anti-symmetric' ones since they do produce an increment of tension at first order in $\|\mathbf{u}'\|$.

Usually, the longitudinal vibrations are discarded. Indeed compressive waves are not regarded in the literature although they can be found numerically of for cable with high tension. In this work, we will consider it.

Anti-symmetric modes

Anti-symmetric modes have been obtained historically via assuming that the increment of tension due to vibration is negligible and that the vibration is mainly in the normal direction. Let us make following formal assumptions:

- $\frac{\|\mathbf{q}'\|-1}{\|\mathbf{q}'\|}$ can be considered constant with S;
- The normal vibration given by V are of primary interest in (4.28) so that U can be considered of second order;
- The variation of the curvature function $\mathcal{K}$ are neglected so we make a first order approximation of it;
- The vibration does not produce any tension variation so that $EA\,(U' - \mathcal{K}V)$, corresponding to the additional tension (see (4.12)) is zero.

Then, our assumptions allows to simplify (4.28) as follows:

$$\omega^2 V + k^2 V'' = 0 \ , \tag{4.29}$$

where $k^2 = \dfrac{1}{\epsilon}\dfrac{\varepsilon}{1+\varepsilon}$.
As done in previous paragraph, V admits as solution

$$V = q_1 \cos\left(\frac{\omega}{k}S\right) + q_2 \sin\left(\frac{\omega}{k}S\right) \quad ; \quad (q_1, q_2) \in \mathbb{R}^2 \ . \tag{4.30}$$

From the homogeneous boundary conditions, the normal vibration is given by

$$V_k = q_1 \sin\left(\frac{n\pi}{l}S\right) \ ; \ n \in \mathbb{N}^* \ , \quad q_1 \in \mathbb{R} \ . \tag{4.31}$$

The geometric compatibility condition is given by

$$U' - \mathcal{K}V = 0 \ . \tag{4.32}$$

Then

$$U = p_1 - q_1 \frac{\mathcal{K}l}{n\pi} \cos\left(n\pi S\right) \quad , \quad (p_1, q_1) \in \mathbb{R}^2 \ . \tag{4.33}$$

Applying homogeneous boundary conditions to U yields

$$U(0) = 0 \iff p_1 = q_1 \frac{\mathcal{K}l}{n\pi} \ , \tag{4.34}$$

and then

$$U(l) = 0 \iff 0 = q_1 \frac{\mathcal{K}l}{n\pi} \left[1 - \cos\left(n\pi\right)\right] \ . \tag{4.35}$$

Then n must be even to satisfy $U(l) = 0$ creating a normal vibration which possesses a vibration node at $S = \frac{l}{2}$. This is the reason why those vibrations are often denoted as anti-symmetric modes.
As a summary, a mode is given by

$$\omega_n = 2n\frac{k\pi}{l} \; ; \; n \in \mathbb{N} \; , \tag{4.36}$$

$$V_n = q_{1,n} \sin\left(\frac{2n\pi}{l}S\right) \; , \tag{4.37}$$

$$U_n = q_{1,n}\frac{\mathcal{K}l}{n\pi}\sin\left(\frac{n\pi}{l}S\right)^2 \; , \tag{4.38}$$

$$q_{1,n} = \frac{2\sqrt{2}n\pi}{\sqrt{4ln^2\pi^2 + 3l^3\mathcal{K}^2}} \; . \tag{4.39}$$

In this case the constant $q_{1,k}$ normalizes the modes in the sense of the $\mathcal{L}^2$-norm i.e.

$$\left(\int_0^l V_n^2 + U_n^2 \mathrm{d}S\right)^{\frac{1}{2}} = 1 \; . \tag{4.40}$$

Note that those modes are not orthogonal in the sense of the $\mathcal{L}^2$ norm. Indeed, for $n_2 > n_1$, we have that

$$\int_0^l V_{n_1}V_{n_2} + U_{n_1}U_{n_2}\mathrm{d}S = \frac{2l^3\mathcal{K}^2}{\sqrt{4n_1^2\pi^2 + 3l^3\mathcal{K}^2}\sqrt{4n_2^2\pi^2 + 3l^3\mathcal{K}^2}} \; . \tag{4.41}$$

When the longitudinal displacement is discarded, those modes become orthogonal. This assumption is often coined as the 'condensed cable' assumption in the literature but the latter is not considered in this work.

Symmetric modes

Let us make following assumptions:

- $\frac{\|\mathbf{q}'\|-1}{\|\mathbf{q}'\|}$ can be considered constant with S;
- The normal vibration given by V is of primary interest in (4.28) so that U can be considered of second order;
- The variation of the curvature function $\mathcal{K}$ are neglected so that we make a first order approximation of it;
- The vibration produces a tension variation which is only a function of time. Then the function $\frac{1}{\epsilon}(U' - \mathcal{K}V)$, corresponding to the rescaled additional tension, can be considered as constant with space and its non-vanishing value is given by τ.

The assumptions made allows to consider a simplified version of (4.28) which is

$$\omega^2 V + k^2 V'' = -\mathcal{K}\tau \; , \tag{4.42}$$

where $k^2 = \frac{1}{\epsilon}\left(\frac{\varepsilon}{1+\varepsilon}\right)$.
The latter implies that

$$V = q_1\cos\left(\frac{\omega}{k}S\right) + q_2\sin\left(\frac{\omega}{k}S\right) - \frac{\mathcal{K}}{\omega^2}\tau \quad ; \quad (q_1, q_2) \in \mathbb{R}^2 \; . \tag{4.43}$$

From compatibility condition, we have that

$$U = p_1 + q_1 \frac{k\mathcal{K}}{\omega} \sin\left(\frac{\omega}{k} S\right) - q_2 \frac{k\mathcal{K}}{\omega} \cos\left(\frac{\omega}{k} S\right) + \left(\epsilon - \frac{\mathcal{K}^2}{\omega^2}\right) S\tau \ , \tag{4.44}$$

where $(q_1, q_2, p_1) \in \mathbb{R}^3$.
Homogeneous boundary conditions lead to the following system

$$\begin{bmatrix} 1 & 0 & 0 & -\frac{\mathcal{K}}{\omega^2} \\ \cos\left(\frac{\omega}{k} l\right) & \sin\left(\frac{\omega}{k} l\right) & 0 & -\frac{\mathcal{K}}{\omega^2} \\ 0 & -\frac{k\mathcal{K}}{\omega} & 1 & 0 \\ \frac{k\mathcal{K}}{\omega} \sin\left(\frac{\omega}{k} l\right) & -\frac{k\mathcal{K}}{\omega} \cos\left(\frac{\omega}{k} l\right) & 1 & \left(\epsilon - \frac{\mathcal{K}^2}{\omega^2}\right) l \end{bmatrix} \begin{bmatrix} q_1 \\ q_2 \\ p_1 \\ \tau \end{bmatrix} = \mathcal{M} \begin{bmatrix} q_1 \\ q_2 \\ p_1 \\ \tau \end{bmatrix} = \begin{bmatrix} 0 \\ 0 \\ 0 \\ 0 \end{bmatrix} \ . \tag{4.45}$$

We are searching for non trivial solutions, then the system can be recast into the following transcendental equation

$$\det(\mathcal{M}) = 0 \iff 0 = \frac{2k\mathcal{K}^2 \left(1 - \cos\left(\frac{\omega}{k} l\right)\right) - l\omega \left(\mathcal{K}^2 - \epsilon\omega^2\right) \sin\left(\frac{\omega}{k} l\right)}{\omega^3} \ . \tag{4.46}$$

The case $\omega = 0$ is rejected due to singularity. A famous transcendental equation [6] can be obtained by algebraic manipulations via assuming that $\omega \neq k\pi$

$$\mathcal{F}(\omega) = 2k\mathcal{K}^2 \tan\left(\frac{\omega l}{2k}\right) - l\omega \left(\mathcal{K}^2 - \epsilon\omega^2\right) = 0 \ . \tag{4.47}$$

From a practical point of view, only the very first solutions will be of interest since the cubic function rapidly intersects the infinite branch of the tan function. For numerical purposes, using (4.46) instead of (4.47) with a dichotomy scheme appears more reliable.
Once a candidate for ω is found, one can evaluate coefficients as follows

$$\begin{cases} q_1 = \dfrac{\sin\left(\frac{\omega}{k}\right)}{1 - \cos\left(\frac{\omega}{k}\right)} q_2 \\ p_1 = \dfrac{k\mathcal{K}}{\omega} q_2 \\ \tau = \dfrac{\omega^2}{\mathcal{K}} q_1 \end{cases} \ . \tag{4.48}$$

Then q_1 (or q_2) should be tuned so that

$$\int_0^1 V^2 + U^2 \ \mathrm{d}S = 1 \ . \tag{4.49}$$

As τ is assumed to be non-vanishing, the case $1 - \cos\left(\frac{\omega}{k}\right) = 0$ is impossible which is the main difference with the other type of planar vibration. It is noteworthy that anti-symmetric mode can also be found numerically when using equation (4.46), to avoid some mistakes in the process we warn the reader about the importance of checking the condition on τ.

Treatment of the transcendental equation

This equation is numerically challenging, especially with Newton's method. A way to tackle it, is to perform dichotomy on intervals where the tan function changes its sign.
The graphs of the two functions are depicted in Figure 4.3. It can be seen that for X close to $\frac{2`k+1}{2}\pi$, $\tan X$ is greater than the cubic function of X so that dichotomy can be applied in a vicinity of it. The algorithm applied to (4.47) is given in Algorithm 1.

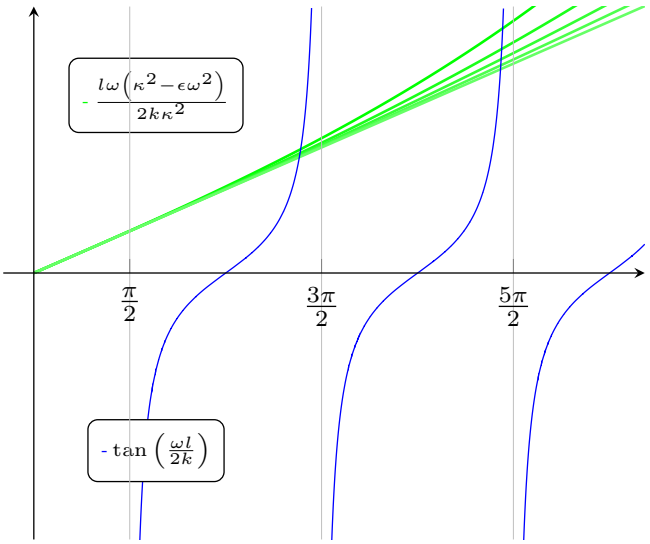

Figure 4.3: Transcendental equation (4.47) for various values of system parameters for various values of slope

Needed: ;
Number of expected solutions: N ;
Coefficient: c ;
Initialize: ;
$X \leftarrow (0, ..., \frac{2N+3}{2}\pi)$ (small mesh) ;
$X^+ \leftarrow X[2;;\text{end}]$;
$X^- \leftarrow X[1;;\text{end}-1]$;
$X^* \leftarrow X^+ \times X^-$;
$\omega \leftarrow X^+[k \text{ such that } X_k^* <= 0]$;
$\bar{\omega} \leftarrow X^-[k \text{ such that } X_k^* <= 0]$;
Limit ω and $\bar{\omega}$ to their first N^{th} components ;
for $1 \leq i \leq 50$ **do**
    $f^+ \leftarrow \mathcal{F}(\frac{\omega+\bar{\omega}}{2})$ (size N);
    $f^- \leftarrow \mathcal{F}(\bar{\omega})$ (size N);
    if $f_k^+ \times f_k^- <= 0$ **then**
        $\omega_k \leftarrow \frac{\omega+\bar{\omega}}{2}$
    end
    if $f_k^+ \times f_k^- > 0$ **then**
        $\bar{\omega}_k \leftarrow \frac{\omega+\bar{\omega}}{2}$
    end
end
Return ω

Algorithm 1: Dichotomy approach for the frequency equation

Longitudinal vibrations (Compression waves)

Longitudinal vibrations are often discarded when it comes to the modal analysis of cables. However, the latter exists. Those modes are often high frequency modes for moderately tensed cables but when cables are very taut, those modes are likely to be contained in the low frequency range. When δ is almost negligible and ϵ becomes larger, the assumption of preponderant vibrations is in default.
We can adapt the developments made for the normal vibrations via assuming following condi-

tions:

- $\frac{\|\mathbf{q}'\|-1}{\|\mathbf{q}'\|}$ can be considered constant with S;
- The longitudinal vibration given by U is of primary interest in (4.28) so that V can be considered of second order;
- The variation of the curvature function $\mathcal{K}$ are neglected so we make a first order approximation of it;
- The vibration produces a slope variation which is a function of time only. Then the function $(V' + \mathcal{K}U)$, corresponding to the rescaled additional tension, can be considered to be constant with space and its non-trivial value is given by τ .

These assumptions allow to consider to simplified system

$$\begin{cases} 0 = \omega^2 U + \dfrac{1}{\epsilon} U'' - \mathcal{K} k^2 \tau \\ 0 = \tau - (V' + \mathcal{K}U) \end{cases} . \tag{4.50}$$

As done previously the latter results into a determinant equation which reduces in

$$\det\left(\widetilde{\mathcal{M}}\right) = 0 \iff 0 = \frac{2k^2\mathcal{K}^2\left(\cos\left(\sqrt{\epsilon}\omega\right) - 1\right) - \sqrt{\epsilon}\omega\left(\omega^2 - k^2\mathcal{K}^2\right)\sin\left(\sqrt{\epsilon}\omega\right)}{\sqrt{\epsilon}\omega^3} , \tag{4.51}$$

that can be recast in the following transcendental form

$$\mathcal{F}^*(\omega) = 2k^2\mathcal{K}^2 \tan\left(\frac{\sqrt{\epsilon}\omega}{2}\right) - \sqrt{\epsilon}\omega\left(\omega^2 - k^2\mathcal{K}^2\right) = 0 . \tag{4.52}$$

The treatment of the latter can be done via the dichotomy approach similarly to the case (4.46). However, for a lot of practical applications subjected to longitudinal vibrations the following approximation provides with an acceptable precision

$$\omega_k = \frac{k\pi}{\sqrt{\epsilon}} \quad , \quad k \in \mathbb{N} . \tag{4.53}$$

Summary

An analytical approximation for the modes of a pinned-pinned cable have been proposed. The assumptions made are of practical interest since the majority of cables are designed in a way that the strains are very small compared to unity. Moreover the assumptions of small (but non-zero) displacements is valid for most tensed cables in practical engineering structures. The influence of the inclination of the cable via the cubic terms in (4.47).

4.1.5 Comparisons with numerical computations

The idea of this section is to compare the analytical approximations proposed and the modes captured by numerical procedures. This also allows to characterize and to quantify the relevance of analytical treatment of the linear vibrations of cable compared to their numerical treatments. One could argue that assumptions are too restrictive and that addressing (4.14-4.16) directly via a numeric solver is the best way to check the quality of the approximation. First a finite difference approach to tackle the modal analysis will be described, then comparisons with our analytical prediction will be performed.

Finite difference method applied to frequency tracing

The Finite Difference Method (FDM) is used to treat (4.14-4.16). First, we assume that separation of spatial and temporal variables holds and that the unknowns are harmonic with regards to time so that

$$\begin{cases} u = Ue^{i\omega t} \\ v = Ve^{i\omega t} \\ w = We^{i\omega t} \end{cases} . \tag{4.54}$$

Injecting (4.54) into (4.14)-(4.16) yields the following system of equations:

$$\begin{cases} 0 = \omega^2\ U + \dfrac{1}{\epsilon}\ \left[U'' - \dfrac{1+2\varepsilon}{1+\varepsilon}\mathcal{K}V' - \dfrac{\varepsilon}{1+\varepsilon}\mathcal{K}^2U - \mathcal{K}'V\right] \\ 0 = \omega^2\ V + \dfrac{1}{\epsilon}\ \left[\dfrac{\varepsilon}{1+\varepsilon}V'' + \dfrac{1+2\varepsilon}{1+\varepsilon}\mathcal{K}U' + \left(\dfrac{\varepsilon}{1+\varepsilon}\right)'V' + \left(\dfrac{\varepsilon}{1+\varepsilon}\mathcal{K}\right)'U - \mathcal{K}^2V\right] \\ 0 = \omega^2\ W + \dfrac{1}{\epsilon}\ \left[\dfrac{\varepsilon}{1+\varepsilon}W'' + \left(\dfrac{\varepsilon}{1+\varepsilon}\right)'W'\right] \end{cases} \tag{4.55}$$

The FDM is used with regard to spatial variable only. It consists of defining a grid over the domain $0 \leqslant S \leqslant 1$ with a constant step $\Delta S = \frac{1}{N}$ where $N \in \mathbb{N}$ is the number of segments used to sample the domain. The unknowns are then approximated by a vector of their value for each point of the grid, in another words:

$$\begin{cases} U(S_k) \approx \mathbf{U}_k \\ V(S_k) \approx \mathbf{V}_k \\ W(S_k) \approx \mathbf{W}_k \end{cases} \quad , \quad S_k = k\Delta S \quad , \quad k = 0, ..., N \tag{4.56}$$

The spatial derivatives are approximated by central difference quotients:

$$\frac{\partial f}{\partial S}(S_k) \approx \frac{f_{k+1} - f_{k-1}}{2\Delta S} \quad , \quad \frac{\partial^2 f}{\partial S^2}(S_k) \approx \frac{f_{k+1} - 2f_k + f_{k-1}}{(\Delta S)^2} \tag{4.57}$$

for any arbitrary function f in the set of the unknowns.
For the value in $S = 0$ and $S = 1$, (4.57) are taken as such by setting that $f_{-1} = 0$ and $f_{N+1} = 0$ respectively.
Reporting the approximations (4.56) and (4.57) into (4.55) yields the following eigenvalue problem:

$$\omega^2\mathbf{Y} + \widetilde{\mathbf{K}}(\epsilon, \varepsilon, \mathcal{K}, \Delta S)\mathbf{Y} = \mathbf{0} \tag{4.58}$$

where the value of ε, $\mathcal{K}$ and their derivatives are computed analytically via using (4.7). The matrix $\widetilde{\mathbf{K}}$ is an equivalent of the tangent stiffness matrix which size is $(3(N+1) \times 3(N+1))$. The vector $\mathbf{Y}$ is taken as follows:

$$\mathbf{Y} = (\mathbf{U}_0, \mathbf{V}_0, \mathbf{W}_0, ..., \mathbf{U}_N, \mathbf{V}_N, \mathbf{W}_N)^\top \tag{4.59}$$

Solving the eigenvalue problem in (4.58) provides with a set of natural frequencies ω_k and a set of eigenvectors $\mathbf{Y}_k$. In practical implementations, the homogeneous boundary conditions are implicitly imposed via discarding the three first and last rows and columns of $\widetilde{\mathbf{K}}$.

Comparisons with analytical developments

The Irvine parameter given as:

$$\lambda_{\text{Irv}} = \frac{\rho g d}{H}\sqrt{\frac{EA}{H\int_0^L \cos(\alpha(S))^3 \mathrm{d}S}} = \sqrt{\frac{\delta}{\epsilon}}\left(\frac{\eta + \delta l}{\sqrt{1 + (\eta + \delta l)^2}} - \frac{\eta}{\sqrt{1+\eta^2}}\right)^{1/2} \tag{4.60}$$

is often used as a plotting parameter for the frequency since the crossovers are related to multiples of $\pi\lambda_{\text{Irv}}$. The latter is also used here since it gives an indicator of both the contribution of the elasticity and the static geometry on the cable frequencies.
When the assumptions given in Section 4.1.4 are satisfied, the predictions of system frequencies are accurate. The veering phenomenon is well reconstituted by both approaches. However, the effect of inclination is not totally caught by the analytical approximations. As a result, analytical approximations do not predict the real system responses for an inclined and near-inextensible cable yet. The qualitative aspect of the frequency curve are well-described and the dynamic content changes are captured, even when modes are switching between normal and longitudinal vibration. Hopefully, those cases are out of the scope when it comes to ropeways. This claim is illustrated in Figures 4.4 and 4.5. One can see that a wide range of tension is well approximated by our analytical approximation. The inclination of the cable does not have significant influence on the precision if the horizontal span remains bigger than the vertical distance. One should outline the fact that higher the frequency is, the less accurate is the analytical approximation. Of course, for most civil engineering studies, low frequencies are of bigger interest so that the comparisons should focus on first modes.

The prediction of frequencies is only one part of the prediction. Indeed the mode-shapes obtained by the analytical prediction and their numerical twins should be compared. Different cases are analyzed to highlight pros and cons of the analytical approximations. The solution computed via FDM is superimposed to the analytically obtained ones. For the cases satisfying our simplifying assumptions, the agreements are qualitatively good. However, the combined effect of the inclination and the inextensibility is not caught by the analytical approximation. This claim is illustrated in Figures 4.6-4.8. Even though the transversal vibrations are well-described, the planar vibration approximation is not always well-suited, especially for the combined case of near-inextensible and inclined cable. The latter is very unfortunate for the case of ropeways in general for recent and practical applications. For this reason, numerical approximation of frequencies and mode shapes seems more reliable and flexible. It should be preferred to describe accurately the physics of chair lifts.

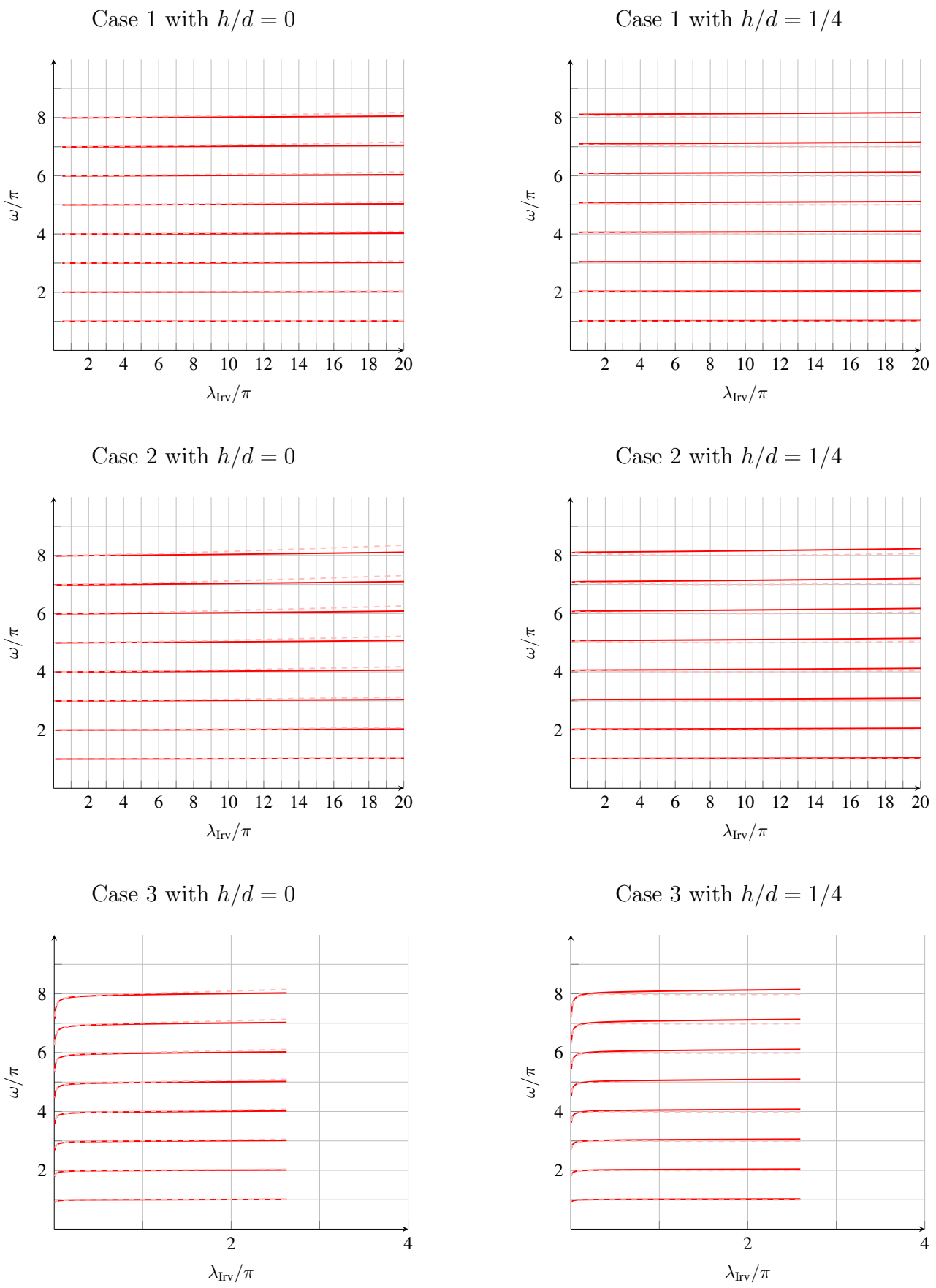

Figure 4.4: Normalized frequency of the out-of-plane modes versus normalized λ_{Irv} parameter ; Computed via analytical approximation (dashed line - - -) and FDM (solid line —)

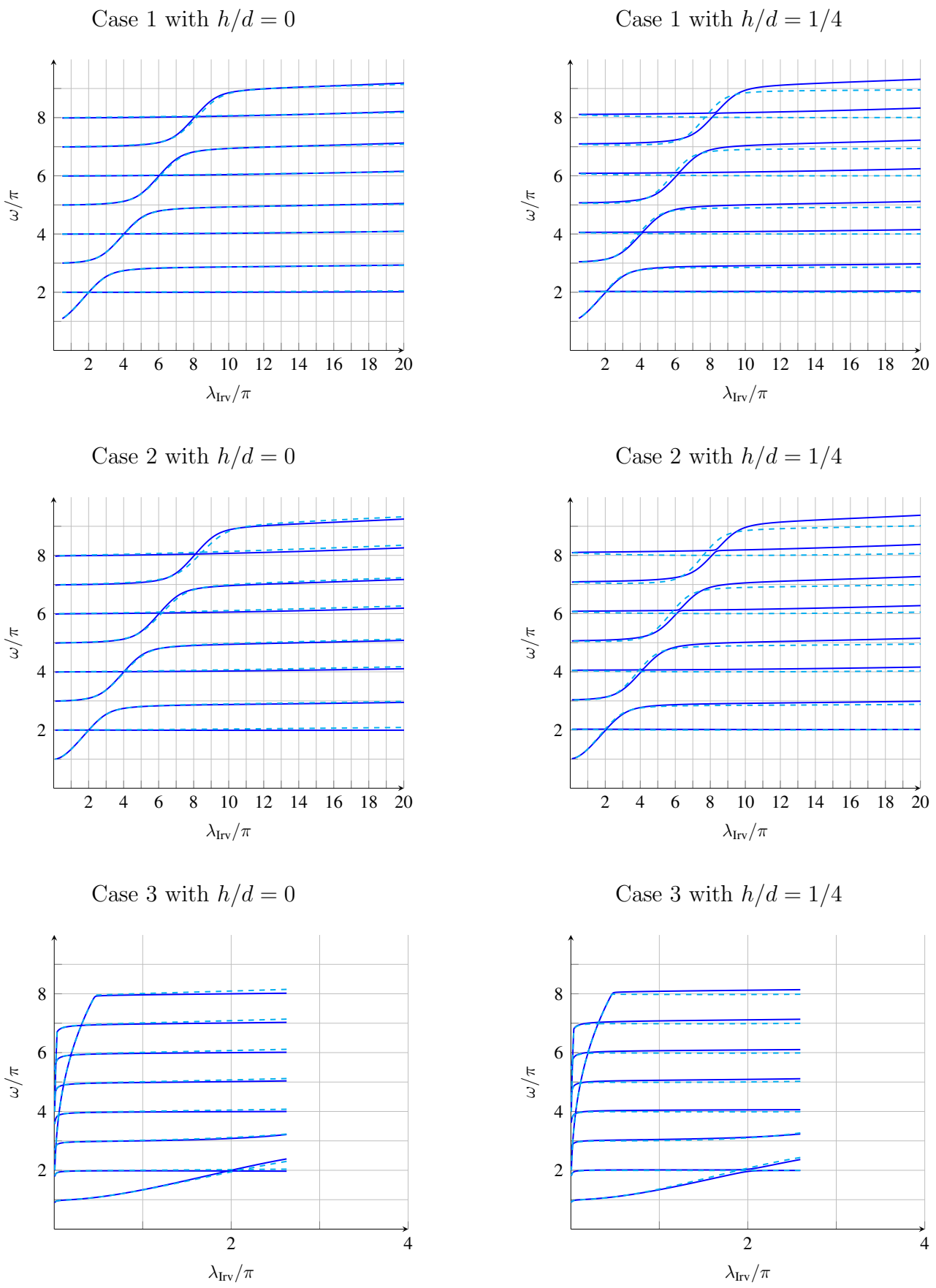

Figure 4.5: Normalized frequency of the in-plane modes versus normalized λ_{Irv} parameter ; Computed via analytical approximation (solid line - - -) and FDM (solid line ——)

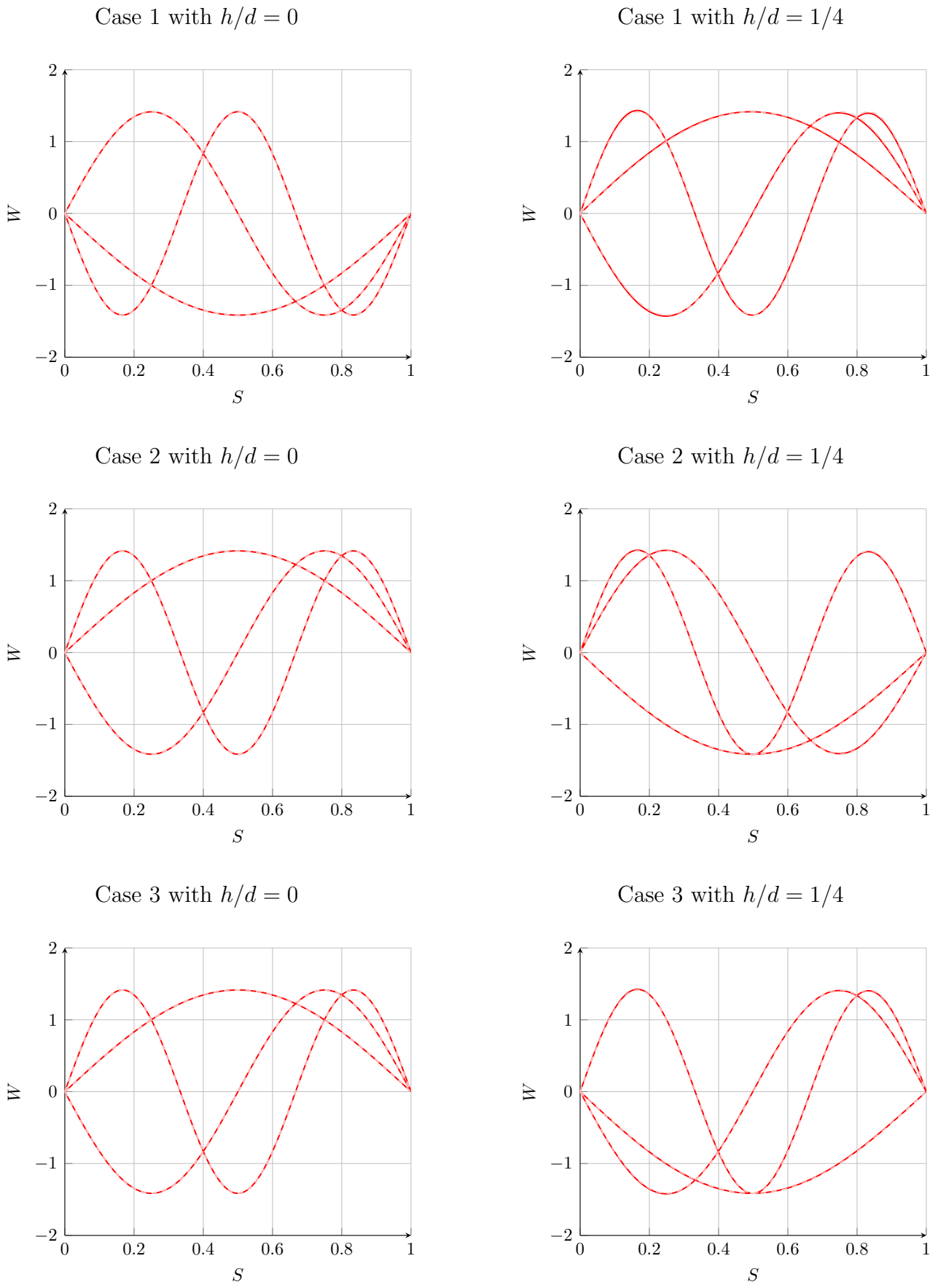

Figure 4.6: Normalized transversal component for the first three out-of-plane modes for $h/d = 0$ and $h/d = 1/4$ for cables given in Table 4.1 ; Computed via analytical approximation (dashed line - - -) and FDM (solid line —)

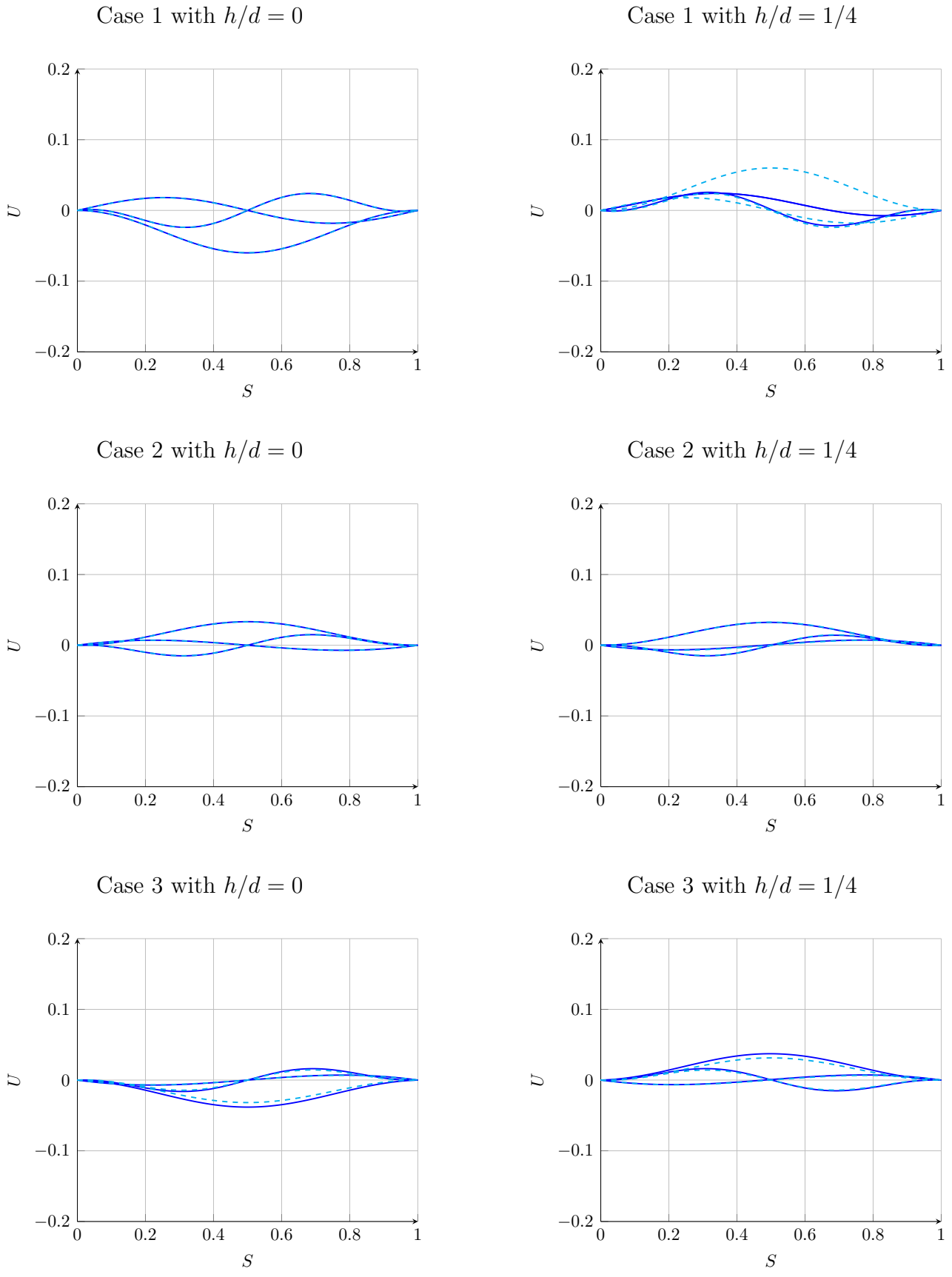

Figure 4.7: Normalized axial component for the first three in-plane modes for $h/d = 0$ and $h/d = 1/4$ for cables given in Table 4.1 ; Computed via analytical approximation (solid line - - -) and FDM (solid line ——)

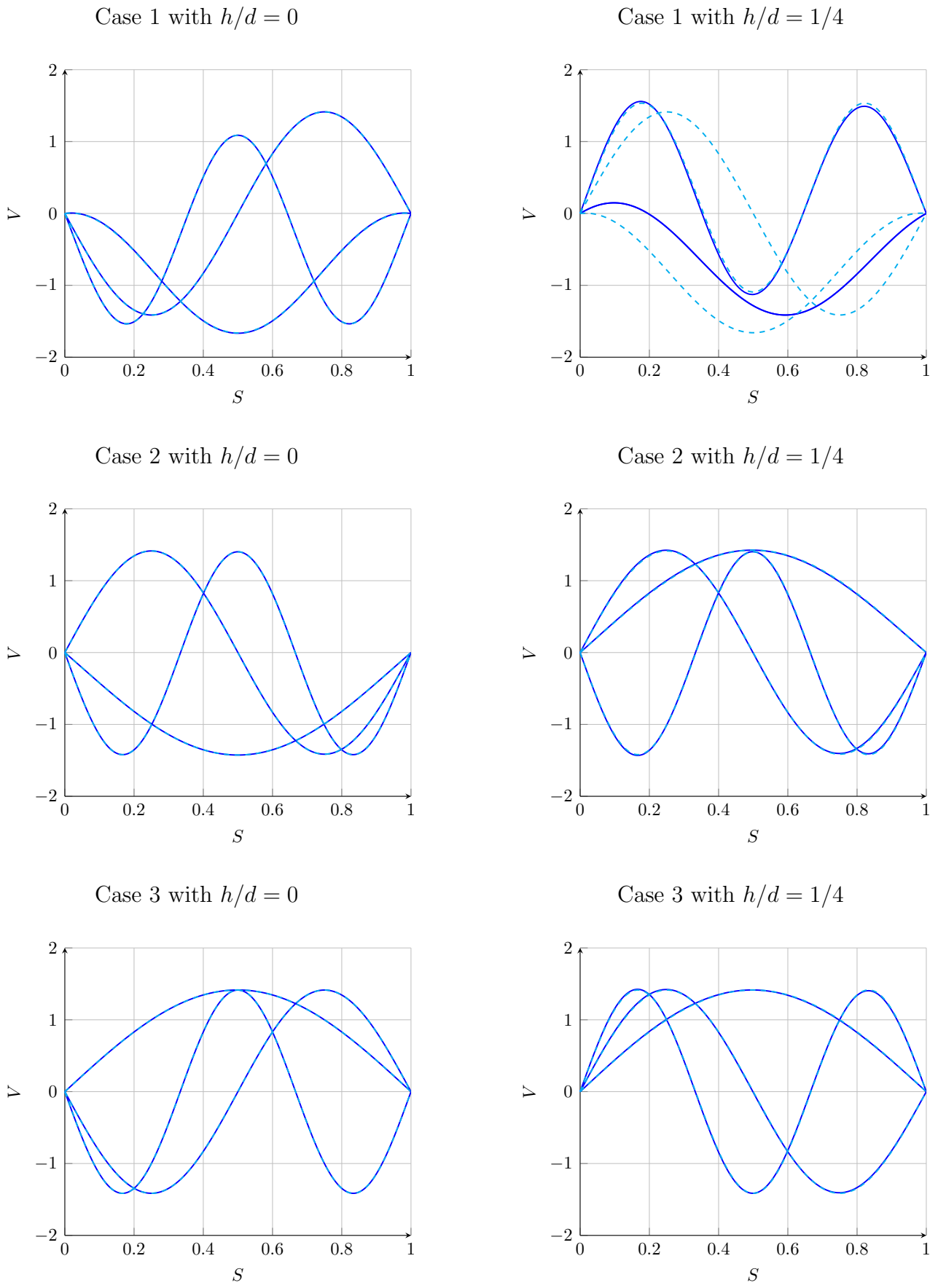

Figure 4.8: Normalized normal component for the first three in-plane modes for $h/d = 0$ and $h/d = 1/4$ for cables given in Table 4.1 ; Computed via analytical approximation (solid line - - -) and FDM (solid line ——)

4.2 Nonlinear oscillations

In this section the equations for the nonlinear dynamics of a hanged cable are presented. Our choice is to keep the influence of the longitudinal motions in the projection and to use numerical based methods that can be applied to general cases with an arbitrary number of degree of freedom.

4.2.1 Ritz-Galerkin procedure

From this statement, one can choose to project the nonlinear dynamics on a family of chosen modes of the linear case computed in Section 4.1. Then the displacement is given by

$$\mathbf{u}(S,t) = \sum_{k=1}^{N} \Phi_k(S)\varphi_k(t) \ , \tag{4.61}$$

where Φ_k is a cable mode shape. Note that, projections can be performed on arbitrary modes. The current internal forces are expanded up to third order in $\|\mathbf{u}'\|$ as follows

$$\begin{aligned}
\frac{1}{\epsilon}\left(\|\mathbf{q}'\|-1\right)\frac{\mathbf{q}'}{\|\mathbf{q}'\|} =& \frac{1}{\epsilon}(\|\mathbf{q}'\|-1)\mathbf{e} \\
&+\frac{1}{\epsilon}\frac{\|\mathbf{x}'\|-1}{\|\mathbf{q}'\|}\mathbf{u}' + \frac{1}{\epsilon}\frac{1}{\|\mathbf{x}'\|}(\mathbf{e}\cdot\mathbf{u}')\mathbf{e} \\
&+\frac{1}{\epsilon}\frac{1}{2\|\mathbf{x}'\|^2}\left(\left[\mathbf{u}'\cdot\mathbf{u}' - 3(\mathbf{e}\cdot\mathbf{u}')^2\right]\mathbf{e} + 2\left[\mathbf{e}\cdot\mathbf{u}'\right]\mathbf{u}'\right) \\
&+\frac{1}{\epsilon}\frac{1}{2\|\mathbf{x}'\|^3}\begin{pmatrix}\left[5(\mathbf{e}\cdot\mathbf{u}')^3 - 3(\mathbf{e}\cdot\mathbf{u}')(\mathbf{u}'\cdot\mathbf{u}')\right]\mathbf{e} \\ +\left[\mathbf{u}'\cdot\mathbf{u}' - 3(\mathbf{e}\cdot\mathbf{u}')^2\right]\mathbf{u}'\end{pmatrix}
\end{aligned} \ . \tag{4.62}$$

The right hand-side of (4.62) can be seen as the superposition of static elastic forces, $f_e(\mathbf{x})$, and incremental elastic forces due to the vibration, $\Delta f_e(\mathbf{x},\mathbf{u})$, i.e.

$$\frac{1}{\epsilon}\left(\|\mathbf{q}'\|-1\right)\frac{\mathbf{q}'}{\|\mathbf{q}'\|} = f_e(\mathbf{x}) + \Delta f_e(\mathbf{x},\mathbf{u}) \ . \tag{4.63}$$

Both are recast in the Frenet basis as follow

$$f_e(\mathbf{x}) = \frac{1}{\epsilon}\begin{bmatrix}\|\mathbf{x}'\|-1\\0\\0\end{bmatrix} \ , \tag{4.64}$$

$$\begin{aligned}
\Delta f_e(\mathbf{x},\mathbf{u}) =& \frac{1}{\epsilon}\begin{bmatrix}u'-\mathcal{K}v\\0\\0\end{bmatrix} + \frac{1}{\epsilon}\frac{\|\mathbf{x}'\|-1}{\|\mathbf{x}'\|}\begin{bmatrix}0\\v'+\mathcal{K}u\\w\end{bmatrix} \\
&+\frac{1}{\epsilon}\frac{1}{2\|\mathbf{x}'\|^2}\begin{bmatrix}(v'+\mathcal{K}u)^2+w^2\\2(u'-\mathcal{K}v)(v'+\mathcal{K}u)\\2(u'-\mathcal{K}v)w\end{bmatrix} \\
&-\frac{1}{\epsilon}\frac{1}{2\|\mathbf{x}'\|^3}\begin{bmatrix}2(u'-\mathcal{K}v)\left[(v'+\mathcal{K}u)^2+w^2\right]\\\left[2(u'-\mathcal{K}v)^2-(v'+\mathcal{K}u)^2-w^2\right](v'+\mathcal{K}u)\\\left[2(u'-\mathcal{K}v)^2-(v'+\mathcal{K}u)^2-w^2\right]w\end{bmatrix}
\end{aligned} \ . \tag{4.65}$$

The full nonlinear governing equation reads

$$\ddot{\mathbf{q}} + \alpha\dot{\mathbf{q}} = \left[f_e(\mathbf{x}) + \Delta f_e(\mathbf{x},\mathbf{u})\right]' + \mathbf{b} + f \ , \tag{4.66}$$

where we recall that $f(S,t)$ is the other forces applied to the cable presented in (2.73). Simplifying (4.66) thanks to (2.78) yields

$$\ddot{\mathbf{u}} + \alpha\dot{\mathbf{u}} - [\Delta f_e(\mathbf{x},\mathbf{u})]' = f \ . \tag{4.67}$$

A Ritz-Galerkin procedure is performed with regards to the inner-product given in (4.25). Here we do not assume any type of dynamics, every terms are retained in the projection. A set of N equations is obtained as follows

$$\int_0^L (\ddot{\mathbf{u}} + \alpha\dot{\mathbf{u}}) \cdot \Phi_j \mathrm{d}S + \int_0^L \Delta f_e(\mathbf{q},\mathbf{u}) \cdot \Phi_j' \mathrm{d}S = \int_0^L f \cdot \Phi_j \mathrm{d}S \quad , \quad 1 \leqslant j \leqslant N \ , \tag{4.68}$$

where the differentiation of vectors with regards to S is done via (2.8).
Depending on the family used for the projection, the mass matrix and stiffness matrix can be full or diagonal. As modes are not necessarily orthogonal, the stiffness matrix can be non-symmetric and the mass matrix non-diagonal. The discrete system is obtained as

$$\mathbf{M}_{jk}\ddot{\varphi}_k + \mathbf{C}_{jk}\dot{\varphi}_k + \mathbf{K}_{jk}\varphi_k + \mathcal{Q}_{jkl}\varphi_k\varphi_l + \mathcal{C}_{jklm}\varphi_k\varphi_l\varphi_m = \mathbf{f}_j \quad , \quad 1 \leqslant j \leqslant N \ , \tag{4.69}$$

where Einstein convention has been used. The formal expression of each tensor is given in (4.76-4.78). To lighten numerical computations, we multiplied by the inverse of the mass matrix and the time is rescaled so that

$$\begin{gathered} \ddot{\varphi}_j + \underbrace{\xi_j\dot{\varphi}_j}_{\text{No summation}} + \mathbf{K}_{jk}\varphi_k + \mathcal{Q}_{jkl}\varphi_k\varphi_l + \mathcal{C}_{jklm}\varphi_k\varphi_l\varphi_m = \mathbf{f}_j \quad , \quad 1 \leqslant j \leqslant N \ , \\ t = \frac{\tau}{\omega_0} \ , \end{gathered} \tag{4.70}$$

for conciseness we did not change the notation for $\mathbf{K}$, $\mathcal{Q}$, $\mathcal{C}$ and $\mathbf{f}$ in (4.70). This kind of models are often coined as reduced-order-models (ROM).
The formal value of the tensors built with the Ritz-Galerkin procedure are given considering that Φ refers to a mode and its subscript refers to its index. The latter can be decomposed in the Frenet basis as follows

$$\Phi_j = \begin{bmatrix} P_j \\ Q_j \\ B_j \end{bmatrix} \tag{4.71}$$

$$\mathbf{M}_{jk} = \int_0^L \Phi_j \cdot \Phi_k \mathrm{d}S \tag{4.72}$$

$$\mathbf{C}_{jk} = \alpha \int_0^L \Phi_j \cdot \Phi_k \mathrm{d}S \tag{4.73}$$

$$\mathbf{f}_j(t) = \int_0^L \Phi_j \cdot f \mathrm{d}S \tag{4.74}$$

As we work in the Frenet basis, the derivative of a given mode reads

$$\Phi_j' = \begin{bmatrix} P_j' - \mathcal{K}Q_j \\ Q_j' + \mathcal{K}P_j \\ B_j' \end{bmatrix} \tag{4.75}$$

The latter allows to take into account the curvature into the first, second and third order expansion of the elastic forces in the nonlinear equations of the motion (4.65) .

$$\mathbf{K}_{jk} = \frac{1}{\epsilon}\int_0^l \left(\begin{bmatrix} P'_k - \mathcal{K}Q_k \\ 0 \\ 0 \end{bmatrix} + \frac{\|\mathbf{q}'\| - 1}{\|\mathbf{q}'\|} \begin{bmatrix} 0 \\ Q'_k + \mathcal{K}P_k \\ B_k \end{bmatrix} \right) \cdot \begin{bmatrix} P'_j - \mathcal{K}Q_j \\ Q'_j + \mathcal{K}P_j \\ B'_j \end{bmatrix} \mathrm{d}S \tag{4.76}$$

$$\mathcal{Q}_{jkl} = \frac{1}{\epsilon}\int_0^l \left(\frac{1}{\|\mathbf{q}'\|^2} \begin{bmatrix} \left(Q'_k + \mathcal{K}P_k\right)\left(Q'_l + \mathcal{K}P_l\right) + B'_k B'_l \\ 2\left(P'_k - \mathcal{K}Q_k\right)\left(Q'_l + \mathcal{K}P_l\right) \\ 2\left(P'_k - \mathcal{K}Q_k\right) B'_l \end{bmatrix} \right) \cdot \begin{bmatrix} P'_j - \mathcal{K}Q_j \\ Q'_j + \mathcal{K}P_j \\ B'_j \end{bmatrix} \mathrm{d}S \tag{4.77}$$

$$\begin{aligned} \mathcal{C}_{jklm} = -\frac{1}{2\epsilon}\int_0^l & \begin{bmatrix} 2\left(P'_k - \mathcal{K}Q_k\right)\left[\left(Q'_l + \mathcal{K}P_l\right)\left(Q'_m + \mathcal{K}P_m\right) + B'_l B'_m\right] \\ \left(Q'_k + \mathcal{K}P_k\right)\left[2\left(P'_l - \mathcal{K}Q_l\right)\left(P'_m - \mathcal{K}Q_m\right) - \left(Q'_l + \mathcal{K}P_l\right)\left(Q'_m + \mathcal{K}P_m\right) - B'_l B'_m\right] \\ B'_k\left[2\left(P'_l - \mathcal{K}Q_l\right)\left(P'_m - \mathcal{K}Q_m\right) - \left(Q'_l + \mathcal{K}P_l\right)\left(Q'_m + \mathcal{K}P_m\right) - B'_l B'_m\right] \end{bmatrix} \\ & \cdot \left(\frac{1}{\|\mathbf{q}'\|^3} \begin{bmatrix} P'_j - \mathcal{K}Q_j \\ Q'_j + \mathcal{K}P_j \\ B'_j \end{bmatrix} \right) \mathrm{d}S \end{aligned} \tag{4.78}$$

4.2.2 Tracking frequency response with arc-length continuation technique

The set of equations given by (4.70) can be numerically treated with the arc-length method [3, 8]. The key idea is to follow the response curve assuming that the latter is smooth and that the system response is periodic. An overview of the method is available in Appendix E. The system is harmonically forced with an arbitrary frequency Ω, in another words we set

$$f(S,t) = F(S)\sin(\Omega t) \ . \tag{4.79}$$

To obtain the system response, we track orbits that remain unchanged by the application of the monodromy matrix [5] and the stability of the response is estimated via evaluating the eigenvalues of the same matrix at a converged state. Indeed, considering an initial condition φ^* the problem reads

$$\mathcal{M}(\varphi^*, \Omega)\ \varphi^*(0) = \varphi^*\left(\frac{2\pi}{\Omega}\right) \ . \tag{4.80}$$

When a couple (φ^*, Ω) satisfies (4.80), then we can judge on the stability of the periodic orbit. The latter will be:

- Stable if all eigenvalues are contained in the unit circle.
- Unstable if at least one eigenvalue is out of the unit circle.

As an example, we are considering the system given by (4.70) where $N = 5$. The latter corresponds to a system where the dynamics are projected on the first five modes of the cable. The dofs entitled as φ_1, φ_3 and φ_5 are corresponding to out-of-plane modes while the dofs entitled as φ_2, φ_4 are corresponding to in-plane modes. The parameters of the application are given in Table 4.2. The response curves are plotted in Figure 4.9. The response is sophisticated and multi-valued, therefore the design of cable requires in-depth analysis of their frequency responses. This simple example also depicts potential large displacements close to resonance. The components of the various tensors in (4.70) are given in (4.76-4.78). To have an idea of the amplitude of displacement for the physical system, (4.61) should be used before any comparison.

Table 4.2: Parameters used for the arc-length continuation example (Physical value of a chair lift span)

EA (MN)	T_0 (kN)	ρ (kg/m)	d (m)	h (m)	μ	$F(S)$ (N)
400	80	6	250	10	0.08	$0.8\,(\mathbf{e}+\mathbf{n}+\mathbf{z})$

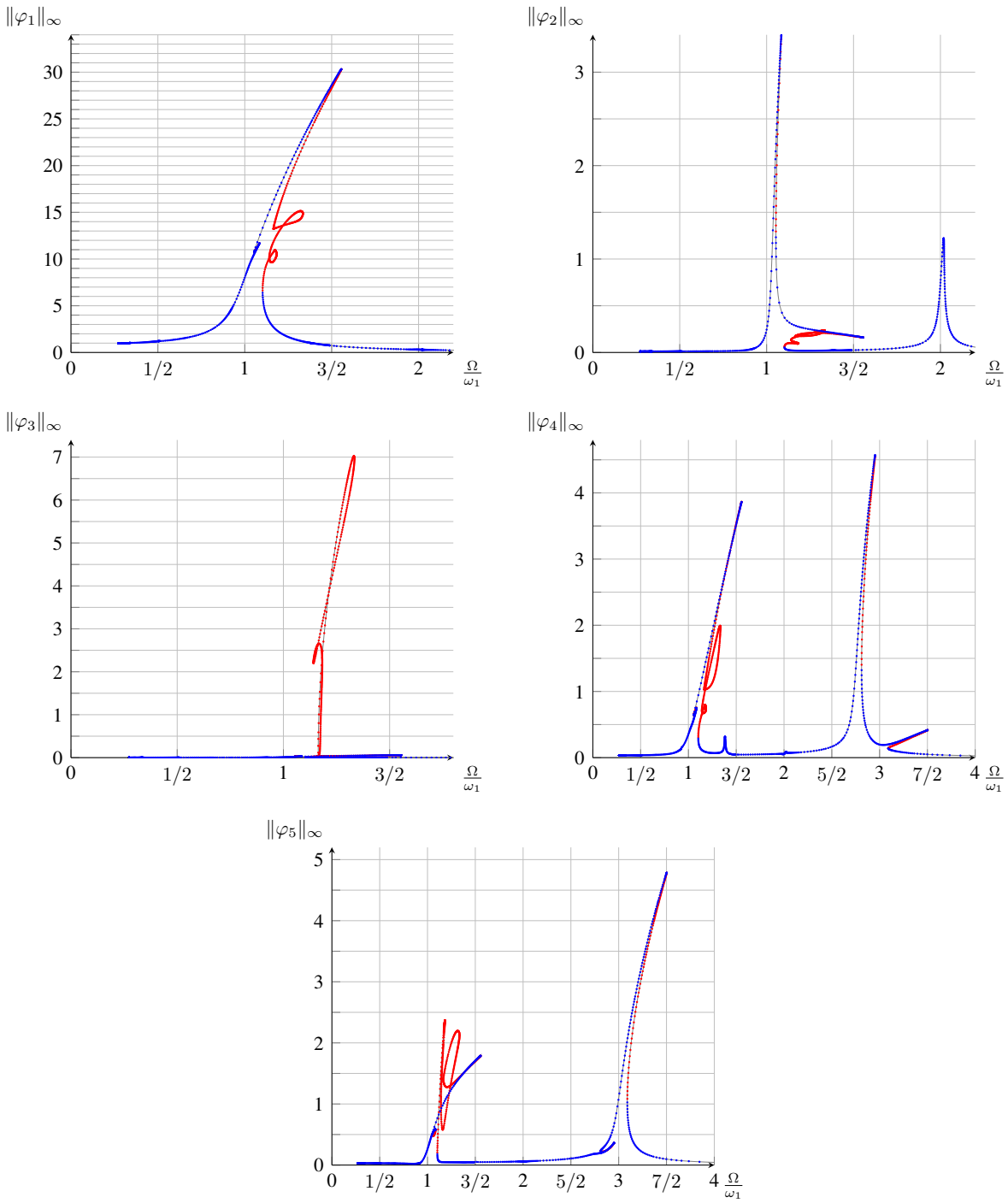

Figure 4.9: Frequency response curves obtained with arc-length continuation technique for a 5 dof system
(dotted line ·····) Stable solutions ; (dotted line ·····) Unstable solutions

4.2.3 Comparison with finite element method

The usage of ROM is mainly driven by its computational efficiency and the possibility of studying analytically small-dofs systems. However, very few comparisons between results of finite element and those of ROM are available.
FEM has been already developed to ensure admissible and accurate solutions [2]. The results obtained via FEM and ROM are different, here we list some differences:

- In FEM, the nonlinear dynamics are integrated with the self-weight effects retained and the assumption of a small displacement is not made.
- In the ROM, amplitudes correspond to modal coordinates so that the displacement profile needs to be built back.
- In the ROM, the vibration around the rest position is an elastic vibration, therefore inextensible/inelastic motions could be roughly approximated.

The goal of this subsection is to compare the predictions made by both methods and to claim on the validity of the ROM. To do such comparisons, we propose the following methodology:

- With the same set of parameters, compute the dynamics of the cable via the ROM and the FEM.
- Build back the cable profile from the ROM according to (4.61)
- Compare the transient trajectories for some given points in the physical domain.
- Compare the evaluation of system amplitude at first and last quarter span and at mid-span in the physical domain with different forcing amplitudes. The latter will be performed via continuation technique on the ROM while the NFEM dynamics will be integrated until a stationary point is reached.

The idea behind this methodology is to compare the same system in the physical domain. As the frequency response corresponds to an asymptotic behavior, we check that the FEM approach and the ROM are providing with similar asymptotic responses for a single span cable. In the end, we are comparing the same system under the same solicitation but with two approaches. The latter comparisons allows to verify the accuracy of the FEM in the nonlinear regimes and also the validity of the assumptions done for the ROM.

Comparisons of transient dynamics

The transient dynamics are of deep interest for engineering applications due to potential high displacements. The ability of reduced-order-model to track such responses could avoid costful computations via refined mesh in NFEM.
Different scenarios are investigated here. We will check system amplitudes close and far from resonances and with different configurations (highly tensed and not so tensed). The set of parameters depicted in Table 4.3 are used for the results depicted in Figures 4.10 - 4.13. The idea between those two different scenarios is that the first case corresponds to a linear regime in the sense that nonlinearities cannot have significant impact on the response whereas in the second case, the geometry and forcing amplitude lead to a response where the nonlinearities are essential to describe the system response. The first (resp. second) case corresponds to the first (resp. second) line of the Table 4.3.
For the quasi-linear regime (taut cable with small forcing amplitude), we see a qualitatively good agreement between both approaches as illustrated in Figure 4.10. The overall motion

Table 4.3: Parameters used for the comparisons between transient dynamics caught via FEM and ROM

Case	EA (MN)	T_0 (kN)	ρ (kg/m)	d (m)	h (m)	α (IS)	$\vec{F}(S)$ (N)	Ω (rad/s)
Quasi linear	400	111.58	5.56	300	10	0.08	$0.0001\,(\mathbf{x}+\mathbf{y}+\mathbf{z})$	2.22
Nonlinear	100	80	5.56	300	15	0.08	$0.8\,(\mathbf{x}+\mathbf{y}+\mathbf{z})$	2.25

Table 4.4: Parameters used for the comparisons between asymptotic dynamics caught via FEM and ROM

Case	EA (MN)	T_0 (kN)	ρ (kg/m)	d (m)	h (m)	α (IS)	$\vec{F}(S)$ (N)
Quasi linear	400	111.58	5.56	300	10	0.2	$0.0001\,(\mathbf{x}+\mathbf{y}+\mathbf{z})$
Nonlinear	100	80	5.56	300	15	0.2	$0.8\,(\mathbf{x}+\mathbf{y}+\mathbf{z})$

of the cable is described similarly so that the maximum amplitudes of vibrations is the same. However, the ROM is way faster in terms of CPU-time due to its low number of dof. The envelop of the cable motion is also well approximated as shown in Figure 4.11. Indeed, both FEM and ROM provide with the same displacement amplitude in this case although it is transient dynamics.
When it comes to the nonlinear case, the qualitative agreement between the two methods holds. However, discrepancies in the longitudinal direction arise. The small differences can be explained by the difference in the treatment of the geometrical nonlinearity since it is linearized up to third order in the ROM. Unfortunately, there is not a method which produce larger values of displacement so that we cannot prefer a method for safer designs.
Computational efficiency is the key parameter to choose one of the approaches, although FEM may be more flexible when it comes to compute the response of more complicated systems (e.g. cable networks, hybrid boundary conditions, beam-cable structures, ...). One could say that ROM allows analytical derivations of the system responses but it relies on very practical knowledge of cable nonlinear dynamics and behaviors [1, 9]. Moreover, the more dofs are of interest, the less intuitive are the analytical derivations. In this case, FEM is a reliable tool to investigate nonlinear dynamics of an unknown cable system and to determine the applicability of the ROM.

Comparisons of asymptotic dynamics

Dynamic simulations are costful especially with NFEM. The ROM is therefore a valuable tool to describe rich dynamical behaviors due to the light computational effort required and its qualitative accuracy. Due to the system dimension, continuation techniques are not practical for tracing the NFEM asymptotic dynamic responses. This is why ROM is better suited for arc-length continuation. A comparison between asymptotic responses of the NFEM dynamics and the ROM response computed via continuation method is proposed here. The goal of this comparison is to assess for the reliability of designs relying of ROM and also for the NFEM ability to trace nonlinear behaviors.
The parameters, used for the computations are given in Table 4.4. Every computations have been performed with a time step such that the smallest period at stake is divided into 2000 intervals.

In Figures 4.14 and 4.15, we can see that the linear regimes are well reconstituted by both

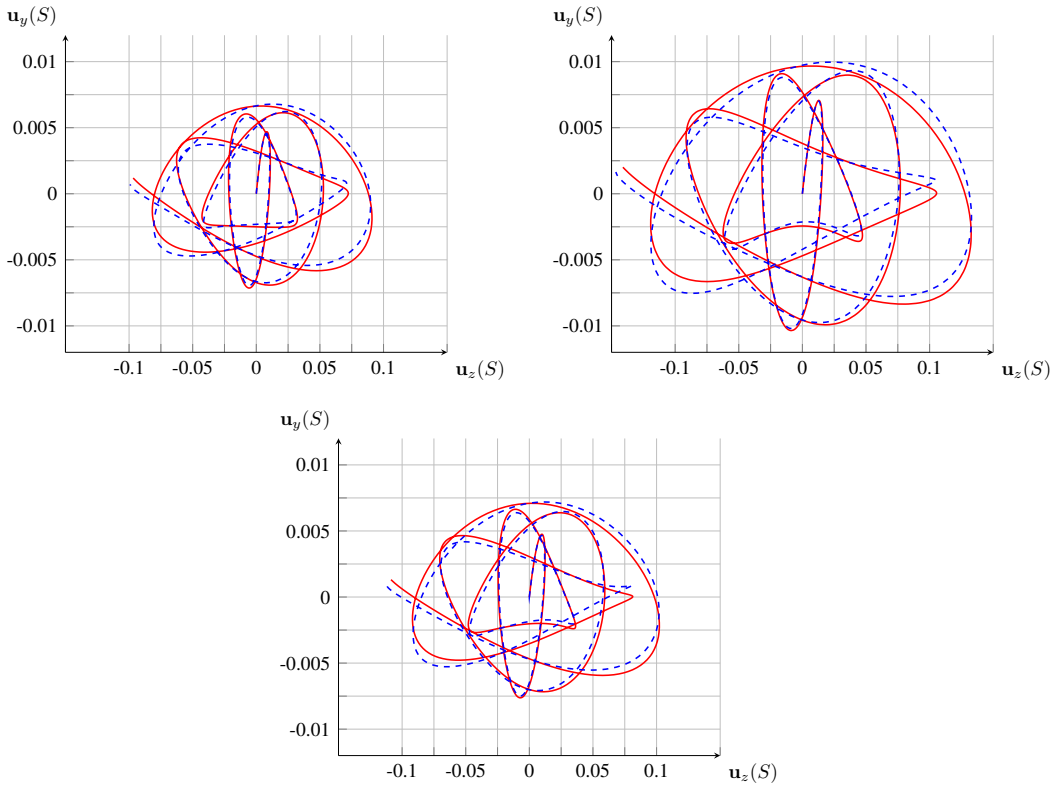

Figure 4.10: Vertical displacement versus transverse displacement (mm) for the first quarter span, mid-span and last quarter span obtained via FEM (solid line —) and via ROM (dashed line - - -) for a transient dynamics in a quasi-linear regime - Parameters are given in Table 4.3

approaches. In this case, the assumptions made for obtaining the ROM do not have any impact on the obtained amplitudes. However the highly-nonlinear regime responses obtained from FEM and the ROM are different. For low frequencies, the two predictions of amplitude are still qualitatively in agreement, but with higher frequencies come more discrepancies. It appears that coupling between modes are not always traced by the ROM and that the latter tends to overestimate the amplitude of displacement. Additional modes may be added in the continuation to catch further details about the nonlinear dynamics however some discrepancy subsist between both approaches in the nonlinear case. Even though the modes obtained via FEM and ROM are the same, it is difficult to keep a good match between dynamic responses when the cable is slacker, inclined and subjected to moderate loads. To accommodate this issue, the usage of ROM should be always supported by another tool, especially in the latter case.

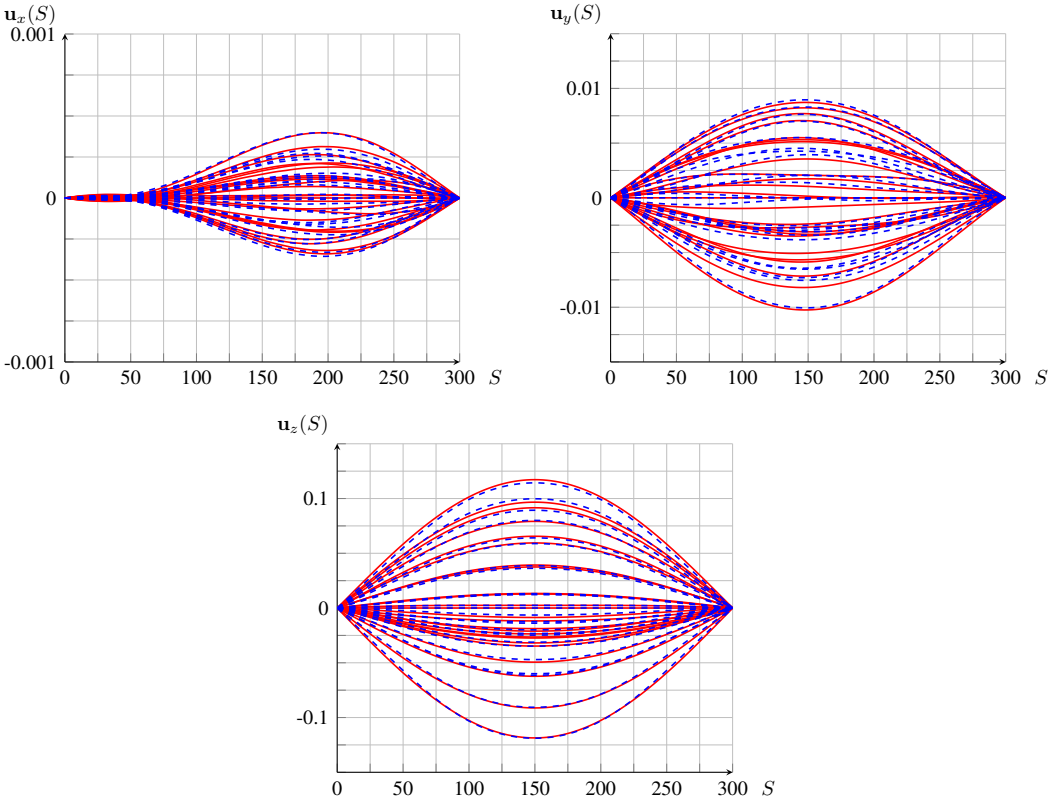

Figure 4.11: Displacement (mm) versus curvilinear abscissa (m) for the **x** direction, **y** direction and **z** direction obtained via FEM (solid line —) and via ROM (dashed line - - -) for a transient dynamics in a quasi-linear regime- Parameters are given in Table 4.3

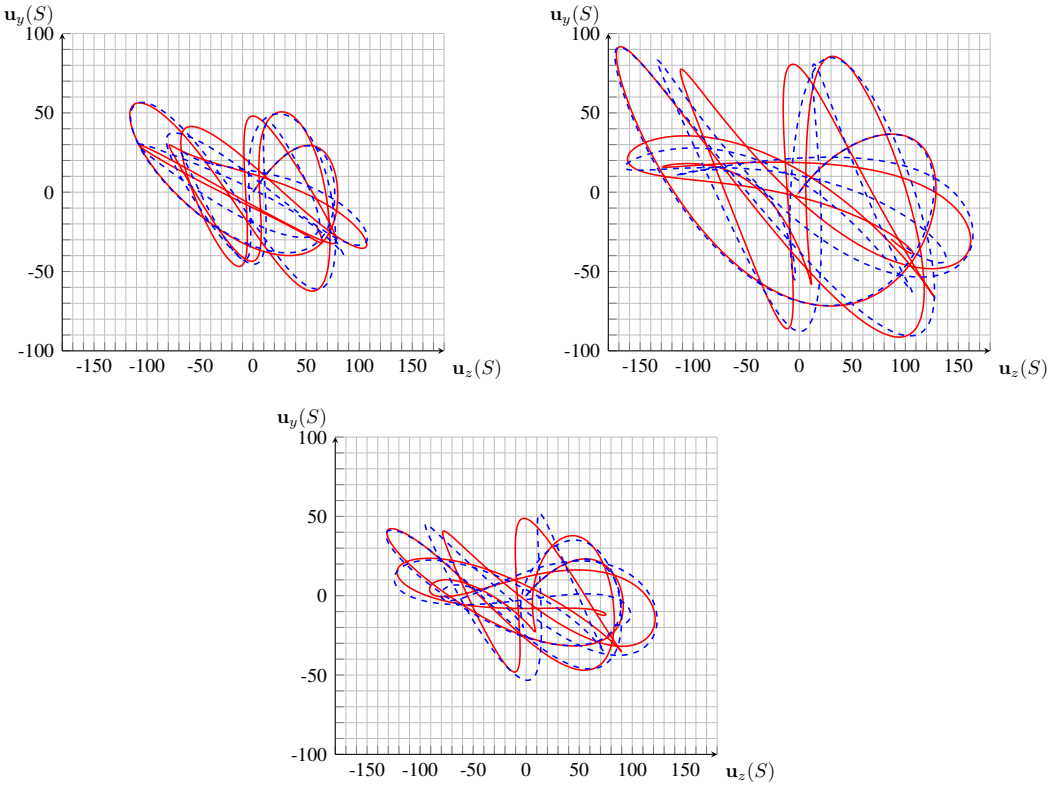

Figure 4.12: Vertical displacement versus transverse displacement (mm) for the first quarter span, mid-span and last quarter span obtained via FEM (solid line —) and via ROM (dashed line - - -) for a transient dynamics in a nonlinear regime - Parameters are given in Table 4.3

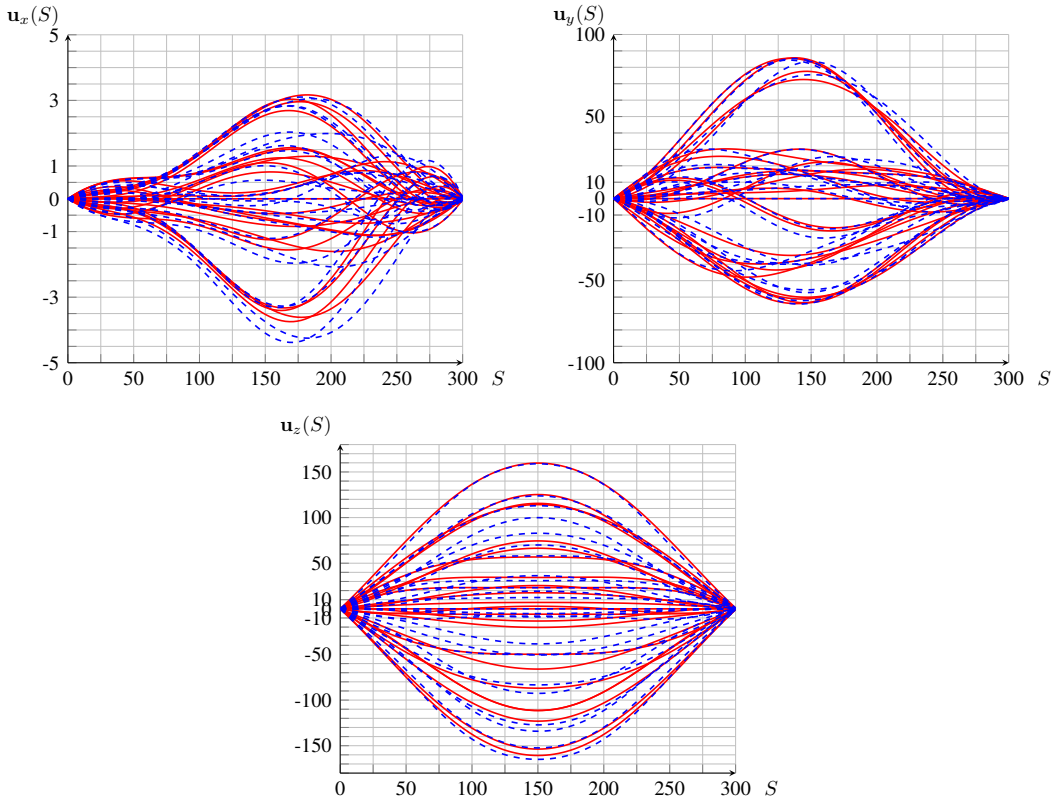

Figure 4.13: Displacement (mm) versus curvilinear abscissa (m) for the **x** direction, **y** direction and **z** direction obtained via FEM (solid line —) and via ROM (dashed line - - -) for a transient dynamics in a nonlinear regime - Parameters are given in Table 4.3

4.3 Approximate treatment via the method of multiple scales

A treatment of the equations (4.70) is proposed via the method of the multiple scales [7]. The latter consists on seeking a solution in the form of a series expansion considering an arbitrary small book-keeping parameter ϵ

$$\varphi_j(t,\epsilon) = \sum_{k=0}^{N} \epsilon^k \varphi_{j,k}\left(T_0, ..., T_N\right) \ , \tag{4.81}$$

where the parameter ϵ artificially connects the physical time t to different time scale as follows

$$T_0 = t \quad , \quad T_k = \epsilon^k t \quad , \quad k = 1, ..., N \ , \tag{4.82}$$

where the time T_0 is coined as the fast-time scale and other time scales are coined as slow-time scales. All those time scales are assumed to be independent and the time differentiation reads

$$\frac{\mathrm{d}}{\mathrm{d}t} = \sum_{k=0}^{N} \epsilon^k \frac{\partial}{\partial T_k} = \sum_{k=0}^{N} \epsilon^k D_k \tag{4.83}$$

$$\frac{\mathrm{d}^2}{\mathrm{d}t^2} = \sum_{k=0}^{N}\sum_{l=0}^{N} \epsilon^{k+l} \frac{\partial^2}{\partial T_k \partial T_l} = \sum_{k=0}^{N}\sum_{l=0}^{N} \epsilon^{k+l} D_k D_l \ , \tag{4.84}$$

where the partial differentiation with respect to a time-scale T_k is denoted D_k for conciseness. We further assume that D_k and D_j commute for all k and j. After having injected the series

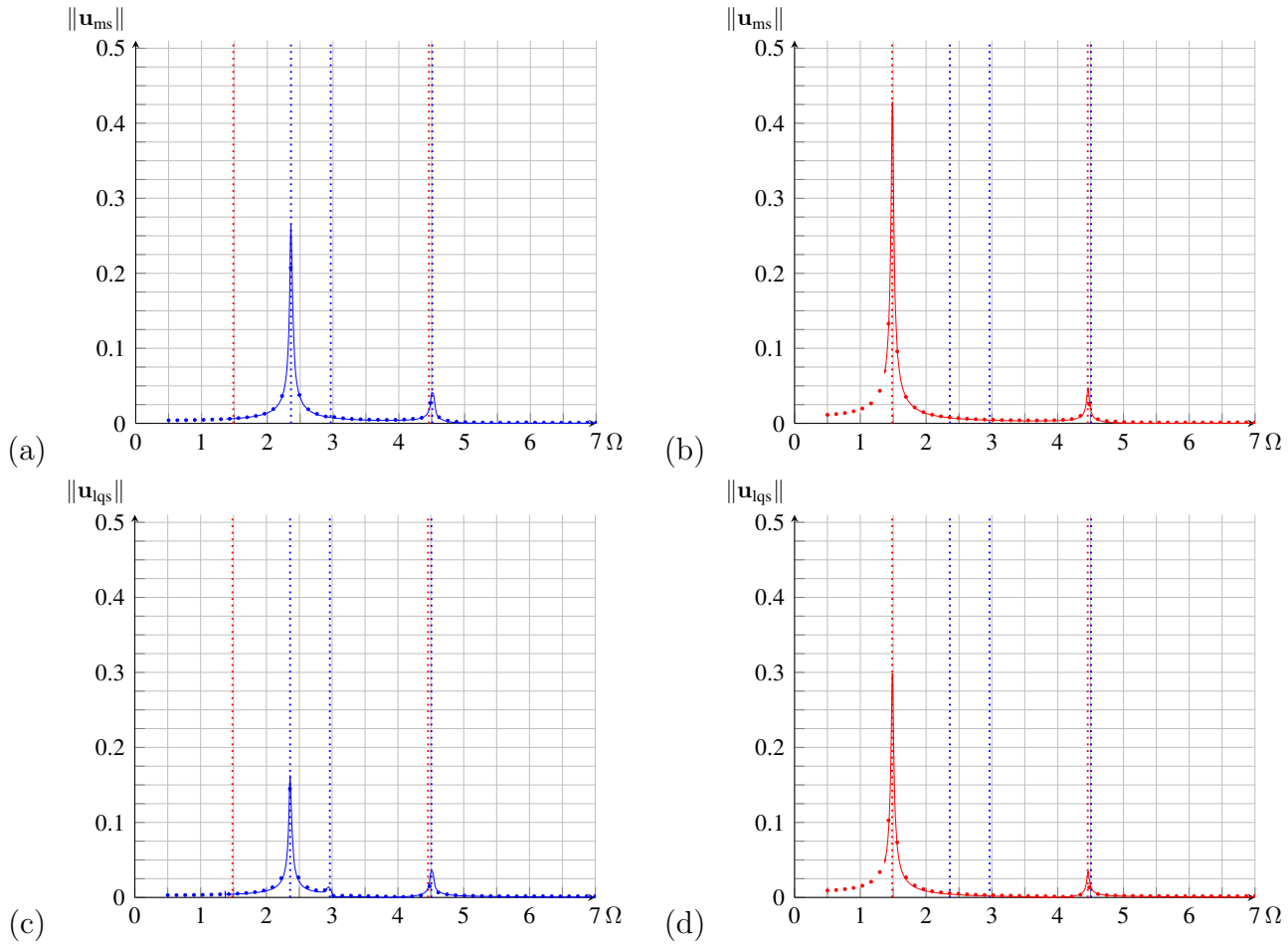

Figure 4.14: Displacement (mm) versus frequency of forcing (rad/s) for the **y** direction and **z** direction obtained via FEM (dots •) and (dots •) and via arc-length continuation endowed in the ROM (solid line —) and (solid line —) in a linear regime - (a) Vertical amplitude at midspan (b) Transversal amplitude at midspan (c) Vertical amplitude at last quarter span (d) Transversal amplitude at last quarter span - Undamped frequencies are plotted vertically - Parameters are given in Table 4.4

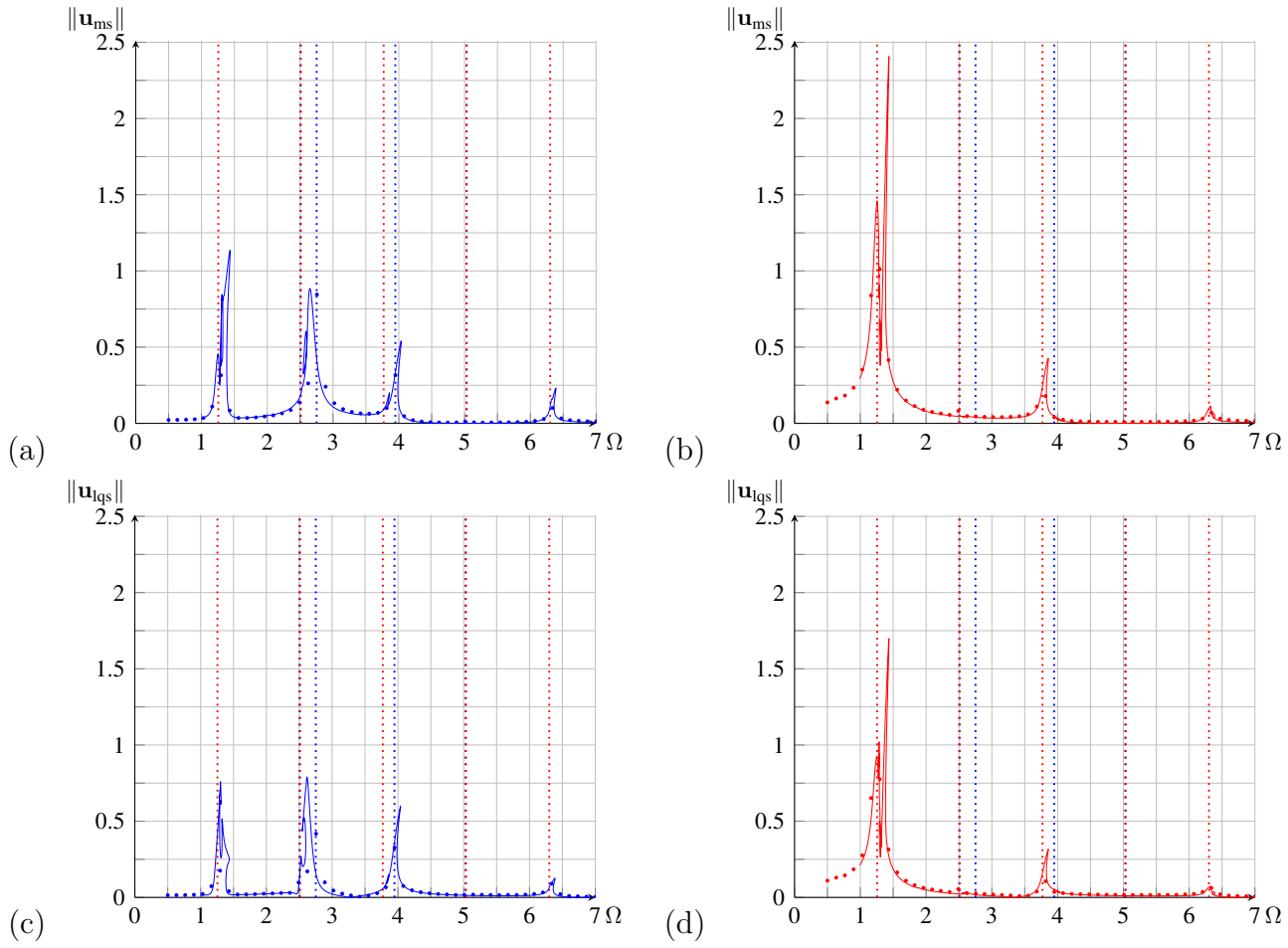

Figure 4.15: Displacement (m) versus frequency of forcing (rad/s) for the **y** direction and **z** direction obtained via FEM (dots •) and (dots •) and via arc-length continuation endowed in the ROM (solid line —) and (solid line —) in a nonlinear regime - (a) Vertical amplitude at midspan (b) Transversal amplitude at midspan (c) Vertical amplitude at last quarter span (d) Transversal amplitude at last quarter span - Undamped frequencies are plotted vertically - Parameters are given in Table 4.4

expansion into the governing equation, one vanishes every coefficient of the obtained series. Generally speaking, this method accommodates very well for stationary solutions that can be seen as perturbations of a linear vibration. For this reason, the actual nonlinear dynamics (4.70) is mapped to the following equation

$$\ddot{\varphi}_j + \epsilon^{\xi} \underbrace{\hat{\xi}_j \dot{\varphi}_j}_{\text{No summation}} + \mathbf{K}_{jk}\varphi_k + \epsilon^{Q}\hat{\mathcal{Q}}_{jkl}\varphi_k\varphi_l + \epsilon^{C}\hat{\mathcal{C}}_{jklm}\varphi_k\varphi_l\varphi_m = \epsilon^{f}\hat{f}_j \quad , \quad 1 \leqslant j \leqslant N \ , \tag{4.85}$$

where the exponents in ϵ^{ξ}, ϵ^{Q}, ϵ^{C} and ϵ^{f} have to be specified depending on the application. A lot of cases can be considered depending on the amplitude of vibration, number and nature of modes used for obtaining the reduced-order model, nature of the forcing and value of the coefficients of the nonlinear terms. In the following, the general case of a primary resonance with N-dofs is detailed and an application to a single-dof projection is done as an example.

4.3.1 General treatment at primary resonance

We are treating here the scenario of an excitation around a main frequency. To treat the latter, assumptions are made so that we remain close to the physics of the cables:

- The motion is incremental so that the amplitude of the incremental displacement is first order in ϵ i.e. $\varphi = \epsilon\varphi_1 + \epsilon^2\varphi_2 + \epsilon^3\varphi_3$;
- Low damping so that its influence only comes at high order of ϵ. In this work, we consider it at second order i.e. $\epsilon^{\xi} = \epsilon^2$;
- The nonlinear dynamics prevail in the behavior so that both quadratic and cubic terms influence should be traced the earliest possible in the solution. In another words, we consider that $\epsilon^{Q} = \epsilon^0$ and $\epsilon^{C} = \epsilon^0$ ($\mathcal{O}(1)$);
- The external forcing relatively small compared to the static tension i.e. $\epsilon^{f} = \epsilon^2$ with a frequency close to the frequency of the mode considered $\Omega = \omega + \epsilon^2\sigma$. As an example we take here a cosine;
- The cable is relatively highly tensed so that most of the modes are favorable to a internal resonance scenario.

The latter set of assumptions results in the following equation

$$\ddot{\varphi}_j + \epsilon^2\hat{\xi}_j\dot{\varphi}_j + \mathbf{K}_{jk}\varphi_k + \hat{\mathcal{Q}}_{jkl}\varphi_k\varphi_l + \hat{\mathcal{C}}_{jklm}\varphi_k\varphi_l\varphi_m = \epsilon^2\hat{f}_j \quad , \quad 1 \leqslant j \leqslant N \ , \tag{4.86}$$

where we have for all $1 \leqslant j \leqslant N$

$$\varphi_j = \epsilon\varphi_{j,1} + \epsilon^2\varphi_{j,2} + \epsilon^3\varphi_{j,3} + \mathcal{O}(\epsilon^4) \tag{4.87}$$

$$\dot{\varphi}_j = \epsilon D_0\varphi_{j,1} + \epsilon^2\left(D_0\varphi_{j,2} + D_1\varphi_{j,1}\right) + \epsilon^3\left(D_0\varphi_{j,3} + D_1\varphi_{j,2} + D_2\varphi_{j,1}\right) + \mathcal{O}(\epsilon^4) \tag{4.88}$$

$$\ddot{\varphi}_j = \epsilon D_0^2\varphi_{j,1} + \epsilon^2\left(D_0^2\varphi_{j,2} + 2D_0D_1\varphi_{j,1}\right) + \epsilon^3\left(D_0^2\varphi_{j,3} + 2D_0D_1\varphi_{j,2} + 2D_0D_2\varphi_{j,1}\right) + \mathcal{O}(\epsilon^4) \tag{4.89}$$

A set of N detuning parameters should be introduced as follows

$$\omega_1 = \Omega + \sigma_1\epsilon^2 \ , \tag{4.90}$$

$$\omega_j = k_j\omega_1 + \sigma_j\epsilon^2 \quad , \quad 2 \leqslant j \leqslant N \ . \tag{4.91}$$

Note that for $2 \leqslant j \leqslant N$, all σ_j should be evaluated and used as a given input data. The actual parameter is σ_1, namely the main detuning. The first order equations are obtained via considering the terms at order ϵ^1 in (4.86), which reads:

$$D_0^2\varphi_{j,1} + \mathbf{K}_{jk}\varphi_{k,1} = 0 \quad , \quad 1 \leqslant j \leqslant N \ . \tag{4.92}$$

The latter can be solved exactly via considering the linear system given by

$$D_0 \begin{bmatrix} D_0\varphi \\ \varphi \end{bmatrix} = \begin{bmatrix} \mathbf{0} & -\mathbf{K} \\ \mathbf{I} & \mathbf{0} \end{bmatrix} \begin{bmatrix} D_0\varphi \\ \varphi \end{bmatrix} \ . \tag{4.93}$$

The latter can be solved exactly with the matrix exponential. However, most of the applications does not require such a tool and often simplifies drastically since the in-plane and out-of-plane dynamics are decoupled at first order.
The first order solutions often consists on a linear combination of harmonics where coefficients are depending of T_1 and T_2 time scales. The second order equations are obtained via considering the terms up to ϵ^2 in (4.86)

$$D_0^2\varphi_{j,2} + \mathbf{K}_{jk}\varphi_{k,2} = -\left(2D_0D_1\varphi_{j,1} + \hat{\mathcal{Q}}_{jkl}\varphi_{k,1}\varphi_{l,1}\right) \quad , \quad 1 \leqslant j \leqslant N \ . \tag{4.94}$$

For this set of equations, the secular terms are removed. The latter corresponds to a non-resonance condition so that the motion remains bounded. A strategy that works on every computer or algebraic manipulation, is to re-use the equations obtained here for higher order equations. As a consequence, for each j, two pieces of information are gathered: the particular solution and the non-resonance condition. The particular solution is obtained via considering the particular solution of (4.94) where every secular terms is removed. The non resonance condition is obtained via applying solvability conditions

$$0 = \left(2D_0D_1\varphi_{j,1} + \hat{\mathcal{Q}}_{jkl}\varphi_{k,1}\varphi_{l,1}\right) \quad , \quad 1 \leqslant j \leqslant N \ , \tag{4.95}$$

where we only keep the resonant term in the blue term. Sometimes, the latter can be done automatically via applying Fredholm alternative [4].
The last step consists on treating the third order part of (4.86) which reads

$$\begin{aligned} D_0^2\varphi_{j,3} + \mathbf{K}_{jk}\varphi_{k,3} = & \frac{f_j}{2}\left(e^{i\Omega T_0} + e^{-i\Omega T_0}\right) \quad , \quad 1 \leqslant j \leqslant N \\ & - \left(2D_0D_1\varphi_{j,2} + D_1^2\varphi_{j,1} + 2D_0D_2\varphi_{j,1} + \hat{\xi}_j D_0\varphi_{j,1}\right) \ . \\ & - \left(\hat{\mathcal{Q}}_{jkl}\varphi_{k,1}\varphi_{l,2} + \hat{\mathcal{Q}}_{jkl}\varphi_{k,2}\varphi_{l,1} + \hat{\mathcal{C}}_{jklm}\varphi_{k,1}\varphi_{l,1}\varphi_{m,1}\right) \end{aligned} \tag{4.96}$$

The only information needed is the non-resonance condition obtained via:

- Writing Ω as a function of ω_j;
- Selecting the secular terms and setting them to 0;
- Injecting the non-resonant conditions obtained from (4.94);
- Using the polar form for every complex coefficients;
- Parting real and imaginary parts;
- Searching for equilibrium points.

Of course each configuration is different and some small adjustments should be done when using the method of multiple scales. The described methodology can be adapted for every primary resonance scenario.

4.3.2 Single-dof projection at primary resonance

We are considering here the case of the projection along a single mode. One should state that if the mode is an in-plane mode then softening or hardening behavior can be expected whereas if the mode is an out-of-plane mode the behavior is strictly hardening.
Indeed, due to the expression of the quadratic tensor given in (4.77), only the planar motion are subjected to quadratic terms whereas out-of-plane motion are only subjected to cubic terms.
Our study consists on a particular case of (4.85) where the following assumptions are taken:

- The motion is incremental so that the amplitude of the incremental displacement is first order in ϵ i.e. $\varphi = \epsilon\varphi_1 + \epsilon^2\varphi_2 + \epsilon^3\varphi_3$;
- The damping influence is considered at second order i.e. $\epsilon^\xi = \epsilon^2$ so that damping only appears in equations at order ϵ^3;
- The quadratic term influence should be traced at order ϵ^2 so that we consider $\epsilon^Q = \epsilon^0$;
- The cubic term influence should be traced at order ϵ^3 so that we consider $\epsilon^C = \epsilon^0$;
- The external forcing term is considered at third order i.e. $\epsilon^f = \epsilon^2$ with a frequency close to the frequency of the mode considered $\Omega = \omega + \epsilon^2\sigma$. Here we use a cosine as an example.

where the subscript $\bullet_j$ has been removed since only one mode is considered for the projection.
In this particular case, (4.85) reduces to

$$\ddot{\varphi} + \epsilon\xi\dot{\varphi} + \omega^2\varphi + \mathcal{Q}\varphi^2 + \mathcal{C}\varphi^3 = \epsilon^3 f \ . \tag{4.97}$$

In the presented case, we have

$$\frac{\mathrm{d}}{\mathrm{d}t} = D_0 + \epsilon D_1 + \epsilon^2 D_2 + ... \ , \tag{4.98}$$

$$\frac{\mathrm{d}^2}{\mathrm{d}t^2} = D_0^2 + 2\epsilon D_1 D_0 + \epsilon^2\left(D_1^2 + 2D_0 D_2\right) + ... \tag{4.99}$$

Injecting all our assumptions in (4.85) yields

$$D_0^2\varphi_1 + \omega^2\varphi_1 = 0 \ , \tag{4.100}$$

$$D_0^2\varphi_2 + \omega^2\varphi_2 = -2D_0D_1\varphi_1 - \mathcal{Q}\varphi_1^2 \ , \tag{4.101}$$

$$\begin{aligned} D_0^2\varphi_3 + \omega^2\varphi_3 = \frac{f}{2}\left(e^{i\omega T_0 + i\sigma T_2} \ + e^{-i\omega T_0 - i\sigma T_2}\right) - \mathcal{C}\varphi_1^3 - 2\mathcal{Q}\varphi_1\varphi_2 - D_1^2\varphi_1 \\ - \xi D_0\varphi_1 - 2D_0D_2\varphi_1 - 2D_1D_0\varphi_2 \end{aligned} \ . \tag{4.102}$$

Let us note that the equation at order ϵ^0 is trivially satisfied. Equation (4.100) gives

$$\varphi_1(T_0, T_1, T_2) = A(T_1, T_2)e^{i\omega T_0} + A^*(T_1, T_2)e^{-i\omega T_0} \ , \tag{4.103}$$

where A^* stands for the complex conjugate of A.
Injecting the solution in (4.101) yields

$$D_0^2\varphi_2 + \omega^2\varphi_2 = -2i\omega D_1 A e^{i\omega T_0} + 2i\omega D_1 A^* e^{-i\omega T_0} - \mathcal{Q}\left(A^2 e^{2i\omega T_0} + 2|A|^2 + (A^*)^2 e^{-2i\omega T_0}\right) \ , \tag{4.104}$$

The stationary solution can be met if $D_1 A = 0$. In another words, as we are looking for periodic motions, the solution cannot be unbounded in time.
It results into the following particular solution

$$\varphi_2(T_0, T_2) = \frac{\mathcal{Q}}{3\omega^2}\left(\left(A(T_2)\right)^2 e^{2i\omega T_0} - 6|A(T_2)|^2 + \left(A^*(T_2)\right)^2 e^{-2i\omega T_0}\right) \ . \tag{4.105}$$

The last equation given by (4.102) is only used to obtain a non-secularity condition. Considering only the terms in factor of $e^{i\omega T_0}$ gives

$$i\xi\omega A + \left(3\mathcal{C} - \frac{10\mathcal{Q}^2}{3\omega^2}\right) A^2 A^* + 2i\omega A' = \frac{f}{2} e^{i\sigma T_2} \ . \tag{4.106}$$

The vibration amplitude is taken in polar form, i.e. $A\left(T_2\right) = r\left(T_2\right) e^{i\theta(T_2)}$. Equation (4.106) is multiplied by $e^{-i\theta}$

$$i\xi\omega r + \left(3\mathcal{C} - \frac{10\mathcal{Q}^2}{3\omega^2}\right) r^3 + 2i\omega r' - 2\omega r\theta' = \frac{f}{2} e^{i\sigma T_2 - \theta} \ . \tag{4.107}$$

The real and imaginary parts of (4.107) are separated as follows

$$\begin{cases} r\theta' = \left(\dfrac{3\mathcal{C}}{2\omega} - \dfrac{5\mathcal{Q}^2}{3\omega^3}\right) r^3 - \dfrac{f}{4\omega}\cos\left(\sigma t_2 - \theta\right) \\ r' = \dfrac{f}{4\omega}\sin\left(\sigma t_2 - \theta\right) - \dfrac{\xi}{2} r \end{cases} . \tag{4.108}$$

The following change of variable is performed: $\tilde{\theta} = \sigma t_2 - \theta$ so that we have eventually

$$\begin{cases} r\tilde{\theta}' = r\sigma + \left(\dfrac{5\mathcal{Q}^2}{3\omega^3} - \dfrac{3\mathcal{C}}{2\omega}\right) r^3 + \dfrac{f}{4\omega}\cos\left(\tilde{\theta}\right) \\ r' = \dfrac{f}{4\omega}\sin\left(\tilde{\theta}\right) - \dfrac{\xi}{2} r \end{cases} . \tag{4.109}$$

The stationary points are obtained for $r' = \tilde{\theta}' = 0$. Squaring and adding both equations give the following relation

$$\frac{f^2}{16\omega^2} = \left[\frac{\xi^2}{4} + \left(\sigma - \left(\frac{3\mathcal{C}}{2\omega} - \frac{5\mathcal{Q}^2}{3\omega^3}\right)\right)^2 r^2\right] r^2 \ . \tag{4.110}$$

The latter may be written otherwise as

$$\sigma = \left(\frac{3\mathcal{C}}{2\omega} - \frac{5\mathcal{Q}^2}{3\omega^3}\right) r^2 \pm \sqrt{\frac{f^2}{16 r^2 \omega^2} - \frac{\xi^2}{4}} \ . \tag{4.111}$$

Solving (4.110) or (4.111) for the couple (r, σ) gives the frequency curve. The sign of $\frac{3\mathcal{C}}{2\omega} - \frac{5\mathcal{Q}^2}{3\omega^3}$ determines if hardening or softening behavior appears in the system.
An application for the first out-of-plane and first in plane mode is proposed and challenged via the arc-length method. The parameters used are given in Table 4.5. The latter results in rescaled parameters according to (4.85) which are given in 4.6. We compare the response curve obtained via MMS and the arc-length method in Figure 4.16.

4.4 Stability investigations via Hill equation

The stability of a solution of (4.70) is of many interest for mechanical engineering. For most applications, the orbital stability is the correct definition that one can expect of a stable solution. The latter can be defined as a solution whose slightly perturbed trajectory remains in a small neighborhood of its periodic orbit. In another words, when the initial condition is perturbed

Table 4.5: Parameters used for the arc-length continuation versus MMS

Attributes	Values
EA (MN)	400
ρ (kg.m^{-1})	5
d (m)	300
h (m)	10
H (kN)	100
$\mathbf{C}$ (IS)	0.08
F (N)	0.3

Table 4.6: Coefficients obtained according to the methodology proposed

Attributes	Values for first OOP mode	Values for first IP mode
ξ	0.0216	0.0216
ω	1.0044	2.0076
$\mathcal{Q}$	0	-0.02489
$\mathcal{C}$	0.0011	0.01749
f	0.4283	0.0320

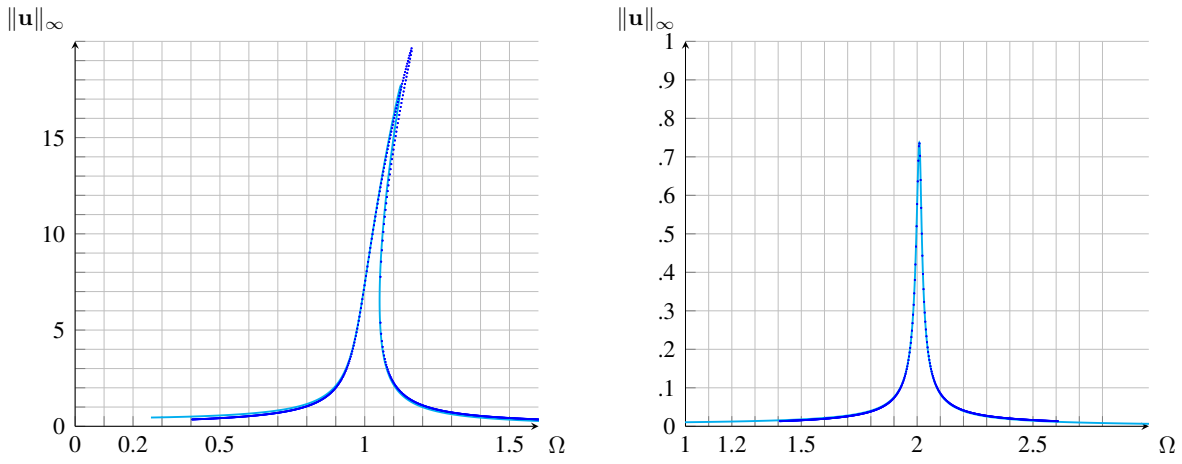

Figure 4.16: Response curves for the first OOP mode and the first IP mode obtained via arc-length method (solid line —) and MMS (dotted line ·····) for a single-dof projection - Parameters are given in Tables 4.5 - 4.6

slightly, the perturbed orbit remains contained in a torus which centered on the periodic orbit. This behavior can be investigated via setting $\tilde{\varphi} = \varphi + \delta$ where φ satisfies (4.70) and injecting this function into (4.70). Then, the equations are expanded at first order so that an equation on δ is obtained

$$\ddot{\delta}_j + \underbrace{\xi_j \dot{\delta}_j}_{\text{No summation}} + \mathbf{K}_{jk}\delta_k + \mathcal{Q}_{jkl}\left(\varphi_k\delta_l + \varphi_l\delta_k\right) + \mathcal{C}_{jklm}\left(\varphi_l\varphi_m\delta_k + \varphi_k\varphi_m\delta_l + \varphi_k\varphi_l\delta_m\right) = 0 \quad 1 \leqslant j \leqslant N \; . \tag{4.112}$$

where the Einstein convention is used for sum.
As φ is a periodic function, equation (4.112) corresponds to a multi-dimensional Hill equation with constant damping. The latter can easily be exploited numerically via the computation of the eigenvalues of the monodromy matrix.
When $N = 1$, the latter simplifies in the following:

$$\ddot{\delta} + \xi\dot{\delta} + \left(\mathbf{K} + 2\mathcal{Q}\varphi + 3\mathcal{C}\varphi^2\right)\delta = 0 \; . \tag{4.113}$$

When quadratic terms are negligible and when the oscillation is mainly composed of the first harmonic which is typical from out of plane cable vibrations close to the main resonance, the latter can be directly mapped to the Mathieu equation as follows

$$\ddot{\delta} + \xi\dot{\delta} + \left(\mathbf{K} + \frac{3\mathcal{C}\Phi^2}{2} + \frac{3\mathcal{C}\Phi^2}{2}\cos\left(2\Omega t\right)\right)\delta = 0 \; . \tag{4.114}$$

For practical applications, the Mathieu equation holds phenomenological mechanisms of instability. Under some rough approximations, the latter can be applied also to in-plane vibrations which opens the possibility of a better design of cable relying on dynamical analysis, see Appendix G for details.
However, practical designs of cable systems require more developments around the questions of Hill equations. Although numerical tools can track any situations, it does not produce the knowledge to better understand the mechanisms of instability intrinsic to the cable dynamics.

Conclusion of the chapter

This chapter gathers most of the known development and provide with essential features of cable simulation. Main results and contributions are:

- The developments of system equations in a unified way with the statics and the linear vibrations;
- Several way of computing modes and frequencies are gathered: analytical approximations, finite difference and finite element and their comparisons;
- A general way to derive a reduced order model more suitable to analytical developments and faster numerical integration;
- A general methodology to catch instability via two tools: the arc-length continuation technique and the use of Hill equations;
- A canvas to derive the method of multiple scales applied to the particular case of an aerial ropeway.

The limitations are the following:

- We lack some experimental validation for the choice of the modes selected in our work;
- Very few applications were done due to a lack of knowledge about the usual solicitation of the aerial ropeway. Every illustration and application are relying on pure assumption and old engineering examples;
- The extension to more sophisticated systems is not straightforward and requires tedious numerical manipulations.

Following improvements could be done:

- More complex cases could be investigated such as including more dofs in the system treated via the method of multiple scales or considering energy exchange with another system (Nonlinear Energy Sink perhaps);
- The general application of Hill equation could be implemented to provide with a predictive tool for engineering;
- Defining criteria to prevent instabilities to happen in reality by the combined use of experiments and the method of multiple scales;

References

[1] Benedettini, F., Rega, G., and Alaggio, R. (1995). Non-linear oscillations of a four-degree-of-freedom model of a suspended cable under multiple internal resonance conditions. *Journal of Sound and Vibrations*, 182:775–798.

[2] Bertrand, C., Acary, V., Ture Savadkoohi, A., and Lamarque, C.-H. (2020). A robust and efficient numerical finite element method for cables. *International Journal for Numerical Method in Engineering*, 121.

[3] Crisfield, M. (1997). *Nonlinear Finite Element Analysis of Solid and Structures*. John Wiley and Sons.

[4] Delves, L. M. and Mohamed, J. L. (1985). *Eigenvalue problems and the Fredholm alternative*. Cambridge University Press.

[5] Floquet, G. (1883). Sur les équations différentielles linéaires à coefficients périodiques. *Annales Scientifiques de l'École Normale Supérieure*, 12.

[6] Irvine, H. M. (1992). *Cable structures*. Dover, New York. OCLC: 831328789.

[7] Nayfeh, A. H. and Mook, D. (1995). *Forced Oscillations of Systems Having a Single Degree of Freedom*. John Wiley & Sons, Ltd.

[8] Sundararajan, P. and Noah, S. (1997). Dynamics of forced nonlinear systems using shooting/arc-length continuation methods - application to rotor systems. *ASME, J. Vib. Acoustic*, 119:9–20.

[9] Warminski, J., Zulli, D., Rega, G., and Latalski, J. (2016). Revisited modelling and multimodal nonlinear oscillations of a sagged cable under support motion. *Meccanica*, 51:2541–2575.

Chapter 5

Applications to aerial ropeways: One-span model

This chapter is concerned with the applications of the developed methodology in Chapter 2 to the particular cases of aerial ropeways. Although the context seems like an engineering application, essential features of discussion are not omitted. Limitations are clearly stated and discussed.
The motivation here is to derive analytical tools for the study of the translating cable mechanics. Our inspiration mainly comes from the suspended bridge community (see review from [2]) which we coupled to a mixed Eulerian-Lagrangian viewpoint. The history of axially moving cable has been detailed in Chapter 1.
First, the equation of motion for an inclined moving cable which is suspended between two eyelets provided a given tension on one eyelet are derived. Then derivations inherent to steady-state solution and linear vibrations of this system are given. Eventually, the parametric instabilities due to axial velocity are discussed.

5.1 Context and modeling choices

We are interested into the equilibrium of a cable which axial velocity is prescribed as v. As the cable flows throughout the span, the studied domain does not remain between boundaries. To bypass this, the following change of coordinate is endowed

$$S(\tilde{S},t) = \tilde{S} + \int_0^t v(t^*)\mathrm{d}t^* \ . \tag{5.1}$$

This change of space variable forces the curvilinear abscissa to span between 0 and L and allows to apply boundary conditions on the particles located respectively at the beginning and at the end of the span. This leads to a mixed Eulerian-Lagrangian description. Moreover the chain rule implies a change for time differentiation, indeed

$$\frac{\mathrm{d}\bullet}{\mathrm{d}t} = \frac{\partial\bullet}{\partial t} + v(t)\frac{\partial\bullet}{\partial S} \ . \tag{5.2}$$

Main assumptions of Chapter 2 remain true. Here we give a simple recalling. The domain is contained in the cartesian space $\mathbb{R}^3$ with the basis $(O,\mathbf{x},\mathbf{y},\mathbf{z})$ and we have in the cartesian space

$$\mathbf{q} = x\ \mathbf{x} + y\ \mathbf{y} + z\ \mathbf{z} \ , \tag{5.3}$$

where the variable S allows to access to every particles of the domain and defines the orientation of it. The tangent vector can be defined for almost every S^* in the sense of the Lebesgue measure

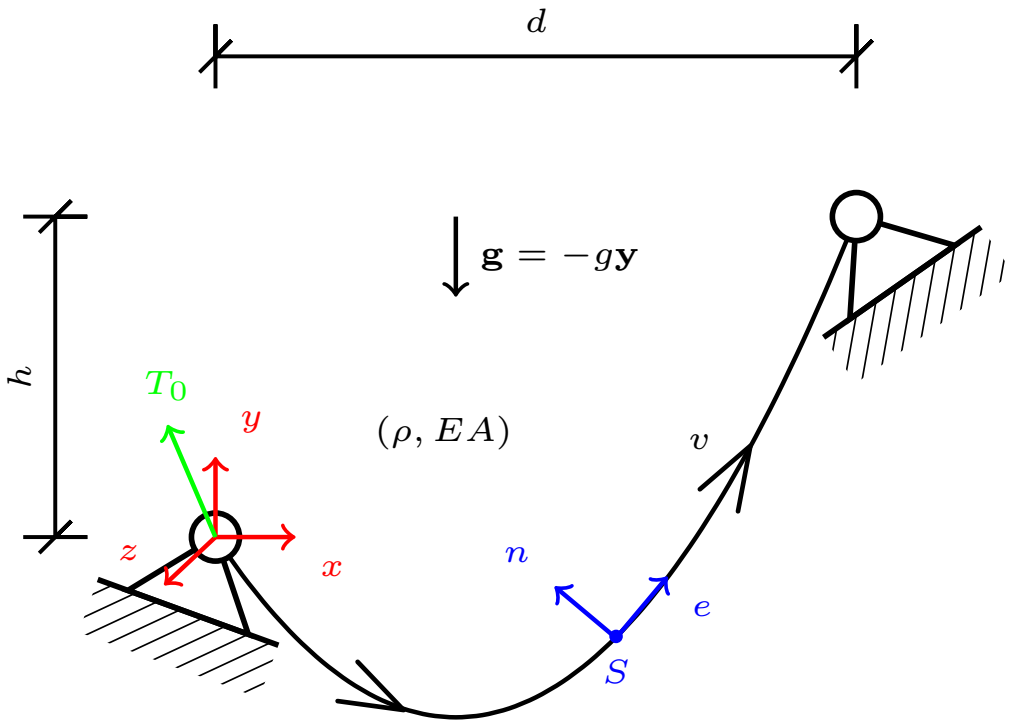

Figure 5.1: Elastic cable translating at velocity v between two ideal supports in the gravitational field g with axial velocity v

as

$$\mathbf{e}(S) = \frac{\mathbf{q}'(S)}{\|\mathbf{q}'(S)\|} \ , \tag{5.4}$$

where $\bullet'$ denotes the differentiation with regards to S. As the cable flows, the word equilibrium stands for a steady-state of the structure. The current cable which spans between q_0 and q_L has an unstretched length L. The cable is assumed to be uniform i.e. is linear density ρ and its rigidity EA are constant along all the span. An initial tension, T_0 is enforced in q_0 and the cable lies in the gravitational field given by g. We further assume that there is no point load applied to the cable. The system of interest is depicted in Figure 5.1. The three-dimensional Cartesian space is equipped with the Euclidean normal basis $(\mathbf{x}, \mathbf{y}, \mathbf{z})$. Due to the geometry of the system and the gravitational field taken along $\mathbf{y}$, we can assume that the steady-state lies into the plane given by $z = 0$. Moreover, with a suitable translation we can assume without loss of generality

$$q_0 = \begin{bmatrix} 0 \\ 0 \\ 0 \end{bmatrix} \quad ; \quad q_L = \begin{bmatrix} d \\ h \\ 0 \end{bmatrix} \quad ; \quad \mathbf{q} = \begin{bmatrix} x \\ y \\ z \end{bmatrix} \ . \tag{5.5}$$

Again, the cable is assumed perfectly flexible, therefore it cannot resist any moment or torque. Only its internal tensile force ensure the balance of forces. The latter is given by the product of a positive scalar quantity called tension, T, and a vector indicating the axial direction in the cable, $\frac{\mathbf{q}'(S,t)}{\|\mathbf{q}'(S,t)\|}$. Moreover, the cable is taken linear elastic and all geometrical non-linearities are kept, then

$$T(S,t) = EA\left(\|\mathbf{q}(S,t)\| - 1\right) \geqslant 0 \ . \tag{5.6}$$

For the sake of conciseness, S and t dependencies of variables are removed from system equations. Motion equations can be derived following indefinite equation of equilibrium

$$\left(T\frac{\mathbf{q}'}{\|\mathbf{q}'\|}\right)' + \mathbf{b} = \rho\gamma \ , \tag{5.7}$$

where $\mathbf{b}$ is the distributed load applied to the cable and γ the Eulerian acceleration. Due to the change of variable, we have

$$\gamma = \ddot{\mathbf{q}} + \dot{v}\mathbf{q}' + 2v\dot{\mathbf{q}}' + v^2\mathbf{q}'' \ , \tag{5.8}$$

where $\dot{\bullet}$ stands for the time differentiation.
Considering that damping, referred as $\tilde{\alpha}$, might be added in the sequel, the full dynamics of such a system are given by

$$\rho\left(\ddot{\mathbf{q}} + 2v\dot{\mathbf{q}}' + v^2\mathbf{q}'' + \dot{v}\mathbf{q}'\right) + \tilde{\alpha}\dot{\mathbf{q}} = EA\left((\|\mathbf{q}'\| - 1)\frac{\mathbf{q}'}{\|\mathbf{q}'\|}\right)' + \mathbf{b} \ . \tag{5.9}$$

The governing equations (5.9) can be rescaled via considering a non-dimensional time $t^* = \frac{Ht}{\rho d^2}$ and a non-dimensional variable $\mathbf{q}^* = \frac{\mathbf{q}}{d}$. After dropping the superscripts $(\cdot)^*$, the rescaled equations are recast in the following form

$$\ddot{\mathbf{q}} + 2\nu\dot{\mathbf{q}}' + \nu^2\mathbf{q}'' + \nu\mathbf{q}' + \alpha\dot{\mathbf{q}} = \frac{1}{\epsilon}\left((\|\mathbf{q}'\| - 1)\frac{\mathbf{q}'}{\|\mathbf{q}'\|}\right)' + \tilde{\mathbf{b}} \ , \tag{5.10}$$

where the following notations are taken

$$\nu^2 = \frac{\rho v^2}{H} \ , \ \epsilon = \frac{H}{EA} \ , \ \tilde{\mathbf{b}} = \frac{d}{H}\mathbf{b} \ , \ \alpha = \frac{d}{\sqrt{\rho H}}\tilde{\alpha} \ , \ l = \frac{L}{d} \ . \tag{5.11}$$

Equation (5.10) corresponds to the dynamics of a translating cable. The additional terms compared to (2.76) are due to inertial forces i.e. centripedal and coriolis forces. The latter can be met also in rotor dynamics [6]. One can expect the behaviors of rotating systems plus the behaviors of cable dynamics.

5.2 Steady-state regime

Most of the time, the cable is assumed to move with a given velocity which is not varying with time. The profile is given by $\mathbf{x}$. The latter case is obtained via setting $\nu = \nu_0$ so that $\dot{\nu} = 0$ and $\tilde{\mathbf{b}} = -\delta\mathbf{y}$ in (5.10) and reads

$$\nu_0^2\mathbf{x}'' = \frac{1}{\epsilon}\left[(\|\mathbf{x}'\| - 1)\,\frac{\mathbf{x}'}{\|\mathbf{x}'\|}\right] - \delta\mathbf{y} \ . \tag{5.12}$$

It is clear that (5.12) is a modified elastic catenary equation, the latter is more visible if we write the following

$$\left[\left(\frac{1}{\epsilon}\left(\|\mathbf{x}'\| - 1\right) - \nu_0^2\,\|\mathbf{x}'\|\right)\mathbf{e}\right]' = \delta\mathbf{y} \ . \tag{5.13}$$

No transverse load is applied so that the equilibrium is planar. Without loss of generality, we can assume the cable first extremity to be pinned in $(0, 0)$ and the second extremity to be

pinned in $(1, h^* = \frac{h}{d})$. This physical situation at stake is depicted in Figure 5.1.
Assuming the following boundary condition

$$\|\mathbf{x}'(0)\| = \frac{T_0}{EA} = \sqrt{1+\eta^2}\frac{H}{EA} = \epsilon\sqrt{1+\eta^2} \quad , \quad \mathbf{e}(0) = \frac{1}{\sqrt{1+\eta^2}}\begin{bmatrix}1\\ \eta\end{bmatrix} \tag{5.14}$$

$$\mathbf{x}(0) = \begin{bmatrix}0\\ 0\end{bmatrix} \quad , \quad \mathbf{x}(L) = \begin{bmatrix}1\\ h^*\end{bmatrix} \ , \tag{5.15}$$

where H is the tension imposed at $S = 0$ and $\eta = \frac{V}{H}$ is the ratio of the vertical component of the internal forces by H. The latter is also linked to the sine of (2.6) at $S = 0$ and L is the reference length of the cable.
It can be shown via direct integration of (5.13) that

$$\mathbf{e} = \frac{1}{\xi}\begin{bmatrix}1\\ \eta + \frac{\delta}{\beta}S\end{bmatrix} \quad , \quad \|\mathbf{x}'\| = \frac{1+\epsilon\beta\xi}{1-\epsilon\nu_0^2} \ , \tag{5.16}$$

$$\xi = \sqrt{1+\left(\eta + \frac{\delta}{\beta}S\right)^2} \quad , \quad \beta = 1 - \epsilon\nu_0^2 - \frac{\nu_0^2}{\sqrt{1+\eta^2}} \ . \tag{5.17}$$

To obtain the profile of the cable, we use the following relation which can be derived by combination of (5.16) with (5.17)

$$\mathbf{x}' = \|\mathbf{x}'\|\,\mathbf{e} = \left[\frac{\xi^{-1}}{1-\epsilon\nu_0^2} + \frac{\epsilon\beta}{1-\epsilon\nu_0^2}\right]\begin{bmatrix}1\\ \eta + \frac{\delta}{\beta}S\end{bmatrix} \ . \tag{5.18}$$

Integrating $\mathbf{q}'$ between $0 \leqslant S \leqslant L$ and L yields the following

$$1 - x(S) = \frac{\beta\epsilon}{1-\epsilon\nu_0^2}(l-S) + \frac{1}{1-\epsilon\nu_0^2}\frac{\beta}{\delta}\left(\sinh^{-1}(\eta + \frac{\delta}{\beta}l) - \sinh^{-1}(\eta + \frac{\delta}{\beta}S)\right) \quad , \tag{5.19}$$

$$\begin{aligned} h^* - y(S) = \ & \frac{\beta\epsilon\eta}{1-\epsilon\nu_0^2}(l-S) + \frac{1}{2}\frac{\epsilon\delta}{1-\epsilon\nu_0^2}(l^2 - S^2) \\ & + \frac{1}{1-\epsilon\nu_0^2}\frac{\beta}{\delta}\left(\sqrt{1+\left(\eta + \frac{\delta}{\beta}l\right)^2} - \sqrt{1+\left(\eta + \frac{\delta}{\beta}S\right)^2}\right) \ . \end{aligned} \tag{5.20}$$

Equations (5.19)-(5.20) provide with the profile of the cable. Admissibility conditions are obtained via solving the nonlinear system obtained via setting $S = 0$

$$\begin{cases} 1 = \dfrac{\beta\epsilon l}{1-\epsilon\nu_0^2} + \dfrac{1}{1-\epsilon\nu_0^2}\dfrac{\beta}{\delta}\left(\sinh^{-1}(\eta + \dfrac{\delta}{\beta}l) - \sinh^{-1}(\eta)\right) \\ h^* = \dfrac{\beta\epsilon\eta l}{1-\epsilon\nu_0^2} + \dfrac{1}{2}\dfrac{\epsilon\delta l^2}{1-\epsilon\nu_0^2} + \dfrac{1}{1-\epsilon\nu_0^2}\dfrac{\beta}{\delta}\left(\sqrt{1+\left(\eta + \dfrac{\delta}{\beta}l\right)^2} - \sqrt{1+\eta^2}\right) \end{cases} \ . \tag{5.21}$$

Eventually, the Frenet basis of the rest configuration reads

$$\mathbf{e} = \frac{1}{\xi}\begin{bmatrix}1\\ \eta + \frac{\delta}{\beta}S\end{bmatrix} \quad , \quad \mathbf{n} = -\frac{1}{\xi}\begin{bmatrix}\eta + \frac{\delta}{\beta}S\\ -1\end{bmatrix} \ . \tag{5.22}$$

The latter obeys the following rule

$$\mathbf{e}' = \mathcal{K}\mathbf{n} \quad , \quad \mathbf{n}' = -\mathcal{K}\mathbf{e} \quad , \quad \mathcal{K} = \frac{\frac{\delta}{\beta}}{1+\left(\eta + \frac{\delta}{\beta}S\right)^2} \ . \tag{5.23}$$

Table 5.1: Critical velocity for some typical parameters and a fictitious unfavorable case

Type	EA (MN)	ρ (kg/m)	v_{crit} (m/s)
Ropeway	235	12.94	4261.5
Carrying hauling rope	40	6	2582
Fictitious cable	1	3	577.4

5.2.1 Remarks

Problem (5.21) reduces to the elastic catenary problem when $\nu_0 = 0$. The extension to the translating elastic catenary proposed here is valid if

$$\epsilon \neq \frac{1}{\nu_0^2} \iff EA \neq \rho v_0^2 \ , \tag{5.24}$$

which corresponds to the case of a critical axial velocity. Physically speaking, it means that the domain travels faster than longitudinal elastic waves creating an apparent vanishing tension. For ropeways, this situation is not expected at all as shown in the Table 5.1 where we added the critical axial velocity. Indeed the maximum in-line velocity in France is 12.5 m/s. Moreover, the introduction of the velocity induces a slight change in the profile and the tension. A first order development shows that both the profile and the tension difference between a translating and a fixed cable order is proportional to $\epsilon\nu_0^2$ which tremendously small.
Even though the translating cable is interesting for its similarities with solid-fluid interaction and the rotor dynamics, the velocity does not change the behavior of the cable much.

5.3 Extension of free vibrations for a translating cable

This section presents the direct extension of the analysis of linear free vibrations to the case of a translating cable. First, the rescaled equations are presented, then the linearized equations are derived briefly in a similar manner than in Chapter 4. Next, we present how to adapt our developed analytical and finite differences methodology for the case of a translating cable.

5.3.1 Undamped vibrations

As presented in details in Chapter 4, the linear vibrations equations for the translating cable are derived. The damping, α, is discarded and we consider the case where $\nu = \nu_0$ so that $\dot{\nu} = 0$ and $\tilde{\mathbf{b}} = -\delta\mathbf{y}$.
Here we develop the modal analysis of the translating cable as an extension of the theory of free vibrations of cables. An incremental dynamics around the established regime is considered by setting $\mathbf{q} = \mathbf{x} + \mathbf{u}$ where $\mathbf{x}$ is the rest profile of the cable.
The displacement $\mathbf{u}$ is decomposed on the Frenet basis taken at the rest configuration as

$$\mathbf{u} = u\ \mathbf{e} + v\ \mathbf{n} + w\ \mathbf{z} \ . \tag{5.25}$$

By using (5.2), we obtain that

$$\dot{\mathbf{u}} = \dot{u}\ \mathbf{e} + \dot{v}\ \mathbf{n} + \dot{w}\ \mathbf{z} \ , \tag{5.26}$$
$$\mathbf{u}' = \ (u' - \mathcal{K}v)\ \ \mathbf{e} + (v' + \mathcal{K}u)\ \ \mathbf{n} + w'\ \mathbf{z} \ , \tag{5.27}$$
$$\ddot{\mathbf{u}} = \ddot{u}\ \mathbf{e} + \ddot{v}\ \mathbf{n} + \ddot{w}\ \mathbf{z} \ , \tag{5.28}$$
$$\dot{\mathbf{u}}' = \ (\dot{u}' - \mathcal{K}\dot{v})\ \ \mathbf{e} + (\dot{v}' + \mathcal{K}\dot{u})\ \ \mathbf{n} + \dot{w}'\ \mathbf{z} \ , \tag{5.29}$$
$$\mathbf{u}'' = \ \left[(u' - \mathcal{K}v)' - \mathcal{K}\,(v' + \mathcal{K}u)\right]\ \mathbf{e} + \left[(v' + \mathcal{K}u)' + \mathcal{K}\,(u' - \mathcal{K}v)\right]\ \mathbf{n} + w''\ \mathbf{z} \ . \tag{5.30}$$

Moreover the current axial vector is linearized at first order as done previously as follows

$$\frac{\mathbf{x}'+\mathbf{u}'}{\|\mathbf{x}'+\mathbf{u}'\|} = \mathbf{e} + \frac{1}{\|\mathbf{x}'\|}\left(\mathbf{u}' - (\mathbf{e}\cdot\mathbf{u}')\mathbf{e}\right) \ . \tag{5.31}$$

Equations (5.26)-(5.30) and (5.31) are injected into (5.10). Then the established regime given by (5.12) is used to simplify the expression so that we obtain in a condensed form

$$\ddot{u} + 2\nu_0\left(\dot{u}' - \mathcal{K}\dot{v}\right) = \frac{1-\epsilon\nu_0^2}{\epsilon}\left[\ (u' - \mathcal{K}v)' - \frac{\varepsilon}{1+\varepsilon}\mathcal{K}(v' + \mathcal{K}u)\ \right] \ , \tag{5.32}$$

$$\ddot{v} + 2\nu_0\left(\dot{v}' + \mathcal{K}\dot{u}\right) = \frac{1-\epsilon\nu_0^2}{\epsilon}\left[\ \mathcal{K}\left(u' - \mathcal{K}v\right) + \left(\frac{\varepsilon}{1+\varepsilon}(v' + \mathcal{K}u)\right)'\ \right] \ , \tag{5.33}$$

$$\ddot{w} + 2\nu_0\dot{w}' = \frac{1-\epsilon\nu_0^2}{\epsilon}\left[\ \frac{\varepsilon}{1+\varepsilon}w'\ \right]' \ , \tag{5.34}$$

where $\varepsilon = \|\mathbf{x}'\| - 1$.
Again, the system of equations given by (5.32)-(5.34) can be seen as an in plane motion superimposed with an out of plane motion. However, an additional term due to the velocity appears in equation and the latter is likely to provoke complex modes. This possibility is presented briefly in Appendix F or detailed the mathematical paper of Lallement and Inman [1].

5.3.2 Treatment via finite difference method

The Finite Difference Method (FDM) is used again to treat (5.32)-(5.34). We assume that separation of spatial and temporal variables holds and that the unknowns are in the following form

$$\begin{cases} u = Ue^{\lambda t} \\ v = Ve^{\lambda t} \\ w = We^{\lambda t} \end{cases} \ . \tag{5.35}$$

Injecting (5.35) into (5.32)-(5.34) and simplifying by $e^{\lambda t}$ yields the following system of equations

$$\begin{cases} 0 = \lambda^2\ U + 2\nu_0\lambda\left(U' - \mathcal{K}V\right) - \dfrac{1-\epsilon\nu_0^2}{\epsilon}\ \left[U'' - \dfrac{1+2\varepsilon}{1+\varepsilon}\mathcal{K}V' - \dfrac{\varepsilon}{1+\varepsilon}\mathcal{K}^2U - \mathcal{K}'V\right] \\ 0 = \lambda^2\ V + 2\nu_0\lambda\left(V' + \mathcal{K}U\right) - \dfrac{1-\epsilon\nu_0^2}{\epsilon}\ \left[\begin{array}{r} \dfrac{\varepsilon}{1+\varepsilon}V'' + \dfrac{1+2\varepsilon}{1+\varepsilon}\mathcal{K}U' + \left(\dfrac{\varepsilon}{1+\varepsilon}\right)'V' \\ + \left(\dfrac{\varepsilon}{1+\varepsilon}\mathcal{K}\right)'U - \mathcal{K}^2V \end{array}\right] \\ 0 = \lambda^2\ W + 2\nu_0\lambda W' - \dfrac{1-\epsilon\nu_0^2}{\epsilon}\ \left[\dfrac{\varepsilon}{1+\varepsilon}W'' + \left(\dfrac{\varepsilon}{1+\varepsilon}\right)'W'\right] \end{cases} . \tag{5.36}$$

The FDM is used with regard to spatial variable only. The latter has been previously presented in (4.56) and (4.57). In the case treated here, the system takes the following form

$$\mathbf{0} = \lambda^2\mathbf{M}\mathbf{Y} + \lambda\mathbf{C}\mathbf{Y} + \mathbf{K}\mathbf{Y} \ . \tag{5.37}$$

The latter can be reorganized into a standard eigenvalue problem as

$$\begin{bmatrix} \mathbf{0} & \mathbf{I} \\ -\mathbf{M}^{-1}\mathbf{K} & -\mathbf{M}^{-1}\mathbf{C} \end{bmatrix}\begin{bmatrix} \mathbf{Y} \\ \lambda\mathbf{Y} \end{bmatrix} = \lambda\begin{bmatrix} \mathbf{Y} \\ \lambda\mathbf{Y} \end{bmatrix} \ . \tag{5.38}$$

As a consequence, λ is a complex value occurring in complex conjugate pairs. Eigenvectors also occur in complex conjugate pairs and are denoted in the literature as complex modes [1] or sometimes damped modes. The natural frequency and the modal damping ratio obtained via considering respectively

$$\omega_k = |\lambda_k| \quad , \quad \alpha_k = -\frac{\mathrm{re}\,(\lambda_k)}{\omega_k} \ . \tag{5.39}$$

5.3.3 Analytical treatment of out-of-plane vibrations

We first focus on (5.34). Due to numerical investigations, we assume the separation of spatio-temporal variables as follows

$$w(S,t) = W(S)e^{i\omega t} \quad ; \quad i^2 = -1 \ , \tag{5.40}$$

which can be inserted into (5.34) and yields

$$\omega^2 W - 2i\nu_0\omega W' + \frac{1-\epsilon\nu_0^2}{\epsilon}\left[\frac{\varepsilon}{1+\varepsilon}W'\right]' = 0 \ . \tag{5.41}$$

The claim made earlier on $\dfrac{\varepsilon}{1+\varepsilon}$ is still valid for the translating case and results into the following differential equation

$$\omega^2 W - 2i\nu_0\omega W' + a^2 W'' = 0 \ , \tag{5.42}$$

where we have set the following

$$a^2 = \frac{1-\epsilon\nu_0^2}{\epsilon}\ \frac{\varepsilon}{1+\varepsilon} \ . \tag{5.43}$$

Once homogeneous boundary conditions are imposed, the system can be solved as follows

$$\begin{aligned} W &= W_0 \exp\left(i\frac{\omega}{a^2}\left(\nu_0 + \sqrt{\nu_0^2+a^2}\right)S\right)\left[1-\exp\left(-2i\frac{\omega}{a^2}\sqrt{\nu_0^2+a^2}S\right)\right] \\ \text{where} \quad \omega_k &= \frac{a^2 k\pi}{\sqrt{\nu_0^2+a^2}} \ , \ k\in\mathbb{N} \end{aligned} \ . \tag{5.44}$$

The modes can be made unit with respect to the following norm

$$\left(\int_0^L g\cdot g^* \mathrm{d}S\right)^{1/2} \ , \tag{5.45}$$

where $(\cdot)^*$ stands for the complex conjugate of $(\cdot)$. Then we have

$$W_k = \sqrt{2}i\exp\left[\frac{i\nu_0 k\pi}{\sqrt{\nu_0^2+a^2}}S\right]\sin\left(k\pi S\right) \ . \tag{5.46}$$

However, those modes are no longer orthogonal due to the fictitious damping added by the axial velocity that breaks the symmetry of the system. We obtained complex mode shapes that can be interpreted as the superposition of two waves that travel forward and backward respectively at celerity $k\pi\left(\dfrac{\nu_0}{\sqrt{\nu_0^2+a^2}}+1\right)$ and $k\pi\left(\dfrac{\nu_0}{\sqrt{\nu_0^2+a^2}}-1\right)$. Moreover, from (5.42) we can see that W_k^* also satisfies the equation. When the velocity vanishes, we recover the obtained modes for the classic case given by (4.23).

5.3.4 Analytical treatment of in-plane vibrations

Let us focus on (5.32) and (5.33). This set of equations is a coupled set of linear equations with continuous coefficients. We assume that the planar displacement is given by

$$u = U(S)e^{i\omega t} \ , \tag{5.47}$$

$$v = V(S)e^{i\omega t} \ , \tag{5.48}$$

which can be inserted into (4.14) and (4.15) and yields

$$\begin{cases} 0 = \omega^2 U - 2i\nu_0\omega\left(U' - \mathcal{K}V\right) + \dfrac{1-\epsilon\nu_0^2}{\epsilon}\left[\left(U' - \mathcal{K}V\right)' - \mathcal{K}\dfrac{\varepsilon}{1+\varepsilon}(V' + \mathcal{K}U)\right] \\ 0 = \omega^2 V - 2i\nu_0\omega\left(V' + \mathcal{K}U\right) + \dfrac{1-\epsilon\nu_0^2}{\epsilon}\left[\mathcal{K}\left(U' - \mathcal{K}V\right) + \left(\dfrac{\varepsilon}{1+\varepsilon}(V' + \mathcal{K}U)\right)'\right] \end{cases} . \tag{5.49}$$

We have seen in Chapter 4 that two different types of mode exist which are the symmetric and anti-symmetric modes. The following developments show that as soon as the velocity of translation is considered, modes are necessarily accompanied by a tension increment so that anti-symmetric modes, that result in no increment of tension at first order, no longer exist.

Non-existence of anti-symmetric modes

We show here that one classical result of the theory of linear vibrations for cables does not hold when axial velocity is considered. Let us make following formal assumptions:

- $\frac{\|\mathbf{q}'\|-1}{\|\mathbf{q}'\|}$ can be considered constant with S;
- The normal vibration given by V is of primary interest in (5.49) so that U can be considered of second order;
- The variation of the curvature function $\mathcal{K}$ are neglected so we make a first order approximation of it;
- The vibration does not produce any tension variation so that $EA\left(U' - \mathcal{K}V\right)$, corresponding to the additional tension (see (4.12)) is zero.

Then, our assumptions allows to simplify (5.49) as follows

$$\omega^2 V - 2i\nu_0\omega U' + a^2 V'' = 0 \ , \tag{5.50}$$

where $a^2 = \dfrac{1-\epsilon\nu_0^2}{\epsilon}\dfrac{\varepsilon}{1+\varepsilon}$.
As done in the previous paragraph, V admits as solution

$$V = V_0 \exp\left[\frac{i\nu_0 k\pi}{\sqrt{\nu_0^2 + a^2}}S\right]\sin\left(k\pi S\right) \ . \tag{5.51}$$

The geometric compatibility condition is given by

$$U' - \mathcal{K}V = 0 \ , \tag{5.52}$$

then

$$U = U_0 - V_0\mathcal{K}\frac{\exp\left[\frac{i\nu_0 k\pi}{\sqrt{\nu_0^2+a^2}}S\right]}{a^2 k\pi}\left[\left(\nu_0^2 + a^2\right)\cos\left(k\pi S\right) - i\nu_0\sqrt{\nu_0^2 + a^2}\sin\left(k\pi S\right)\right] \ . \tag{5.53}$$

Applying homogeneous boundary condition to U yields

$$U(0) = 0 \iff U_0 = V_0 \mathcal{K} \frac{\nu_0^2 + a^2}{a^2 k \pi} \ , \tag{5.54}$$

and then

$$U(1) = 0 \iff 0 = \exp\left[\frac{i\pi k \nu_0}{\sqrt{a^2+\nu_0^2}}\right]\left(i\nu_0\sqrt{a^2+\nu_0^2}\sin(\pi k) - \left(a^2+\nu_0^2\right)\cos(\pi k)\right) + a^2 + \nu_0^2 \ . \tag{5.55}$$

which cannot be satisfied unless $\nu_0 = 0$. This causes the so-called veering in the frequency curves. Indeed, as the anti-symmetric mode no longer exist, the curves no longer intersect each other and the continuum of frequency are separated.
The latter can also be explained by the fact that damping shift vibration nodes positions which breaks the possibility of symmetry. The latter was stated in earlier works as a follow-up from observations of the obtained solutions [3, 7].

In-plane normal vibrations

Let us make following assumptions:

- $\frac{\|\mathbf{q}'\|-1}{\|\mathbf{q}'\|}$ can be considered constant with S;
- The normal vibration given by V is of primary interest in (5.49) so that U can be considered of second order;
- The variation of the curvature function $\mathcal{K}$ are neglected so we make a first order approximation of it;
- The vibration produces a tension variation which is a function of time alone. Then the function $\frac{1-\epsilon\nu_0^2}{\epsilon}\left(U' - \mathcal{K}V\right)$, corresponding to the rescaled additional apparent tension, can be considered to be constant with space and its non-trivial value is given by τ.

Then, system (5.49) simplifies as follows

$$\begin{aligned} 0 &= a^2 V'' - 2i\nu_0\omega V' + \omega^2 V + \mathcal{K}\tau \\ 0 &= \frac{1-\epsilon\nu_0^2}{\epsilon}\left(U' - \mathcal{K}V\right) - \tau \\ a^2 &= \frac{1-\epsilon\nu_0^2}{\epsilon}\,\frac{\varepsilon}{1+\varepsilon} \end{aligned} \ . \tag{5.56}$$

The latter results in

$$V = V_0 \exp\left[\frac{i\omega}{a^2}\left(\nu_0 + \sqrt{\nu_0^2+a^2}\right)S\right] + V_1 \exp\left[\frac{i\omega}{a^2}\left(\nu_0 - \sqrt{\nu_0^2+a^2}\right)S\right] - \frac{\mathcal{K}\tau}{\omega^2} \ , \tag{5.57}$$

$$\begin{aligned} U = U_0 + \tau\left(\frac{\epsilon}{1-\epsilon\nu_0^2} - \frac{\mathcal{K}^2}{\omega^2}\right)S - i\frac{a^2\mathcal{K}\left(V_0/\omega\right)}{\sqrt{\nu_0^2+a^2}+\nu_0}\exp\left[\frac{i\omega}{a^2}\left(\nu_0+\sqrt{\nu_0^2+a^2}\right)S\right] \\ + i\frac{a^2\mathcal{K}\left(V_1/\omega\right)}{\sqrt{\nu_0^2+a^2}-\nu_0}\exp\left[\frac{i\omega}{a^2}\left(\nu_0-\sqrt{\nu_0^2+a^2}\right)S\right] \ . \end{aligned} \tag{5.58}$$

The homogeneous boundary conditions are imposed via the following matrix equation

$$\begin{bmatrix} V(0) \\ V(1) \\ U(0) \\ U(1) \end{bmatrix} = \mathbf{0} \iff \begin{bmatrix} 1 & 1 & 0 & -\frac{\mathcal{K}}{\omega^2} \\ e^{\frac{i\omega}{a^2}\left(\nu_0+\sqrt{\nu_0^2+a^2}\right)} & e^{\frac{i\omega}{a^2}\left(\nu_0-\sqrt{\nu_0^2+a^2}\right)} & 0 & -\frac{\mathcal{K}}{\omega^2} \\ \frac{-ia^2\mathcal{K}}{\omega(\sqrt{\nu_0^2+a^2}+\nu_0)} & \frac{ia^2\mathcal{K}}{\omega(\sqrt{\nu_0^2+a^2}-\nu_0)} & 1 & 0 \\ \frac{-ia^2\mathcal{K}e^{\frac{i\omega}{a^2}\left(\nu_0+\sqrt{\nu_0^2+a^2}\right)}}{\omega(\sqrt{\nu_0^2+a^2}+\nu_0)} & \frac{ia^2\mathcal{K}e^{\frac{i\omega}{a^2}\left(\nu_0-\sqrt{\nu_0^2+a^2}\right)}}{\omega(\sqrt{\nu_0^2+a^2}-\nu_0)} & 1 & \frac{\epsilon}{1-\epsilon\nu_0^2}-\frac{\mathcal{K}^2}{\omega^2} \end{bmatrix} \begin{bmatrix} V_0 \\ V_1 \\ U_0 \\ \tau \end{bmatrix} = \mathbf{0} \ . \tag{5.59}$$

The frequencies are obtained when the kernel of the matrix is non-trivial. By imposing its determinant to be zero and simplifying equations we have

$$\begin{cases} 0 = \cos\left(\frac{\nu_0\omega}{a^2}\right) - \cos\left(\frac{\omega\sqrt{a^2+\nu_0^2}}{a^2}\right) - \frac{\omega\left(\mathcal{K}^2\left(1-\nu_0^2\epsilon\right)-\epsilon\omega^2\right)}{2\mathcal{K}^2\sqrt{a^2+\nu_0^2}\left(1-\nu_0^2\epsilon\right)}\sin\left(\frac{\omega\sqrt{a^2+\nu_0^2}}{a^2}\right) \\ \omega \neq 0 \end{cases} . \tag{5.60}$$

We clearly see that our development directly extend the case without velocity. By setting $\nu_0 = 0$ in (5.60) we obtain the classical transcendental equation for the cable in plane frequencies (4.46).

In-plane longitudinal vibrations

The normal vibrations are often considered preponderant in cable dynamics, however scenarios involving highly tensed cable or high frequency responses require the consideration of the longitudinal displacement.
The longitudinal vibrations can also be traced via assuming the following:

- $\frac{\|\mathbf{q}'\|-1}{\|\mathbf{q}'\|}$ can be considered constant with S.
- The longitudinal vibration given by U are of primary interest in (5.49) so that V can be considered of second order.
- The variation of the curvature function $\mathcal{K}$ are neglected so we make a first order approximation of it.
- The vibration produces a slope variation which is a function of time only. Then the function $(V' + \mathcal{K}U)$, corresponding to the rescaled additional tension, can be considered to be constant with space and its non-trivial value is given by τ.

These assumptions allow to consider to simplified system

$$\begin{cases} 0 = \omega^2 U - 2i\nu_0\omega U' + c^2 U'' - a^2\mathcal{K}\tau \\ 0 = \tau - (V' + \mathcal{K}U) \\ a^2 = \dfrac{1-\epsilon\nu_0^2}{\epsilon}\,\dfrac{\varepsilon}{1+\varepsilon} \\ c^2 = \dfrac{1-\epsilon\nu_0^2}{\epsilon} \end{cases} , \tag{5.61}$$

then

$$U = U_0 \exp\left[\frac{i\omega}{c^2}\left(\nu_0 + \sqrt{\nu_0^2+c^2}\right)S\right] + U_1 \exp\left[\frac{i\omega}{c^2}\left(\nu_0 - \sqrt{\nu_0^2+c^2}\right)S\right] + \frac{a^2\mathcal{K}\tau}{\omega^2} , \tag{5.62}$$

$$\begin{aligned} V = V_0 + \tau\left(1-\frac{a^2\mathcal{K}^2}{\omega^2}\right)S + i\frac{c^2\mathcal{K}\left(U_0/\omega\right)}{\sqrt{\nu_0^2+c^2}+\nu_0}\exp\left[\frac{i\omega}{c^2}\left(\nu_0+\sqrt{\nu_0^2+c^2}\right)S\right] \\ - i\frac{c^2\mathcal{K}\left(U_1/\omega\right)}{\sqrt{\nu_0^2+c^2}-\nu_0}\exp\left[\frac{i\omega}{c^2}\left(\nu_0-\sqrt{\nu_0^2+c^2}\right)S\right] . \end{aligned} \tag{5.63}$$

As done previously, applying homogeneous boundary conditions results into a determinental equation which reduces in

$$\mathcal{F}^*(\omega) = \frac{\omega(\omega - a\mathcal{K})(a\mathcal{K} + \omega)\sin\left(\frac{\omega\sqrt{c^2+\nu_0^2}}{c^2}\right)}{a^2\mathcal{K}^2\sqrt{c^2+\nu_0^2}} - 2\cos\left(\frac{\omega\sqrt{c^2+\nu_0^2}}{c^2}\right) + 2\cos\left(\frac{\nu_0\omega}{c^2}\right) = 0\ . \quad (5.64)$$

The treatment of the latter can be done via the dichotomy approach similarly to the case (4.46). However, for a lot of practical applications subjected to longitudinal vibrations the following approximation provides an acceptable precision

$$\omega_k = \frac{c^2 k\pi}{\sqrt{\nu_0^2 + c^2}}\ ,\ k \in \mathbb{N}\ . \quad (5.65)$$

5.3.5 Numerical applications and comparisons with analytical results

For the purpose of comparing analytic treatments and numerical solution, Table 4.1 contains the parameters used to check our methodology. As a reminder, the first case is a near-inextensible case, the second is typical for a ropeway and the last one is chosen since it corresponds to a fictitious cable for which the dynamical behavior is equally parted between longitudinal and normal vibrations. As visible on Figures 5.2 and 5.3, the prediction is accurate for the frequencies. The proposed analytical approach is able to trace the modal content accurately. Small discrepancies happen similarly to the fixed-cable approximation proposed when the assumptions are not relevant for the case considered especially for the case of the modal shape which partition in real and imaginary part is not caught in the combined case of an inclined and near inextensible cable.

	Type	EA (MN)	ρ (kg/m)	d (m/s)	h (m)	v_0 (m/s)
Case 1	Ropeway	235	12.94	100	$\{0, 33\}$	8
Case 2	Carrying hauling rope	40	6	100	$\{0, 33\}$	8
Case 3	Fictitious cable	1	3	100	$\{0, 33\}$	8

5.3.6 Cross-overs for the translating cable case

As explained previously, the translating cable only exhibits modes accompanied with a constant tension increment. This phenomenon comes with a stalling in the cross-over zones depicted for the fixed cable in Figure 3.19. The cross over phenomenon is annihilated by the velocity and curves depart from each other. The latter is made visible on Figure 5.4 where the non-dimensional frequencies are plotted versus the Irvine parameter (cf (3.115)). We see that the bigger the velocity is, the larger the stall between frequencies becomes. Those veering phenomenon, where two curves approaches from each other are accompanied by a abrupt variation of the eigenvector shape in those zones.

Although the frequency plot is changing slightly in the presence of a translating velocity, the modal shape exchanges and abrupt variations of the modes in the zones where curves are close to each other remains similar. The main difference relies in the complex values of the eigenvectors and the eigenvalues.

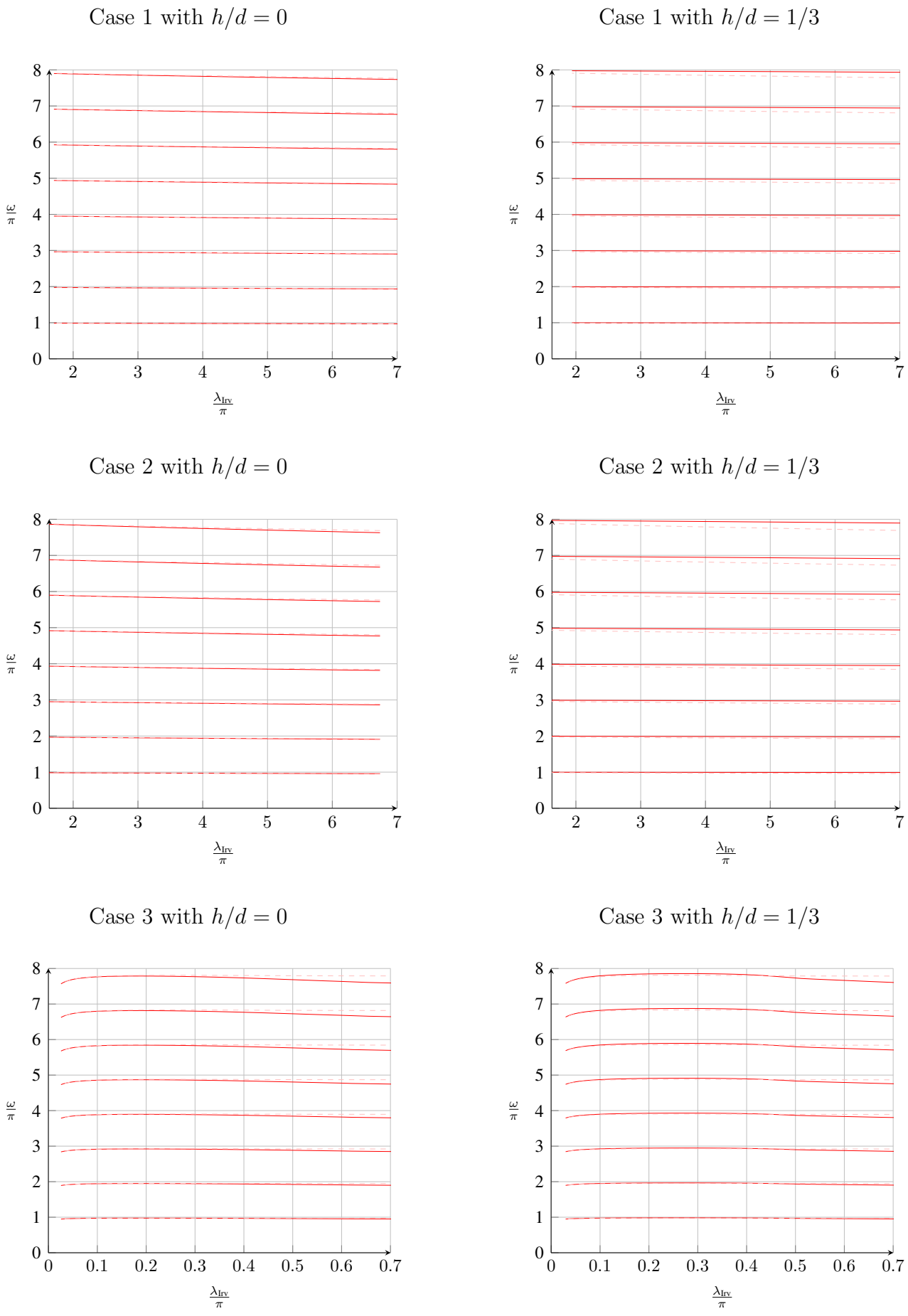

Figure 5.2: Normalized frequency of the out-of-plane modes versus normalized λ_{Irv} parameter ; Computed via analytical approximation (dashed line - - -) and FDM (solid line —)

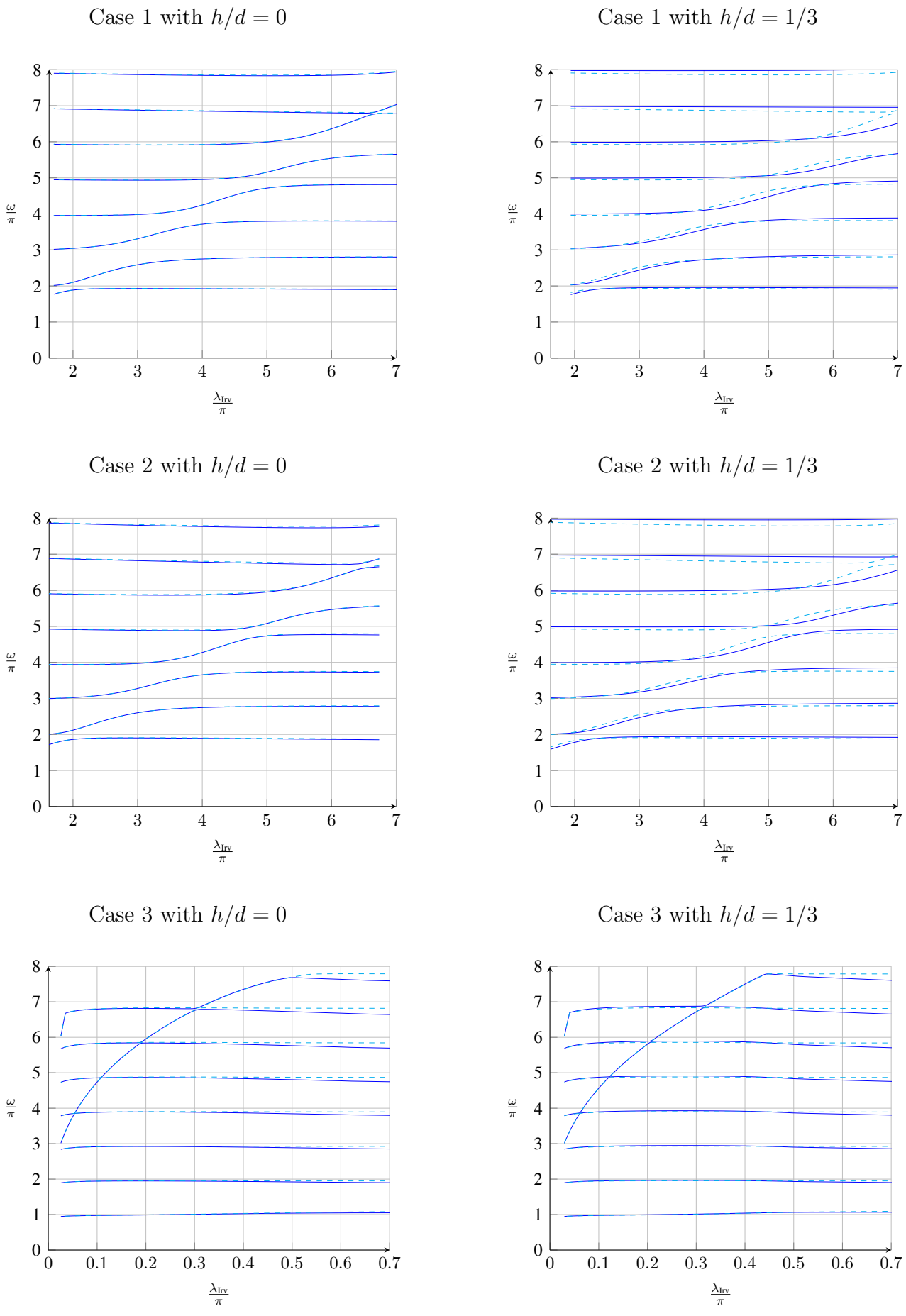

Figure 5.3: Normalized frequency of the in-plane modes versus normalized λ_{Irv} parameter ; Computed via analytical approximation (solid line - - -) and FDM (solid line ——)

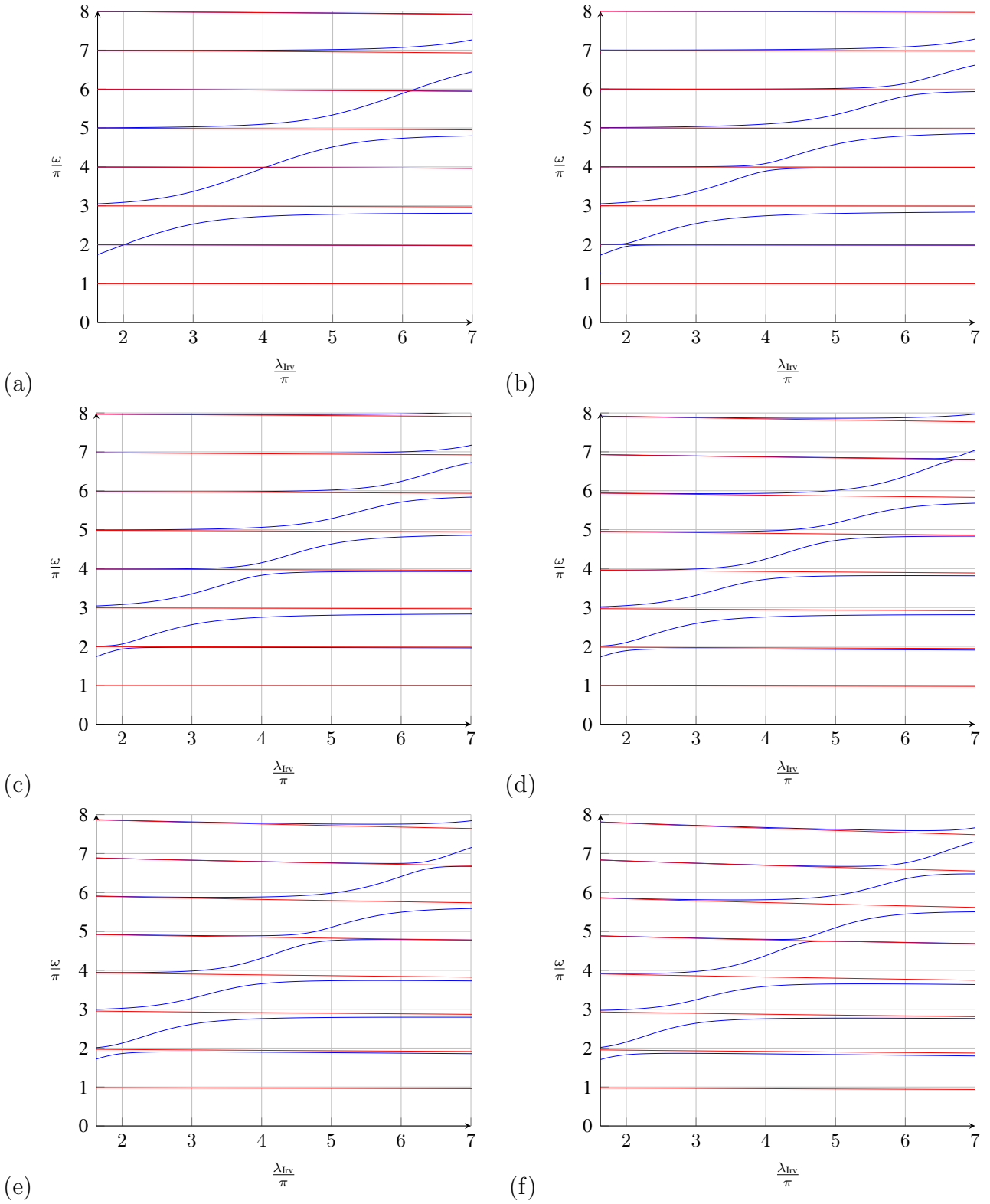

Figure 5.4: Non-dimensional frequencies versus Irvine's parameter. Out-of-plane modes (solid line —) and in-plane modes (solid line —) are depicted with varying velocities and parameters given in Table 5.2. (a) $v_0 = 0$, (b) $v_0 = 3$, (c) $v_0 = 5$, (d) $v_0 = 8$, (e) $v_0 = 10$ and (f) $v_0 = 12$

Table 5.2: Parameters used for the calculation of the frequency plot examples

EA (MN)	T_0 (kN)	ρ (kg/m)	d (m)	h (m)	v_0 (m/s)
100	85	5	100	5	$\in \{0, 3, 5, 8, 10, 12\}$

Table 5.3: Parameters used for the calculation of the Campbell diagram example

EA (MN)	T_0 (kN)	ρ (kg/m)	d (m)	h (m)	v_0 (m/s)
100	85	5	100	5	$\in [0, 120]$

5.3.7 Discussion about the translating cable modes

Frequencies and modes of the translating cable are an extension of the fixed cable vibrations. However the physical interpretation and its applicability for the cable-car should be discussed. The eigenvalues λ_k are complex and come as conjugate pairs. As for rotating systems, the triplet $(\nu_0^2, \mathrm{re}(\lambda_k), \mathrm{im}(\lambda_k))$ gives access to the Campbell diagram and the decay rate of the translating cable [6, 9]. In theory, one can identify critical speed for which the system exhibits unbounded amplitude. In the case of cable-cars, the critical speed obtained is far from any velocity used in realistic application, see Figure 5.5 where the critical speed is obtained when singularities are met or when a non-zero real part is met. In the case depicted here with the set of parameters given in Table 5.3, the critical speed obtained numerically is 89.86 m/s.
Moreover, those modes are not practical for studying the nonlinear dynamics of a translating cable since the original system is a real-valued system and the Ritz-Galerkin projection procedure is a sesquilinear form. The latter transforms the real system into a complex system which has not been shown to converge numerically and not being tractable by the means of the method of multiple scales.
Although the proposed analysis is straightforward, its usage for realistic cable-car situations is irrelevant. Then instabilities should be traced with a nonlinear analysis of the dynamics. The modes used for the projection should be the fixed-cable modes so that the system remains real-valued and the methodology described in Section 4.2 is applicable.

5.4 Nonlinear dynamics of the translating cable

In this section, we discuss the possibility of tracing the dynamic response of a translating cable given in (5.10) by the means of the methodology described in Section 4.2.
We assume the following:

- $\mathbf{q} = \mathbf{x} + \mathbf{u}$ where $\mathbf{x}$ is the permanent regime given by (5.9) and $\mathbf{u}$ is a dynamic perturbation of the stationary profile

- the non-dimensional velocity of translation $\nu = \nu_0 + \nu_1(t)$ corresponds to a fluctuation ν_1 around a mean value ν_0

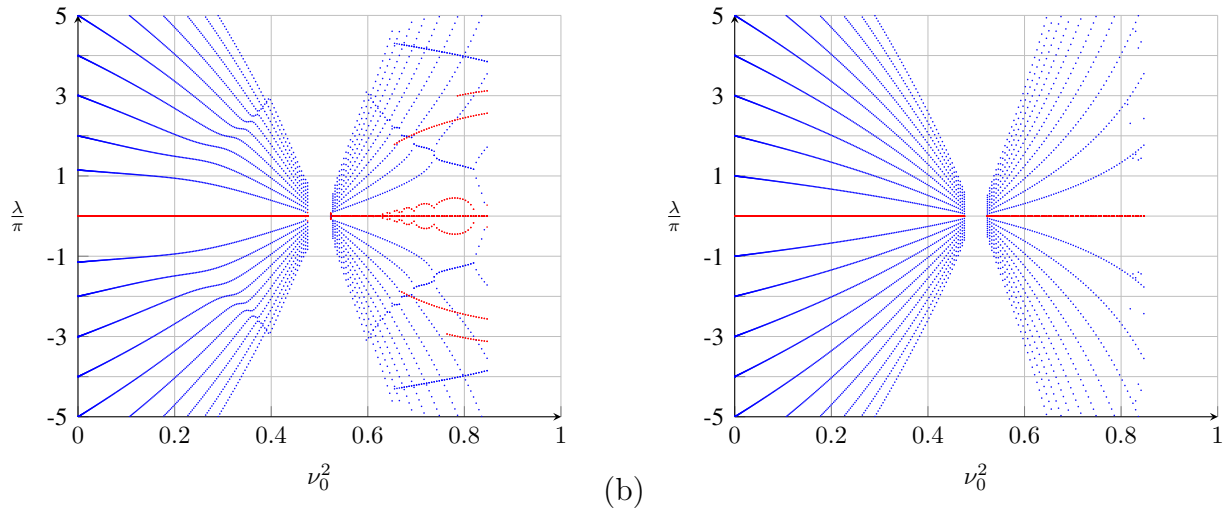

Figure 5.5: Complex frequencies versus non-dimensional velocity parameter. The real part (dotted line ·····) and imaginary part (dotted line ·····) are plotted for the (a) planar modes and the (b) transversal modes

For the sake of the reader we recall every equations needed just below

$$\begin{cases} \ddot{\mathbf{q}} + 2\nu\dot{\mathbf{q}}' + \nu^2\mathbf{q}'' + \nu\mathbf{q}' + \alpha\dot{\mathbf{q}} = \dfrac{1}{\epsilon}\left((\|\mathbf{q}'\| - 1)\dfrac{\mathbf{q}'}{\|\mathbf{q}'\|}\right)' + \delta\mathbf{y} + f \\ \left[\left(\dfrac{1}{\epsilon}(\|\mathbf{x}'\| - 1) - \nu_0^2\|\mathbf{x}'\|\right)\mathbf{e}\right]' = \delta\mathbf{y} \quad ; \quad \dot{\mathbf{x}} = \mathbf{0} \\ \mathbf{q} = \mathbf{x} + \mathbf{u} \\ \nu = \nu_0 + \nu_1(t) \end{cases} . \tag{5.66}$$

All the latter can be simplified and expanded at third order as

$$\ddot{\mathbf{u}} + 2(\nu_0 + \nu_1)\dot{\mathbf{u}}' + \dot{\nu}_1(\mathbf{x}' + \mathbf{u}') + \alpha\dot{\mathbf{u}} = \frac{1}{\epsilon}\left(\mathbf{u}' - \frac{\mathbf{u}'}{\|\mathbf{x}'\|}\right)' - (\nu_0 + \nu_1)^2\mathbf{u}'' + \Delta f_e(\mathbf{x}, \mathbf{u})' + f \ , \tag{5.67}$$

where the expression of $\Delta f_e(\mathbf{x}, \mathbf{u})$ is given in (4.65) and corresponds to the incremental elastic forces induced by the dynamic perturbation.
Physically speaking, this equation describes the vibration around the stationary regime of the cable. In order to treat it, we apply the methodology detailed in Section 4.2. The incremental motion is taken as follows

$$\mathbf{u}(S, t) = \sum_{k=1}^{N} \Phi_k(S)\varphi_k(t) \quad ; \quad N \in \mathbb{N}^* \ , \tag{5.68}$$

where $(\Phi_k)_{k\in\mathbb{N}}$ is the family of the fixed-cables modes obtained from the stationary regime $\mathbf{x}$. The modes are computed via (4.14)-(4.16), the latter are used for two main reasons. The first one is the fact that the system of equation remains a system with real coefficient and the second one is that the differences between the fixed and translating case are relatively small when ν_0 remains in the domain of engineering applications.
Using the same projection technique presented in (4.68), we can obtain the following system of equations

$$\begin{aligned} &\mathbf{M}_{jk}\ddot{\varphi}_k + \left[\mathbf{C}_{jk} + \mathbf{C}_{jk}^{\nu_0} + \mathbf{C}_{jk}^{\nu_1}(t)\right]\dot{\varphi}_k + \left[\mathbf{K}_{jk} + \mathbf{K}_{jk}^{\nu_0} + \mathbf{K}_{jk}^{\nu_1}(t)\right]\varphi_k \\ &\quad + \mathcal{Q}_{jkl}\varphi_k\varphi_l + \mathcal{C}_{jklm}\varphi_k\varphi_l\varphi_m = \mathbf{f}_j^{\nu_1}(\mathbf{x}, t) + \mathbf{f}_j(t) \end{aligned} \quad , \quad 1 \leqslant j \leqslant N \ , \tag{5.69}$$

where the Einstein convention is used and where

$$\mathbf{M}_{jk} = \int_0^l \Phi_j \cdot \Phi_k \mathrm{d}S \ , \tag{5.70}$$

$$\mathbf{C}_{jk} = \alpha \int_0^l \Phi_j \cdot \Phi_k \mathrm{d}S \ , \tag{5.71}$$

$$\mathbf{C}_{jk}^{\nu_0} = 2\nu_0 \int_0^l \Phi_j \cdot \Phi_k' \mathrm{d}S \ , \tag{5.72}$$

$$\mathbf{C}_{jk}^{\nu_1}(t) = 2\nu_1(t) \int_0^l \Phi_j \cdot \Phi_k' \mathrm{d}S \ , \tag{5.73}$$

$$\mathbf{K}_{jk} = \frac{1}{\epsilon} \int_0^l \left(\begin{bmatrix} P_k' - \mathcal{K}Q_k \\ 0 \\ 0 \end{bmatrix} + \frac{\|\mathbf{q}'\| - 1}{\|\mathbf{q}'\|} \begin{bmatrix} 0 \\ Q_k' + \mathcal{K}P_k \\ B_k \end{bmatrix} \right) \cdot \begin{bmatrix} P_j' - \mathcal{K}Q_j \\ Q_j' + \mathcal{K}P_j \\ B_j' \end{bmatrix} \mathrm{d}S \ , \tag{5.74}$$

$$\mathbf{K}_{jk}^{\nu_0} = -\nu_0^2 \int_0^l \Phi_k' \cdot \Phi_j' \mathrm{d}S \ , \tag{5.75}$$

$$\mathbf{K}_{jk}^{\nu_1}(t) = \dot{\nu}_1(t) \int_0^l \Phi_k' \cdot \Phi_j \mathrm{d}S + \left(2\nu_0\nu_1(t) + \nu_1^2(t)\right) \int_0^l \Phi_k' \cdot \Phi_j' \mathrm{d}S \ , \tag{5.76}$$

$$\mathcal{Q}_{jkl} = \frac{1}{\epsilon} \int_0^l \left(\frac{1}{\|\mathbf{q}'\|^2} \begin{bmatrix} \left(Q_k' + \mathcal{K}P_k\right)\left(Q_l' + \mathcal{K}P_l\right) + B_k' B_l' \\ 2\left(P_k' - \mathcal{K}Q_k\right)\left(Q_l' + \mathcal{K}P_l\right) \\ 2\left(P_k' - \mathcal{K}Q_k\right) B_l' \end{bmatrix} \right) \cdot \begin{bmatrix} P_j' - \mathcal{K}Q_j \\ Q_j' + \mathcal{K}P_j \\ B_j' \end{bmatrix} \mathrm{d}S \ , \tag{5.77}$$

$$\mathcal{C}_{jklm} = -\frac{1}{2\epsilon} \int_0^l \begin{bmatrix} 2\left(P_k' - \mathcal{K}Q_k\right)\left[\left(Q_l' + \mathcal{K}P_l\right)\left(Q_m' + \mathcal{K}P_m\right) + B_l' B_m'\right] \\ \left(Q_k' + \mathcal{K}P_k\right)\left[2\left(P_l' - \mathcal{K}Q_l\right)\left(P_m' - \mathcal{K}Q_m\right) - \left(Q_l' + \mathcal{K}P_l\right)\left(Q_m' + \mathcal{K}P_m\right) - B_l' B_m'\right] \\ B_k'\left[2\left(P_l' - \mathcal{K}Q_l\right)\left(P_m' - \mathcal{K}Q_m\right) - \left(Q_l' + \mathcal{K}P_l\right)\left(Q_m' + \mathcal{K}P_m\right) - B_l' B_m'\right] \end{bmatrix} \cdot \left(\frac{1}{\|\mathbf{q}'\|^3} \begin{bmatrix} P_j' - \mathcal{K}Q_j \\ Q_j' + \mathcal{K}P_j \\ B_j' \end{bmatrix} \right) \mathrm{d}S \ , \tag{5.78}$$

$$\mathbf{f}_j^{\nu_1}(\mathbf{x}, t) = \left(2\nu_0\nu_1(t) + \nu_1^2(t)\right) \int_0^l \mathbf{x}' \cdot \Phi_j' \mathrm{d}S - \dot{\nu}_1(t) \int_0^l \mathbf{x}' \cdot \Phi_j \mathrm{d}S \ , \tag{5.79}$$

$$\mathbf{f}_j(t) = \int_0^l \Phi_j \cdot f \mathrm{d}S \ . \tag{5.80}$$

Once $\nu_1(t)$ is chosen, several cases can be investigated. Two main scenarios are of interest:

- A periodic fluctuation around the mean value which creates a parametric excitation
- A breaking or accelerating scenario

The first scenario paves the way to stability analysis both analytically and numerically.

5.4.1 Periodic solicitations for the ropeway

The possible periodic solicitations for the ropeway are due to the following main mechanisms:

- A periodic fluctuation of the in-line velocity. The latter comes from the command of the motor station. The axial velocity is decomposed as a constant part ν_0 and a fluctuation $\nu_1(t) = V \sin(\Omega t)$ and $f = 0$.

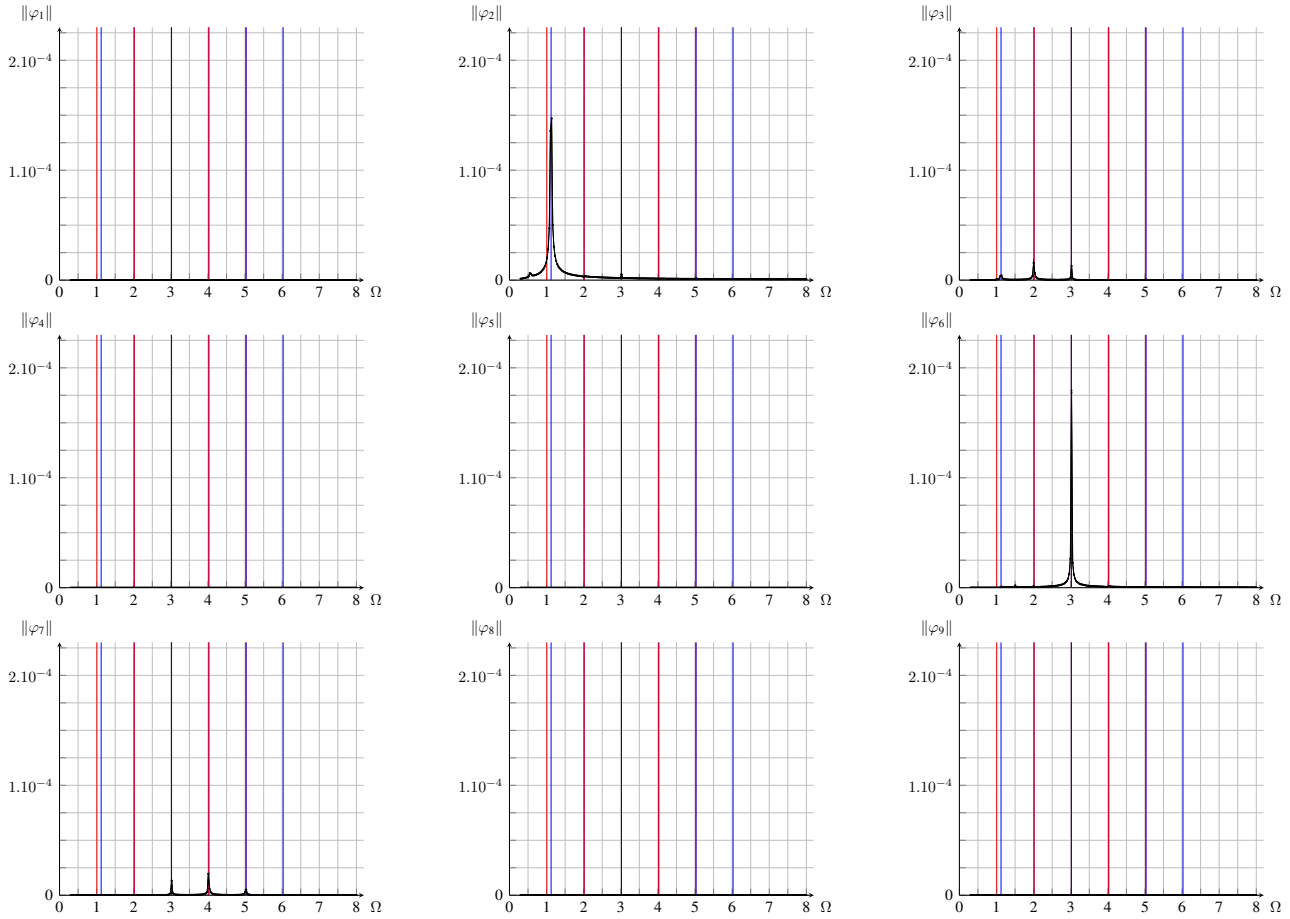

Figure 5.6: Response curves of each modes (solid line —) for a cable translating at velocity $\nu(t) = \nu_0 + V\sin(\Omega t)$ - OOP frequencies (solid line —) and IP frequencies (solid line —) are plotted vertically - Parameters in Table 5.4

- The charge and discharge of the cable by the car. Indeed each time the car enters the line it creates an increment of force (idealized view). It can also be seen as a force moving along the curvilinear abscissa. The force f is specified afterwards.
- External solicitation that can be approximated by a periodic function of time. The latter has already been studied in Section 4.2.

The first case is a direct fallout of Section 5.4. Typical time-integration profiles of the non-dimensional system are provided in Figures 5.7-5.10 and an example of frequency response is available in Figure 5.6. As visible in Figures 5.7-5.10 and 5.6, the displacement is dominated by the planar modes. However the amplitudes of fluctuation are not enough to produce strong nonlinear phenomena. The response is mostly linear in the sense that amplitude peaks are centered around the linear frequencies. However, the out-of-plane modes remain important for the dynamics since without it, we could lose some resonance phenomenon for transverse modes. As a conclusion, sudden large amplitudes of oscillation are not directly due to the fluctuation of the velocity. We clearly see in the case presented that the amplitude is not enough to be considered as big. Moreover, the amplitude of the fluctuation is less likely to increase much.

Those observations go in favor of the investigation of other scenarios as a source of sudden large oscillations. The most likely is the periodic load and deload of the cable. The latter is intrinsic to the cable-car, indeed each vehicle is distant from a given length of the following one. The

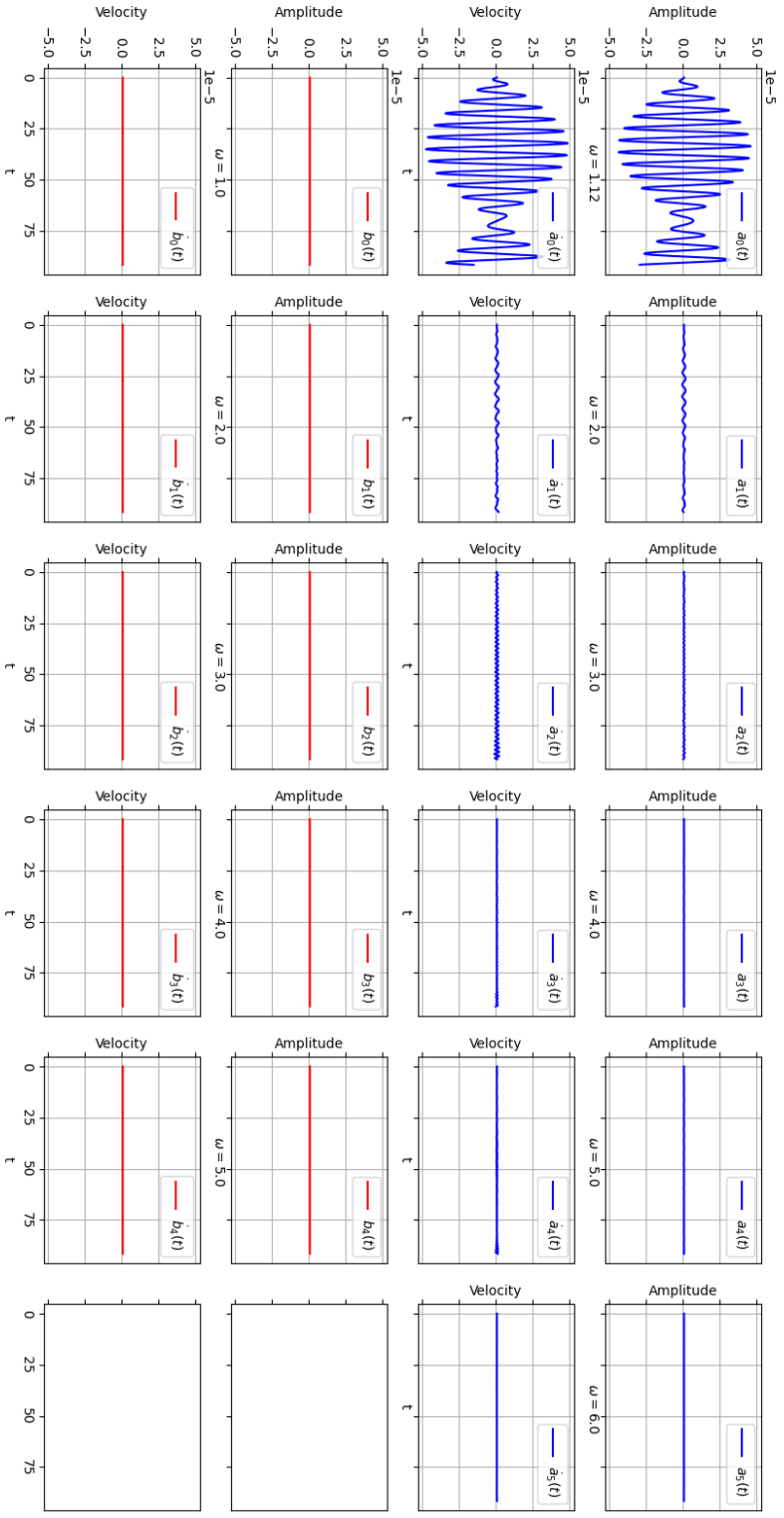

Figure 5.7: First seconds of time integration for $\Omega = 1.03$ rad/s - IP dofs (solid line —) OOP dofs (solid line —) - Parameters in Table 5.4

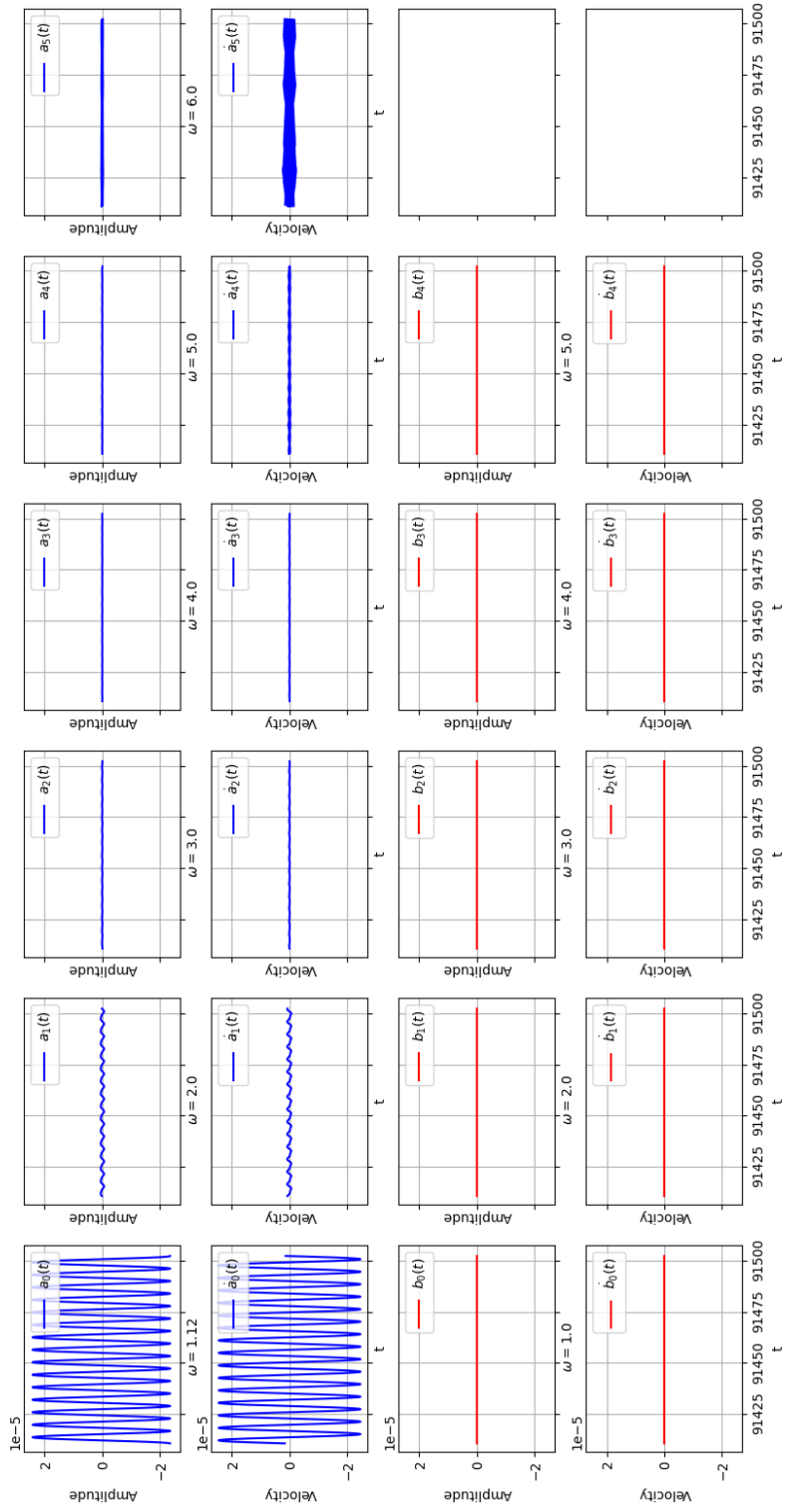

Figure 5.8: Last seconds of time integration for $\Omega = 1.03$ rad/s - IP dofs (solid line —) OOP dofs (solid line —) - Parameters in Table 5.4

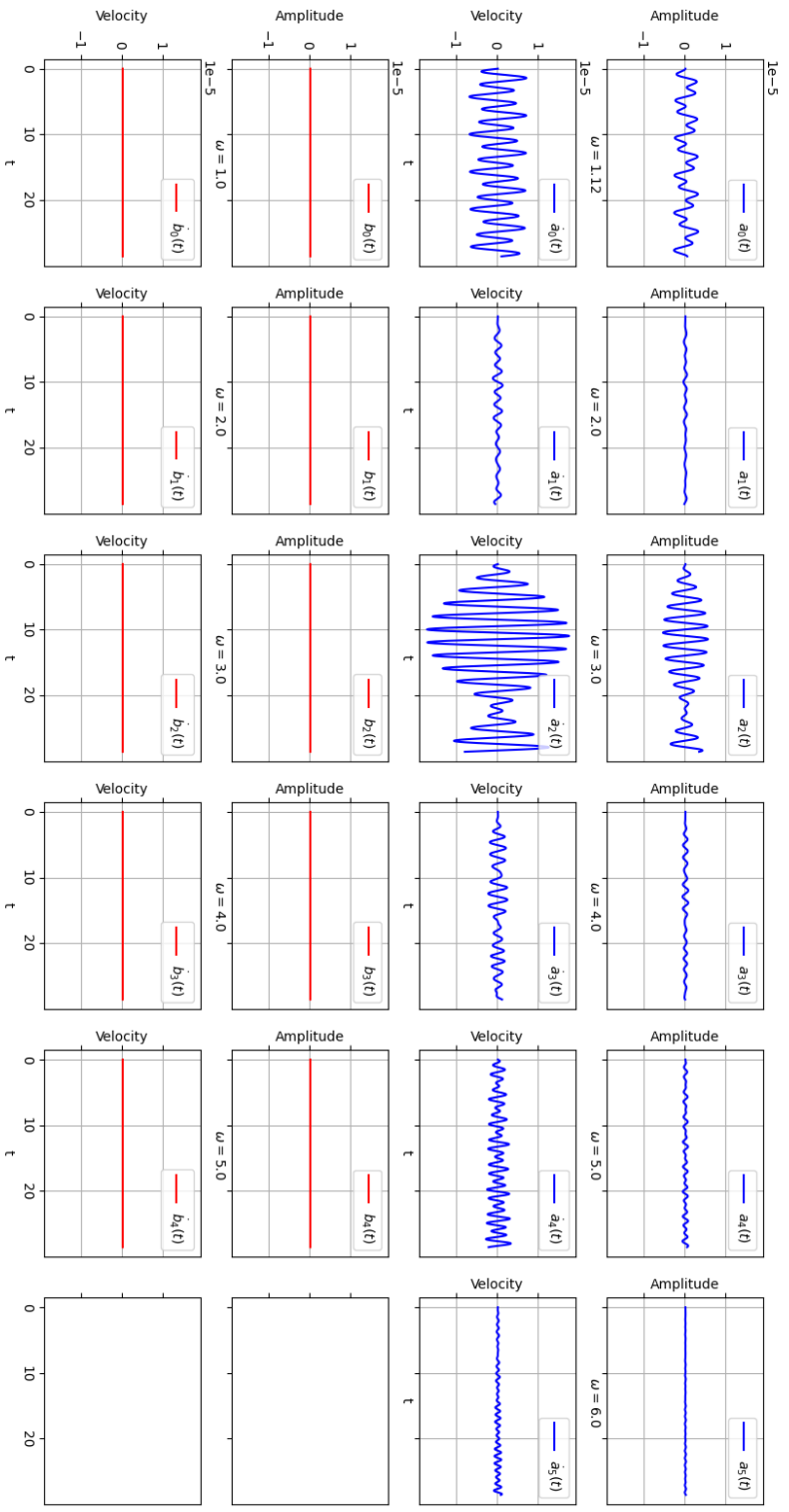

Figure 5.9: First seconds of time integration for $\Omega = 3.3$ rad/s - IP dofs (solid line —) OOP dofs (solid line —) - Parameters in Table 5.4

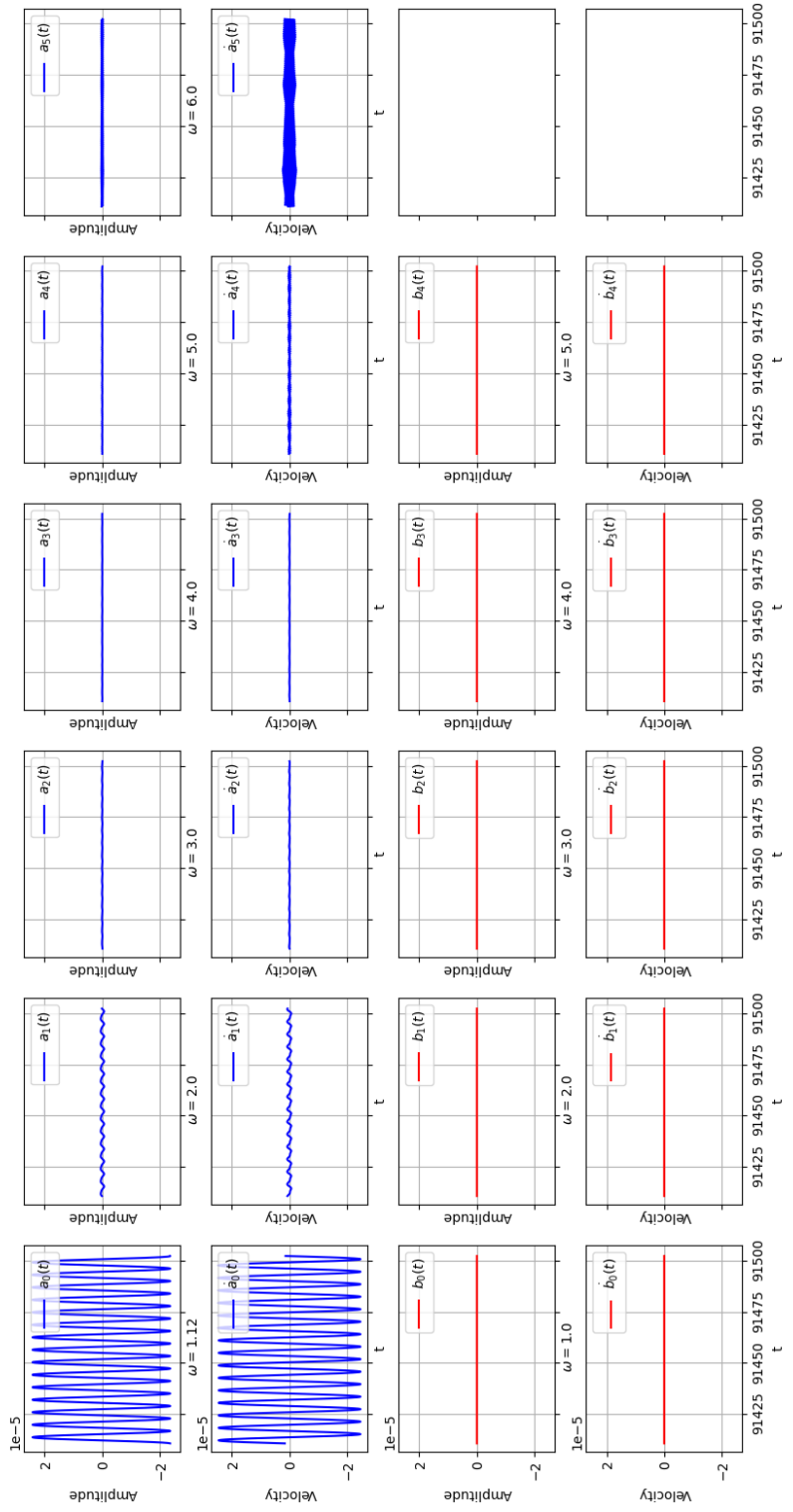

Figure 5.10: Last seconds of time integration for $\Omega = 3.3$ rad/s - IP dofs (solid line —) OOP dofs (solid line —) - Parameters in Table 5.4

Table 5.4: Parameters used to plot the frequency curves of the translating cable with fluctuating velocity

EA (MN)	ρ (kg/m)	H (kN)	d (m)	h (m)	v_0 (m/s)	v_1 (m/s)	α (IS)
100	5	80	80	5	5	0.1	0.2

	ω_1	ω_2	ω_3	ω_4	ω_5	ω_6	ω_7	ω_8	ω_9
(rad/s)	1	1.114	1.999	1.999	2.998	3.003	3.996	3.996	4.992

Table 5.5: Parameters used to plot the response of the translating cable due to braking

EA (MN)	ρ (kg/m)	H (kN)	d (m)	h (m)	v_0 (m/s)	Rayleigh damping
100	5	80	80	5	5	8%

ratio of this distance by the in-line velocity provide with the period of forcing. The amplitude of forcing is the weight of the car in first approach.
A more precise and complex model is to trace the motion of the car along the curvilinear abscissa in order to catch the influence of the mobile mass on the dynamics [4, 5]. The latter approach is not done here but an alternative via FEM is proposed in Chapter 6.
The external forcing is very general. It can be wind, temperature variations (if thermo-mechanical coupling is considered), passenger behavior or any periodic event that would cause a displacement or an applied force to the cable. Most of those cases are a fallout of the methodology presented in Sections 4.2 and 5.4.

5.4.2 Emergency braking

The case of an emergency braking is studied here. We assume that the cable is flowing at a velocity ν_0 and that suddenly the cable is stopped via imposing the following velocity

$$\nu : t \longrightarrow \begin{cases} \nu_0 & , \quad -\infty < t \leqslant 0 \\ \dfrac{t}{t_a}\nu_0 & , \quad 0 < t \leqslant t_a \\ 0 & , \quad t_a < t < +\infty \end{cases} , \tag{5.81}$$

which plot is given in Figure 5.11 via using the parameters set available in Table 5.5.
We see that the model proposed is not able to explain the sudden large amplitude of oscillations when physical values are used. The braking should be further investigated via more complete models and FEM approach which can include friction and the presence of obstacles.

5.5 Dynamical analysis: a case study

In this section we investigate the stability of the translating cable. As explained in last section, the situation where the axial velocity exhibits a fluctuation around its mean value is not a valuable scenario to explain large oscillations in cable-car engineering.
We are investigating here the possibility given by periodic load and deload of the cable combined to a constant velocity of translation. The stability of the system can be investigated by the means of evaluating the eigenvalues of the monodromy matrix for the periodic solutions found

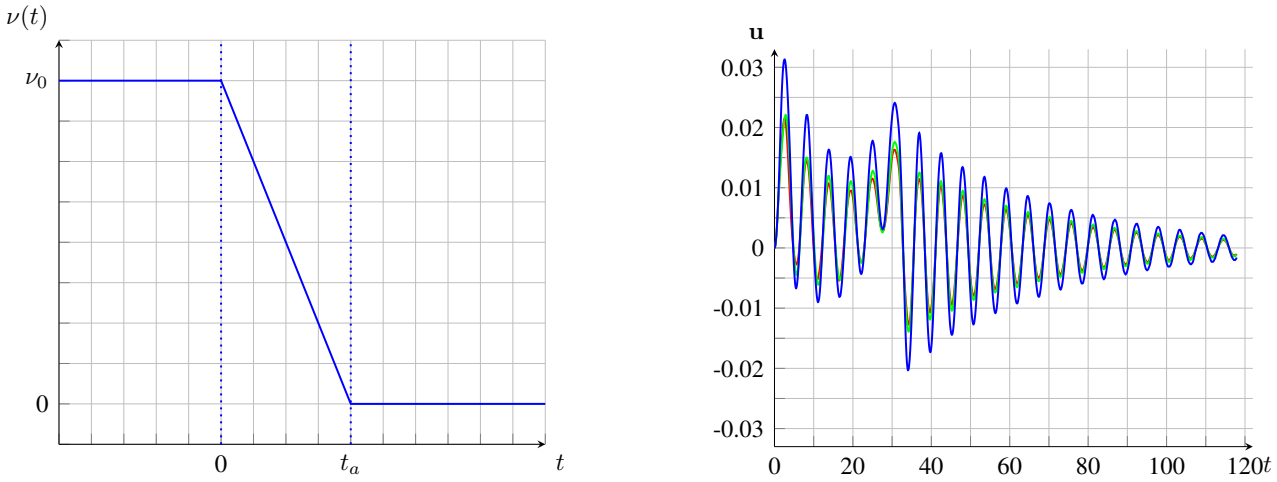

Figure 5.11: Amplitude of the first quarter span (solid line —) , the midspan (solid line —) and the last quarter span (solid line —) when the braking is applied to the cable

via the arc-length method (see Appendix E for details).
It should be noted that in engineering situations, the term 'stability' is misunderstood and misused. Indeed, it often implies that the system undergoes sudden large oscillations. This mechanism that can be explained by the coexistence of two attractive solutions ; one which exhibits small amplitudes and another one whose amplitude is large. The other mechanism that could explain the sudden large amplitudes of displacement is the possibility of parametric resonance made possible by the term (5.76) in the equation.
This section presents some application of (5.69) which illustrates both possibilities. In order to simulate the excitation of the cable by the car, we assume that a periodic force is applied to the "left end" of the cable. We simplified the solicitation drastically but still believe the latter to represent the key mechanism at stake. We consider

$$f : (S,t) \longrightarrow \left\{ F_0 \sin(\Omega t) \quad , \quad 0 \leqslant S \leqslant \frac{l}{20} \quad , \quad 0 \leqslant S \leqslant \frac{l}{20} \right\} . \tag{5.82}$$

Following our methodology we obtain $\mathbf{f}(t)$ which allows to investigate the sensibility of the span to this kind of solicitation. We could also investigate a sum of atoms such that at every $t_k = \frac{2k\pi}{\Omega}$ the force F_0 is applied to the first meters of the span. This is out of the scope of the study led here.
The situation is illustrated in Figure 5.12.

5.5.1 Coexistence of multiple solutions and internal resonance

The parameters used are given in Table 5.6. In this particular case, we used a Rayleigh damping of 8%: $\mathbf{C} = 8\%\mathbf{M} + 8\%\mathbf{K}$. The six first modes were used to build the ROM. The response curves are plotted mode per mode in Figure 5.13. The main component of the response is the first planar mode given by φ_2. This prediction via arc-length is challenged via direct-time integration and both responses are superimposed. We only plot the location of the system in the amplitude domain when the transient regime stops, we see here that high jumps may occur in this kind of situations, see Figure 5.16. Those jumps are likely to occur close to unstable zones. The amplitude of motion can be multiplied by 4 close to the main peak. The same plot in terms of kinetic energy is depicted in Figure 5.15 where we see that different energy levels are coexisting at the same frequency.
The internal resonance is always difficult to represent. Plots can suggest that curves are buckling, looping or crossing each other. However, depending on the dimension of the plot, complex

Figure 5.12: Real life illustration of the studied case - Bad Gastein aerial ropeway - Photo credits: https://www.seilbahn.net/sn/index1.php

Table 5.6: Parameters used to plot the response curves of the translating cable with punctual forcing

EA (MN)	ρ (kg/m)	H (kN)	d (m)	h (m)	v_0 (m/s)	P (kN)	Rayleigh damping
40	4	84	80	5	5	1962	8%

	ω_1	ω_2	ω_3	ω_4	ω_5	ω_6
(rad/s)	1	1.0264	1.9995	1.9997	2.9985	2.9994
Type	OOP	IP	IP	OOP	OOP	IP

connections between branches are revealed. 2D-plots can mislead our judgment and even occult part of the dynamics as shown in the 3D-representation of the response curves in Figure 5.14. The internal resonance is therefore more visible when response curves are plotted on a 3D-axis $(\Omega, \varphi_j, \varphi_k)$ with $k \neq j$. In the case presented here we see a connection between every modes in the zone given by $3 \leqslant \Omega \leqslant 4$. The classical representation of a loop should therefore be interpreted in a twisted shape in a 7 dimensional space formed by the frequency range and the space of amplitudes.
The latter illustrates the multiple internal resonances the cable is subjected to. The latter makes the analysis a real challenge and the dynamic design of cable structures a hard task. In first approach, we could try to find ways to avoid the huge jumps maybe via the use of a tune-mass damper or a nonlinear energy sinks [8]. The latter is left for further research.

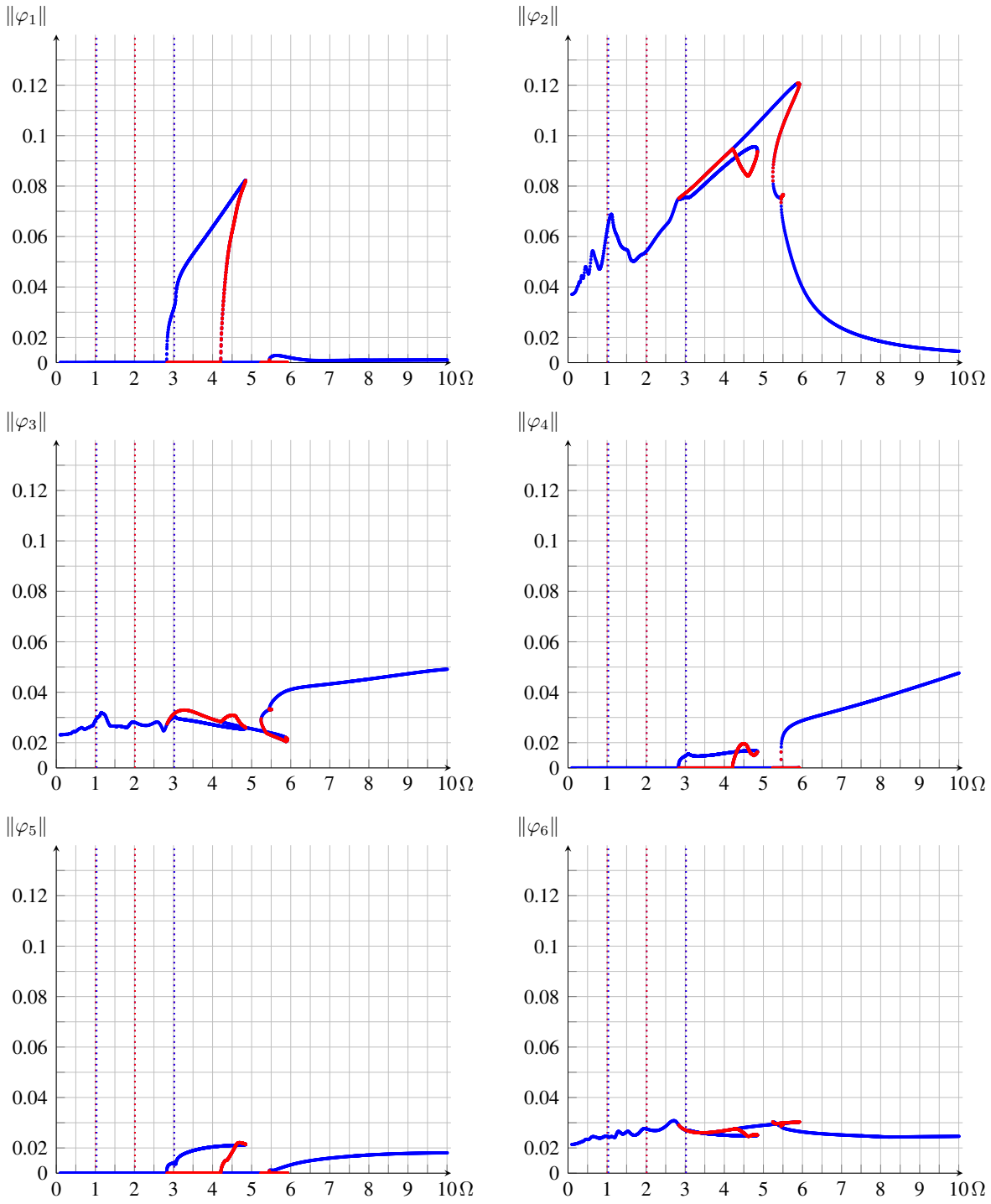

Figure 5.13: Frequency response curves obtained with arc-length continuation technique for the cable subjected to punctual forcing
(dotted line ·····) Stable solutions ; (dotted line ·····) Unstable solutions

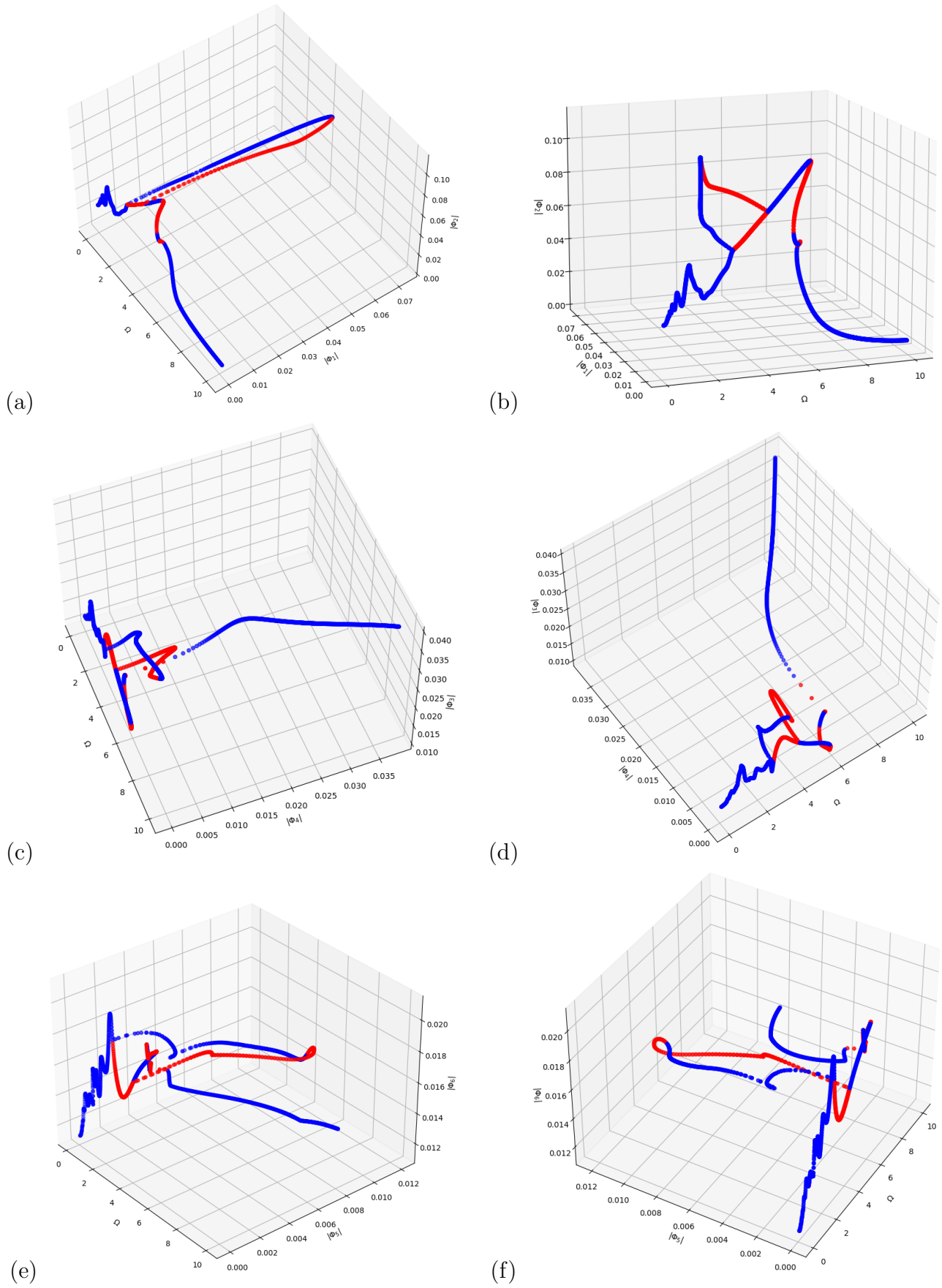

Figure 5.14: Frequency response curves plotted in 3D plots
(dotted line ·····) Stable solutions ; (dotted line ·····) Unstable solutions ; (a-b) First and second modes, (c-d) third and fourth modes, (e-f) fifth and sixth modes

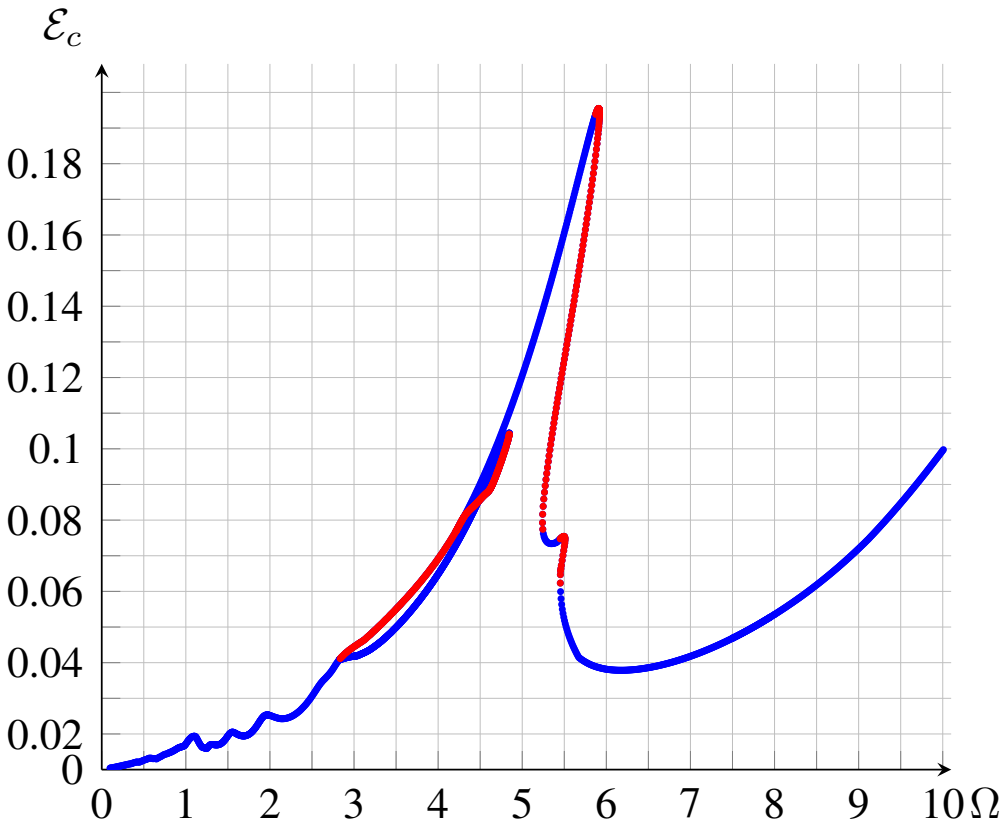

Figure 5.15: Frequency response curves obtained with arc-length continuation technique for the cable subjected to punctual forcing (Kinetic energy of the whole system) (dotted line ·····) Stable solutions ; (dotted line ·····) Unstable solutions

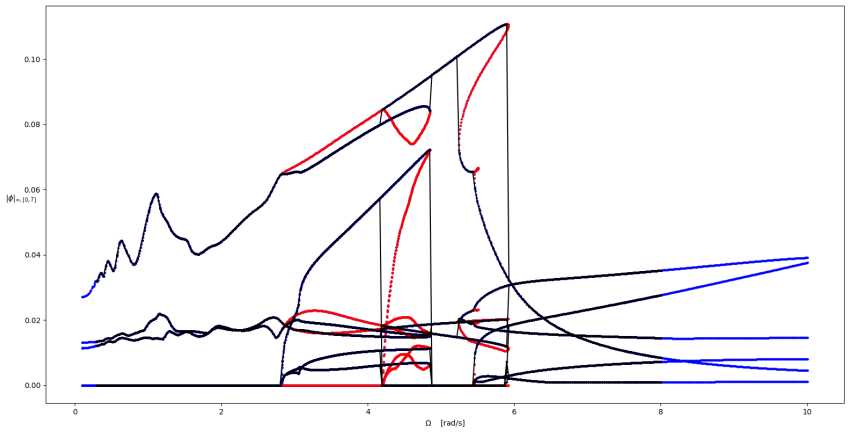

Figure 5.16: All Frequency response curves obtained with arc-length continuation technique and solution obtained from time integration (solid line —)
(dotted line ·····) Stable solutions ; (dotted line ·····) Unstable solutions

Conclusion of the chapter

This chapter consists mainly on extension and applications of the tools developed in the Chapter 4. We have seen that even in a simplified manner, the cable-car installation remains a challenge for design. Main contributions and results are:

- The extension of the classical theory of vibration for the translating cable case;
- A proof for the non-existence of anti-symmetric modes when the axial velocity is non-zero;
- A strategy to simulate the influence of the velocity on the dynamics of cables;
- Preliminary results about the instability occurring on a single span due to velocity related solicitations;
- We have shown that the velocity in itself does not suffice to produce instability and that the solicitation explaining instability is much more complex.

The limitations are the following:

- No experimental data are available to validate the model and there is not a straightforward way of obtaining them;
- The proposed methodology is accurate to trace when an instability occurs in the mathematical sense, the link with sudden large amplitude should be done with care;
- The single-span view lacks the global view of the installation which could occult some interesting phenomenon.

Some research perspectives are:

- Exploring the other ways opened with the translating cable modes;
- Enriching the methodology to account for multiple spans;
- Including the moving mass as a solicitation;
- Pumping the energy of instabilities with active or passive strategy.

Chapter 6

Applications to aerial ropeways: Full-installation model

This chapter is dedicated to a global application of all the presented tools in this manuscript. The main component is Chapter 3. However, some small pieces of the manuscript are used here to propose a methodology believed to be applicable to a carrying hauling rope.
As it is difficult to make it general due to the numerous parameter at play, the focus is drawn to a particular chair-lift installation known to be problematic and subjected to huge sudden large displacements.
This installation denominated the "TSD du Bouquet" was subjected to sudden large oscillations. This phenomenon is often called in french "pompage" in engineering studies. This installation has been dismantled but we have access to the line geometry and to the mechanical properties of the cable. All along this chapter, we use it as an illustration to provide a methodology on the modeling of a global installation using the tools of the previous chapters.

6.1 Context and modeling choices

Let us consider the equilibrium of the installation. Four main components can be listed:

- The cable
- The carriers (punctual masses)
- The stations (sheaves)
- The roller batteries (obstacles)

Each element is described independently from the other. Here we model the system with a tension station at the bottom and a drive station at the top. Every component is visible in Figure 6.1.

6.1.1 The cable

The cable is considered to be uniform with linear density ρ constant along the curvilinear abscissa. The same consideration holds for its rigidity EA. The cable at rest is L meters long. We use a given nominal tension T_0 at the bottom station so that the top tension remains bounded by a maximum value $T_{\max}$.
The damping α is always critical to infer for FEM applications. As a matter of fact, the latter should be small compared to the tension at play so that its influence remains low but still

Table 6.1: Parameters of the cable used in the "TSD des Bouquetins"

EA (MN)	ρ (kg/m)	v_0 (m/s)	T_0 (kN)	α (IS)	m_{veh} (kg)	d_{veh} (m)	μ (NA)
40	4	4	84	4.8	400	36.6	0.1

avoids numerical instabilities[1]. The cable is discretized in element with two nodes. The vector of node displacements is given by $\mathbf{q}$.

6.1.2 The carriers

The carriers are modeled as punctual masses m_{veh}. Vehicles are separated by a given cable segment of d_{veh}. In the model each vehicle is directly attached satisfying the distance requirement. The physical values of the cable and the vehicles are gathered in Table 6.1.

6.1.3 The stations

The stations are modeled as horizontal sheaves. They are given namely by (Γ_1, Γ_2). The top station, Γ_2, is considered to be the drive station which pulls the cable at a driven velocity $v(t)$. The drive sheave has a R_{Γ_2} radius. The bottom station, Γ_1, is a return sheave of a given radius R_{Γ_1}. Sheaves' centers are respectively located at $(x_{\Gamma_1}, y_{\Gamma_1}, z_{\Gamma_1})$ and $(x_{\Gamma_2}, y_{\Gamma_2}, z_{\Gamma_2})$.
In our simulation, the sheaves are modeled with the following constraints

$$\mathbf{g}(\mathbf{q}) = \sqrt{\left(\mathbf{q}^{(3i)} - x_{\Gamma_j}\right)^2 + \left(\mathbf{q}^{(3i+2)} - z_{\Gamma_j}\right)^2} - R_{\Gamma_j} \geqslant 0 \text{ and } \mathbf{q}_{\Gamma_j}^{(3i+1)} = y_{\Gamma_j} \quad , \quad \begin{matrix} i \in \text{nodes} \\ j = 1, 2 \end{matrix} \quad , \tag{6.1}$$

or

$$\mathbf{g}(\mathbf{q}) = \sqrt{\left(\mathbf{q}^{(3i)} - x_{\Gamma_j}\right)^2 + \left(\mathbf{q}^{(3i+2)} - z_{\Gamma_j}\right)^2} - R_{\Gamma_j} \geqslant 0 \text{ and } |\mathbf{q}_{\Gamma_j}^{(3i+1)} - y_{\Gamma_j}| \leqslant \epsilon \quad , \quad \begin{matrix} i \in \text{nodes} \\ j = 1, 2 \end{matrix} \quad , \tag{6.2}$$

where ϵ maintains the cable in place.
Friction is considered for both sheaves. More realistic models could embed the motion of the return sheave so that the tension remains equal to the nominal tension. This constraint is out of the scope here.

6.1.4 Roller batteries

The cable is being supported or compressed by roller batteries to guide it. As a mean of simplification, the roller batteries are not represented as an assembly of cylinder but as a global cylinder. Each roller batteries is identified by the tower holding it namely $(p_k)_{k \in \text{towers}}$. Most of the installation are parallel in the sense that each tower on the way up has a twin on the way down. Friction is supposed to occur on the roller batteries.
In our simulation, the roller batteries are modeled as the following constraints

$$\mathbf{g}(\mathbf{q}) = \sqrt{\left(\mathbf{q}^{(3i)} - x_{p_j}\right)^2 + \left(\mathbf{q}^{(3i+1)} - y_{p_j}\right)^2} - R_{p_j} \geqslant 0 \text{ and } \mathbf{q}_{p_j}^{3i+2} = z_{p_j} \quad , \quad \begin{matrix} i \in \text{nodes} \\ j = 1, 2 \end{matrix} \quad , \tag{6.3}$$

[1]The author admits that long sessions of trial and error allowed to eventually find parameters that were physically reasonable and numerically practicable

Table 6.2: Geometric parameters of the installation "TSD du Bouquet"

Structural element	Γ_1	p_0	p_1	p_2	p_3	p_4	p_5	p_6	p_7	Γ_2
x (m)	25	40	79.71	146.56	222.57	394.98	479.37	623.41	694.13	709.13
y (m)	0	0	16.86	41.03	67.96	126.17	154.04	195.99	212.67	212.67
R (m)	2.5	12	12	12	12	12	12	12	12	2.5

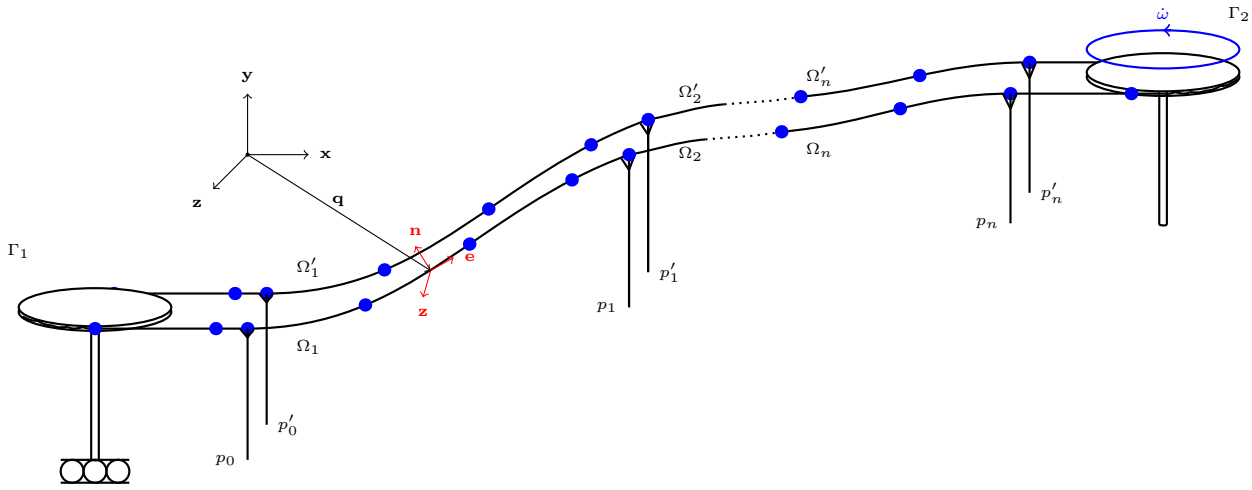

Figure 6.1: Example of carrying hauling rope heaved by its top station at angular velocity $\dot{\omega}$ - The carriers are located via (•)

or

$$\mathbf{g}(\mathbf{q}) = \sqrt{\left(\mathbf{q}^{(3i)} - x_{p_j}\right)^2 + \left(\mathbf{q}^{(3i+1)} - y_{p_j}\right)^2} - R_{p_j} \geqslant 0 \text{ and } ||\mathbf{q}_{p_j}^{3i+2} - z_{p_j}|| \leqslant \epsilon \quad , \quad \begin{matrix} i \in \text{nodes} \\ j = 1, 2 \end{matrix} \quad , \tag{6.4}$$

where ϵ maintains the cable in place.
More realistic model could embed different shape of roller batteries which is out of the scope of the following application.
The parameters used for both the stations and the roller batteries are given in Table 6.2.

6.1.5 Friction considerations

We choose here to model the friction via a Coulomb law. In the particular cases of an aerial ropeway, the design often relies on the assumption of constant line speed. As a result, the static equilibrium of a tower given by (2.108) directly simplifies

$$T_2 = T_1 e^{\mu_{p*} \Delta\theta} \ , \tag{6.5}$$

where $\Delta\theta$ is the wrapped angle. We see here that radius does not enter into the tension variation. In engineering application, the coulomb coefficient of a roll, μ_{p_j} is arbitrarily taken at 10%. This value is kept in the whole study. For the sheaves, we need to have $\mu \geqslant 1$ to guarantee enough tension continuity and the cable to be pulled.
We know that those values are high compared to engineering values but this example aims also to assess for the robustness of the model. In our study, the friction is modeled as proposed in (3.95) which is believed more general.

6.1.6 Imposed velocity

In order to impose the velocity in Γ_2, we formulate the friction problem thanks to (3.95) or (3.99) on the relative tangent velocity which is

$$\mathbf{u}_{T,k+1} = \mathbf{H}_T \mathbf{v}_{k+1} - v(t_{k+1}) \ . \tag{6.6}$$

Two possibilities comes with this formulation:

- The cable sticks to the drive sheave so the cable moves at velocity v
- The cable slips so the cable moves with a lower velocity than v

6.2 Initialization of the model

A critical steps for the evolution problem to work is a good initial condition. In this section we describe each steps required to obtain an acceptable initial cable profile. The proposed methodology is the following:

- Initialize with joined catenary
- Set the roller batteries and the sheaves
- Initialize the FEM mesh
- Stabilize the statics with the DRM

6.2.1 The 3D cable element

As we are developing a three-dimensional application, we used the inextensible catenary equation in the 3D-space. For a homogeneous cable of length L whose tips are hinged on $\mathbf{q}_0$ and $\mathbf{q}_L$ The latter reads

$$\mathbf{q}_L - \mathbf{q}_0 = \begin{bmatrix} \frac{H}{\rho g} \log\left(\eta + \frac{\rho g}{H} + \sqrt{1 + \left(\eta + \frac{\rho g L}{H}\right)^2 + \zeta^2}\right) - \log\left(\eta + \sqrt{1 + \eta^2 + \zeta^2}\right) \\ \frac{H}{\rho g}\left(\sqrt{1 + \left(\eta + \frac{\rho g L}{H}\right)^2 + \zeta^2} - \sqrt{1 + \eta^2 + \zeta^2}\right) \\ \frac{H\zeta}{\rho g} \log\left(\eta + \frac{\rho g}{H} + \sqrt{1 + \left(\eta + \frac{\rho g L}{H}\right)^2 + \zeta^2}\right) - \log\left(\eta + \sqrt{1 + \eta^2 + \zeta^2}\right) \end{bmatrix} , \tag{6.7}$$

where $\eta = \frac{V}{H}$ and $\zeta = \frac{Z}{H}$ are the ratio of the initial vertical and transversal component of the cable forces by the horizontal component of the cable forces.
The elasticity does not matter for the mesh initialization. However it is considered for the rest of the computation.
Note that (6.7) can be directly transformed into an equivalent system where T_0 is imposed via setting $H = \frac{T_0}{\sqrt{1+\eta^2+\zeta^2}}$.

6.2.2 Initialization with joined catenary

The ropeway works at a given nominal tension T_0. We can use (6.7) in a sequence of problems which starts at the first cable located between Γ_1 and p_0, then we solve for each cable located between p_k and p_{k+1} and for p_5 and Γ_2.
The same goes for the down stream part. As a result, we have two lines: one going upstream

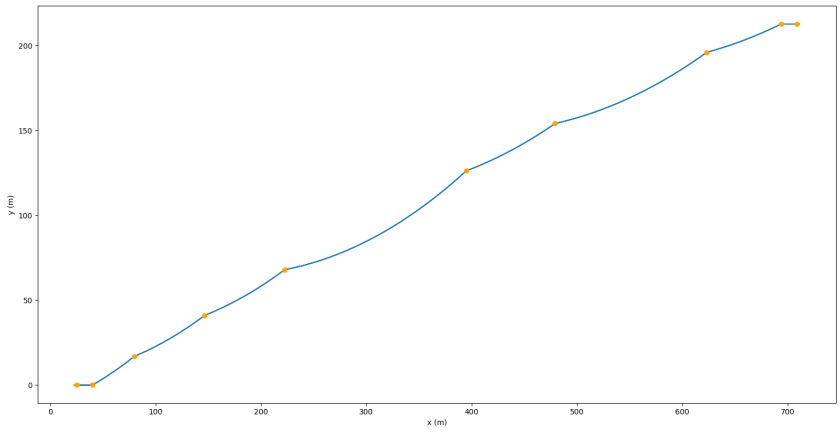

Figure 6.2: Initialization of the upstream part of the line via the $3D$-catenary equation (solid line —) . The towers are the junction between cables (dots •)

Table 6.3: Main characteristics of the cables for the upstream part of the line "TSD du Bouquet"

Span	$\Gamma_1 \to p_0$	$p_0 \to p_1$	$p_1 \to p_2$	$p_2 \to p_3$	$p_3 \to p_4$	$p_4 \to p_5$	$p_5 \to p_6$	$p_6 \to p_7$	$p_7 \to \Gamma_2$
T_0 (kN)	84	84	88.13	94.04	100.63	114.87	121.68	131.94	136.01
L (m)	14.97	43.07	71.02	80.57	182.7	88.73	150.04	72.47	14.95
η	-0.022	0.358	0.261	0.247	0.118	0.234	0.141	0.168	-0.013

and one going downstream. The result is plotted in Figure 6.2. For the first guess, the weight of the vehicles are averaged on each span. The latter results for the studied case in a $\rho = \rho_{\text{cable}} + \rho_{\text{veh}} = 25$ kg/m. This is only temporarily to shoot a first guess for the system.
The results obtained for the considered installation given by Tables 6.1 and 6.2 are gathered in Table 6.3.

6.2.3 Set the roller batteries and the sheaves

We can also access to the theoretical support reaction via the internal forces of each cables. The vertical component is important to chose whether the roller battery is a compression or a supporting one. The profile of the internal forces are plotted in Figure 6.3. The latter allows to access the jump of vertical forces which corresponds to the opposite of the force exerted by the roller batteries on the cable.

$$R_{p_k} = V(p_k^-) - V(p_k^+) \tag{6.8}$$

If the reaction is positive (resp. negative), the roller battery is below (resp. above). The table 6.4 presents the reaction force of the roller batteries for the upstream line. Indeed, the location given in Table 6.2 are the location of the summit of the tower. So the cylinder playing the role of obstacle is placed above or below in accordance with the nature of the roller battery (compression or support).

As the sheaves are used as starting and finishing points for the sequence of catenary problems, they do not represent an additional problem

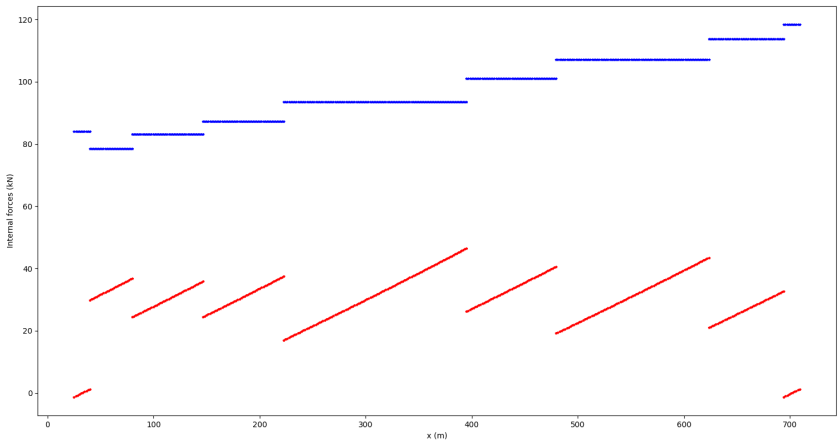

Figure 6.3: Internal forces of the upstream line versus curvilinear abscissa - Horizontal component (dotted line ·····) and vertical component (dotted line ·····)

Table 6.4: Roller battery reaction for the upstream part of the line "TSD du Bouquet"

Structural element	Γ_1	p_0	p_1	p_2	p_3	p_4	p_5	p_6	p_7	Γ_2
R (kN)	1.84	−26.5	16.68	17.06	30.5	30.48	30.98	31.89	41.45	1.83
Roller batteries (C or S)	S	C	S	S	S	S	S	S	S	S

6.2.4 Initialize the FEM mesh

Another result coming from the calculations, is the length of each cable. The whole length of the installation is built by summation. The latter is used to equally part the cable into FE segments. Around each sheaves (Γ_1 and Γ_2) the profile is imposed via considering a wrapped angle of π. The cable segments wrapped along the sheaves are directly connected to the other segments building a global mesh. At the first step, the cable possibly penetrates locally the cylinders used as obstacle. In order to rectify it, we used the gradient of the constraints (6.3) to have an admissible guess as follows

$$\mathbf{q} \longleftarrow \mathbf{q} - (1+\varepsilon)\nabla_{\mathbf{q}}\mathbf{g}^{\top}\mathbf{q} \ , \tag{6.9}$$

where $\epsilon > 0$ is a small positive parameter. The procedure is illustrated in Figure 6.4. The external load vector can be decomposed as the self-weight of the cable and the added weight of the chairs. The latter is built according to the formulas given in (3.17) where we have set

$$\mathbf{b}(S) = \rho_{\text{cable}} + \delta_{S_{\text{veh}}}(S) m_{\text{veh}} \ , \tag{6.10}$$

A visualization of this external force vector is proposed in Figure 6.5. The assembly is done straightforwardly via building a diagonal per block matrix. Only the last element is treated separately, the later assembly embeds a constraint of equality between the first and last node. Therefore for the first $N-1$ elements

$$\mathbf{K}[3e:3e+6, 3e:3e+6] \longleftarrow \mathbf{K}[3e:3e+6, 3e:3e+6] + \mathbf{K}^e \quad , \quad e \in \text{elements} - N \ , \tag{6.11}$$

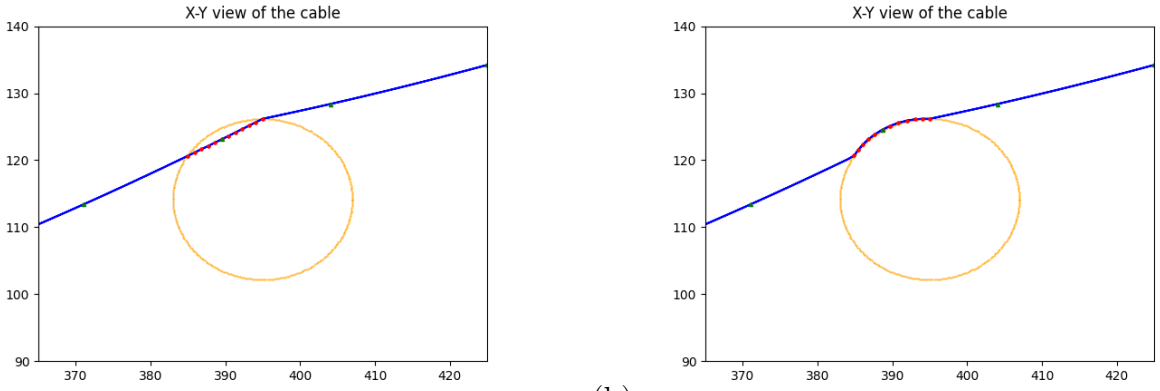

(a) (b)

Figure 6.4: Mesh in the vicinity of p_4 - (a) Before and (b) after the mesh correction

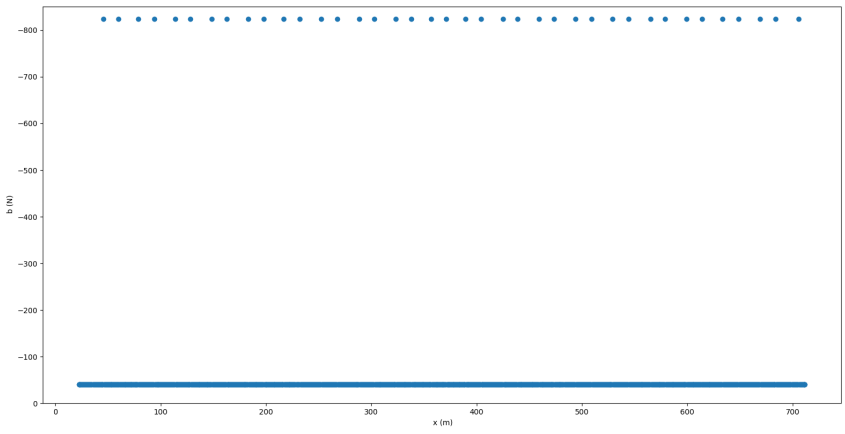

Figure 6.5: Vertical component of the load vector for the FEM application of the carrying hauling rope

and for the last element, $e = N$, we set

$$\mathbf{K}[3N:3N+3,3N:3N+3] \longleftarrow \mathbf{K}[3N:3N+3,3N:3N+3] + \mathbf{K}^N[0:3,0:3] \ , \tag{6.12}$$

$$\mathbf{K}[3N:3N+3,0:3] \longleftarrow \mathbf{K}[3N:3N+3,0:3] + \mathbf{K}^N[0:3,3:6] \ , \tag{6.13}$$

$$\mathbf{K}[0:3,0:3] \longleftarrow \mathbf{K}^N[3:6,3:6] \ , \tag{6.14}$$

$$\mathbf{K}[0:3,3N:3N+3] \longleftarrow \mathbf{K}^N[3:6,0:3] \ . \tag{6.15}$$

6.2.5 Stabilize the statics with the DRM

Using the technique described in 3.2.4, the actual static configuration is obtained. The FEM combined with the frictional dynamics 3.4.5 allows to get the influence of the friction and the obstacle on both the profile and the tension. Moreover the presence of punctual masses instead of distributed weight induces more sophisticated tension profile that are not analytically tractable.
In the proposed application, a very simplistic application of the DRM is endowed to fasten the computation of the damping matrix. We use

$$\mathbf{C}_k = 0.6\mathbf{M} + 0.4\mathbf{K}_k \tag{6.16}$$

The latter is sufficient to obtain the static position of the ropeway without computing modes at each iteration which is computationally expensive in the presented case. The obtained profile is plotted in Figures 6.6 and 6.7.

6.3 Dynamic analysis

This section briefly presents one example of transient dynamics and modal analysis applied to the presented installation.

6.3.1 Transient dynamics of the ropeway

The ropeway is taken from its static position and the top station is driven at 4 m/s.
To do so, the relative velocity of a contacting point to the sheave is computed as

$$\mathbf{u}_{T,k+1} = \mathbf{H}_T\mathbf{v}_{k+1} - v(t_{k+1}) \ . \tag{6.17}$$

The velocity of the drive sheave, $v(t_{k+1})$, may be specified differently in order to account for another scenario which includes acceleration or braking.
The time profiles can be obtained via using (3.95). With this numerical scheme, one can access to the trajectory of one carrier, the force at each roller battery and also the force developed by the sheaves via the Lagrange multipliers.

6.3.2 Modal analysis of the ropeway

According to Section 3.6, we can compute the modes of the installation. The latter is made via constraining the motion in the tangent manifold of the dynamics. In another word we apply the given methodology to $\mathbf{g}$ as given in (6.1) and (6.3). The equalities are taken explicitly in the form of

$$\mathbf{a}(\mathbf{q}) = \mathbf{A}\mathbf{q} \ , \tag{6.18}$$

where $\mathbf{A}$ selects the vertical dofs that remain stucked in the stations and the transversal dofs that remain stucked in the roller batteries.

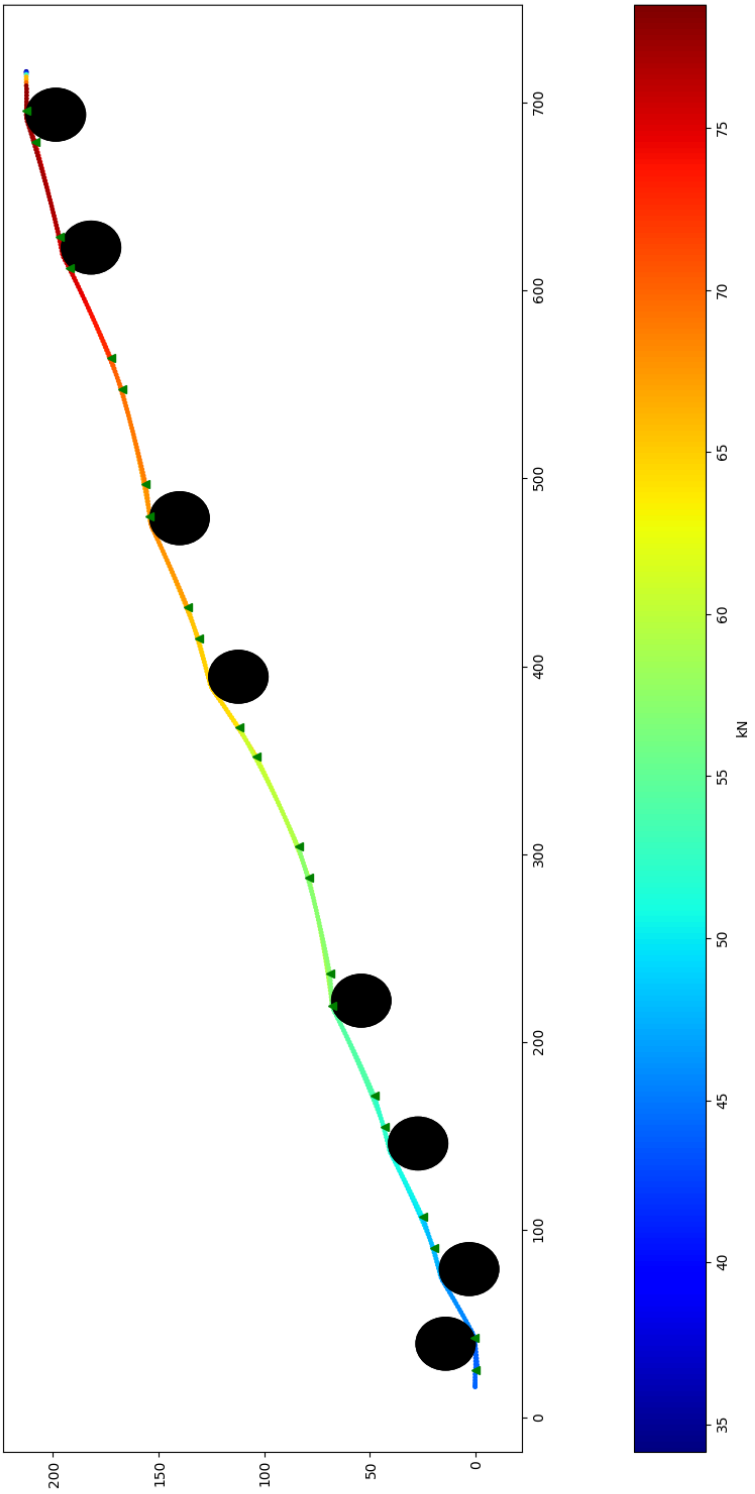

Figure 6.6: XY-view of the full installation obtained by FEM. The chairs are located with ◀ and the tension is depicted as shown by the colorbar

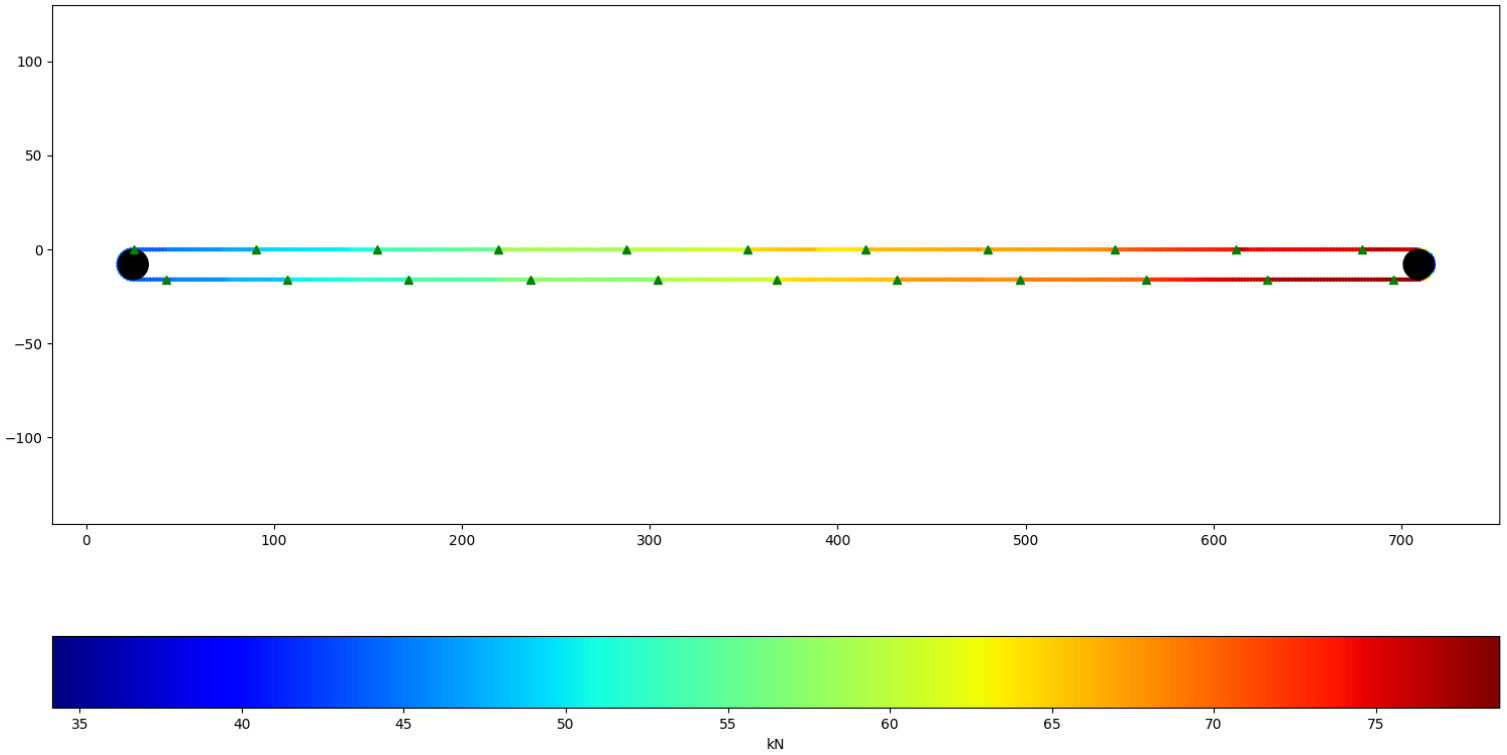

Figure 6.7: XZ-view of the full installation obtained by FEM. The chairs are located with ▲ and the tension is depicted as shown by the colorbar

Global modes can be caught by this methodology. Interestingly, the modes can still be parted into a family of planar modes (contained in the $x-y$ plane) and a family of transversal modes (contained in the $x-z$ plane). For the transversal modes, the behavior of each span seems independent because no vibrations are coexisting on different spans. Moreover the span with the biggest sag seem to respond at lowest frequencies. However for planar modes, the spans seem to be connected with their neighbor span and with the parallel span. The latter is interesting to explain to unexpected growth that happen in reality and goes in favor of complex interaction between spans. This claim is illustrated by Figures 6.8 and 6.9 which are representing the first fifteen modes of the hauling rope. Other application of those modes can lead to qualitative estimation of the instability observed in reality. For instance, modes can be used to build a linear system associated to the ropeway. Although the behavior is nonsmooth and nonlinear, it can be used to get a first idea of the possible displacement of a span.
The idea is to build a one-dof undamped oscillator with one mode. The latter is done via considering a first-order expansion of system variable around the equilibrium as done in Section 3.6. The latter results in

$$\mathbf{0} = \widetilde{\mathbf{M}}\ddot{\mathbf{q}} + \widetilde{\Delta\mathbf{K}}(\mathbf{q})\mathbf{q} + \widetilde{\mathbf{f}} \,, \tag{6.19}$$

where

$$\begin{cases} \widetilde{\mathbf{M}} = (\mathbf{QP})^\top \mathbf{M} (\mathbf{QP}) \\ \widetilde{\Delta\mathbf{K}}(\mathbf{q}) = (\mathbf{QP})^\top \Delta\mathbf{K}(\mathbf{q}) (\mathbf{QP}) \\ \widetilde{\mathbf{f}} = (\mathbf{QP})^\top \mathbf{f} \end{cases} , \tag{6.20}$$

and $\mathbf{P}$ is an orthogonal basis of $\nabla_{\mathbf{q}}\mathbf{a}$ and $\mathbf{Q}$ is an orthogonal basis of $(\nabla_{\mathbf{q}}\mathbf{g}_{\mathcal{A}}\mathbf{P})$. The nodal force vector in (6.19) should be constructed so that it is consistent with the excitation the ropeway is subjected to. Then (6.19) can be projected on one given mode as follows

$$\mathbf{0} = \Phi_j^\top \widetilde{\mathbf{M}} \Phi_j \ddot{\mathbf{q}}_{\Phi_j} + \Phi_j^\top \widetilde{\Delta\mathbf{K}}(\mathbf{q}) \Phi_j \mathbf{q}_{\Phi_j} + \Phi_j^\top \widetilde{\mathbf{f}} \,, \tag{6.21}$$

where Φ_j is one chosen mode and $\mathbf{q}_{\Phi_j}$ is the amplitude associated to this chosen mode.

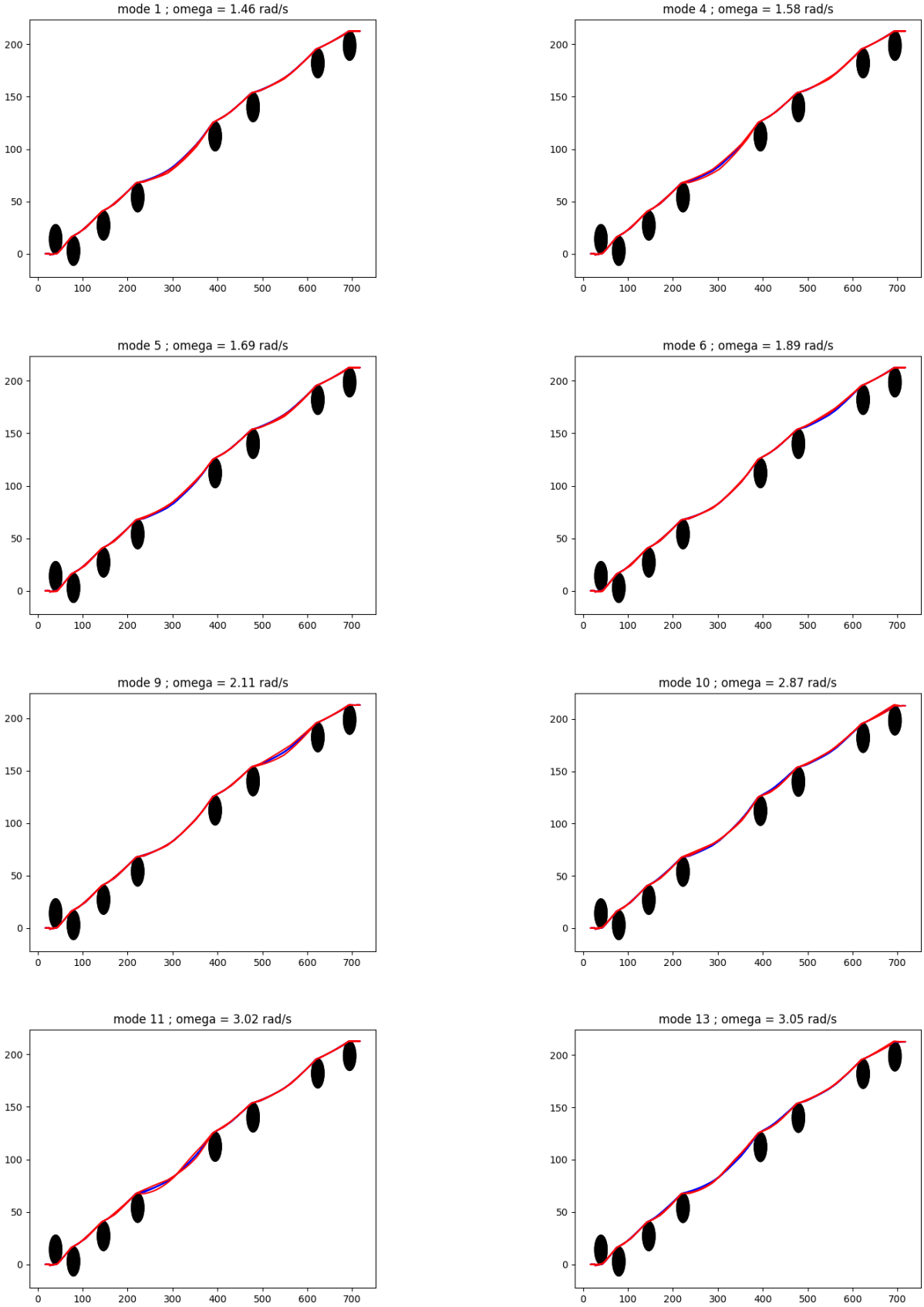

Figure 6.8: Modes contained in the $x - y$ plane obtained for the presented installation according to the methodology given in Section 3.6

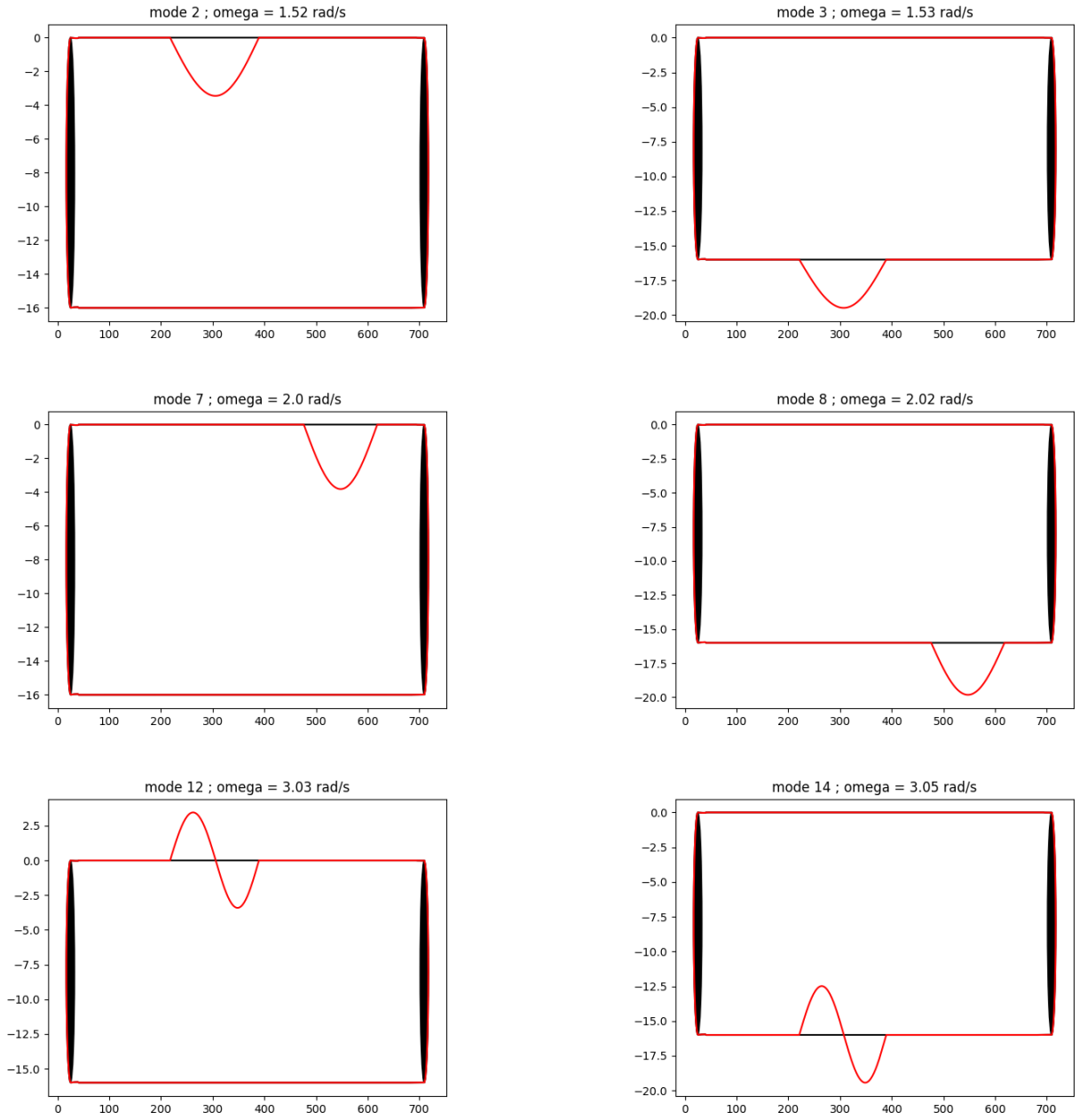

Figure 6.9: Modes contained in the $x - z$ plane obtained for the presented installation according to the methodology given in Section 3.6

Conclusion of the chapter

This chapter is dedicated to the applications of the Chapter 3 to the particular case of the full installation. Here, efforts are made to remain as general as possible for a single cable structure. First, modeling choices are given in detail. Then an application of the DRM 3.2.4 for the case of a unilaterally constrained cable is presented. Subsequently, we give an example of transient dynamics of a full-installation closer to the actual physics of the ropeways. Eventually, Section 3.6 is used to derive global modes for the hauling rope and a methodology to trace growing oscillation is given. Main interests are:

- The development of a sketch of methodology to simulate a hauling cable installation;
- A complex application of the tools developed in the presented research works.

The limitations are the following:

- The numerical procedure relies on low-order schemes and therefore requires high CPU-time;
- No simple guidelines have been developed for the generic installations and the proposed simplified tools rely on linear dynamics.

Following improvements could be done:

- Investigate the possibility of faster numerical results via generalization of a α- generalized time integration scheme specific for the dynamic relaxation method applied to this constraint cable systems;
- Include more nonsmooth dynamics content for the simplified tools;
- Confront the obtained results with robust and reliable experiment to validate or invalidate the proposed methods;
- Include the flexural and torsional stiffness in order to model the physics more accurately.

References

[1] Lallement, G. and Inman, D. (1995). A tutorial on complex eigenvalues. *Proceedings of SPIE - The international society for optical engineering.*

[2] Rega, G. (2004). Nonlinear vibrations of suspended cables - Part I: Modeling and analysis. *Applied Mechanics Reviews*, 57(6):443.

[3] Simpson, A. (1972). On the oscillatory motions of translating elestic cables. *20 of Sound and Vibration*, 290:177–189.

[4] Sofi, A. (2013). Nonlinear in-plane vibrations of inclined cables carrying moving oscillators. *Journal of Sound and Vibrations*, 332:1712–1724.

[5] Sofi, A. and Muscolino, G. (2007). Dynamic analysis of suspended cables carrying moving oscillators. *International Journal of Solids and Structues*, 44:6725–6743.

[6] Subbiah, R.and Littleton, J. E. (2018). *Rotor and Structural Dynamics of Turbomachinery: A Practical Guide for Engineers and Scientists.* Springer International Publishing.

[7] Triantafyllou, M. (1985). The dynamics of translating cables. *Journal of Sound and Vibrations*, 103(3):171–182.

[8] Vakakis, A. F., Gendelman, O. V., Bergman, L. A., McFarland, D. M., Kerschen, G., and Lee, Y. S. (2009). *Nonlinear Targeted Energy Transfer in Mechanical and Structural Systems*. Springer Netherlands.

[9] Wilfred, C. (1924). Protection of steam turbine disk wheels from axial vibration. *Transactions of the ASME*, pages pp 31—160.

Chapter 7

Conclusion and perspectives

This PhD dissertation presents our investigations on the modeling of aerial ropeways including the influence of punctual loads, the interaction between the cable and the roller batteries and the interaction between the cable and the sheaves.

7.1 Results

Chapter 1 is a literature review which presents the existing trends in terms of cable modeling and simulations. Two main blocks are existing separately which are the analytical methods and the numerical methods. The lack of mix between those two aspects induces that models are too simplistic to model complex phenomenons or too sophisticated to study the influences of some parameters on the simulation results. Both approaches may be complementary if incorporated properly into one work which was the initial purpose of this dissertation.

Chapter 2 presents the mechanics of inextensible and elastic cables in a very general way. The derivations of system equations according to the principle of calculus of variations allows to obtain complex system models including a formalism for non-compressible cable. The classical results of the catenary solution and the parabolic approximations are recalled in this particular framework and prospective developments about impact and friction are introduced.

Chapter 3 gives some insights about the use of finite element method applied to the particular case of cable. The numerical challenges inherent to the problem of cable are addressed in order to formulate a cable finite element which can undergo large displacements without any compression. The latter is coupled to the nonsmooth dynamics culture to show its compatibility with impact and friction. Those developments are innovative since the interaction between the cable and sheave are formulated and treated via an inclusion. This allows to simulate a lot of practical situations including belt-drive simulation, cable-roll interaction or impacts along a convex obstacle for which the finite element method is one of the only tool able to compute equilibriums.

Chapter 4 recalls the classical theory of linear vibrations for cables. The latter is valid for incremental vibrations around an equilibrium. The latter is presented in the framework of the Frenet basis and is used to introduce a methodology to derive arbitrary reduced-order-models for tracing the nonlinear dynamics of a fixed-fixed cable. The application of the arc-length method for those has been endowed to show the ability of the method to catch sophisticated dynamical mechanisms. Moreover basic developments have been recalled to treat system equations via the method of multiple scales. The finite element method applied to cable dynamics

and this historical way of computing the cable responses are compared in several situations. It has been shown that in the framework of fixed-fixed cable undergoing incremental displacement and simple loads, the finite element is unnecessarily complicated.

Chapters 5 and 6 are specific applications of the developed tools. A generalization of free vibrations to the case of translating cable is proposed even though it is shown unable to explain the self-excitation or large amplitude in real applications. The "pompage" phenomenon seems to be initiated by the entry and exit of carriers on each span which is directly linked to the line speed. The latter can be simulated with reduced-order-models in a simplified manner or via the finite element method which is also able to compute reaction forces, friction and the support/cable interactions.

This PhD lead to the following publications:

- C. Bertrand, A. Ture Savadkoohi, and C.-H. Lamarque. Nonlinear oscillations of a pendulum cable with the effects of the friction and the radius of the support. Nonlinear Dynamics, 96:1303–1315, 2019 ;
- C. Bertrand, C. Plut, A. Ture Savadkoohi, and C.-H. Lamarque. On the modal response of mobile cables. Engineering Structures, 210, 2020 ;
- C. Bertrand, V. Acary, A. Ture Savadkoohi, and C.-H. Lamarque. A robust and efficient numerical finite element method for cables. International Journal for Numerical Method in Engineering, 121, 2020 ;
- C. Bertrand, A. Ture Savadkoohi, V. Acary, and C.-H. Lamarque. Reduced-order model for the non-linear dynamics of cables [accepted]. Journal of Engineering Mechanics, 2022.

and the following international congresses:

- **About the modal response of mobile cables**, Recent Advances in Nonlinear Mechanics (RANM), May 2019 Lodz, Poland
- **Equilibrium of a non-compressible cable subjected to unilateral constraints**, European Nonlinear Oscillation Conference (ENOC), 17-22 July 2022, Lyon, France
- **A robust numerical implementation of cable finite elements**, International Congress of Theoretical and Applied Mechanics (ICTAM), 23-28 August 2020+1, Milano, Italy
- **Numerical dynamics of a cable subjected to frictional impact**, Conference on the Numerical Solution of Differential and Differential-Algebraic Equations (NUMDIFF), 6-10 September 2021, Halle, Germany

7.2 Perspectives

Several aspects of this work could be improved. Some improvements are research related while some are linked with engineering and practical adaptations.

7.2.1 Perspectives for modeling

- The developed cable models could be further investigated in an algebraic manner to investigate the existence and (non-)uniqueness of solutions. Indeed the equations given in (2.49), (2.53) and (2.69) have not been investigated thoroughly

- The cable constitutive law used is a Hooke's law. The latter could be switch to more sophisticated constitutive law to account for thermal gradients, viscous phenomenon and also torsion. The torsion is the most interesting for engineering application since its coupling with traction could lead to explanation of dynamical instabilities observed in reality

- The conditions of existence and (non-)uniqueness have not been investigated enough in the author opinion for the case of a cable subjected to an obstacle. The latter could first be addressed with given geometries and then more general conditions.

- Comparing the obtained results with in-depth analysis of experimental results could drastically improve the modeling issues of this work. Some real-scale experimental test would enhance every further work on the subject.

7.2.2 Perspectives for analytical approaches

- The reduced-order-models developed here are relying on the theory of linear vibrations of cables. The latter could be enriched with the complex modes obtained in the last chapters. Moreover, the nonlinear effects linked to the geometry could be investigated via nonlinear modes instead of linear ones.

- Some analytical treatments of system equations could be developed to have engineering design tools for the case of multi-span installation. Further investigations via the method of multiple scales or perturbation method could provide interesting tools for design.

- A question to be answered is also the relevance of the nonlinear terms kept in the derivations. The quintic nonlinearity could be introduced in reduced-order-model at least to verify its futility with regard ti the cubic one.

- Investigate the influence of a nonlinear energy sinks on the large amplitude responses of the cable in order to control it. The latter can be done with or without the presence of obstacles.

7.2.3 Perspectives for numerical approaches

- Despite the efforts made, the dynamics captured by finite element method requires very thin time steps to ensure stability and robustness. Some other numerical schemes as HHT-schemes of α-generalized method could be implemented to further improve the quality of the obtained time profiles. The latter could work in the sense that a lot of the high-frequency content could be cut from the responses.

- Developing a full installation model that could cope with the actuators displacements and charge/discharge of passengers would improve the realism of the model. The geometry of the line could be precised for the tower and the sheaves to account for more complex obstacle geometries.

- A comparison with the geometrical exact beams could lead to further improvements of the simulations. Those models can cope with torsion and flexion so that the relevance of those mechanical phenomena in the case of aerial ropeways could be set once and for all.

Appendix A

Computation of the admissibility conditions for the extensible catenary

This appendix is a reminder of the extensible catenary equations. Depending on parameters, two cases are proposed:

- Case 1 = Inputs: initial horizontal component of tension H, linear density ρ, cross-section rigidity EA, horizontal span length d and vertical span length h. Unknowns: L and η
- Case 2 = Inputs: initial axial tension T_0, linear density ρ, cross-section rigidity EA, horizontal span length d and vertical span length h. Unknowns: L and η
- Case 3 = Inputs: reference length L, linear density ρ, cross-section rigidity EA, horizontal span length d and vertical span length h. Unknowns: H and η
- Case 4 = Inputs: reference length L, linear density ρ, cross-section rigidity EA, horizontal span length d and vertical span length h. Unknowns: T_0 and η

To prepare some Newton iterations, the nonlinear system and the Jacobian are presented. The derivations made here are valid for a physical system which has not been made non-dimensional.

Case 1

We recall here the notable quantity of the catenary. The details of derivations are available in the main part of the manuscript (chapter 2).

$$
\begin{aligned}
T(S) &= H\sqrt{1+\left(\eta+\frac{\rho g}{H}S\right)^2}\\
\mathbf{e}(S) &= \frac{1}{\sqrt{1+\left(\eta+\frac{\rho g}{H}S\right)^2}}\begin{bmatrix}1\\ \eta+\frac{\rho g}{H}S\end{bmatrix}\\
\mathbf{n}(S) &= -\frac{1}{\sqrt{1+\left(\eta+\frac{\rho g}{H}S\right)^2}}\begin{bmatrix}\eta+\frac{\rho g}{H}S\\ -1\end{bmatrix}\\
x(S) &= d-\frac{H(L-S)}{EA}-\frac{H}{\rho g}\left(\sinh^{-1}(\eta+\frac{\rho g}{H}L)-\sinh^{-1}(\eta+\frac{\rho g}{H}S)\right)\\
y(S) &= h-\frac{\eta H(L-S)}{EA}-\rho g\frac{L^2-S^2}{2EA}-\frac{H}{\rho g}\left(\sqrt{1+\left(\eta+\frac{\rho g}{H}L\right)^2}-\sqrt{1+\left(\eta+\frac{\rho g}{H}S\right)^2}\right)
\end{aligned}
$$

The admissibility condition are to be formulated as follows

$$\begin{cases} 0 = & d - \dfrac{HL}{EA} - \dfrac{H}{\rho g}\left(\sinh^{-1}(\eta + \dfrac{\rho g}{H}L) - \sinh^{-1}(\eta)\right) \\ 0 = & h - \dfrac{\eta HL}{EA} - \rho g \dfrac{L^2}{2EA} - \dfrac{H}{\rho g}\left(\sqrt{1 + \left(\eta + \dfrac{\rho g}{H}L\right)^2} - \sqrt{1+\eta^2}\right) \end{cases}$$
$$\leftrightarrow \quad \mathbf{0} = \mathcal{F}(L, \eta)$$

The Jacobian matrix of $\mathcal{F}$ is given by

$$\mathcal{J}(L,\eta) = \begin{bmatrix} \frac{\partial \mathcal{F}_1}{\partial L}(L,\eta) & \frac{\partial \mathcal{F}_1}{\partial \eta}(L,\eta) \\ \frac{\partial \mathcal{F}_2}{\partial L}(L,\eta) & \frac{\partial \mathcal{F}_2}{\partial \eta}(L,\eta) \end{bmatrix}$$

where

$$\frac{\partial \mathcal{F}_1}{\partial L}(L,\eta) = -\frac{H}{EA} - \frac{1}{\sqrt{1 + \left(\eta + \frac{\rho g L}{H}\right)^2}}$$

$$\frac{\partial \mathcal{F}_1}{\partial \eta}(L,\eta) = \frac{H}{\rho g}\left(\frac{1}{\sqrt{1+\eta^2}} - \frac{1}{\sqrt{1 + \left(\eta + \frac{\rho g L}{H}\right)^2}}\right)$$

$$\frac{\partial \mathcal{F}_2}{\partial L}(L,\eta) = -\frac{\eta H}{EA} - \frac{\rho g L}{EA} - \frac{\eta + \frac{\rho g L}{H}}{\sqrt{1 + \left(\eta + \frac{\rho g L}{H}\right)^2}}$$

$$\frac{\partial \mathcal{F}_2}{\partial \eta}(L,\eta) = -\frac{HL}{EA} + \frac{H}{\rho g}\left(\frac{\eta}{\sqrt{1+\eta^2}} - \frac{\eta + \frac{\rho g L}{H}}{\sqrt{1 + \left(\eta + \frac{\rho g L}{H}\right)^2}}\right)$$

Case 2

The admissibility condition are to be formulated as follows

$$\begin{cases} 0 = d - \dfrac{T_0 L}{EA\sqrt{1+\eta^2}} - \dfrac{T_0}{\rho g \sqrt{1+\eta^2}}\left(\sinh^{-1}(\eta + \dfrac{\rho g\sqrt{1+\eta^2}}{T_0}L) - \sinh^{-1}(\eta)\right) \\ 0 = h - \dfrac{\eta T_0 L}{EA\sqrt{1+\eta^2}} - \rho g \dfrac{L^2}{2EA} - \dfrac{T_0}{\rho g\sqrt{1+\eta^2}}\left(\sqrt{1 + \left(\eta + \dfrac{\rho g\sqrt{1+\eta^2}}{T_0}L\right)^2} - \sqrt{1+\eta^2}\right) \end{cases}$$

$$\leftrightarrow \quad \mathbf{0} = \mathcal{F}(L, \eta)$$

The Jacobian matrix of $\mathcal{F}$ is given by

$$\mathcal{J}(L,\eta) = \begin{bmatrix} \frac{\partial \mathcal{F}_1}{\partial L}(L,\eta) & \frac{\partial \mathcal{F}_1}{\partial \eta}(L,\eta) \\ \frac{\partial \mathcal{F}_2}{\partial L}(L,\eta) & \frac{\partial \mathcal{F}_2}{\partial \eta}(L,\eta) \end{bmatrix}$$

where

$$\frac{\partial \mathcal{F}_1}{\partial L}(L,\eta) = -\frac{T_0}{EA\sqrt{1+\eta^2}} - \frac{1}{\sqrt{1+\left(\eta+\frac{\rho g\sqrt{\eta^2+1}L}{T_0}\right)^2}}$$

$$\frac{\partial \mathcal{F}_1}{\partial \eta}(L,\eta) = \frac{\eta T_0 L}{EA\sqrt{1+\eta^2}^3} - \frac{T_0}{\rho g\sqrt{1+\eta^2}}\left(\frac{1+\frac{\rho g L\eta}{T_0\sqrt{1+\eta^2}}}{\sqrt{1+\left(\eta+\frac{\rho g\sqrt{1+\eta^2}L}{T_0}\right)^2}} - \frac{1}{\sqrt{1+\eta^2}}\right) + \frac{\eta T_0}{\rho g\sqrt{1+\eta^2}^3}\left(\sinh^{-1}\left(\eta+\frac{\rho g\sqrt{1+\eta^2}L}{T_0}\right) - \sinh^{-1}(\eta)\right)$$

$$\frac{\partial \mathcal{F}_2}{\partial L}(L,\eta) = -\frac{\eta T_0}{EA\sqrt{1+\eta^2}} - \frac{\rho g L}{EA} - \frac{\eta+\frac{\rho g\sqrt{\eta^2+1}L}{T_0}}{\sqrt{1+\left(\eta+\frac{\rho g\sqrt{\eta^2+1}L}{T_0}\right)^2}}$$

$$\frac{\partial \mathcal{F}_2}{\partial \eta}(L,\eta) = -\frac{L\left(EA\sqrt{1+\eta^2}+T_0\sqrt{1+\left(\eta+\frac{g\sqrt{\eta^2+1}L\rho}{T_0}\right)^2}\right)}{EA\sqrt{1+\eta^2}^3\sqrt{1+\left(\eta+\frac{g\sqrt{\eta^2+1}L\rho}{T_0}\right)^2}}$$

Case 3

The admissibility condition are to be formulated as follows

$$\begin{cases} 0 = d - \dfrac{HL}{EA} - \dfrac{H}{\rho g}\left(\sinh^{-1}(\eta+\dfrac{\rho g}{H}L) - \sinh^{-1}(\eta)\right) \\ 0 = h - \dfrac{\eta HL}{EA} - \rho g\dfrac{L^2}{2EA} - \dfrac{H}{\rho g}\left(\sqrt{1+\left(\eta+\dfrac{\rho g}{H}L\right)^2} - \sqrt{1+\eta^2}\right) \end{cases}$$
$$\leftrightarrow \quad \mathbf{0} = \mathcal{F}(H,\eta)$$

The Jacobian matrix of $\mathcal{F}$ is given by

$$\mathcal{J}(L,\eta) = \begin{bmatrix} \frac{\partial \mathcal{F}_1}{\partial H}(H,\eta) & \frac{\partial \mathcal{F}_1}{\partial \eta}(H,\eta) \\ \frac{\partial \mathcal{F}_2}{\partial H}(H,\eta) & \frac{\partial \mathcal{F}_2}{\partial \eta}(H,\eta) \end{bmatrix}$$

where

$$\frac{\partial \mathcal{F}_1}{\partial H}(H,\eta) = -\frac{L}{EA} - \frac{1}{\rho g}\left(\sinh^{-1}(\eta + \frac{\rho g}{H}L) - \sinh^{-1}(\eta)\right) - \frac{L}{H}\frac{1}{\sqrt{1+\left(\eta+\frac{\rho g L}{H}\right)^2}}$$

$$\frac{\partial \mathcal{F}_1}{\partial \eta}(H,\eta) = \frac{H}{\rho g}\left(\frac{1}{\sqrt{1+\eta^2}} - \frac{1}{\sqrt{1+\left(\eta+\frac{\rho g L}{H}\right)^2}}\right)$$

$$\frac{\partial \mathcal{F}_2}{\partial H}(H,\eta) = -\frac{\eta L}{EA} - \frac{1}{\rho g}\left(\sqrt{1+\left(\eta+\frac{\rho g}{H}L\right)^2} - \sqrt{1+\eta^2}\right) + \frac{L}{H}\frac{\eta+\frac{\rho g L}{H}}{\sqrt{1+\left(\eta+\frac{\rho g L}{H}\right)^2}}$$

$$\frac{\partial \mathcal{F}_2}{\partial \eta}(H,\eta) = -\frac{HL}{EA} + \frac{H}{\rho g}\left(\frac{\eta}{\sqrt{1+\eta^2}} - \frac{\eta+\frac{\rho g L}{H}}{\sqrt{1+\left(\eta+\frac{\rho g L}{H}\right)^2}}\right)$$

Case 4

$$\begin{cases} 0 = d - \dfrac{T_0 L}{EA\sqrt{1+\eta^2}} - \dfrac{T_0}{\rho g\sqrt{1+\eta^2}}\left(\sinh^{-1}(\eta + \dfrac{\rho g\sqrt{1+\eta^2}}{T_0}L) - \sinh^{-1}(\eta)\right) \\ 0 = h - \dfrac{\eta T_0 L}{EA\sqrt{1+\eta^2}} - \rho g\dfrac{L^2}{2EA} - \dfrac{T_0}{\rho g\sqrt{1+\eta^2}}\left(\sqrt{1+\left(\eta+\dfrac{\rho g\sqrt{1+\eta^2}}{T_0}L\right)^2} - \sqrt{1+\eta^2}\right) \end{cases}$$

$\leftrightarrow \quad \mathbf{0} = \mathcal{F}(T_0,\eta)$

The Jacobian matrix of $\mathcal{F}$ is given by

$$\mathcal{J}(L,\eta) = \begin{bmatrix} \frac{\partial \mathcal{F}_1}{\partial T_0}(T_0,\eta) & \frac{\partial \mathcal{F}_1}{\partial \eta}(T_0,\eta) \\ \frac{\partial \mathcal{F}_2}{\partial T_0}(T_0,\eta) & \frac{\partial \mathcal{F}_2}{\partial \eta}(T_0,\eta) \end{bmatrix}$$

where

$$\frac{\partial \mathcal{F}_1}{\partial T_0}(T_0,\eta) = -\frac{L}{EA} - \frac{1}{\rho g}\left(\sinh^{-1}(\eta + \frac{\rho g\sqrt{1+\eta^2}}{T_0}L) - \sinh^{-1}(\eta)\right) - \frac{L\sqrt{1+\eta^2}}{T_0}\frac{1}{\sqrt{1+\left(\eta + \frac{\rho g L\sqrt{1+\eta^2}}{T_0}\right)^2}}$$

$$\frac{\partial \mathcal{F}_1}{\partial \eta}(T_0,\eta) = \frac{H}{\rho g}\left(\frac{1}{\sqrt{1+\eta^2}} - \frac{1}{\sqrt{1+\left(\eta + \frac{\rho g L}{H}\right)^2}}\right)$$

$$\frac{\partial \mathcal{F}_2}{\partial T_0}(T_0,\eta) = -\frac{\eta L}{EA} - \frac{1}{\rho g}\left(\sqrt{1+\left(\eta + \frac{\rho g\sqrt{1+\eta^2}}{T_0}L\right)^2} - \sqrt{1+\eta^2}\right) + \frac{L\sqrt{1+\eta^2}}{T_0}\frac{\eta + \frac{\rho g L\sqrt{1+\eta^2}}{T_0}}{\sqrt{1+\left(\eta + \frac{\rho g L\sqrt{1+\eta^2}}{T_0}\right)^2}}$$

$$\frac{\partial \mathcal{F}_2}{\partial \eta}(T_0,\eta) = -\frac{T_0 L}{\sqrt{1+\eta^2}EA} + \frac{T_0}{\rho g\sqrt{1+\eta^2}}\left(\frac{\eta}{\sqrt{1+\eta^2}} - \frac{\eta + \frac{\rho g L\sqrt{1+\eta^2}}{T_0}}{\sqrt{1+\left(\eta + \frac{\rho g L\sqrt{1+\eta^2}}{T_0}\right)^2}}\right)$$

Appendix B

Calculus of variations

This Appendix is a reminder about Calculus of Variations. The notations used here are specific to this appendix.
Two cases are presented: the first one is the one dimensional case and the second is its extension to the curvilinear domains to $\mathbb{R}^d$.

B.1 One-Dimensional Case

In this section, $x \in \mathbb{R}$ is a variable and f is a scalar function such that:

$$f : \begin{bmatrix} x & \longrightarrow f(x) \\ ]a,b[& \longrightarrow \mathbb{R} \end{bmatrix} \tag{B.1}$$

and f is assumed continuously differentiable. We assume that the values of f are given in a and b. Let us consider the following functional:

$$\mathcal{S}(f) = \int_a^b \mathcal{L}(f(x), f'(x), x)\mathrm{d}x \tag{B.2}$$

We are concerned with finding extremal values of $\mathcal{S}$ for the set of functions that are satisfying the boundary conditions in a and b. The idea is to apply $\mathcal{S}$ to a function $f + \epsilon g$ such that $g(a) = g(b) = 0$ and ϵ is an arbitrary small parameter. The first order variation of $\mathcal{S}$ reads:

$$\mathrm{d}\mathcal{S} = \mathcal{S}(f + \epsilon g) - \mathcal{S}(f) \tag{B.3}$$

We may develop at first order in ϵ the latter as follows

$$\mathrm{d}\mathcal{S} = \epsilon \int_a^b \frac{\partial \mathcal{L}}{\partial f} g + \frac{\partial \mathcal{L}}{\partial f'} g' \mathrm{d}x + \mathcal{O}(\epsilon^2) \tag{B.4}$$

Using integral by part with the second integral term yields:

$$\int_a^b \frac{\partial \mathcal{L}}{\partial f'} g'(x)\ \mathrm{d}x = \left[\frac{\partial \mathcal{L}}{\partial f'} g\right]_a^b - \int_a^b \frac{\mathrm{d}}{\mathrm{d}x}\left(\frac{\partial \mathcal{L}}{\partial f'}\right) g\ \mathrm{d}x \tag{B.5}$$

Using the fact that $g(a) = g(b) = 0$ and factorizing by g inside the integral yields:

$$\mathrm{d}\mathcal{S} = \epsilon \int_a^b \left[\frac{\partial \mathcal{L}}{\partial f} - \frac{\mathrm{d}}{\mathrm{d}x}\left(\frac{\partial \mathcal{L}}{\partial f'}\right)\right] g\ \mathrm{d}x + \mathcal{O}(\epsilon^2) \tag{B.6}$$

If f is an extreme point of $\mathcal{S}$, then $\mathrm{d}\mathcal{S}$ should vanish at first order for all g. Thus,

$$\forall g \in \mathcal{C}^1(]a,b[) \text{ s.t.} g(a) = g(b) = 0 \quad , \quad \int_a^b \left[\frac{\partial \mathcal{L}}{\partial f} - \frac{\mathrm{d}}{\mathrm{d}x} \left(\frac{\partial \mathcal{L}}{\partial f'} \right) \right] g \, \mathrm{d}x = 0 \tag{B.7}$$

As a consequence, f should satisfy the following differential equation:

$$\frac{\partial \mathcal{L}}{\partial f} - \frac{\mathrm{d}}{\mathrm{d}x} \left(\frac{\partial \mathcal{L}}{\partial f'} \right) = 0 \tag{B.8}$$

The latter is often coined as the Lagrange-Euler equation and the $\mathcal{L}$ is called the Lagrangian of the system.

Appendix C

Computation of the admissibility conditions for the cable-pulley super-element

This appendix regroups the compatibility conditions for the cable-pulley super-element. Configurations provided here are the following:

- Equilibrium contained in the $(\mathbf{x}, \mathbf{y})$-plane
  - The cable is above the pulley (Support Configuration)
  - The cable is below the pulley (Compression Configuration)
- Equilibrium is 3D and contained in the $(\mathbf{x}, \mathbf{y})$-plane
  - The cable is above the pulley (3D - Support Configuration)
  - The cable is below the pulley (3D - Compression Configuration)

Support configuration

The admissibility is given by

$$
\begin{aligned}
\text{(C1):}\quad & \begin{cases} 0 = x_p - \dfrac{R\left(\eta_1 + \frac{\rho g}{H_1} L_1\right)}{\sqrt{1 + \left(\eta_1 + \frac{\rho g}{H_1} L_1\right)^2}} - x_0 - \dfrac{H_1}{\rho g}\left(\sinh^{-1}(\eta_1 + \dfrac{\rho g}{H_1} L_1) - \sinh^{-1}(\eta_1)\right) \\ 0 = y_p + \dfrac{R}{\sqrt{1 + \left(\eta_1 + \frac{\rho g}{H_1} L_1\right)^2}} - y_0 - \dfrac{H_1}{\rho g}\left(\sqrt{1 + \left(\eta_1 + \dfrac{\rho g}{H_1} L_1\right)^2} - \sqrt{1 + \eta_1^2}\right) \end{cases} \\
\text{(P):}\quad & \left\{ H_2\sqrt{1 + \eta_2^2} = H_1\sqrt{1 + \left(\eta_1 + \dfrac{\rho g}{H_1} L_1\right)^2}\, e^{\mu(\tan^{-1}(-\eta_2) - \tan^{-1}(\eta_1))} \right. \\
\text{(C2):}\quad & \begin{cases} 0 = x_2 - x_p + \dfrac{R\eta_2}{\sqrt{1 + \eta_2^2}} - \dfrac{H_2}{\rho g}\left(\sinh^{-1}(\eta_2 + \dfrac{\rho g}{H_2} L_2) - \sinh^{-1}(\eta_2)\right) \\ 0 = y_2 - y_p - \dfrac{R}{\sqrt{1 + \eta_2^2}} - \dfrac{H_2}{\rho g}\left(\sqrt{1 + \left(\eta_2 + \dfrac{\rho g}{H_2} L_2\right)^2} - \sqrt{1 + \eta_2^2}\right) \end{cases}
\end{aligned}
\tag{C.1}
$$

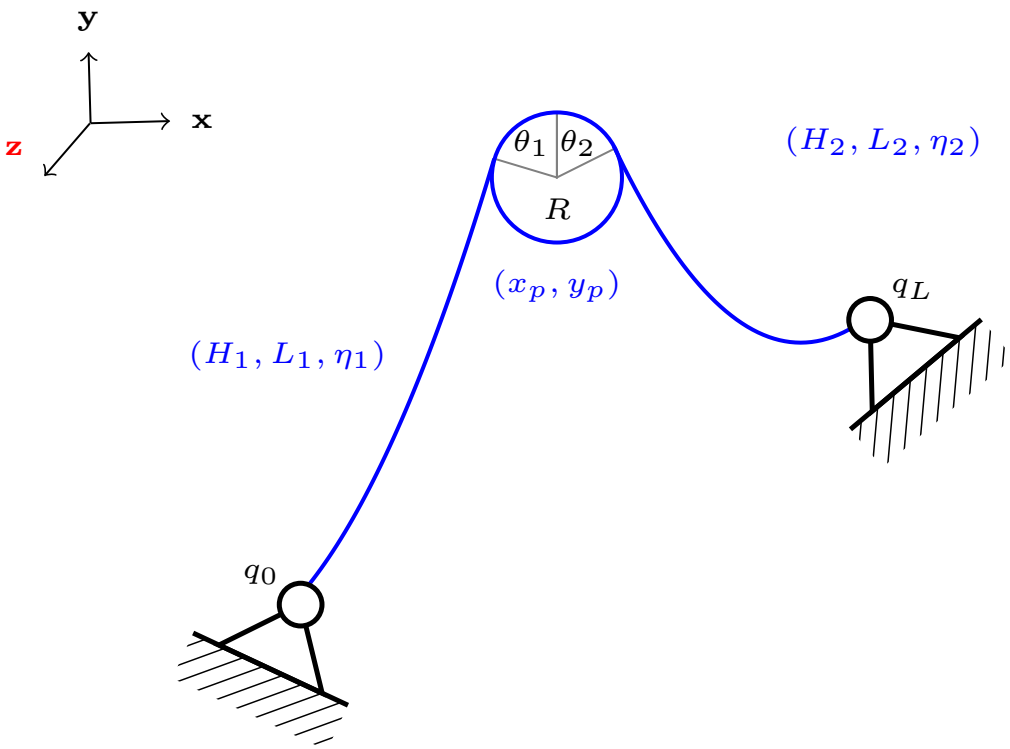

Compression configuration

The admissibility is given by

$$
\text{(C1):}\quad \begin{cases} 0 = x_p - \dfrac{R\left(\eta_1 + \frac{\rho g}{H_1}L_1\right)}{\sqrt{1+\left(\eta_1 + \frac{\rho g}{H_1}L_1\right)^2}} - x_0 - \dfrac{H_1}{\rho g}\left(\sinh^{-1}(\eta_1 + \dfrac{\rho g}{H_1}L_1) - \sinh^{-1}(\eta_1)\right) \\ 0 = y_p - \dfrac{R}{\sqrt{1+\left(\eta_1 + \frac{\rho g}{H_1}L_1\right)^2}} - y_0 - \dfrac{H_1}{\rho g}\left(\sqrt{1+\left(\eta_1 + \dfrac{\rho g}{H_1}L_1\right)^2} - \sqrt{1+\eta_1^2}\right) \end{cases}
$$

$$
\text{(P):}\quad \left\{ H_2\sqrt{1+\eta_2^2} = H_1\sqrt{1+\left(\eta_1 + \frac{\rho g}{H_1}L_1\right)^2}\, e^{\mu(\tan^{-1}(\eta_2)-\tan^{-1}(-\eta_1))} \right.
$$

$$
\text{(C2):}\quad \begin{cases} 0 = x_2 - x_p - \dfrac{R\eta_2}{\sqrt{1+\eta_2^2}} - \dfrac{H_2}{\rho g}\left(\sinh^{-1}(\eta_2 + \dfrac{\rho g}{H_2}L_2) - \sinh^{-1}(\eta_2)\right) \\ 0 = y_2 - y_p - \dfrac{R}{\sqrt{1+\eta_2^2}} - \dfrac{H_2}{\rho g}\left(\sqrt{1+\left(\eta_2 + \dfrac{\rho g}{H_2}L_2\right)^2} - \sqrt{1+\eta_2^2}\right) \end{cases}
\tag{C.2}
$$

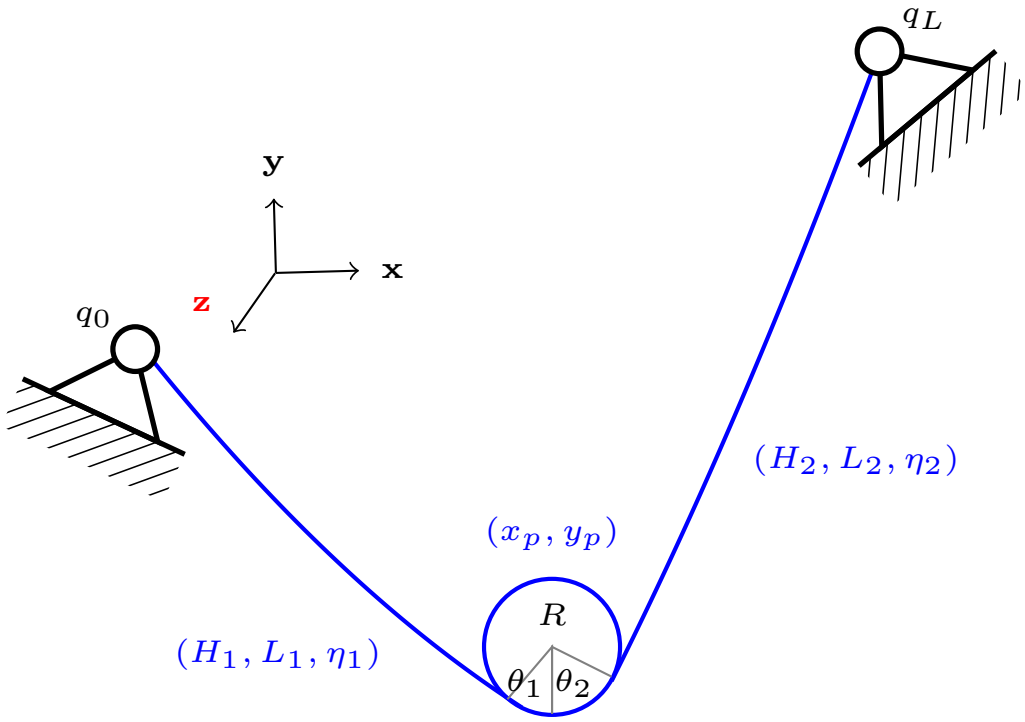

3D - Support configuration

The admissibility is given by

$$
\begin{aligned}
\text{(C1):} & \begin{cases} 0 = x_p - \dfrac{R\left(\eta_1 + \frac{\rho g}{H_1} L_1\right)}{\sqrt{1 + \left(\eta_1 + \frac{\rho g}{H_1} L_1\right)^2}} - x_0 - \dfrac{H_1}{\rho g}\left(\sinh^{-1}(\eta_1 + \dfrac{\rho g}{H_1} L_1) - \sinh^{-1}(\eta_1)\right) \\ 0 = y_p + \dfrac{R}{\sqrt{1 + \left(\eta_1 + \frac{\rho g}{H_1} L_1\right)^2}} - y_0 - \dfrac{H_1}{\rho g}\left(\sqrt{1 + \left(\eta_1 + \dfrac{\rho g}{H_1} L_1\right)^2} - \sqrt{1 + \eta_1^2}\right) \end{cases} \\
\text{(P):} & \left\{ H_2\sqrt{1 + \eta_2^2} = H_1\sqrt{1 + \left(\eta_1 + \dfrac{\rho g}{H_1} L_1\right)^2}\, e^{\mu(\tan^{-1}(-\eta_2) - \tan^{-1}(\eta_1))} \right. \\
\text{(C2):} & \begin{cases} 0 = x_2 - x_p + \dfrac{R\eta_2}{\sqrt{1 + \eta_2^2}} - \dfrac{H_2}{\rho g}\left(\sinh^{-1}(\eta_2 + \dfrac{\rho g}{H_2} L_2) - \sinh^{-1}(\eta_2)\right) \\ 0 = y_2 - y_p - \dfrac{R}{\sqrt{1 + \eta_2^2}} - \dfrac{H_2}{\rho g}\left(\sqrt{1 + \left(\eta_2 + \dfrac{\rho g}{H_2} L_2\right)^2} - \sqrt{1 + \eta_2^2}\right) \end{cases}
\end{aligned}
\tag{C.3}
$$

3D - Compression configuration

The admissibility is given by

$$
\begin{aligned}
\text{(C1):}\quad & \begin{cases} 0 = x_p - \dfrac{R\left(\eta_1 + \frac{\rho g}{H_1} L_1\right)}{\sqrt{1 + \left(\eta_1 + \frac{\rho g}{H_1} L_1\right)^2}} - x_0 - \dfrac{H_1}{\rho g}\left(\sinh^{-1}(\eta_1 + \dfrac{\rho g}{H_1} L_1) - \sinh^{-1}(\eta_1)\right) \\ 0 = y_p - \dfrac{R}{\sqrt{1 + \left(\eta_1 + \frac{\rho g}{H_1} L_1\right)^2}} - y_0 - \dfrac{H_1}{\rho g}\left(\sqrt{1 + \left(\eta_1 + \dfrac{\rho g}{H_1} L_1\right)^2} - \sqrt{1 + \eta_1^2}\right) \end{cases} \\
\text{(P):}\quad & \begin{cases} H_2\sqrt{1+\eta_2^2} = H_1\sqrt{1 + \left(\eta_1 + \dfrac{\rho g}{H_1} L_1\right)^2}\, e^{\mu(\tan^{-1}(\eta_2) - \tan^{-1}(-\eta_1))} \end{cases} \\
\text{(C2):}\quad & \begin{cases} 0 = x_2 - x_p - \dfrac{R\eta_2}{\sqrt{1+\eta_2^2}} - \dfrac{H_2}{\rho g}\left(\sinh^{-1}(\eta_2 + \dfrac{\rho g}{H_2} L_2) - \sinh^{-1}(\eta_2)\right) \\ 0 = y_2 - y_p - \dfrac{R}{\sqrt{1+\eta_2^2}} - \dfrac{H_2}{\rho g}\left(\sqrt{1 + \left(\eta_2 + \dfrac{\rho g}{H_2} L_2\right)^2} - \sqrt{1+\eta_2^2}\right) \end{cases}
\end{aligned}
\tag{C.4}
$$

Appendix D

Log-decrement technique

Notations used here are specific to this chapter and only used in the following.

We are interested in the solution of the following differential equation

$$m\ddot{x}(t) + 2\xi\dot{x}(t) + kx(t) = 0 \tag{D.1}$$

The latter can be recast into

$$\ddot{x}(t) + 2\xi\omega\dot{x}(t) + \omega^2 x(t) = 0 \tag{D.2}$$

We are looking to a system which is freely vibrating with damping then we must have

$$\Delta = 4\omega^2\left(\xi^2 - 1\right) < 0 \tag{D.3}$$

The solution is given as

$$x(t) = A_0 \exp(-\xi\omega t)\cos(\omega\sqrt{1-\xi^2}t + \Phi) \tag{D.4}$$

We want to quantity the rate of decay between two successive maximum of amplitude. The pseudo period of the motion is given by

$$T_d = \frac{2\pi}{\omega\sqrt{1-\xi^2}} \tag{D.5}$$

We can evaluate the wanted ratio as

$$\frac{x(t+T_d)}{x(t)} = \exp\left(-\xi\omega T_d\right) \tag{D.6}$$

Composing by Neperian logarithm we have

$$\log\frac{x(t+T_d)}{x(t)} = -\xi\omega T_d = -\frac{2\xi\pi}{\sqrt{1-\xi^2}} \tag{D.7}$$

The latter formulae is of practical interest to identify damping from experimental data. The decrease of the amplitude is depicted in Figure D.1.

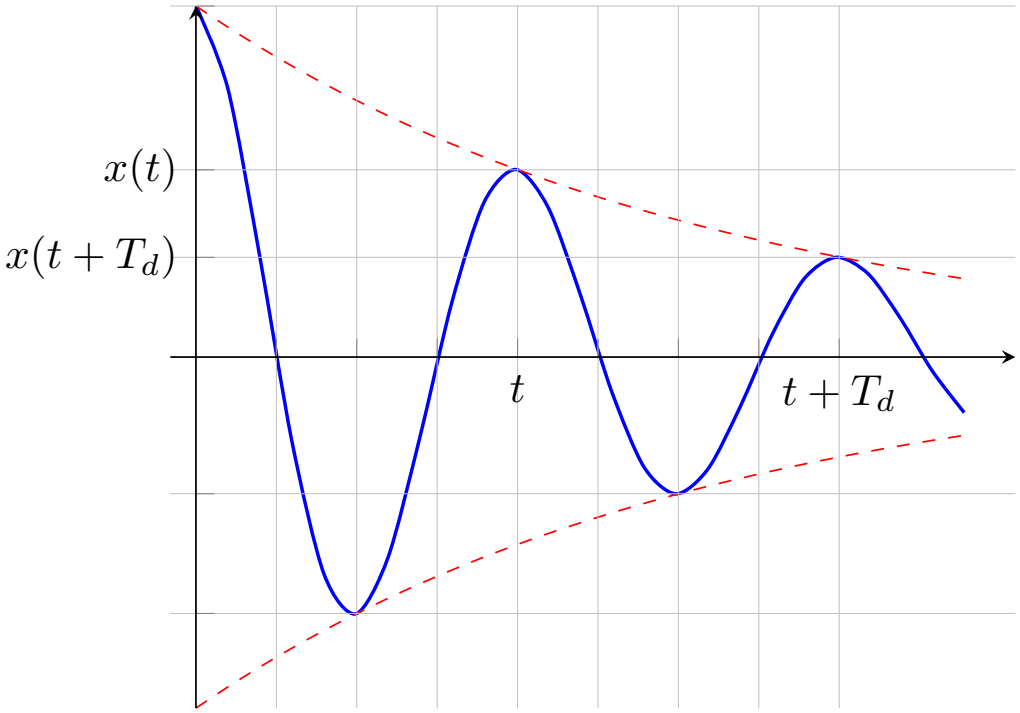

Figure D.1: A damped oscillation (solid line —) accompanied with its envelop (dashed line - - -)

Appendix E

Computation of periodic solutions via the arc-length method

The notations used in this chapter are valid for this chapter only. The latter is self-standing and can be read independently from the manuscript.

Governing Equations

Let us consider a general evolution problem under state-space formalism as

$$\dot{z} = f(z, t) \tag{E.1}$$

where the state-space variable belongs to $\mathbb{R}^d$ with $d \in \mathbb{N}$.
Considering arbitrary initial condition $z_0 \in \mathbb{R}^d$, the latter can be numerically integrated for $t \in [0, T]$ with any suitable numerical scheme.

Periodic Solutions under Period Forcing

A particular case of (E.1) is obtained when a periodic forcing is applied to a given mechanical system. In this case, it is assumed that the system response will be periodic with the same period, T, as the forcing applied with pulsation Ω to the system. Mathematically speaking

$$\forall t \geqslant 0, \quad z(z_0, T + t) = z(z_0, t) \quad ; \quad T = \frac{2\pi}{\Omega} \tag{E.2}$$

These solutions are given by by (E.2). The unknowns of this problem are the tuple given by the initial condition z_0 and the frequency of forcing Ω. The frequency-curve, which consists on plotting the maximum amplitude of the periodic motion versus the frequency, is a common representation of the solution to this problem.

Monodromy Matrix

When studying the periodic solution of an ODE, the monodromy matrix appears naturally when computing the Jacobian of (E.2) with regards to the initial condition. Indeed,

$$\frac{\partial}{\partial z_0} \left(z(z_0, T) - z_0 \right) = \frac{\partial z}{\partial z_0}(z_0, T) - \mathbf{I} \tag{E.3}$$

The monodromy matrix is therefore obtained as

$$\mathbf{M}(z_0, T) = \frac{\partial z}{\partial z_0}(z_0, T) \tag{E.4}$$

The latter is not easy to derive especially when it comes to nonlinear multi-dimensional problems. That is the reason why it often computed numerically via numerical differentiation as

$$\mathbf{M}_{ij}(z_0, T) \approx \frac{z_i(z_0 + \delta e_j, T) - z_i(z_0, T)}{\delta} \quad , \quad e_j = (0, ..., 0, 1, 0, ..., 0)^\top \tag{E.5}$$

At a converged state, this matrix also gives insight about the stability of a periodic solution. Indeed, it is interesting to know how the system reacts to a small perturbation. The system variable may remain in a torus centered on the periodic orbit or the system behavior could change radically. This information is contained in the eigenvalues of $\mathbf{M}$. Those eigenvalues are called Floquet multipliers and two cases are of major interest

- $\forall i \quad |\lambda_i| < 1$: The motion is stable
- $\exists i \quad |\lambda_i| \geqslant 1$: The motion is unstable

Arc-length Continuation Technique

Obtaining the frequency-curve requires to solve the following nonlinear problem

$$\begin{cases} \dot{z} = f(z, t) \\ h(z_0, \Omega) = \ z(z_0, t = T, \Omega) - z_0 = \mathbf{0} \end{cases} \tag{E.6}$$

Several approaches may be endowed to solve (E.6) among which brutal computations and shooting methods. We are here interested into the arc-length continuation technique which is suitable to trace continuum of periodic solutions. The latter resides in the introduction of a path to follow when searching for periodic solutions. An arc-length coordinate, s, is introduced in order to impose the solution to follow a path. In another words, the curve given by (z_0, Ω) is assumed continuous and differentiable so that a tangent direction to this curve may be defined almost everywhere in the Lebesgue sense. The philosophy is as follows

- Start from an admissible point (z_0, Ω)
- Advance forward in the tangent direction given by v with a step-length Δs : Prediction step
- Correct the prediction by following the orthogonal direction to v : Correction Step

This methodology is illustrated by schematic E.1

Prediction Step

Let us assume that we have a solution of (E.6) given by (z_0, Ω), a tangent direction is computed as follows

$$v = \left(\Delta z_0^\dagger, \Delta\Omega^\dagger\right) \text{ such that } \begin{cases} 0 = \dfrac{\partial h}{\partial z_0}\Delta z_0^\dagger + \dfrac{\partial h}{\partial \Omega}\Delta\Omega^\dagger \\ 1 = \left(\Delta z_0^\dagger\right)^\top \left(\Delta z_0^\dagger\right) + \left(\Omega^\dagger\right)^2 \end{cases} \tag{E.7}$$

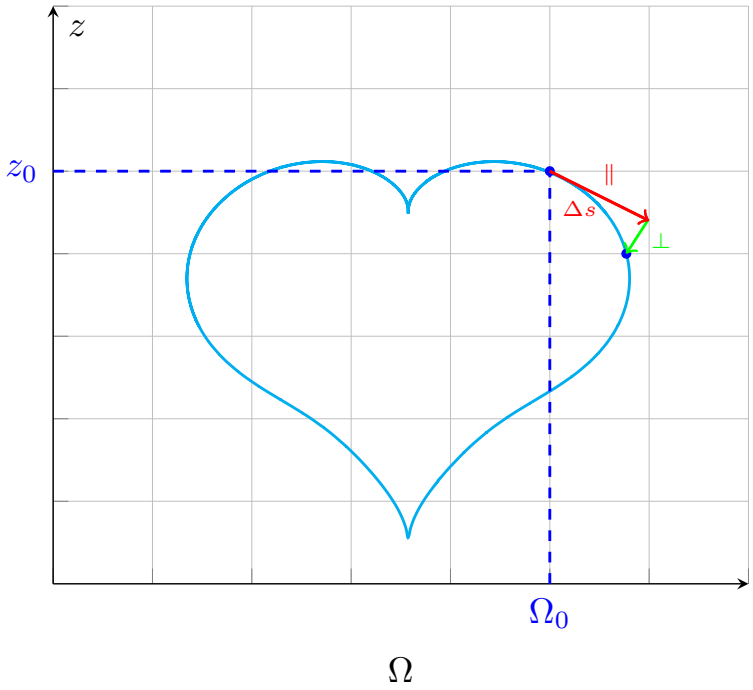

Figure E.1: Illustration of the prediction and correction process in the Arc-length Continuation method

First equation corresponds to the tangent derivation and second one is the unit constraint. The unit constraint is obtained by setting

$$\begin{cases} a = \Delta\Omega^{\dagger} \\ a\Delta z = \Delta z_0^{\dagger} \end{cases} \rightarrow a = \pm \left(1 + (\Delta z)^{\top} (\Delta z)\right)^{-\frac{1}{2}} \tag{E.8}$$

and the expression of the tangent direction is obtained by solving

$$\frac{\partial h}{\partial z_0}\Delta z = -\frac{\partial h}{\partial \Omega} \tag{E.9}$$

We can obtain the next guess as

$$\begin{bmatrix} z_0^{k+1} \\ \Omega^{k+1} \end{bmatrix} = \begin{bmatrix} z_0^{k} \\ \Omega^{k} \end{bmatrix} + \Delta s \; v \tag{E.10}$$

where Δs is a step-length parameter chosen by the user.
It is clear from (E.8) that two choices arise for the value of a. As the continuation technique is designed to follow a path, we should choose the one that conserves the path direction, i.e. we should impose

$$v^{k+1} \cdot v^{k} > 0 \tag{E.11}$$

As a consequence, the sign of a is given by

$$\text{sign}(a) = \text{sign}\left((\Delta z_0)^{k} \cdot (\Delta z) + \Delta\Omega^{k}\right) \tag{E.12}$$

Correction Step

A correction should be performed on the prediction done in the previous step. We are solving the following nonlinear equation

$$h(z_0 + \Delta z_0, \Omega + \Delta z_0) = \mathbf{0} \tag{E.13}$$

with the orthogonality constraint as follows

$$v \cdot \begin{bmatrix} \Delta z_0 \\ \Delta\Omega \end{bmatrix} = 0 \quad \text{i.e.} \quad \Delta z_0^\dagger \cdot \Delta z_0 + \Delta\Omega^\dagger \Delta\Omega = 0 \tag{E.14}$$

Endowing a Newton-Raphson procedure leads to the following problem

$$\begin{bmatrix} \frac{\partial h}{\partial z_0} & \frac{\partial h}{\partial \Omega} \\ \Delta z_0^\dagger & \Delta\Omega^\dagger \end{bmatrix} \begin{bmatrix} \Delta z_0 \\ \delta\Omega \end{bmatrix} = - \begin{bmatrix} -h(z_0, \Omega) \\ 0 \end{bmatrix} \tag{E.15}$$

or equivalently

$$\begin{bmatrix} \mathbf{M}(z_0, \Omega) - \mathbf{I} & \frac{\partial h}{\partial \Omega} \\ \Delta z_0^\dagger & \Delta\Omega^\dagger \end{bmatrix} \begin{bmatrix} \Delta z_0 \\ \delta\Omega \end{bmatrix} = - \begin{bmatrix} -h(z_0, \Omega) \\ 0 \end{bmatrix} \tag{E.16}$$

which is a problem of dimension $d + 1$.
A convergence criteria should be chosen by the user, for instance

$$\frac{\|h(z_0, \Omega)\|}{\|z_0\|} \leqslant \varepsilon \quad \text{or} \quad \frac{\|\Delta z_0\|}{\|z_0\|} \leqslant \varepsilon \tag{E.17}$$

The computation of $\frac{\partial h}{\partial \Omega}$ is done numerically and we have

$$\frac{\partial h}{\partial \Omega} = \frac{\partial z}{\partial \Omega}(z_0, T) + \frac{\partial T}{\partial \Omega}\frac{\partial z}{\partial t}(z_0, T) \tag{E.18}$$

which takes sense numerically as

$$\frac{\partial z}{\partial \Omega}(z_0, T) \approx \frac{z(z_0, T, \Omega + \delta) - z(z_0, T, \Omega - \delta)}{2\delta} \tag{E.19}$$

$$\frac{\partial T}{\partial \Omega}\frac{\partial z}{\partial t}(z_0, T) \approx -\frac{2\pi}{\Omega^2} f(z(T), T) \tag{E.20}$$

Appendix F

Damped oscillations: 1-dof analysis

Notations used here are specific to this chapter and only used in the following.

We are interested in the solution of the following differential equation

$$\ddot{x}(t) + 2\xi\omega\dot{x}(t) + \omega^2 x(t) = 0 \quad ; \quad 0 \leq \xi \leq 1/\sqrt{2} \tag{F.1}$$

If seek for x in the following form

$$x = e^{\lambda t} \tag{F.2}$$

then (F.1) reduces to solve

$$\lambda^2 + \xi\omega\lambda + \omega^2 = 0 \tag{F.3}$$

The determinant of (F.3) reads

$$\Delta = 4(\xi^2 - 1)\omega^2 < 0 \tag{F.4}$$

The solution of (F.1) is then given by

$$x(t) = X_1 e^{\lambda_1 t} + X_2 e^{\lambda_2 t} \tag{F.5}$$

where

$$\lambda_1 = -\xi\omega + i\omega\sqrt{1-\xi^2} \tag{F.6}$$

$$\lambda_2 = -\xi\omega - i\omega\sqrt{1-\xi^2} \tag{F.7}$$

We see that the eigenfrequencies of the differential equation do not coincide with the expected system frequency ω but we have following properties

$$|\lambda_i| = \omega \quad ; \quad i = 1, 2 \tag{F.8}$$

$$\frac{\mathrm{Re}(\lambda_i)}{|\lambda_i|} = \xi \quad ; \quad i = 1, 2 \tag{F.9}$$

Since eigenfrequencies of the system depart from physical frequencies, one can ask the frequency of resonance of the system. To have an idea, let us excite the system given by (F.1) with an arbitrary harmonic forcing at frequency Ω

$$\ddot{x}(t) + 2\xi\omega\dot{x}(t) + \omega^2 x(t) = Ae^{\Omega t} \tag{F.10}$$

We can take a look at the transfer function of the latter as

$$X = H(\Omega)A \tag{F.11}$$

where

$$H(\Omega) = \frac{1}{\omega^2 + 2i\xi\omega\Omega - \Omega^2} \tag{F.12}$$

The modulus of the latter is given by

$$|H(\Omega)| = \frac{1}{\sqrt{\left(\omega^2 - \Omega^2\right)^2 + 4(\xi\omega\Omega)^2}} \tag{F.13}$$

Even if the amplification remains finite when $\xi \neq 0$, the maximum of amplitude can be determined when the derivative of $|H|$ is zero which means

$$\Omega = \omega\sqrt{1 - 2\xi^2} \tag{F.14}$$

Of course the latter is consistent for the undamped case but we seen than the maximum amplification will not arise at ω but it is shifted to Ω. Then following frequencies can be considered

$$\text{(Undamped/natural frequency)} \quad : \quad \omega \tag{F.15}$$

$$\text{(Damped frequency)} \quad : \quad \lambda = -\xi\omega \pm i\omega\sqrt{1 - \xi^2} \tag{F.16}$$

$$\text{(Resonant frequency)} \quad : \quad \Omega = \omega\sqrt{1 - 2\xi^2} \tag{F.17}$$

Appendix G

Mathieu type equation

Notations used here are specific to this chapter and only used in the following.

We are interested into the stability of the solution of the following differential equation

$$\ddot{x}(t) + [\delta + 2\varepsilon\cos(2t)]\, x(t) = 0 \quad , \quad \varepsilon \ll 1 \tag{G.1}$$

By stability we mean that the solution obtained should remain periodic and bounded. This problem is treated via an expansion of system variable x as

$$x(t) = x_0(t) + \varepsilon x_1(t) + \varepsilon^2 x_2(t) + \mathcal{O}(\varepsilon^2) \tag{G.2}$$

Moreover it is assumed that δ can be expansed into

$$\delta = \delta_0 + \varepsilon\delta_1 + \varepsilon^2\delta_2 + \mathcal{O}(\varepsilon^2) \tag{G.3}$$

In pratical application, δ often corresponds to a multiple of a frequency perturbed by a small quantity. In other words, δ_0 corresponds to $0, 1, 2^2, ..., k^2$ and δ_i are perturbation at order ε^i. Equations (G.1-G.3) can be combined to obtain the following set of equations

$$\ddot{x}_0(t) + \delta_0 x_0(t) = 0 \tag{G.4}$$
$$\ddot{x}_1(t) + \delta_0 x_1(t) = -\left[\delta_1 + 2\cos(2t)\right] x_0(t) \tag{G.5}$$
$$\ddot{x}_2(t) + \delta_0 x_2(t) = -\left[\delta_1 + 2\cos(2t)\right] x_1(t) - \delta_2 x_0(t) \tag{G.6}$$

From (G.4), it is seen that

$$x_0(t) = A_0\cos(\sqrt{\delta_0}t) + B_0\sin(\sqrt{\delta_0}t) \tag{G.7}$$

The solution for x_0 can be injected into (G.5). However, we are interested into solutions that remains bounded in time t. So resonant terms should be eliminated from the right-hand side. Before going any further we should split our study into different cases which are $\delta_0 = 0$, $\delta_0 = 1$ and the rest. The key idea is to build one curve for cos and another one for sin giving δ as a function of ε.

Case $\delta_0 = 0$

When δ_0 is set to 0, $x_0 = 1$. The system at order ε^1 reads

$$\ddot{x}_1(t) = -\left[\delta_1 + 2\cos(2t)\right] x_0(t) \tag{G.8}$$

The latter imposes that $\delta_1 = 0$ and that

$$x_1(t) = \frac{\cos(2t)}{2} \tag{G.9}$$

It can be injected into (G.6) which yields

$$\ddot{x}_2(t) = -\cos(2t)^2 - \delta_2 \tag{G.10}$$
$$= -\frac{\cos(4t)}{2} - \left(\delta_2 + \frac{1}{2}\right) \tag{G.11}$$

Then we have to set $\delta_2 = -\frac{1}{2}$. This first investigation yields the first transition curve as

$$\delta = -\frac{\varepsilon^2}{2} \tag{G.12}$$

Case $\delta_0 = 1$

When $\delta_0 = 1$, $x_0(t) = A_0\cos(t) + B_0\sin(t)$. The equations for particular solutions at order ε^1 reads

$$\ddot{x}_1(t) + x_1(t) = -\left[\delta_1 + 2\cos(2t)\right]\cos(t) = -(\delta_1 + 1)\cos(t) - \cos(3t) \tag{G.13}$$
$$\ddot{x}_1(t) + x_1(t) = -\left[\delta_1 + 2\cos(2t)\right]\sin(t) = -(\delta_1 - 1)\sin(t) - \sin(3t) \tag{G.14}$$

The particular solution for x_1 is obtained as

$$\delta_1 = -1 \rightarrow x_1(t) = \frac{\cos(3t)}{8} \tag{G.15}$$
$$\delta_1 = 1 \rightarrow x_1(t) = \frac{\sin(3t)}{8} \tag{G.16}$$

The latter is injected into (G.6) and provides

$$\ddot{x}_2(t) + \delta_0 x_2(t) = \left[1 - 2\cos(2t)\right]\frac{\cos(3t)}{8} - \delta_2\cos(t) \tag{G.17}$$
$$\ddot{x}_2(t) + \delta_0 x_2(t) = -\left[1 + 2\cos(2t)\right]\frac{\sin(3t)}{8} - \delta_2\sin(t) \tag{G.18}$$

i.e.

$$\ddot{x}_2(t) + \delta_0 x_2(t) = \frac{\cos(3t)}{8} - \frac{\cos(5t)}{8} - \left(\frac{1}{8} + \delta_2\right)\cos(t) \rightarrow \delta_2 = -\frac{1}{8} \tag{G.19}$$
$$\ddot{x}_2(t) + \delta_0 x_2(t) = -\frac{\sin(3t)}{8} - \frac{\sin(5t)}{8} - \left(\frac{1}{8} + \delta_2\right)\sin(t) \rightarrow \delta_2 = \frac{1}{8} \tag{G.20}$$

which gives two transition curves as

$$\delta = 1 - \varepsilon + \frac{1}{8}\varepsilon^2 \tag{G.21}$$
$$\delta = 1 + \varepsilon + \frac{1}{8}\varepsilon^2 \tag{G.22}$$

Case $\delta_0 = k^2$ with $k > 1$

In order to remain bounded we have the following conditions for δ_1

$$\ddot{x}_1(t) + k^2 x_1(t) = -\delta_1 \cos(kt) - \cos\left((2-k)t\right) - \cos\left((2+k)t\right) \tag{G.23}$$
$$\ddot{x}_1(t) + k^2 x_1(t) = -\delta_1 \cos(kt) + \sin\left((2-k)t\right) - \sin\left((2+k)t\right) \tag{G.24}$$

The particular solution for x_1 is obtained as

$$\delta_1 = 0 \rightarrow x_1(t) = \frac{\cos\left((2+k)t\right)}{4(1+k)} + \frac{\cos\left((2-k)t\right)}{4(1-k)} \tag{G.25}$$
$$\delta_1 = 0 \rightarrow x_1(t) = \frac{\sin\left((2+k)t\right)}{4(1+k)} - \frac{\sin\left((2-k)t\right)}{4(1-k)} \tag{G.26}$$

The latter is injected into (G.6) and provides

$$\ddot{x}_2(t) + k^2 x_2(t) = -\frac{\cos\left((4-k)t\right)}{4(1-k)} - \frac{\cos\left((4+k)t\right)}{4(1+k)} - \left(\delta_2 + \frac{1}{2(1-k^2)}\right)\cos(kt) \tag{G.27}$$
$$\ddot{x}_2(t) + k^2 x_2(t) = \frac{\sin\left((4-k)t\right)}{4(1-k)} - \frac{\sin\left((4+k)t\right)}{4(1+k)} - \left(\delta_2 + \frac{1}{2(1-k^2)}\right)\sin(kt) \tag{G.28}$$

We see here that two cases occur for $k = 2$ and for $k \geq 3$. If $k = 2$ then The first term of the right hand side is secular in addition to the last one, yielding

$$\delta_2 = \frac{5}{12} \tag{G.29}$$
$$\delta_2 = -\frac{1}{12} \tag{G.30}$$

The latter depicts two transition curves as

$$\delta = 4 + \frac{5}{12}\varepsilon^2 \tag{G.31}$$
$$\delta = 4 - \frac{1}{12}\varepsilon^2 \tag{G.32}$$

Otherwise transition curves are given by

$$\delta = k^2 + \frac{\varepsilon^2}{2(k^2-1)} \tag{G.33}$$

The unstable zones are often represented onto a $\delta - \varepsilon$ graph, see Figure G.1.

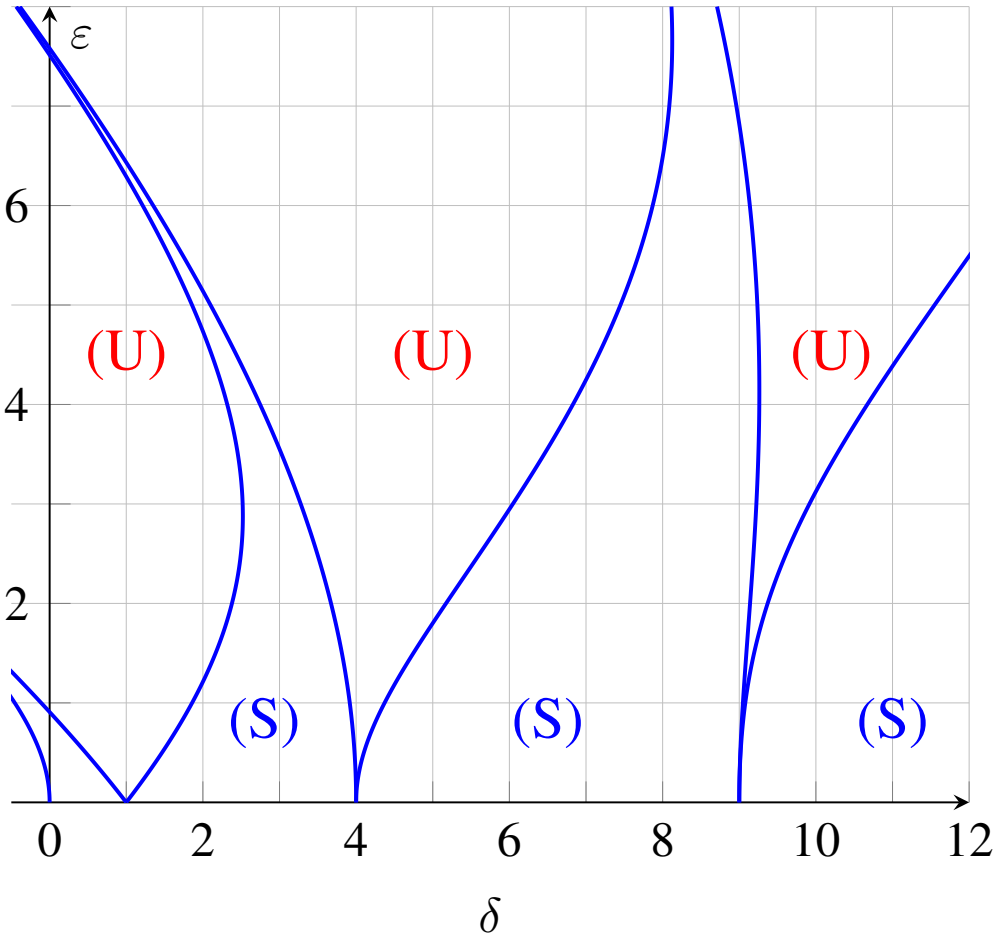

Figure G.1: Stable (S) and unstable (U) zones of the Mathieu type equation